



Navigating Vascular Complexity: Insights from hiPSC-derived Vascular Cells to Advanced 3D Models

Elana M. Meijer

Navigating Vascular Complexity:
Insights from hiPSC-derived Vascular Cells
to Advanced 3D Models

Elana M. Meijer

Navigating Vascular Complexity: Insights from hiPSC-derived Vascular Cells to Advanced 3D Models

ISBN: 978-94-6483-775-9

Provided by thesis specialist Ridderprint, ridderprint.nl

Printing: Ridderprint

Layout and design: Daisy Zunnebeld, persoonlijkproefschrift.nl

Cover lay-out: Daisy Zunnebeld, persoonlijkproefschrift.nl

Cover design: Adora Arts

Copyright 2024 © Elana M. Meijer

The Netherlands. All rights reserved. No parts of this thesis may be reproduced, stored in a retrieval system or transmitted in any form or by any means without permission of the author.

Navigating Vascular Complexity

Insights From hiPSC-derived vascular cells to Advanced 3D
Models

De Diversiteit van het Vasculaire Stelsel
Inzichten uit hiPSC afgeleide Vasculaire Cellen en Geavanceerde 3D-Modellen

(met een samenvatting in het Nederlands)

Proefschrift

ter verkrijging van de graad van doctor aan de
Universiteit Utrecht
op gezag van de
rector magnificus, prof. dr. H.R.B.M. Kummeling,
ingevolge het besluit van het college voor promoties
in het openbaar te verdedigen op

woensdag 1 mei 2024 des middags te 12.15 uur

door

Elana Marianne Meijer

geboren op 25 mei 1995
te Amsterdam

Promotor:

Prof. dr. M.C. Verhaar

Copromotor:

Dr. K.L. Cheng

Beoordelingscommissie:

Prof. dr. C.V.C. Bouten

Dr. J. Essers

Prof. dr. ir. J. Malda

Dr. Y.M. Ruigrok

Prof. dr. J.P.G. Sluijter (voorzitter)

Contents

Chapter 1	General introduction	6
PART 1	Generation and use of hiPSC derived vascular cells	
Chapter 2	Implementation of pericytes in vascular regeneration strategies	32
Chapter 3	3D human iPSC Blood Vessel Organoids as a Source of Flow-Adaptive Vascular Cells for Creating a Human-Relevant 3D-Scaffold Based Macrovascular Model	80
Chapter 4	Induction of Fenestrae in hiPSC-Derived Endothelial cells for Disease modeling	116
Chapter 5	The Effect of Mechanical Stimuli on the Phenotypic Plasticity of Induced Pluripotent Stem Cell-Derived Vascular Smooth Muscle Cells in a 3D Hydrogel	144
PART 2	The application of mechanical stimuli in advanced 3D models	
Chapter 6	Contributions of Wall Stretch and Shear Stress to Vascular Regulation: Molecular Mechanisms of Homeostasis and Expansion	176
Chapter 7	A complex three-dimensional microfluidic model that mimics the early stage events in the human atherosclerotic artery	208
PART 3	Matrigel-free vascular organoid culture	
Chapter 8	Matrigel-free alternatives for hiPSC-derived blood vessel organoid culture	242
Chapter 9	General Discussion	266
Appendices	Nederlandse Samenvatting	281
	Dankwoord	288
	List of publications	293
	Curriculum Vitae	294

CHAPTER

1



General introduction

Preface

The field of regenerative medicine is highly interdisciplinary, focusing on replacing or restoring the function of diseased tissues through a variety of approaches. Over the past years, cells, biomaterial scaffolds or a combination of both showed promising results in mediating regenerative responses. However, one of the major issues in tissue restoration or replacement is lack of (functional) vasculature¹. Without blood vessel support, organ function is impaired, due to the lack of sufficient nutrient and oxygen exchange within the tissue microenvironment. This limits tissue survival, and cell proliferation and differentiation, necessary for regenerative responses. Most tissues require a vascular bed within 150 μm , which is approximately the diffusion limit of oxygen². Vascularization strategies can either focus on the stimulation of vessel formation at the transplantation site or the use of a pre-vascularized construct directly for implantation. Research in this field is thus not limited to the tissue of interest, but also the connected vasculature.

The complex and tissue dependent structure of blood vessels provides unique mechanical features for blood flow regulation. Disturbance in their physiology by vascular occlusion or damage of the vascular wall compromises circulation, depriving connected tissues from oxygen and nutrients. These events result in tissue hypoxia, a state in which there is not enough oxygen to maintain tissue homeostasis, leading to organ failure. Depending on the location of the lesion or occlusion, vascular pathologies can result in among others brain aneurysms, stroke, kidney failure and myocardial infarction (MI). Currently, vascular pathologies are the leading cause of death worldwide³.

The main function of the vascular system is to nourish all the tissues and organs in the human body. The blood flow in the human body starts at the arterial outlets of the heart, courses through the entire body and returns at the venous inlets of the heart. Nutrients and oxygen are delivered through the vascular system and metabolic byproducts and waste are removed⁴. To investigate underlying mechanisms of disease development, various *in vitro* models have been established that recapitulate the unique characteristics of blood vessels. In addition, regeneration of the vasculature gained great interest over the past years, aiming for solutions to restore tissue perfusion upon vascular damage or occlusion. To produce alternative vascular substitutes, both the natural composition and function of the vascular tissue of interest should be incorporated in the model.

In this thesis multiple aspects of the vasculature and vascular development are studied. By exploring vascular cells and their heterogenous properties in advanced three-dimensional (3D) models, the studies presented in this thesis provide insights in the possibilities for developing (patient-specific) disease models for therapeutic screening, and (pre-)vascularization strategies for regenerative medicine.

Arteries, Veins, and Capillaries: The Vascular Diversity

Vasculature is roughly classified into macro- and microvasculature. Macrovasculature includes arteries and veins, and microvasculature describes vessels with a diameter smaller than 150 μm including terminal arterioles, venules, and capillaries.

Blood vessels are, except for capillaries, all composed of three layers: (i) the tunica adventitia, the outer layer with elastic fibers and collagen, that provides structural support and maintains the shape of the vessel; (ii) the tunica media, the middle layer, composed of elastic and muscular tissue which regulates the vessel diameter; (iii) the tunica intima, the inner layer, composed of a monolayer of endothelial cells (ECs), providing a flat surface that is exposed to the blood flow. The amount and composition of extracellular matrix (ECM) components in each layer is dependent on vessel function and the tissue the vessel is providing for⁵. ECM is composed of two main classes of macromolecules: proteoglycans (PGs) and fibrous proteins. The main fibrous proteins include collagens, elastins, laminins and fibronectins⁶. PGs form a hydrated gel in the extracellular interstitial space, providing buffering, hydration and force-resistant properties to the ECM⁶. These components provide unique characteristics for different parts of the vasculature. For example, elastic arteries are generally composed of a more collagen-and-elastin-rich matrix compared to veins and smaller vessels^{7,8}.

Capillaries are responsible for the exchange of fluids and solutes between the intra- and extra-vascular compartments⁹. They are composed of a monolayer of ECs, supported by the basement membrane and a layer of mural cells, pericytes. Within the human body, three different types of capillaries are present. Continuous non-fenestrated capillaries are the most common, where both the endothelial monolayer and the basement membrane are continuous, only allowing small molecules (< 1 nm) to pass. Continuous fenestrated capillaries have small pores in the EC membrane, but an intact basement membrane, enabling rapid exchange of substances with a size of approximately 6-12 nm. These capillaries are present in the endocrine system, the kidneys, and the small intestines. Sinusoidal capillaries display gaps in both EC and basement membrane, allowing exchange of the largest molecules (>50

nm). Sinusoidal capillaries are present in the liver and the spleen¹⁰. Some regions within the capillary system are also involved in storage and the release of specific blood cells, located in the lungs, gut and liver¹¹.

Endothelial Cells: Key Players in Vascular Physiology

Vascular ECs originate in the mesoderm through vasculogenesis, as reviewed elsewhere¹²⁻¹⁴. ECs are polarized, with the luminal side directly exposed to blood cells and components and the basolateral side separated from surrounding tissues by a glycoprotein basement membrane. EC subtypes throughout the vascular system include arterial, venous, capillary, and lymphatic ECs. The various subtypes of ECs originate from mesodermal progenitor cells and undergo (hem-)angioblast differentiation. Numerous studies have explored the source of endothelial cells and the pathways through which they develop into various subtypes¹⁵. However, the precise differentiation pathways leading to distinct EC subtypes remain incompletely elucidated. It's unknown whether all ECs follow a uniform developmental pathway or if the emergence of EC subtypes is governed by lineage-restricted populations^{14, 16-18}.

The main functions of the endothelium include active control of vasoconstriction and vasodilation, innate immunity and exchange of solutes, fluids, hormones, and macromolecules between the intra- and extra-vascular compartments. ECs are actively involved in the suppression of the vascular smooth muscle cells (VSMCs) in the tunica media to avoid their outgrowth into the tunica intima layer¹⁹. ECs are interconnected either through tight junctions or adherent junctions in the intercellular clefts. The tight junctions between individual ECs facilitate transport and help to maintain cell polarity between the luminal and abluminal side of the ECs. Adherent junctions initiate and maintain cell-cell contact and interactions with surrounding cells²⁰. Most junctional markers are not unique expressed by ECs. These include platelet/endothelial cell adhesion molecule (PECAM)-1 (or CD31), which is e.g. also expressed in monocytes, and vascular endothelial (VE)-cadherin, which is expressed in ECs, but also in trophoblasts and fetal stem cells^{21, 22}. A combination of these markers is often used to characterize ECs and visualize the tight junctions in EC monolayers.

The structural heterogeneity of ECs was first identified via Electron Microscopy (EM) studies in the 1960's²³. A decade later, successful isolation and characterization of Human Umbilical Cord ECs (HUVECs) was reported^{24, 25}. While it is documented that distinct vascular segments exhibit variations in protein expression profiles^{26, 27}, the predominant choice in most *in vitro* investigations remains HUVECs. To study

endothelial interactions in health and disease, not only tissue specific ECs should be considered, but also the use of ECs in more advanced 3D cell culture setup, since ECs only partly maintain their phenotype in 2D culture *in vitro*^{28, 29}.

Vascular ECs are subject to various mechanical forces, including radial forces resulting from intravascular pressure, such as tangential forces occurring within the vessel wall due to the balance between cell-cell interactions and vasomotion, as well as axial shear forces arising from the friction between the flowing blood and the vessel wall. Under physiologic conditions, finely tuned equilibrium exists between endothelial-derived factors responsible for vasodilation and vasoconstriction, culminating in the preservation of vascular homeostasis³⁰. In addition to changes in cell morphology, ECs respond to defined flow stimuli with electrochemical activities and altered gene expression^{31, 32}. These include an increase of nitric oxide (NO) release when shear stress increases. This occurs by rapid endothelial NO synthase (eNOS) activation with upregulation of eNOS gene expression and the transcription activation of the eNOS promoter¹⁹. However, to maintain vascular stability and homeostasis, the support of mural cells is required.

Mural Cell Heterogeneity: Implications for Vascular Physiology

The endothelial monolayer is supported by a population of mural cells. In larger vessels including arteries, arterioles and veins, ECs receive structural support from VSMCs, which envelop the endothelial monolayer in multi-layered sheets. Their interactions stabilize the vessel and help regulate vessel contractility and tone^{33, 34}. In capillaries and post-capillary venules, ECs are supported by pericytes. They are present in a pericyte/EC ratio between 1:1 and 1:10, depending on their location. Pericytes are localized primarily along endothelial cell-cell junctions, branch points and in areas that need to maintain high levels of barrier function such as the blood-brain barrier (BBB)^{35, 36}. Platelet Derived Growth Factor BB (PDGFBB) – Platelet Derived Growth Factor Receptor Beta (PDGFR β) interactions are required to recruit both VSMCs and pericytes to vessels. PDGFBB is secreted by ECs and binds to the receptor on the mural cells³⁷. The origin of mural cells is rather heterogenous. Lineage tracing studies show that VSMCs in the head and nervous system appear to originate in the neural crest, while VSMCs in the gut, liver and lung have a mesothelial origin and differentiate into VSMCs via an epithelial to mesenchymal transition^{38, 39}. Pericytes arise either from the neural crest or the mesoderm, depending on their destined location^{39, 40}.

VSMCs show high plasticity, possessing multi differential capacities in response to different stimuli. This is beneficial in physiological conditions during vascular development, remodeling or replacement but can also lead to unexpected and unwanted phenotypic switches in response to disease. VSMCs express multiple phenotypes, roughly divided into contractile and synthetic. In mature arteries, VSMCs are mainly restricted to their contractile phenotype, allowing the vessel to contract and maintain its geometry while withstanding pressure. In smaller vessels, contractile VSMCs are responsible for the regulation of blood flow distribution by reducing and increasing the diameter of the vessels⁴¹. The contractility of VSMCs is regulated by active substances excreted by the ECs and triggered by an ionized calcium influx⁴². Contractile VSMCs are non-proliferative, non-migratory and produce little ECM. During vascular development in embryogenesis, angiogenesis and vasculogenesis, VSMCs acquire a synthetic phenotype. Synthetic VSMCs are highly proliferative, contribute to ECM production and migrate towards the newly formed endothelium to form a functional tunica media for the new vessel. Once the vessel is matured, the synthetic VSMCs switch back to their contractile state. *Visa versa*, following vascular injury, contractile VSMCs undergo a phenotypic transition to a synthetic state. This transition involves downregulation of gene expression associated with contractility, rearrangement of the cellular cytoskeleton, and a morphological shift from an elongated spindle-like shape to a flattened rhomboid configuration. Additionally, synthetic VSMCs exhibit increased proliferation rates and an increased secretion of matrix metalloproteinases (MMPs), which collectively contribute to extracellular matrix (ECM) remodeling and facilitate the process of vascular repair.

Within the context of vascular pathologies, the biological signals derived from vascular injury often cause VSMCs to stay in their proliferative synthetic state. Consequently, VSMCs overproduce MMPs, collagen, and elastin, leading to undesirable remodeling of the ECM within the vasculature. Vascular pathologies characterized by this detrimental ECM remodeling include atherosclerosis, hypertension-associated vascular remodeling, and restenosis following angioplasty or stent placement.

In vitro characterization of synthetic VSMCs based on gene expression patterns is complex. Certain investigations have reported elevated expression levels of specific markers such as osteopontin (OPN), MMP-9, epiregulin (EREG), and vimentin (VIM) in synthetic cells. However, these cells are typically characterized by the absence or reduced expression of contractile markers, including Smooth Muscle Actin Alpha (α SMA), Calponin, and Myosin Heavy Chain, as employed in their delineation⁴³⁻⁴⁵.

Multiple factors influence the phenotypic state of VSMCs in health and disease. Cytokines, growth factors, environmental stiffness and mechanical stress all contribute to their phenotypic state, as reviewed elsewhere⁴⁶. To this day, most studies have still relied on differentiated VSMCs with unclear embryonic origin, purity, or functional phenotype. This phenotypic heterogeneity poses a significant challenge in their application for human disease modeling as well as regenerative medicine. The successful replication of physiological function relies on the presence of contractile VSMCs, whereas in vascular diseases as well as tissue (re)generation, synthetic VSMCs play critical roles. This translates into a challenge for iPSC-derived VSMCs to accurately represent various disease conditions *in vitro* or express the desired cellular phenotypes in different phases of vascular tissue engineering. In **Chapter 5** of this thesis, we provide an in-depth exploration of various influencing factors that guide phenotypic transition in hiPSC-derived VSMCs.

Angiogenesis and Vasculogenesis: Building the Vascular Network

During embryonic development, the cardiovascular system emerges as the first functional organ system. Vascular cells also play a crucial role in imparting essential regulatory signals, that facilitate the development of various other tissue types, such as those found in the pancreas and the nervous system.⁴⁷⁻⁵¹ During embryonic development, the vascular system also plays a major role in lymph regulation, systemic function of the endocrine system, as well as immunological surveillance and inflammation. The process commonly referred to as “neovascularization”, describing the development of new blood vessels, can be categorized into two distinct mechanisms: angiogenesis and vasculogenesis. Angiogenesis is defined as sprouting from pre-existing blood vessels whereas vasculogenesis is *de novo* vessel formation from endothelial progenitor cells (EPCs), ECs or other stem cells.

Angiogenesis commences from specific subset of ECs known as “tip cells,” which initiate the process of angiogenic expansion within capillaries. These tip cells respond to the presence of vascular endothelial growth factor A (VEGFA) and orient themselves along a VEGFA gradient, facilitated by the interaction between VEGFA and its receptor, vascular endothelial growth factor receptor 2 (VEGFR2)⁵². Subsequently, in the migration phase, the interaction of VEGFA with VEGFR2 promotes the proliferation of ECs and induces the formation of vascular tubes, sprouting from the original vessel⁵³. In the concluding maturation stage, EC proliferation is inhibited whereas new capillaries migrate, with an emphasis on stabilizing the newly formed vascular tubes. This stabilization is facilitated by mural

cells, which can be either pericytes or VSMCs. The last stage, maturation, consists of inhibition of endothelial proliferation and migration of new capillaries to fuse with the pre-existing vascular network to facilitate blood perfusion.

The precise *in vivo* mechanisms driving vasculogenesis remains elusive. In quail embryos, blood island clusters within the embryonic yolk sac exhibit a configuration comprising of an outer layer of angioblasts that undergo differentiation into flattened ECs, enveloping an inner cluster of rounded primitive blood cells. Subsequently, these ECs sprout and connect to another blood island cluster to develop the vascular plexus⁵⁴⁻⁵⁷. In mice, a somewhat similar process is described, where primitive blood cells form a band wrapping around the proximal yolk sac. This interaction with angioblasts induces EC differentiation. Mature ECs subsequently wrap around the circulating blood cells, although the precise mechanism underlying this process remains to be fully elucidated⁵⁸. Studies involving human embryos have not been feasible for ethical reasons. Given the complexity of studying vasculogenesis *in vivo*, researchers have resorted to *in vitro* models as valuable tools for elucidating the underlying mechanisms. These models include both 2D and 3D cell cultures, co-culture studies and the use of (vascular) organoids.

Both vasculogenesis and angiogenesis play crucial roles in the maintenance of tissue homeostasis. Disruption of this balance can lead to various pathologies characterized by excessive development of new vessels. These pathologies include among others hypertension, cancer, and atherosclerosis⁵⁹⁻⁶¹. Defects in the angiogenesis mechanism, leading to excess or impaired vascular sprouting can cause brain ischemia, respiratory distress, neurodegeneration and osteoporosis⁶². The exploration of the mechanisms and molecular pathways governing both vasculogenesis and angiogenesis holds the promise of identifying novel therapeutic targets for addressing these vascular pathologies.

Vascular Replacement: Challenges and Innovations for Large Blood Vessels

Cardiovascular diseases (CVD) encompass a range of conditions including coronary artery disease (CAD), peripheral artery disease (PAD), myocardial infarction (MI), heart failure, and stroke, which collectively represent the leading cause of global mortality^{63,64}. These pathologies frequently co-occur with comorbidities including diabetes, hypertension, and depression. CAD, PAD, and MI are characterized by the irreversible damage to the affected blood vessels. Recent research efforts

have predominantly focused on establishing functionally perfusable vasculature within ischemic heart tissues, primarily through therapeutic neovascularization strategies^{65,66}.

The earliest vascular replacement surgery in 1906 used a patient's own vein segment to replace a diseased vessel⁶⁷. The long-term outcomes were suboptimal, prompting research into techniques for collection, processing and storage of suitable human grafts and the exploration into synthetic alternatives⁶⁷. Current clinical approaches for addressing CAD and PAD include angioplasty, stent placement, or surgical bypass grafting. In the context of surgical bypass grafting, autologous vessels with small diameters (<6 mm), such as the saphenous vein or the internal thoracic artery, are frequently used. While considered the gold standard, these autologous grafts require invasive harvesting procedures and may not always be suitable for vessel replacement upon explantation from the harvesting site. Additionally, the lifespan of venous grafts is limited due to high chances of intimal hyperplasia development, a pathological vascular remodeling resulting from the proliferation and migration of VSMCs into the tunica intima layer⁶⁸⁻⁷¹. Five years following surgical intervention, the average patency rates for venous grafts range between only 25% and 55%^{72,73}.

For larger vessels, synthetic polymers like Polytetrafluoroethylene (PTFE), Gore-Tex, and Dacron are used in surgical vascularization. However, these are not suitable for replacement of smaller diameter vessels due to the high risk of thrombotic occlusions⁷⁴⁻⁷⁶. Ongoing research explores the incorporation of living cells to stimulate physiological remodeling at graft anastomosis sites.

Adopting a tissue engineering approach, ideally utilizing autologous materials, offers the potential to design grafts tailored to specific target tissues and clinical needs. Scaffold-based approaches represent the most widespread strategy for tissue-engineered vascular graft (TEVG) development. The presence of physical support in a tubular structure facilitates cell behavior similar to the *in vivo* conditions. Synthetic polymers, already used in clinical applications, offer the advantage of tunable final properties to meet clinical requirements. However, challenges with synthetic materials include the lack of binding sites for invading cells and the necessity to ensure an anti-thrombogenic lumen. Tested polymers include predominantly biodegradable polyesters such as polyglycolic acid (PGA), poly-lactic acid (PLA), poly-L-lactic acid (PLLA) and polycaprolactone (PCL)⁷⁷. Bioabsorbable elastomers such as polyurethanes (PU) and Poly(glycerol-sebacate) (PGS) exhibit good biocompatibility, supporting EC proliferation on the luminal side and VSMC infiltration^{78,79}. A significant study in 1999 employed PGA grafts seeded with VSMCs,

demonstrating promising results in small and large animal models⁸⁰. This study ultimately led to clinical trials in patients with end-stage renal disease^{81, 82}. While initial results were encouraging, patency rates dropped to only 28% after one year, requiring interventions to restore graft patency. These reports indicate that further optimization of current synthetic grafts designs are desired.

One of the limitations of synthetic polymers is their lack of bioactivity. Consequently, natural polymers, primarily ECM-based, have been utilized to create vascular grafts. ECM-derived proteins maintain natural cellular binding sites, enhance material biocompatibility, and secrete factors to stimulate cellular colonization and proliferation. Commonly used natural polymers in tissue engineering include collagen, gelatin, elastin, and fibrin. Various techniques have been used to create vessel-like structures from these materials, including electrospinning⁸³, gel-based mold casting^{84, 85} and freeze drying^{86, 87}. While some studies have reported encouraging results with using natural polymers, they often exhibit reduced mechanical strength compared to synthetic alternatives and are susceptible to degradation, which may result in rupture and aneurysm formation post-implantation⁸⁸⁻⁹¹.

In vascular tissue engineering, the utilization of decellularized materials is also often employed to achieve a balance between structural stability and biological functionality. When derived from allogeneic or xenogeneic sources, decellularization is necessary to prevent an immunogenic response. Results of clinical studies reported various challenges associated with the immunogenicity and patency of decellularized grafts, but some studies have shown promising results with increased patency rates (up to 66.7% after 5 years)⁹²⁻⁹⁵. Hybrid approaches, combining synthetic and natural materials, offer another possibility to combine structural stability and biological activity. One example includes a PEG-fibrin hydrogel, where VSMC progenitors are mixed in with the gel supported by a layer of electrospun PU fibers⁹⁶. However, these methods often require extended culturing times and advanced bioreactors to mimic *in vivo* conditions for maturation of the construct.⁹⁷⁻⁹⁹

Microvascular Regeneration: From Concept to Clinical Implications

Successful upscaling of tissue-engineered constructs remains limited due to the diffusion limits of oxygen and nutrients, as well as waste removal by the surrounding vasculature. The generation of microvascular structures is therefore a critical component of tissue engineering. Three critical characteristics of functional

microvasculature *in vivo* encompass a hollow endothelialized lumen, a highly organized network structure and a complex signaling environment that dynamically regulates and drives vascular function¹⁰⁰.

Self-assembling TEVGs are the most popular option for construct pre-vascularization and (re-) generation of vascular structures. These approaches are based on the fundamental concept that, when placed within a 3D environment and exposed to appropriate stimuli, vascular cells possess the intrinsic capacity to self-organize into complex tissues. Several techniques have been explored in this context, including the use of cell-laden sheets that can be rolled into tubular structures, aggregation-based methods, where organoids or cell structures are developed within a 3D matrix, and bioprinting, which often involves mixing cells within a supporting scaffold material⁷⁷.

Within the scope of self-assembling strategies, organoids have attracted much scientific attention. Organoids are small, self-organizing tissue structures that replicate many of the developmental, structural, and functional properties of their full-sized counterparts¹⁰¹. The emergence of interest in combining tissue organoids with vascularization represents a significant advancement in the field of tissue engineering^{102, 103}. Various approaches have been explored, including the co-culturing of vascular cells with tissue specific cells, aiming at the formation of EC-based tubular structures within the organoids^{102, 104, 105}. In 2019, the first blood vessel organoids were generated, exhibiting characteristics of small vascular structures composed of ECs and vascular mural cells¹⁰⁴. Although EC tube formation is often successful in these protocols, *in vitro* perfusion and achieving vessel stability within these structures remains challenging. The implantation of these pre-vascularized structures, however, has shown promise in overcoming these challenges. Upon implantation, pre-vascularized structures often rapidly self-establish connections with the host vasculature, allowing for the perfusion of the preassembled vascular network and further maturation of the organoid or construct^{104, 106, 107}.

The technology of bioprinting is an additional promising tool for microvascular tissue engineering. Bioprinting techniques include extrusion-based bioprinting, lithographic printing and melt electro writing. These techniques fabricate 3D objects and structures in a layer-by-layer manner, either with or without the deposition of cells onto or within the printing material¹⁰⁸. One of the major advantages of these techniques is that they allow precise control over the location of placement, density, and ratio of cells within the biomaterial. However, challenges in this field include cell survival upon longer printing times for complex structures, ensuring proper vessel

formation and maturation, vessel stability upon implantation and the scalability in terms of time and costs for larger tissue constructs. An innovation in the 3D bioprinting techniques is the use of volumetric bioprinting. The printing procedure is inspired by computed tomography (CT) principles, facilitating the manufacturing of intricate objects through the use of dynamic 2D light fields. Volumetric bioprinting facilitates the rapid production of entire cell-laden constructs featuring arbitrary size and architectural complexity, typically achievable within a time frame spanning seconds to tens of seconds¹⁰⁹. This approach typically allows high cell survival rates during the crosslinking process. Nevertheless, a disadvantage of this technique is the lack of control of the placement of the cells during crosslinking. An alternative approach could involve seeding cells into a pre-printed construct, offering a potential solution.

In addition to printing vascular networks, 3D printing and casting are used to create microfluidic devices. A microfluidic device is composed of microchannels, chambers or other microstructures molded or printed onto a chip. These platforms can replicate the intricate architecture of microvasculature, facilitating the generation of tissue constructs that closely resemble *in vivo* conditions^{110, 111}. Researchers use microfluidic systems to investigate vascular dynamics, endothelial barrier function, and cellular interactions, shedding light on vascular pathologies like atherosclerosis and enabling the study of angiogenesis¹¹². Moreover, these devices accelerate drug screening, personalized medicine, and regenerative therapies by allowing controlled assessment of cellular responses within microvascular networks, thus holding great promise for the field of regenerative medicine.

Reprogramming for Regeneration: iPSCs and Vascular Tissue Engineering

In recent years, the application of induced pluripotent stem cells (iPSCs) in the field of tissue engineering has witnessed a remarkable expansion. Human iPSCs are generated through a reprogramming process from adult human cells such as skin fibroblasts, resulting in pluripotency. Pluripotency offers these cells the unique ability to differentiate into diverse cell types, similar to embryonic stem cells (ESCs). The first reprogramming of human cells to iPSCs in 2006 marked a significant milestone in regenerative medicine by offering an alternative to ESCs, bypassing ethical concerns surrounding the use of ESCs¹¹³. In the context of vascular tissue engineering, hiPSCs have the potential to create patient-specific applications. HiPSCs derived from individual patients embed the genetic background of the patients in the application. This personalized approach holds promise for enhancing the

fields of personalized drug screening and transplantation of personalized tissue-engineered constructs. Furthermore, the use of autologous material can significantly improve the rates of survival and overall success following implantation procedures.

Numerous protocols for differentiating hiPSCs into ECs and mural cells have been published in the past years^{114, 115}. Most protocols describe differentiation into a population of a single vascular cell type. The concept of hiPSC differentiation is based on understanding cellular differentiation in embryology. In the context of vascular ECs, their proliferation from mesodermal origins into ECs is mediated by the presence of VEGF and is modulated by microRNA-21 (Mir21) and transforming growth factor beta (TGF β). Early experimental approaches involved the co-culturing of ECs with stromal cells which are known to secrete these factors to facilitate EC differentiation. Nonetheless, this co-culture strategy yielded suboptimal outcomes in terms of both the quantity and diversity of resulting differentiated ECs¹¹⁶. In 2013, Rufaihah et al showed that BMP4 plays a crucial role in differentiating iPSCs into the mesoderm lineage¹¹⁷. This insight has been incorporated into more recent experimental procedures. Additionally, differentiation efficiency is dependent on the presence of growth factors as well as structural support of the culture. Structural support can include the use of ECM like gels using Fibrin, Matrigel, Collagen or synthetic alternatives¹¹⁸. In terms of structural heterogeneity between the different populations, hiPSC to EC differentiation protocols have so far aimed for differentiation towards arterial, lymphatic, and venous subtypes, marking a noteworthy advancement in this field^{117, 119, 120}.

Regarding VSMCs, the majority of hiPSC differentiation protocols typically result in VSMCs with a wide spectrum of phenotypic and developmental characteristics, ranging from synthetic to contractile. Although attempts to selectively enrich lineage-specific or contractile VSMCs from non-VSMCs have yielded some degree of success, a substantial portion of documented research studies have leaned upon differentiated VSMCs that lack clear delineation in terms of their embryonic origin, purity, maturation status, or functional phenotype¹¹⁵.

Pioneering work, primarily using murine and human ESCs, led to the first report by Taura et al. of generating mural cells (VSMCs and pericytes) from hiPSC lines¹²¹. Lee et al. established hiPSC lines derived from vascular somatic cells and successfully differentiated them into smooth muscle-like cells closely resembling human aortic VSMCs in terms of gene expression, epigenetics, and functional properties¹²². Following studies aimed to improve the differentiation and purification of hiPSC-derived VSMCs, resulting in various differentiation protocols yielding VSMCs

expressing ACTA2 at levels exceeding 90%¹²³⁻¹²⁵. These findings collectively represent significant progress in the field of VSMC differentiation, with ongoing efforts to enhance the quality and understanding of these cells.

Fully differentiated VSMCs exhibit a capacity for phenotype switching between their synthetic state and contractile phenotype. Research has demonstrated that this phenotypic switch can be regulated *in vitro* through the modulation of certain key factors. Specifically, cultivation with low serum levels and PDGF-BB deprivation leads to the development of a contractile SMC phenotype characterized by elevated MYH11 expression¹²⁶. These contractile VSMCs display distinct morphological, cytoskeletal, and functional features, including more condensed cell morphology, organized cytoskeletal proteins, active caveolae, and enhanced contractility¹²⁶⁻¹²⁹. Alternatively, high serum levels supplemented with PDGF-BB and TGF- β 1 induce the transition towards a synthetic phenotype, characterized by low MYH11 levels and increased extracellular matrix protein production¹²⁷. Researchers have used these defined VSMCs to engineer more elastic and functional vascular smooth muscle tissue constructs.

Recently, co-culture protocols aiming at the generation of both ECs and mural cells from one hiPSC source have been increasingly used. hiPSC derived early vascular cells can mature into both ECs and pericytes together in a codifferentiation protocol, facilitating both differentiation pathways¹³⁰. In an engineered synthetic hyaluronic acid (HA)-based hydrogel, this co-culture self-developed into a microvascular network that, upon implantation, integrates with host vasculature and establishing blood flow. In 2019, the first blood vessel organoids were characterized as 3D co-cultures composed of hiPSC-derived ECs and mural cells. These vascular organoids demonstrated the remarkable capacity to establish connections with the host's vascular network when implanted under the renal capsule of mice¹⁰⁴. Through the combination of precise hiPSC differentiation methods and sophisticated 3D models, it becomes feasible to create personalized disease models tailored to individual tissue regions. This development also holds significant promise for the future of vascular tissue engineering¹³¹.

Disease Modeling Approaches: From Cells to Systems

CAD or atherosclerosis is the most common form of CVD characterized by lipid accumulation and inflammation in the large arteries. Clinical complications include MI and stroke. Atherosclerotic plaques are characterized by the continual accumulation and alteration of lipids, inflammatory cells, smooth muscle cells and

necrotic cells within the inner layer of the vessel wall¹³². Lesion growth reduces blood flow and instable lesions can rupture, resulting in complete obstruction of the blood flow and induce MI or stroke, depending on the location of the clot.

Atherosclerosis mostly occurs in regions of arteries that exhibit turbulent blood flow, such as bifurcations. Disturbed blood flow can result in disturbance of the EC barrier, characterized by leaky tight junctions and therefore increased permeability of the EC monolayer. This promotes the uptake of plasma low-density lipoprotein (LDL) and triglyceride (TG) rich lipoproteins either by trans-endothelial transport or diffusion at the cell-cell junctions¹³³. Subsequent activation of the ECs in response to lipid oxidation promotes adhesion of monocytes, leukocytes, and other inflammatory mediators^{134, 135}. Following initiation, there is a progressive accumulation of lipids and foam cells, accompanied by the infiltration of other leukocytes, T cells particularly, into the atherosclerotic lesion, where they interact with macrophages. Over time, foam cells undergo apoptosis, leading to the development of necrotic cores characterized by cellular debris and cholesterol deposits. Simultaneously, VSMCs switch from their contractile to a proliferative state and migrate towards the subendothelial region, forming a protective “fibrous cap” that reinforces the structural integrity of the atherosclerotic lesion, limiting the risk of rupture. Lesions characterized by thick fibrous caps tend to exhibit greater stability. Several determinants impacting lesion stability have been identified, including the senescence of SMCs and ECs. Notably, macrophages are involved in the destabilization of atherosclerotic plaques by increasing inflammation and producing proteolytic enzymes that compromise the integrity of the fibrous cap¹³².

Atherosclerotic disease models mostly use rodents, as certain strains are known to develop atherosclerotic lesions when placed on high fat, high cholesterol diets. However, it is recognized that these models exhibit differences in various immune and mechanical facets when compared to the human condition, thereby limiting clinical translation^{136, 137}. *In vitro* atherosclerosis models include co-culture studies to study the interaction between vascular cells and other cells, as well as tissue engineered constructs to study vascular development and the influence of mechanic factors on developmental pathways¹³⁸⁻¹⁴¹. The use of microfluidic systems in *in vitro* atherosclerosis research opens possibilities for recreating physiologically relevant vessel anatomy by including flow dynamics in the system. The integration of such models in combination with patient-specific cell populations would give comprehensive insights into the onset and progress of atherosclerotic lesions, with the promising prospect of tailoring personalized therapeutic interventions.

Outline of this thesis

Current findings and developments in the vascular field highlight the heterogeneity and complexity of the vascular system, necessitating the creation of condition-specific options for vascular replacement or pre-vascularization strategies, as well as disease modeling. **In the first part of this thesis**, we focus on the generation and use of suitable vascular cells for tissue engineering purposes and disease modeling, using hiPSC-derived vascular organoids as the main source. We hypothesize that human iPSCs and iPSC-derived cells can be utilized for micro-and macrovascular regeneration strategies and disease modeling, in an application tailored approach. **In the second part of this thesis**, we explore the application of mechanical stimuli in advanced 3D models. Our aim is to construct models that closely replicate physiological conditions, providing a more nuanced understanding of the impact of mechanical stretch and shear stress on the onset and progression of vascular disease. **To conclude this thesis**, we strive to develop a Matrigel-free protocol for differentiating vascular organoids, thereby enhancing the clinical translatability of the utilized cell lines.

The first part of this thesis starts with **Chapter 2, Implementation of pericytes in vascular regeneration strategies**. Here the importance of using tissue specific cells for regenerative purposes is discussed in detail. The origin of pericytes is as heterogeneous and complex as their function and is defined in a tissue- and context specific manner. The importance of improving our understanding of this great variety in pericytes is highlighted by the ongoing interest in these cells within different research fields including basic vascular biology, and vascular contribution and response to disease in different organ systems. In this chapter, we provide an overview of the literature for graft (pre)-vascularization strategies and highlight the possible advantages of using tissue-specific pericytes for specific TE organ grafts.

In **Chapter 3, 3D Human iPSC Blood Vessel Organoids as a Source of Flow-Adaptive Vascular Cells for Creating a Human-Relevant 3D-Scaffold Based Macrovascular Model**, the suitability of human iPSC organoid-derived vascular cells for TE on synthetic scaffolds is described. While human and animal studies have advanced our understanding of CVD mechanisms, the complex interplay of dynamic factors *in vivo* provides limits to in dept causality studies. Human-focused *in vitro* vascular models, often combining cells and biomaterial scaffolds, offer controlled simulations for studying disease and tissue behavior in an *in vitro* biomimetic

environment. In this chapter, we differentiated, validated and used two distinct vascular cell populations from hiPSC-derived vascular organoids; organoid derived endothelial cells (ODECs) and organoid-derived mural cells (ODMCs).

In depth validation of the ODECs was conducted and described in chapter 3, whereas in **Chapter 4, Manipulating human iPSC-derived endothelial cells to emulate fenestrated vasculature: A new method for the induction and regulation of fenestrations**, the capacity of ODECs to adapt different endothelial cell phenotypes was evaluated. Considerable endothelial heterogeneity exists across the vascular system, necessitating the capability to differentiate tissue-specific cells originating from the same (donor) source. For the first time, we here investigated the capacity of hiPSC-derived ECs to adapt a fenestrated phenotype by using the stimulation of growth factors in a 2D culture system.

In **Chapter 5, Induce and control the phenotypic switch in iPSC derived Vascular Smooth Muscle Cells in a 3D hydrogel**, the ODMCs were compared to aortic VSMCs to study their capacity to undergo the phenotypic switch. Understanding disease processes in vascular biology is crucial for developing targeted therapies and regenerative strategies. However, challenges in replicating physiological functions with hiPSC-derived VSMCs underscore the need for a deeper understanding of environmental factors shaping cell phenotypes. In this chapter we assessed the effect of growth factors, hydrogel stiffness and cyclic strain on the phenotype of both VSMCs and ODMCs.

In the second part of this thesis, we continue to investigate the impact of mechanical forces on vascular (re)modeling are discussed in **Chapter 6, Contributions of Wall Stretch and Shear Stress to Vascular Regulation: Molecular Mechanisms of Homeostasis and Expansion**. The incorporation of mechanical stimuli is crucial for replicating the physiological conditions in the blood vessels, as well as to provide clues to guide vascular adaptation (as shown e.g. in **chapter 5**). **Chapter 6** summarizes the impact of mechanical factors in both angiogenesis as vasculogenesis, focusing on various activation pathways by mechanosensors, which transduce mechanical stimuli into a vascular regulatory responses.

Studying vascular pathologies *in vitro* is challenging because of the complexity of the disease (development) and interacting factors from surrounding tissues. Using a microfluidic chip, we created an atherosclerosis-on-a-chip model, described in **Chapter 7; A complex three-dimensional microfluidic model that mimics the early-stage events in the human atherosclerotic artery**. Traditionally explored

through rodent models and two- or three-dimensional human cell cultures, recent progress in microfluidic technology holds promise for studying atherosclerosis in *in vitro* human cell microfluidic systems. These advancements introduce crucial flow dynamics, such as shear stress, and help bridge the gap between large-scale bioreactors and more cost-effective chip-format assays. The system described in **chapter 7** provides an advanced platform for 3D studies of vascular cell/immune cell interactions in early-stage atherosclerosis. This novel microfluidics model also provides live-confocal imaging with side-to-side comparison of healthy human macrovessels with atherosclerotic vessels, offering a humanized platform for more in-depth mechanistic studies and drug testing.

In vitro (bio)medical research animal (by)products are often used for cell culture. In 3D cell culture, the most used natural hydrogel is Matrigel, which was also used in the original vascular organoid differentiation protocol¹⁰⁴. Since Matrigel is derived from carcinogenic mouse tissue and the composition of the gel is batch dependent, it's not suitable for regenerative purposes and transplantation of tissue engineered constructs. To conclude this thesis, we developed a new protocol to replace the Matrigel in the original vascular organoid differentiation protocol, described in **Chapter 8; Animal-free alternatives for Matrigel in hiPSC-derived blood vessel organoid culture**. By replacing Matrigel with vitronectin (hiPSC coating) and fibrin gel (3D organoid culture), we are working towards a Matrigel-free organoid culture. This will be beneficial for future regenerative therapies and transplantable cell- or organoid-based constructs. In **Chapter 9**, the main findings of this thesis are highlighted and discussed in the context of the application of hiPSC derived cells in vascular regeneration and vascular disease modeling.

References

1. Heller M, Bauer HK, Schwab R, et al. The impact of intercellular communication for the generation of complex multicellular prevascularized tissue equivalents. *J Biomed Mater Res A*. 2020;108(3):734-48.
2. Colton CK. Implantable biohybrid artificial organs. *Cell Transplant*. 1995;4(4):415-36.
3. Mathers CD, Loncar D. Projections of global mortality and burden of disease from 2002 to 2030. *PLoS Med*. 2006;3(11):e442.
4. Herman IP. *Physics of the human body*: Springer; 2016.
5. Tennant M, McGeachie JK. Blood vessel structure and function: a brief update on recent advances. *Aust N Z J Surg*. 1990;60(10):747-53.
6. Frantz C, Stewart KM, Weaver VM. The extracellular matrix at a glance. *J Cell Sci*. 2010;123(Pt 24):4195-200.
7. Hu M, Ling Z, Ren X. Extracellular matrix dynamics: tracking in biological systems and their implications. *J Biol Eng*. 2022;16(1):13.
8. Bou-Gharios G, Ponticos M, Rajkumar V, et al. Extra-cellular matrix in vascular networks. *Cell Prolif*. 2004;37(3):207-20.
9. Michel CC, Curry FE. Microvascular permeability. *Physiol Rev*. 1999;79(3):703-61.
10. Sarin H. Physiologic upper limits of pore size of different blood capillary types and another perspective on the dual pore theory of microvascular permeability. *J Angiogenesis Res*. 2010;2:14.
11. Kruger-Genge A, Blocki A, Franke RP, et al. Vascular Endothelial Cell Biology: An Update. *Int J Mol Sci*. 2019;20(18).
12. Tavian M, Cortes F, Robin C, et al. [The hemangioblast, common precursor of endothelial and hematopoietic cells]. *Transfus Clin Biol*. 2000;7(3):238-41.
13. Augustin HG, Kozian DH, Johnson RC. Differentiation of endothelial cells: analysis of the constitutive and activated endothelial cell phenotypes. *Bioessays*. 1994;16(12):901-6.
14. De Val S, Black BL. Transcriptional control of endothelial cell development. *Dev Cell*. 2009;16(2):180-95.
15. Aquino JB, Sierra R, Montaldo LA. Diverse cellular origins of adult blood vascular endothelial cells. *Dev Biol*. 2021;477:117-32.
16. Coultas L, Chawengsakophak K, Rossant J. Endothelial cells and VEGF in vascular development. *Nature*. 2005;438(7070):937-45.
17. Risau W, Flamme I. Vasculogenesis. *Annu Rev Cell Dev Biol*. 1995;11:73-91.
18. Vogeli KM, Jin SW, Martin GR, et al. A common progenitor for haematopoietic and endothelial lineages in the zebrafish gastrula. *Nature*. 2006;443(7109):337-9.
19. Mehta D, Malik AB. Signaling mechanisms regulating endothelial permeability. *Physiol Rev*. 2006;86(1):279-367.
20. Aird WC. Phenotypic heterogeneity of the endothelium: I. Structure, function, and mechanisms. *Circ Res*. 2007;100(2):158-73.
21. Garlanda C, Dejana E. Heterogeneity of endothelial cells. Specific markers. *Arterioscler Thromb Vasc Biol*. 1997;17(7):1193-202.
22. Aird WC. Spatial and temporal dynamics of the endothelium. *J Thromb Haemost*. 2005;3(7):1392-406.

23. Weibel ER, Palade GE. New Cytoplasmic Components in Arterial Endothelia. *J Cell Biol.* 1964;23(1):101-12.
24. Jaffe EA, Hoyer LW, Nachman RL. Synthesis of antihemophilic factor antigen by cultured human endothelial cells. *J Clin Invest.* 1973;52(11):2757-64.
25. Gimbrone MA, Jr., Cotran RS, Folkman J. Human vascular endothelial cells in culture. Growth and DNA synthesis. *J Cell Biol.* 1974;60(3):673-84.
26. Kumar S, West DC, Ager A. Heterogeneity in endothelial cells from large vessels and microvessels. *Differentiation.* 1987;36(1):57-70.
27. Page C, Rose M, Yacoub M, et al. Antigenic heterogeneity of vascular endothelium. *Am J Pathol.* 1992;141(3):673-83.
28. Unger RE, Krump-Konvalinkova V, Peters K, et al. In vitro expression of the endothelial phenotype: comparative study of primary isolated cells and cell lines, including the novel cell line HPMEC-ST1.6R. *Microvasc Res.* 2002;64(3):384-97.
29. Majewska A, Wilkus K, Brodaczewska K, et al. Endothelial Cells as Tools to Model Tissue Microenvironment in Hypoxia-Dependent Pathologies. *Int J Mol Sci.* 2021;22(2).
30. Tesauro M, Cardillo C. Obesity, blood vessels and metabolic syndrome. *Acta Physiol (Oxf).* 2011;203(1):279-86.
31. Resnick N, Gimbrone MA, Jr. Hemodynamic forces are complex regulators of endothelial gene expression. *FASEB J.* 1995;9(10):874-82.
32. Reinhart WH. Shear-dependence of endothelial functions. *Experientia.* 1994;50(2):87-93.
33. Owens GK. Regulation of differentiation of vascular smooth muscle cells. *Physiol Rev.* 1995;75(3):487-517.
34. Abraham S, Kogata N, Fassler R, et al. Integrin beta1 subunit controls mural cell adhesion, spreading, and blood vessel wall stability. *Circ Res.* 2008;102(5):562-70.
35. Ando K, Fukuhara S, Izumi N, et al. Clarification of mural cell coverage of vascular endothelial cells by live imaging of zebrafish. *Development.* 2016;143(8):1328-39.
36. Bergers G, Song S. The role of pericytes in blood-vessel formation and maintenance. *Neuro Oncol.* 2005;7(4):452-64.
37. Smyth LCD, Rustenhoven J, Park TI, et al. Unique and shared inflammatory profiles of human brain endothelia and pericytes. *J Neuroinflammation.* 2018;15(1):138.
38. Majesky MW. Developmental basis of vascular smooth muscle diversity. *Arterioscler Thromb Vasc Biol.* 2007;27(6):1248-58.
39. Pouget C, Pottin K, Jaffredo T. Sclerotomal origin of vascular smooth muscle cells and pericytes in the embryo. *Dev Biol.* 2008;315(2):437-47.
40. Armulik A, Genove G, Betsholtz C. Pericytes: developmental, physiological, and pathological perspectives, problems, and promises. *Dev Cell.* 2011;21(2):193-215.
41. Christensen KL, Mulvany MJ. Location of resistance arteries. *J Vasc Res.* 2001;38(1):1-12.
42. Kim HR, Appel S, Vetterkind S, et al. Smooth muscle signalling pathways in health and disease. *J Cell Mol Med.* 2008;12(6A):2165-80.
43. Zhao D, Li J, Xue C, et al. TL1A inhibits atherosclerosis in apoE-deficient mice by regulating the phenotype of vascular smooth muscle cells. *J Biol Chem.* 2020;295(48):16314-27.
44. Tierney JW, Evans BC, Cheung-Flynn J, et al. Therapeutic MK2 inhibition blocks pathological vascular smooth muscle cell phenotype switch. *JCI Insight.* 2021;6(19).
45. Owens GK, Kumar MS, Wamhoff BR. Molecular regulation of vascular smooth muscle cell differentiation in development and disease. *Physiol Rev.* 2004;84(3):767-801.

46. Cao G, Xuan X, Hu J, et al. How vascular smooth muscle cell phenotype switching contributes to vascular disease. *Cell Commun Signal*. 2022;20(1):180.
47. Yebra M, Diaferia GR, Montgomery AM, et al. Endothelium-derived Netrin-4 supports pancreatic epithelial cell adhesion and differentiation through integrins alpha2beta1 and alpha3beta1. *PLoS One*. 2011;6(7):e22750.
48. Weinstein BM. Vessels and nerves: marching to the same tune. *Cell*. 2005;120(3):299-302.
49. Magenheim J, Ilovich O, Lazarus A, et al. Blood vessels restrain pancreas branching, differentiation and growth. *Development*. 2011;138(21):4743-52.
50. Serini G, Bussolino F. Common cues in vascular and axon guidance. *Physiology (Bethesda)*. 2004;19:348-54.
51. Honma Y, Araki T, Gianino S, et al. Artemin is a vascular-derived neurotropic factor for developing sympathetic neurons. *Neuron*. 2002;35(2):267-82.
52. Liu ZJ, Shirakawa T, Li Y, et al. Regulation of Notch1 and Dll4 by vascular endothelial growth factor in arterial endothelial cells: implications for modulating arteriogenesis and angiogenesis. *Mol Cell Biol*. 2003;23(1):14-25.
53. Gerhardt H, Golding M, Fruttiger M, et al. VEGF guides angiogenic sprouting utilizing endothelial tip cell filopodia. *J Cell Biol*. 2003;161(6):1163-77.
54. Pardanaud L, Altmann C, Kitos P, et al. Vasculogenesis in the early quail blastodisc as studied with a monoclonal antibody recognizing endothelial cells. *Development*. 1987;100(2):339-49.
55. Drake CJ. Embryonic and adult vasculogenesis. *Birth Defects Res C Embryo Today*. 2003;69(1):73-82.
56. Sabin FR. Preliminary note on the differentiation of angioblasts and the method by which they produce blood-vessels, blood-plasma and red blood-cells as seen in the living chick. 1917. *J Hematother Stem Cell Res*. 2002;11(1):5-7.
57. Moore MA, Metcalf D. Ontogeny of the haemopoietic system: yolk sac origin of in vivo and in vitro colony forming cells in the developing mouse embryo. *Br J Haematol*. 1970;18(3):279-96.
58. Ferkowicz MJ, Yoder MC. Blood island formation: longstanding observations and modern interpretations. *Exp Hematol*. 2005;33(9):1041-7.
59. Zarei M, Khazaei M, Sharifi MR, et al. Coronary angiogenesis during experimental hypertension: is it reversible? *J Res Med Sci*. 2011;16(3):269-75.
60. Papetti M, Herman IM. Mechanisms of normal and tumor-derived angiogenesis. *Am J Physiol Cell Physiol*. 2002;282(5):C947-70.
61. Costa PZ, Soares R. Neovascularization in diabetes and its complications. Unraveling the angiogenic paradox. *Life Sci*. 2013;92(22):1037-45.
62. Carmeliet P. Angiogenesis in life, disease and medicine. *Nature*. 2005;438(7070):932-6.
63. Metra M, Zaca V, Parati G, et al. Cardiovascular and noncardiovascular comorbidities in patients with chronic heart failure. *J Cardiovasc Med (Hagerstown)*. 2011;12(2):76-84.
64. Group WCRCW. World Health Organization cardiovascular disease risk charts: revised models to estimate risk in 21 global regions. *Lancet Glob Health*. 2019;7(10):e1332-e45.
65. Clayton ZE, Sadeghipour S, Patel S. Generating induced pluripotent stem cell derived endothelial cells and induced endothelial cells for cardiovascular disease modelling and therapeutic angiogenesis. *Int J Cardiol*. 2015;197:116-22.

66. Kim H, Park SJ, Park JH, et al. Enhancement strategy for effective vascular regeneration following myocardial infarction through a dual stem cell approach. *Exp Mol Med*. 2022;54(8):1165-78.
67. Guevara-Noriega KA, Martinez-Toiran A, Alvarez-Concejo B, et al. Historical overview of vascular allografts transplantation. *Vasc Endovasc Rev*. 2019;2:19-22.
68. Goldman S, Zadina K, Moritz T, et al. Long-term patency of saphenous vein and left internal mammary artery grafts after coronary artery bypass surgery: results from a Department of Veterans Affairs Cooperative Study. *J Am Coll Cardiol*. 2004;44(11):2149-56.
69. van Dijk D, Spoor M, Hijman R, et al. Cognitive and cardiac outcomes 5 years after off-pump vs on-pump coronary artery bypass graft surgery. *JAMA*. 2007;297(7):701-8.
70. Collins P, Webb CM, Chong CF, et al. Radial artery versus saphenous vein patency randomized trial: five-year angiographic follow-up. *Circulation*. 2008;117(22):2859-64.
71. Kim KB, Cho KR, Jeong DS. Midterm angiographic follow-up after off-pump coronary artery bypass: serial comparison using early, 1-year, and 5-year postoperative angiograms. *J Thorac Cardiovasc Surg*. 2008;135(2):300-7.
72. Belkin M, Knox J, Donaldson MC, et al. Infrainguinal arterial reconstruction with nonreversed greater saphenous vein. *J Vasc Surg*. 1996;24(6):957-62.
73. Sayers RD, Raptis S, Berce M, et al. Long-term results of femorotibial bypass with vein or polytetrafluoroethylene. *Br J Surg*. 1998;85(7):934-8.
74. Takagi H, Goto SN, Matsui M, et al. A contemporary meta-analysis of Dacron versus polytetrafluoroethylene grafts for femoropopliteal bypass grafting. *J Vasc Surg*. 2010;52(1):232-6.
75. Jackson MR, Belott TP, Dickason T, et al. The consequences of a failed femoropopliteal bypass grafting: comparison of saphenous vein and PTFE grafts. *J Vasc Surg*. 2000;32(3):498-504; -5.
76. van Det RJ, Vriens BH, van der Palen J, et al. Dacron or ePTFE for femoro-popliteal above-knee bypass grafting: short- and long-term results of a multicentre randomised trial. *Eur J Vasc Endovasc Surg*. 2009;37(4):457-63.
77. Carrabba M, Madeddu P. Current Strategies for the Manufacture of Small Size Tissue Engineering Vascular Grafts. *Front Bioeng Biotechnol*. 2018;6:41.
78. Gao J, Crapo PM, Wang Y. Macroporous elastomeric scaffolds with extensive micropores for soft tissue engineering. *Tissue Eng*. 2006;12(4):917-25.
79. Rai R, Tallawi M, Grigore A, et al. Synthesis, properties and biomedical applications of poly (glycerol sebacate)(PGS): A review. *Progress in polymer science*. 2012;37(8):1051-78.
80. Niklason LE, Gao J, Abbott WM, et al. Functional arteries grown in vitro. *Science*. 1999;284(5413):489-93.
81. Gui L, Niklason LE. Vascular Tissue Engineering: Building Perfusable Vasculature for Implantation. *Curr Opin Chem Eng*. 2014;3:68-74.
82. Lawson JH, Glickman MH, Ilzecki M, et al. Bioengineered human acellular vessels for dialysis access in patients with end-stage renal disease: two phase 2 single-arm trials. *Lancet*. 2016;387(10032):2026-34.
83. Soffer L, Wang X, Zhang X, et al. Silk-based electrospun tubular scaffolds for tissue-engineered vascular grafts. *J Biomater Sci Polym Ed*. 2008;19(5):653-64.

84. Boccafoschi F, Rajan N, Habermehl J, et al. Preparation and characterization of a scaffold for vascular tissue engineering by direct-assembling of collagen and cells in a cylindrical geometry. *Macromol Biosci.* 2007;7(5):719-26.
85. Schutte SC, Chen Z, Brockbank KG, et al. Cyclic strain improves strength and function of a collagen-based tissue-engineered vascular media. *Tissue Eng Part A.* 2010;16(10):3149-57.
86. Engbers-Buijtenhuijs P, Buttafoco L, Poot AA, et al. Biological characterisation of vascular grafts cultured in a bioreactor. *Biomaterials.* 2006;27(11):2390-7.
87. Zhang L, Ao Q, Wang A, et al. A sandwich tubular scaffold derived from chitosan for blood vessel tissue engineering. *J Biomed Mater Res A.* 2006;77(2):277-84.
88. Swartz DD, Russell JA, Andreadis ST. Engineering of fibrin-based functional and implantable small-diameter blood vessels. *Am J Physiol Heart Circ Physiol.* 2005;288(3):H1451-60.
89. Huynh TN, Tranquillo RT. Fusion of concentrically layered tubular tissue constructs increases burst strength. *Ann Biomed Eng.* 2010;38(6):2226-36.
90. Lovett M, Eng G, Kluge JA, et al. Tubular silk scaffolds for small diameter vascular grafts. *Organogenesis.* 2010;6(4):217-24.
91. Li X, Xu J, Nicolescu CT, et al. Generation, Endothelialization, and Microsurgical Suture Anastomosis of Strong 1-mm-Diameter Collagen Tubes. *Tissue Eng Part A.* 2017;23(7-8):335-44.
92. Katzman HE, Glickman MH, Schild AF, et al. Multicenter evaluation of the bovine mesenteric vein bioprostheses for hemodialysis access in patients with an earlier failed prosthetic graft. *J Am Coll Surg.* 2005;201(2):223-30.
93. Chemla ES, Morsy M. Randomized clinical trial comparing decellularized bovine ureter with expanded polytetrafluoroethylene for vascular access. *Br J Surg.* 2009;96(1):34-9.
94. Lindsey P, Echeverria A, Cheung M, et al. Lower Extremity Bypass Using Bovine Carotid Artery Graft (Artegraft): An Analysis of 124 Cases with Long-Term Results. *World J Surg.* 2018;42(1):295-301.
95. Olausson M, Patil PB, Kuna VK, et al. Transplantation of an allogeneic vein bioengineered with autologous stem cells: a proof-of-concept study. *Lancet.* 2012;380(9838):230-7.
96. McMahon RE, Qu X, Jimenez-Vergara AC, et al. Hydrogel-electrospun mesh composites for coronary artery bypass grafts. *Tissue Eng Part C Methods.* 2011;17(4):451-61.
97. Zhao J, Qiu H, Chen DL, et al. Development of nanofibrous scaffolds for vascular tissue engineering. *Int J Biol Macromol.* 2013;56:106-13.
98. Gong W, Lei D, Li S, et al. Hybrid small-diameter vascular grafts: Anti-expansion effect of electrospun poly epsilon-caprolactone on heparin-coated decellularized matrices. *Biomaterials.* 2016;76:359-70.
99. Koch S, Flanagan TC, Sachweh JS, et al. Fibrin-poly lactide-based tissue-engineered vascular graft in the arterial circulation. *Biomaterials.* 2010;31(17):4731-9.
100. Seymour AJ, Westerfield AD, Cornelius VC, et al. Bioprinted microvasculature: progressing from structure to function. *Biofabrication.* 2022;14(2).
101. Clevers H. Modeling Development and Disease with Organoids. *Cell.* 2016;165(7):1586-97.
102. Zhang S, Wan Z, Kamm RD. Vascularized organoids on a chip: strategies for engineering organoids with functional vasculature. *Lab Chip.* 2021;21(3):473-88.

103. Azizoglu DB, Cleaver O. Blood vessel crosstalk during organogenesis-focus on pancreas and endothelial cells. *Wiley Interdiscip Rev Dev Biol.* 2016;5(5):598-617.
104. Wimmer RA, Leopoldi A, Aichinger M, et al. Human blood vessel organoids as a model of diabetic vasculopathy. *Nature.* 2019;565(7740):505-10.
105. Takasato M, Er PX, Chiu HS, et al. Kidney organoids from human iPSCs contain multiple lineages and model human nephrogenesis. *Nature.* 2016;536(7615):238.
106. Takebe T, Sekine K, Enomura M, et al. Vascularized and functional human liver from an iPSC-derived organ bud transplant. *Nature.* 2013;499(7459):481-4.
107. Mansour AA, Goncalves JT, Bloyd CW, et al. An in vivo model of functional and vascularized human brain organoids. *Nat Biotechnol.* 2018;36(5):432-41.
108. Moroni L, Boland T, Burdick JA, et al. Biofabrication: A Guide to Technology and Terminology. *Trends Biotechnol.* 2018;36(4):384-402.
109. Bernal PN, Delrot P, Loterie D, et al. Volumetric Bioprinting of Complex Living-Tissue Constructs within Seconds. *Adv Mater.* 2019;31(42):e1904209.
110. Wang X, Sun Q, Pei J. Microfluidic-Based 3D Engineered Microvascular Networks and Their Applications in Vascularized Microtumor Models. *Micromachines (Basel).* 2018;9(10).
111. Prabhakarparndian B, Shen MC, Pant K, et al. Microfluidic devices for modeling cell-cell and particle-cell interactions in the microvasculature. *Microvasc Res.* 2011;82(3):210-20.
112. van Dijk CGM, Brandt MM, Poulis N, et al. A new microfluidic model that allows monitoring of complex vascular structures and cell interactions in a 3D biological matrix. *Lab Chip.* 2020;20(10):1827-44.
113. Takahashi K, Yamanaka S. Induction of pluripotent stem cells from mouse embryonic and adult fibroblast cultures by defined factors. *Cell.* 2006;126(4):663-76.
114. Jang S, Collin de l'Hortet A, Soto-Gutierrez A. Induced Pluripotent Stem Cell-Derived Endothelial Cells: Overview, Current Advances, Applications, and Future Directions. *Am J Pathol.* 2019;189(3):502-12.
115. Stephenson M, Reich DH, Boheler KR. Induced pluripotent stem cell-derived vascular smooth muscle cells. *Vasc Biol.* 2020;2(1):R1-R15.
116. Choi KD, Yu J, Smuga-Otto K, et al. Hematopoietic and endothelial differentiation of human induced pluripotent stem cells. *Stem Cells.* 2009;27(3):559-67.
117. Rufaihah AJ, Huang NF, Kim J, et al. Human induced pluripotent stem cell-derived endothelial cells exhibit functional heterogeneity. *Am J Transl Res.* 2013;5(1):21-35.
118. Zhang S, Dutton JR, Su L, et al. The influence of a spatiotemporal 3D environment on endothelial cell differentiation of human induced pluripotent stem cells. *Biomaterials.* 2014;35(12):3786-93.
119. Katt ME, Linville RM, Mayo LN, et al. Functional brain-specific microvessels from iPSC-derived human brain microvascular endothelial cells: the role of matrix composition on monolayer formation. *Fluids Barriers CNS.* 2018;15(1):7.
120. Giacomelli E, Bellin M, Sala L, et al. Three-dimensional cardiac microtissues composed of cardiomyocytes and endothelial cells co-differentiated from human pluripotent stem cells. *Development.* 2017;144(6):1008-17.
121. Taura D, Sone M, Homma K, et al. Induction and isolation of vascular cells from human induced pluripotent stem cells--brief report. *Arterioscler Thromb Vasc Biol.* 2009;29(7):1100-3.

122. Lee TH, Song SH, Kim KL, et al. Functional recapitulation of smooth muscle cells via induced pluripotent stem cells from human aortic smooth muscle cells. *Circ Res.* 2010;106(1):120-8.
123. Lin B, Kim J, Li Y, et al. High-purity enrichment of functional cardiovascular cells from human iPS cells. *Cardiovasc Res.* 2012;95(3):327-35.
124. Ge X, Ren Y, Bartulos O, et al. Modeling supra-avalvular aortic stenosis syndrome with human induced pluripotent stem cells. *Circulation.* 2012;126(14):1695-704.
125. Yang L, Geng Z, Nickel T, et al. Differentiation of Human Induced-Pluripotent Stem Cells into Smooth-Muscle Cells: Two Novel Protocols. *PLoS One.* 2016;11(1):e0147155.
126. Wanjare M, Kuo F, Gerecht S. Derivation and maturation of synthetic and contractile vascular smooth muscle cells from human pluripotent stem cells. *Cardiovasc Res.* 2013;97(2):321-30.
127. Eoh JH, Shen N, Burke JA, et al. Enhanced elastin synthesis and maturation in human vascular smooth muscle tissue derived from induced-pluripotent stem cells. *Acta Biomater.* 2017;52:49-59.
128. Wanjare M, Kusuma S, Gerecht S. Perivascular cells in blood vessel regeneration. *Biotechnol J.* 2013;8(4):434-47.
129. Wanjare M, Kusuma S, Gerecht S. Defining differences among perivascular cells derived from human pluripotent stem cells. *Stem Cell Reports.* 2014;2(5):561-75.
130. Kusuma S, Facklam A, Gerecht S. Characterizing human pluripotent-stem-cell-derived vascular cells for tissue engineering applications. *Stem Cells Dev.* 2015;24(4):451-8.
131. Sundaram S, One J, Siewert J, et al. Tissue-engineered vascular grafts created from human induced pluripotent stem cells. *Stem Cells Transl Med.* 2014;3(12):1535-43.
132. Bjorkegren JLM, Lusic AJ. Atherosclerosis: Recent developments. *Cell.* 2022;185(10):1630-45.
133. Zhang X, Sessa WC, Fernandez-Hernando C. Endothelial Transcytosis of Lipoproteins in Atherosclerosis. *Front Cardiovasc Med.* 2018;5:130.
134. Michel JB, Martin-Ventura JL, Nicoletti A, et al. Pathology of human plaque vulnerability: mechanisms and consequences of intraplaque haemorrhages. *Atherosclerosis.* 2014;234(2):311-9.
135. Xu J, Shi GP. Vascular wall extracellular matrix proteins and vascular diseases. *Biochim Biophys Acta.* 2014;1842(11):2106-19.
136. Emini Veseli B, Perrotta P, De Meyer GRA, et al. Animal models of atherosclerosis. *Eur J Pharmacol.* 2017;816:3-13.
137. Getz GS, Reardon CA. Animal models of atherosclerosis. *Arterioscler Thromb Vasc Biol.* 2012;32(5):1104-15.
138. Chen J, Zhang X, Millican R, et al. Recent Progress in in vitro Models for Atherosclerosis Studies. *Front Cardiovasc Med.* 2021;8:790529.
139. Dorweiler B, Torzewski M, Dahm M, et al. A novel in vitro model for the study of plaque development in atherosclerosis. *Thromb Haemost.* 2006;95(1):182-9.
140. Robert J, Weber B, Frese L, et al. A three-dimensional engineered artery model for in vitro atherosclerosis research. *PLoS One.* 2013;8(11):e79821.
141. Wada Y, Sugiyama A, Kohro T, et al. In vitro model of atherosclerosis using coculture of arterial wall cells and macrophage. *Yonsei Med J.* 2000;41(6):740-55.

PART 1

CHAPTER

2



Implementation of pericytes in vascular regeneration strategies

Elana M. Meijer, Christian G.M. van Dijk, Rafael Kramann, Marianne C. Verhaar,
Caroline Cheng

Tissue Engineering Part B: Reviews, 2022 28(1), 1-21.

Abstract

For the survival and integration of complex large-sized tissue engineered (TE) organ constructs that exceed the maximal nutrients and oxygen diffusion distance required for cell survival, graft (pre-)vascularization to ensure medium or blood supply is crucial. To achieve this, the morphology and functionality of the micro-capillary bed should be mimicked by incorporating vascular cell populations including endothelium and mural cells. Pericytes play a crucial role in microvascular function, blood vessel stability, angiogenesis and blood pressure regulation. In addition, tissue-specific pericytes are important in maintaining specific functions in different organs, including vitamin A storage in the liver, renin production in the kidneys and maintenance of the Blood-Brain-Barrier (BBB). Together with their multipotential differentiation capacity, this makes pericytes the preferred cell type for application in TE grafts. The use of a tissue-specific pericyte cell population that matches the TE organ may benefit organ function. In this review we provide an overview of the literature for graft (pre-)vascularization strategies and highlight the possible advantages of using tissue-specific pericytes for specific TE organ grafts.

Impact statement

The use of a tissue-specific pericyte cell population that matches the TE organ may benefit organ function. In this review we provide an overview of the literature for graft (pre-)vascularization strategies and highlight the possible advantages of using tissue-specific pericytes for specific TE organ grafts.

Introduction

Charles-Marie Benjamin Rouget was the first scientist who described a population of contractile cells surrounding the endothelium of small blood vessels. Initially named Rouget cells ¹, this cell type was renamed after their peri-endothelial location by Karl Wilhelm Zimmermann and since then referred to as pericytes (peri: around, cyte: cell) ². Pericytes can be found in almost all organs and tissues throughout the body and are primarily defined by their distinct morphology. Pericytes can be distinguished from endothelial cells (ECs) by their prominent nuclei and limited cell cytoplasm with long projections. Embedded in the basement membrane (BM) of the vasculature, they embrace the ECs ³, allowing efficient communication between the two cell types.

The origin of pericytes is as heterogeneous and complex as their function and is defined in a tissue- and context specific manner. Genetic lineage tracing experiments ⁴⁻⁹ have revealed the contribution of the neural crest region to the development of pericytes in the face, brain and thymus, whereas pericytes in the liver, lung and gut have been traced back to cells of the mesothelium lineage. The origin of pericytes and lineage tracing by identification of cell specific markers in different tissues have been extensively reviewed elsewhere ¹⁰⁻¹² and we will come to this also in a section below.

Pericytes can be identified by markers such as the cell-surface presence of Platelet Derived Growth Factor beta (PDGFR β) and Neuro/Glial Antigen 2 (NG2). In different tissues and organs in the body, different pericyte subtypes can be found, and their morphology and expression level of various markers is dependent on their tissue-specific function and maturation state ^{13, 14}. To date, a single suitable marker has not been identified and pericyte isolation and characterization remains a challenge, depending on the location. Pericytes are involved in the regulation of many vascular related homeostatic processes; including blood pressure regulation, angiogenesis, and blood vessel remodeling ^{15, 16}. The multipotent role of pericytes highlights the ongoing interest of different research fields including basic vascular biology, and vascular contribution and response to disease in different organs in this particular type of vascular cell.

Modern medicine increasingly shifts its focus towards studying the regenerative capacity of the human body. The research field of tissue engineering (TE) could aid in restoring damaged organs with functional tissue grafts. In that respect, research focused on vascular regeneration is of great importance, since full vascularization

of newly engineered (graft) tissue remains a considerable hurdle^{17, 18}. *In vitro*, expansion of TE construct requires a constant increase in nutrients and oxygen supplies, which in most cases is provided by access to medium in a bioreactor in combination with or without perfusion, depending on the construct's need and size. The maximum size to which graft constructs can grow *ex vivo* without intra-tissue flow of medium is limited. Most cells require a minimal distance of 500-1000 μm from a nearby blood or medium source to ensure survival, expansion and preservation of their natural function¹⁹. Upon implantation, TE constructs require immediate re-establishment of the oxygen and nutrient supply by the recipient's circulation for graft survival. Although spontaneous vascularization is often observed^{17, 20}, natural ingrowth of the recipient's vascular network into implanted tissue takes time, thus compromising the integrity of the implant in the time period before the blood flow is well established. Successful transplantation of TE constructs therefore requires additional strategies to enhance graft vascularization. Introduction of blood flow after implantation can be accelerated by pre-vascularization of large TE grafts *ex vivo* and involves the creation of a vascular tree which can then be surgically connected via the macrovessels (arteries and veins) to the recipient's circulation. An in-depth understanding of all vascular cell types and their interaction in homeostasis is required to develop new strategies to create these complex vascular trees. For the vascular region where the exchange of nutrients and oxygen takes place, one has to mimic the morphology and function of the micro-capillary bed, which consists of microvascular structures in the micrometer range (5-10 μm in lumen diameter) that grow in between organ structures. The out- and inlets to the micro-capillary bed need to be connected to a course of small arterioles and venules (10-1000 μm in diameter) that finally branch out into semi-small diameter macrovessels (>1000 μm to 3000 μm) that can function as connection sites for surgical anastomosis. At the moment, research in the field is mainly focused on TE of macro-vessels and their usage in coronary bypasses or hemodialysis²¹ and far less on introducing connectivity with a TE microvascular bed to create complex hierarchical vascular trees.

TE based on polymer scaffolds may provide promising alternatives for the replacement of these small caliber macrovessels by native or full synthetic grafts²². In this approach, the goal is full restoration of vascular tissue by cell coverage of synthetic scaffolds that are designed to mimic the native vessel structurally, containing the same mechanical properties to withstand local hemodynamic forces. Various materials, including poly(ϵ -caprolactone) (PCL), PCL bis-urea, expanded polytetrafluoroethylene (EPTFe) or ureido-pyrimidinone (UPy) based materials, but

also natural polymers like collagen and fibrin have been used so far to synthesize these scaffolds and have been tested in various *in vitro* cell seeding protocols as well as in *in situ* cellularization strategies²³⁻²⁸.

However, as indicated before, successful vascularization of a large (>500 μm) TE organ graft also requires a microvascular bed. A functional microvascular network exchanges gasses and nutrients, removes metabolic byproducts and for smaller TE organ grafts it may directly function by itself as an access point to integrate with the host vasculature after implantation. Except for their diameter range, microvessels are distinguished from macrovessels by the type of perivascular mural cells; macrovessels are supported by vascular smooth muscle cells (vSMCs) whereas microvessels are supported by pericytes. In TE, numerous studies have used mesenchymal stem/stromal cells (MSCs) as a mural cell pool for vascularization grafts due to their ability to differentiate and function as pericyte-like cells²⁹⁻³¹. Pericytes themselves share many characteristic features with MSCs. Not only do subpopulations of pericytes express MSC markers (CD146+/CD34-/CD73+/CD90+)³²⁻³⁴, like MSCs, they also demonstrate high plasticity and are capable of multipotent stem-cell like behavior^{31, 35}. However, it remains an open question whether all pericytes are MSC like or all MSC are pericytes.

Multiple studies have used pericytes of different origins to recreate microvascular structures in angiogenic assays³⁶⁻³⁸. As pericyte function is partly tissue type dependent, TE graft function could be improved if a tissue-specific pericyte is used to support the capillary bed. Furthermore, pericytes are specialized cells that are crucial for the stability of the native micro-vasculature, and thus can considerably contribute to vessel stabilization and endothelial barrier maintenance in vascularized TE grafts.

Vascular tissue engineering (VTE) of a microvascular bed in soft tissue requires the reconstruction of capillaries using different vascular cell types in combination with a supporting material, usually biological or synthetic hydrogels in combination with bioactive factors. So far, mainly endothelial cells and supporting cells such as MSCs have been investigated in VTE applications, but little is known about the use of pericytes in TE organ grafts. In this review, we present an overview of pericyte function in blood vessel formation and review pericyte subtypes and their specific functions in different tissues. This knowledge can be used to create soft tissue-specific vascularized grafts with optimal pericyte support.

Pericytes in blood vessel formation and EC cross-signaling

Pericyte-endothelial interactions are necessary for the development and maintenance of a functional microcirculation in different tissues^{3, 39}. Various molecular mechanisms are involved in this interaction; including the activity of matrix metalloproteinases (MMPs), and PDGF/PDGFR β , Angiopoietin-1/Tyrosine Kinase-2 (Angpt1/Tie2), transforming growth factor β (TGF β) and sphingosine 1-phosphate (S1P) signaling. Each of these also play an important role in angiogenesis (Figure 1)⁴⁰.

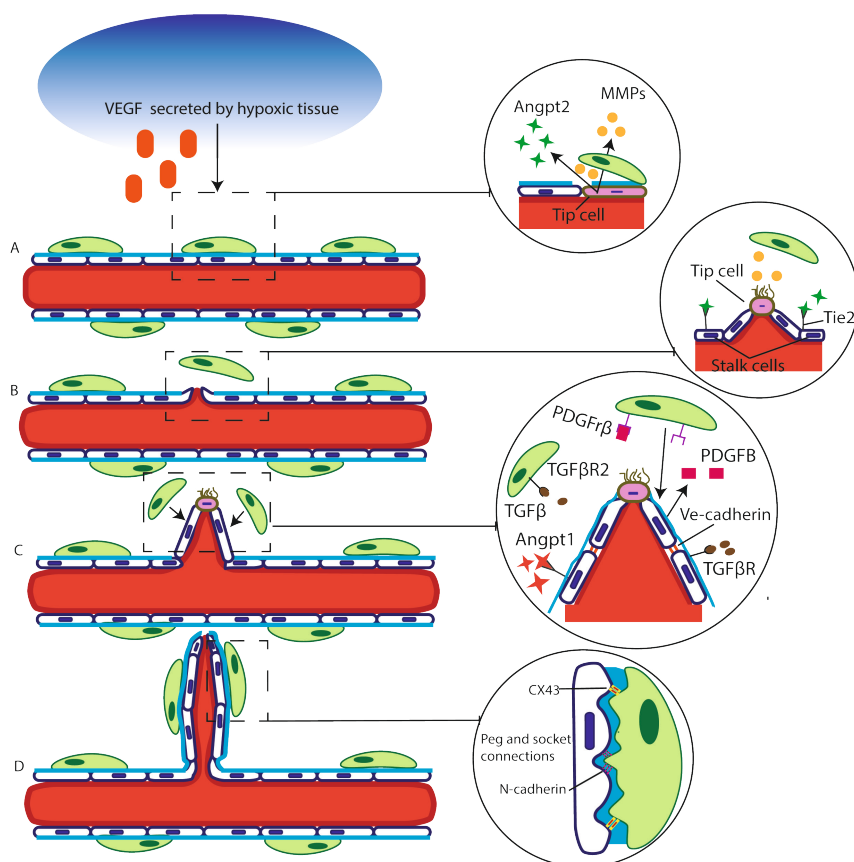


Figure 1. Pericyte and endothelial cross-signaling in angiogenesis.

(A) Pro-angiogenic factors such as vascular endothelial growth factor (VEGF) are secreted by hypoxic tissue and activates endothelial cells (ECs) in a nearby blood vessel. (B) The activated tip cell loosens endothelial tight junctions and secretes angiopoietin 2 (Angpt2) to induce pericyte detachment and vessel destabilization, and produces matrix metalloproteinases (MMPs) to break down the basement membrane. The tip cell migrates away from the vessel wall and sprouts towards a gradient of pro-angiogenic factors, followed by stalk cells. (C) Stalk cells secrete platelet derived growth factor B (PDGFB) to attract PDGF receptor β (PDGFR β) positive pericytes. Paracrine factors Angpt1 and transforming growth factor β (TGF β) are released by pericytes to promote endothelial maturation and barrier formation via the Angpt1 and -2 Tie2 receptor and TGF β R. This results in upregulation of tight junctions such as vascular endothelial (VE)-cadherin. (D) The new capillary forms new peg and socket connections between EC and pericyte, including adherens junction neural (N)-cadherin and gap-junction complex connexin43 (CX43). Meanwhile, a new basement membrane is produced by both EC and pericyte. All this results in neovessel stabilization and maturation.

Angiogenesis, the process in which vessels sprout from pre-existing blood vessels, starts when hypoxic tissue secretes pro-angiogenic factors such as vascular endothelial growth factor (VEGF), which activates ECs in a nearby blood vessel.

The activated ECs (now referred to as tip cells) loosen the endothelial tight junctions bonds and start to secrete angiopoietin 2 (Angpt2) and matrix metalloproteinases (MMPs) in order to break down the BM. This allows the tip cells as well as nearby pericytes to migrate away from the original vessel, with the tip cells sprouting towards a gradient of pro-angiogenic factors. Besides tip cells, the highly proliferative endothelial stalk cells are responsible for establishing new tight junctions to create neovessels. Stalk cells follow behind the tip cell and contribute to the formation of the lumen of the new capillary, which remains connected to the existing blood vessel. The newly created neovessels are unstable and require pericyte recruitment to ensure survival. For this, ECs secrete PDGFB to attract PDGFR β positive pericytes, leading to pericyte coverage and enabling pericytes and ECs interaction via various molecular mechanisms such as Angpt1, TGF β and S1P mediated paracrine stimulation to initiate maturation by promoting the formation of a tight vascular barrier. Excellent reviews describe this global angiogenic process in more detail ⁴¹⁻⁴⁴.

Regarding pericytes and ECs interactions in angiogenesis, essential molecular pathways that guide pericyte behavior should be further elucidated. VEGFA is also secreted by pericytes and therefore, pericytes located at the top of the sprout, could help guide tip cell migration during sprouting ^{45,46}. The importance of PDGF/PDGFR β cross signaling for capillary stabilization has been illustrated in endothelium specific PDGFB knock out mice, which develop vessels without pericyte coverage, resulting in unstable neovessels, micro aneurysms and increased microvascular leakage ^{39, 47-49}. Pericyte-endothelial cell contact also activates TGF β , which inhibits EC proliferation but stimulates pericyte proliferation and therefore promotes blood vessel maturation ⁵⁰. The importance of the TGF β pathway is confirmed by studies where absence of TGF β in mice results in abnormal vasculature development characterized by lack of pericytes coverage, inflammation, (neo)vessel instability and rupture ^{51,52}. The stabilization of newly formed blood vessels is further driven by Angpt1, which is a ligand produced by pericytes and vSMCs and binds to the endothelium specific Tie2 receptor. Angpt1 is a natural inhibitor of vascular permeability as it tightens junctions of established vessels ⁴⁴. Other studies suggest that Angpt1 facilitates EC-dependent release of growth factors including TGF β and PDGFB, stimulating once again pericyte recruitment and blood vessel maturation as described earlier ^{53,54}. In addition to Angpt1, during the initial phase of angiogenesis, upregulation of Angpt2 initiates sprouting by inducing pericyte detachment and vessel destabilization. In the absence of endothelial survival factors, Angpt2 functions as a context dependent antagonist or agonist of the Tie2 receptor and upregulation of Angpt2 leads to vessel regression, which is unfavorable in newly formed capillaries ⁴⁴. Based on this, the balance in Angpt1/Angpt2 ratio thus determines vascular homeostasis

and is essential in regulating neovessel formation and maturation. Furthermore, EC and pericyte interaction is regulated by the S1P pathway. S1P supports the vascular endothelial barrier by promoting secretion of extracellular matrix (ECM) components and upregulation of junction proteins N-cadherin and VE-cadherin as well as downregulation of vascular destabilizing factors, such as Angpt2⁵⁵.

Besides these paracrine pathways, pericytes and ECs also communicate via direct contact. Pericytes share a BM with the ECs and form direct connections through gaps within this membrane. Called peg and socket connections, these sites are enriched with tight- and gap junctions, which are cell-cell junction complexes that contain high levels of junction proteins such as N-cadherin and gap junction protein Connexin 43 (Cx43)⁵⁶. This direct intercellular communication is essential for the transfer of intracellular mediators and synchronization of the intracellular environment between adjacent cells, and is particularly important for the transmission of the mechanical contractile force from the pericytes to the endothelium^{57, 58}. Both paracrine signaling and direct cell-cell contact play an important role in pericyte/EC interaction in angiogenesis but also in other pericyte-dependent functions.

Currently, there are different perceptions on the interaction between pericytes and endothelial sprouts in different tissues¹⁵. The most commonly accepted view is that pericyte recruitment is orchestrated by stalk cells that form the new capillary and actively recruit pericytes for vascular support⁵⁹. For example, research in the retinal angiogenesis field shows that the retinal vascular network remains immature and is prone to rarefaction by ineffective stabilization until pericytes recruitment⁴⁸. In this case, capillary coverage is generally associated with the end of the proliferative stage and the beginning of vascular maturation and establishment of capillary function.

However, pericytes may also play a role in the earliest phase of angiogenesis. Studies in the corpus luteum for example, suggest that the early steps in sprout formation consists of formation of pseudopodic extensions by pericytes that penetrate basal lamina of the vascular segment⁴⁶. These extensions then establish contacts with surrounding cells⁴⁶. The above-mentioned examples illustrate that the interaction between ECs and pericytes may be different in different angiogenic conditions, and in different tissue environment⁶⁰.

Besides their role in vessel formation, pericytes are essential in promoting vessel maturation and tight vascular barrier formation. Preserving vascular barrier function is also one of the pericytes main functions during blood vessel homeostasis. Depending on their locations, pericytes cover between 22% and 99%

of the endothelium in capillaries and are also present in pre capillary arterioles and post capillary venules⁶¹. This coverage appears to correlate positively with endothelial barrier properties, with large pericyte coverage resulting in reduced EC turnover^{16, 62}, whereas low coverage results in enhanced EC proliferation and sprouting capacity. In tissues with severely restricted endothelial permeability, such as the brain (blood-brain-barrier, BBB) and placenta (blood-placenta-barrier), there is typically a higher number of pericytes coverage to sustain barrier control compared to other tissues. Other important functions of pericytes include their contractile regulation of blood flow, their contribution in the formation of ECM and their multipotency to switch between phenotype and cell type. These pericyte functions may differ between different locations in different tissues, resulting in a heterogeneous pool of pericyte phenotypes.

Subpopulations of organ-specific pericytes and their function in the local microvasculature.

Pericytes can typically be identified by electron microscopy in connective tissues, nervous tissues and muscle tissues, and are observed in fenestrated, sinusoid and continuous capillaries^{3, 63}. Based on their morphology, they can be defined as cells embedded in the vascular BM that extend thin foot processes along and around ECs. Different pericyte pools in various tissues can be distinguished based on their origin, morphology, the expression of molecular markers and their tissue-specific function. In the following section, we elaborate on the organization of different pericyte subtypes in the microvasculature of a selection of tissues with a high density of pericytes and/or specific pericyte function (Figure 2). This is followed by a discussion of the possible use and contribution of different pericytes subtypes in VTE of organ grafts in the subsequent paragraph.

Brain

The vascular bed of the central nervous system (CNS) sustains an extremely tight barrier called the BBB, which is impermeable to the passive transport of cells, proteins, and bioactive compounds in the circulation. The capillary wall consists of non-fenestrated endothelium with individual ECs connected by tight junctions enriched in ZO-1. At the basolateral side, pericytes are embedded in the capillary BM nearby astrocyte end-feet, which are also in contact with the vessel wall. Together with microglia and neurons, they form the neurovascular unit (NVU)⁶⁴.

Pericytes in brain tissue emerge from either neural crest cells or mesothelial cells that have undergone epithelial-to-mesenchymal transition^{65, 66}. Their coverage of ECs in the brain is the highest compared to all other sites throughout the body, with

an estimated pericyte to EC ratio of 1:1 to 1:4^{11,67-69}. Various studies have indicated that the high pericyte coverage rate of cerebral microvasculature is essential for brain homeostasis, and is critical for BBB maturation and maintenance^{10,15,70}. Brain pericytes are crucial for the regulation of micro-capillary vasomotion, and they actively contract and relax to regulate the cerebral blood flow (CBF) in response to changes in neuronal activity^{71,72}. Pericyte extensions are enriched in contractile proteins such as alpha-Smooth Muscle Actin (α SMA), tropomyosin, and myosin, which give rise to their contractile ability⁷³. Loss of pericytes in PDGFR $\beta^{+/-}$ mice in the murine brain led to a decrease in capillary density during aging, induced vascular dysfunction, diminished capillary perfusion and led to BBB breakdown⁷⁴. In a similar study a reduction in pericyte numbers in the BBB also caused loss of tight junctions and increased the permeability of the vascular barrier⁷⁵.

In addition to common mural cell markers including PDGFR β , NG2, α SMA, desmin and CD146, brain pericytes express the brain specific marker CD13 (Table 1). Park *et al.* describe two pericyte populations in the brain, that are either CD90 negative or positive⁷⁶. The CD90⁻ population of brain pericytes is polygonal shaped and displays a contractile pericyte phenotype that produces greater amounts of ECM components and expresses higher levels of the mature pericyte marker α SMA. CD90⁻ pericytes are primarily involved in maintaining the neurovasculature, regulating vessel diameter, and moderating immune responses. The CD90⁺ population is spindle shaped and expresses higher amounts of mesenchymal markers CD146 and CD73. This population appears to be more pre-mature, may be considered the primary source for replenishing lost pericytes, and may be responsible for remodeling vasculature during angiogenesis, while possibly being involved in scar formation⁷⁶.

Table 1. Tissue specific pericytes

Subpopulations	Molecular markers
Brain pericytes	PDGFRβ + NG2 + α-SMA - NG2 + CD146 + CD13 + Desmin - Smyth <i>et al.</i> 2018 [68] PDGFRβ + NG2 + α-SMA + NG2 + GFAP - CD45 - Smyth <i>et al.</i> 2018 [68]*
	PDGFRβ + NG2 + α-SMA + NG2 + CD146 + CD13 + CD90 + CD140b CD105 + Park <i>et al.</i> 2016 [76]
	PDGFRβ + NG2 + α-SMA + NG2 + CD146 + CD13 + CD90 - CD140b CD105 + Park <i>et al.</i> 2016 [76]*
Liver pericytes	PDGFRβ + NG2 + α-SMA NG2 + Vimentin + CD90 - CD140b + Gerlach <i>et al.</i> 2012 [80]
Tubulointerstitial Pericytes	PDGFRβ + NG2 + α-SMA + NG2 + Coll1a1 + Lin <i>et al.</i> 2008 [97]
	PDGFRβ + NG2 + α-SMA NG2 + CD73 + PDGFRα + CD45 - Rojas <i>et al.</i> 2012 [98]
Mesangial cells	PDGFRβ + NG2 + α-SMA + NG2 + Coll1a1 - Lin <i>et al.</i> 2008 [97]
	PDGFRβ + NG2 + α-SMA NG2 + CD73 + PDGFRα + CD45 - Rojas <i>et al.</i> 2008 [98]
Podocytes	Nephrin Podocin α-actinin CD2AP + Podocalyxin Synaptopodin WT1 + GLEPP-1 + Testagrossa <i>et al.</i> 2013 [100] ****
Lung pericytes	PDGFRβ + NG2 + α-SMA - NG2 + CD146 + PDGFRα + AquaporinV - CD31 - CD45 - Hung <i>et al.</i> 2017 [122]
	PDGFRβ + NG2 + α-SMA - NG2 + Desmin Rock <i>et al.</i> 2011 [125]
	PDGFRβ + NG2 + α-SMA + NG2 + CD146 + Calponin + CD90 + CD73 + 3g5 + CD31 - CD45 - Yuan <i>et al.</i> 2015 [124]

Table 1. Tissue specific pericytes (continued)

Subpopulations	Molecular markers
Cardiac pericytes	
Nees <i>et al.</i> 2012 [130]	PDGFrβ + α-SMA + NG2 + Calponin 3g5 +
Chen <i>et al.</i> 2015 [136]	PDGFrβ + α-SMA + NG2 + CD146 + PDGFrα +
Avolio <i>et al.</i> 2015 [137]	PDGFrβ + NG2 + Vimentin CD34 +

* Second population described in the same paper

** In activated state

*** Positive in neonatal kidney, negative in adult kidney

**** Review summary

Liver

The microvascular bed in the liver consists of sinusoids, a structure similar to a fenestrated capillary, but with open pores in the endothelium whereas fenestrated endothelium sustains diaphragms covered pores. This discontinuous endothelium permits mixing of the oxygen-rich blood from the hepatic artery with the nutrient-rich blood from the portal vein. Sinusoidal ECs are supported by Kupffer cells and liver pericytes. Liver pericytes are commonly named hepatic stellate cells (HSCs) and reside in the space between parenchymal cells and sinusoidal ECs of the hepatic lobule, also called the space of Disse⁷⁷. Genetic lineage tracing studies revealed that HSCs originate from the septum transversum mesenchyme^{8, 78, 79}. HSCs express PDGFR β , NG2 and vimentin at all times (Table 1)⁸⁰. In addition, in rodents, HSCs in a quiescent state can be identified via the expression of glial fibrillary acidic protein (GFAP), which is also commonly expressed by astrocytes in the central nervous system, in addition to desmin. In the liver injury induced activated state they can be identified by increased expression of α SMA⁸¹. However, there are discrepancies between rodent- and human markers and further research is required to identify specific markers for human HSCs^{82, 83}.

HSCs constitute about 13% of the sinusoidal cell population and exert various functions. The exact ratio of pericytes to ECs has not been investigated. In the healthy liver, quiescent HSCs actively store vitamin A lipid droplets, and this particular cell pool constitutes the largest reservoir of vitamin A in the body⁸⁴. In addition, they contribute to the 3D architecture of the liver tissue by secreting ECM components (collagen, fibronectin, laminin and CNN family member 1), matrix degrading metalloproteinases (MMPs) and their inhibitors (TIMPs) to regulate ECM turnover in the space of Disse^{85, 86}. In line with the general vaso-regulatory capabilities of pericytes, HSCs has been shown to respond to endothelin 1 (ET-1) to modulate cellular contraction^{87, 88} and regulate sinusoidal tone^{89, 90}.

During acute or chronic liver injury, immune cells secrete chemokines including TGF β 1 and PDGF resulting in rapid activation of HSCs, driving them from quiescent to a transdifferentiated state in which they resemble highly proliferative, migratory, and contractile myofibroblasts^{90, 91}. These collagen type I and α SMA-expressing cells migrate to the site of inflammatory or ischemic injury and produce ECM components that accumulate and form scar tissue in the space of Disse that eventually leads to loss of sinusoidal pores in the endothelium⁹². The vitamin A storage capacity of quiescent HSCs is typically lost during this trans-differentiation^{92, 93}.

Kidney

Three different pericyte subtypes have been identified in the kidney: tubulointerstitial pericytes, mesangial cells and podocytes. Tubulointerstitial pericytes are located in the tubulointerstitial space of peritubular capillaries, including in branched vessels from the vasa recta, responsible for returning blood to the cortical vasculature ^{94, 95}. Mesangial cells are considered a specialized subset of pericytes located in the glomerulus that make up the mesangium. Podocytes are also located within the glomerulus wrapping around the capillaries that form the actual glomerulus within the Bowman's capsule to form the renal filtration system. During renal development all stromal cells, including renal pericytes, derive from the odd-skipped-related 1 (Osr1)+ intermediate mesoderm ⁹⁶. In mature kidney, the pericyte to EC ratio is estimated between 1:2.5 and 1:17, depending on the location: the pericyte coverage peaks in the outer medulla, where regulation of blood flow to match reabsorption demands is greatest ⁹⁷.

Both α SMA and NG2 are expressed in the pericytes of the neonatal kidney, with a decline in expression of these pericyte markers observed after birth ⁹⁸. Mesangial cells and tubulointerstitial pericytes also express PDGFR β , PDGFR α , RGS5, desmin, vimentin, CD73 (ecto-5'-nucleotidase) and CD45 ⁹⁹. Podocytes show a distinctively different marker profile with expression of nephrin, podocin, α -actinin-4, CD2-associated protein (CD2AP), podocalyxin, synaptopodin, WT1, CD10 (CALLA) and GLEPP-1 ¹⁰⁰. Although it is still an ongoing discussion whether podocytes can be considered real pericytes, they share similar functions (such as endothelial barrier stabilization, see below). In addition, they are vital for glomerular filtration and therefore should be taken into account in relation to renal VTE ^{16, 101, 102}. An overview of renal pericyte markers is specified in table 1. During glomerular development, podocytes produce a number of angiogenic growth factors, including VEGF-A, VEGF-C, Angpt1, and ephrinB2, whereas adjacent ECs express their cognate receptors ¹⁰³. Together with ECs in the glomerular capillary loop and the glomerular basement membrane (GBM) they form the filtration barrier. A podocyte can be divided into three different structural and functional segments; the cell body, the major processes and the foot processes. The foot processes arise from the major processes, enwrap the glomerular capillaries and comprise a slit diaphragm, which is a meshwork of proteins including nephrin, podocalyxin, and P-cadherin, that participate in podocyte signaling ¹⁰⁴. In the mature kidney, podocytes play an important role in blood filtration and produce urine by filtration through the slit diaphragm, which connects with foot processes from neighboring cells ^{105, 106}. Together with glomerular ECs, podocytes and mesangial cells form a glomerular functional unit, the basic filtration unit in the kidney ¹⁰⁷.

Mesangial cells are more often described as specialized pericytes rather than podocytes, as they display additional pericyte characteristic functions such as providing structural support for the capillaries in the glomerulus and controlling glomerular filtration. In the healthy kidney, mesangial cells contribute to the ECM by predominately depositing type IV collagen, laminin and fibronectin⁹⁵. Moreover, mesangial cells express many receptors for vasoactive agents, such as angiotensin II and endothelin. Combined with their contractile capacity this allows them to play a significant role in regulating glomerular hemodynamics by altering glomerular vascular resistance^{108, 109}

Pericytes of the branched descending vasa recta (DVR) bundles, which are the small vessels around the loop of Henle, and pericytes in the proximal tubule and the distal tubule are difficult to study due to the inaccessibility of the medulla *in vivo*. An isolated DVR model demonstrates that pericytes in this region regulate both vasoconstriction and dilation in response to vasoactive agents^{110, 111}. Moreover, they may regulate blood flow by altering the coverage of EC surface^{10, 70}. Additional data demonstrated that pericytes in the DVR express α SMA for regulation of vessel diameter and contribute to medullary blood flow regulation¹¹². During kidney injury, peritubular pericytes are activated and migrate from the vessels to the interstitial space to trans-differentiate into myofibroblasts, which leads to capillary destabilization and regression¹¹³. A glioma-associated oncogene 1 (Gli1) positive subpopulation of interstitial kidney pericytes act as a major source of renal myofibroblasts after injury, and can thus be considered myofibroblast progenitors [114]. These Gli1+ pericytes detach from the renal capillaries after the injury event, and this depletion induces capillary rarefaction and proximal tubular damage^{114, 115}.

Another pivotal kidney specific function is Erythropoietin (EPO) production by peritubular pericytes. EPO stimulates red blood cell synthesis in the bone marrow and is secreted by the kidney in response to cellular hypoxia. Studies suggest that pericytes are the main EPO producing cells^{116, 117}, and that during chronic kidney disease (CKD) pericytes differentiate into myofibroblasts with subsequent decrease in EPO production, leading to renal anemia¹¹⁷. Pericytes are also identified as renin producing cells in the human kidney, as described by the group of Stefanska *et al.*¹¹⁸, and thus they contribute to the regulation of the Renin-Angiotensin-Aldosterone-System (RAAS), which mediates the effective circulating volume in the body.

Lung

Lung pericytes originate from the mesoderm and mesothelium and are derived from mesenchymal progenitor cells (MPCs)⁹. The lung pericyte to EC ratio is estimated to be 1:10, which is relatively low compared to the ratio in other organs such as brain and kidney. Lung pericytes are found along all sites of the broncho-vascular bundle, embedded within the capillary BM of the alveoli¹¹⁹. A large part of the lung pericyte cell body and the larger processes are separated from ECs by the BM, whereas the finer foot processes penetrate the BM and are in direct contact with the ECs. Electron microscopy showed that lung pericytes function as bridge regions between separate capillary segments by sending long processes to adjacent segments, establishing close contact across these structures¹²⁰. Several studies have investigated the expression of molecular markers in the lung pericytes. PDGFR β and NG2 are, as in other pericyte subpopulations, highly expressed in lung pericytes. Other prominent mesenchymal markers found in isolated human lung pericytes include CD73, CD90, and the hyaluronan receptor CD44¹²¹⁻¹²⁴. α SMA expression is found in the pre- and post- capillary vessels of the lung, but not in the rest of the pulmonary capillaries¹²⁵. In addition, expression of endoglin (CD105) and PDGFR α is observed and considered to be characteristic for human lung pericytes (Table 1).

Most studies of lung pericytes have focused on their function in lung fibrosis and pulmonary hypertension^{119, 125, 126}, whereas pericyte function in lung homeostasis remains largely uncharacterized. Functional studies regarding embryonic lung development in which pericytes were depleted by using a PDGFR β -blocking antibody in postnatal pups, resulted in early embryonic lethality due to abnormal vasculogenesis¹²⁷. Application of Cre-loxP technology to induce targeted ablation of pericytes within the lung, did not lead to changes in vascular permeability, suggesting that lung pericytes may not be as critical in maintaining the vascular barrier function compared to e.g. brain pericytes¹²². Nevertheless, impaired maturation of MPCs into pericytes in a fibrotic mouse model worsened lung fibrosis and increased microvascular dysfunction. This suggests that MPC differentiation into mature, functional pericytes is integral to lung healing in response to injury¹²⁸. Studies in other animal models suggest that lung pericytes contribute to inflammation and fibrosis, and regulate microvascular permeability and stability^{120, 124, 129}. The interaction of pericytes with their cellular neighbors in case of disturbed homeostasis and the environmental cues for pericyte activation in the lungs thus requires further research.

Heart

Considered as cardiac stem cells, cardiac pericytes (CPs) are of mesenchymal origin and are derived from the mesenchymal angioblast during development¹³⁰. Additional evidence indicates that CPs are derived from epicardium specifically¹³¹. Cardiac pericytes show a characteristic morphology, with a star-shaped body and long antler-like branched processes¹³⁰. Cardiomyocyte contraction in particular demands sufficient high oxygen and nutrients levels, which is facilitated by the dense, highly perfused cardiac microvascular bed. The ratio of pericytes to ECs in the heart is estimated to range from 1:2 to 1:3¹³⁰. Cardiac pericytes are primarily found in the capillaries but are also present in the intima of arterioles and venules^{132, 133}. This last population is identified to contribute to restenosis following arterial injury and originates and expands in the intima, in contrast to the other CP populations¹³⁴. During the progression of restenosis, adventitial pericytes migrate to the vessel lumen and give rise to α SMA-positive cells forming the neo-intima. Therapeutic targeting of this specific population may aid in restenosis control¹³⁵.

A few research groups have been able to isolate and characterize CP subpopulations, reporting variations in origin, location and molecular markers. The group of Nees *et al.* found a pericyte population expressing typical pericyte molecular markers NG2, PDGFR β , α SMA, calponin and 3g5¹³⁰. The group of Chen *et al.* isolated pericytes from fetal and adult hearts expressing CD146, NG2, PDGFR β , PDGFR α , α SMA¹³⁶. Another population was identified in human neonatal hearts, by the group of Avolio *et al.* who demonstrated their present in arterioles and capillaries. This specific subpopulation uniquely expressed progenitor EC marker CD34 in addition to NG2, vimentin and PDGFR β ¹³⁷.

CPs regulate vascular permeability and angiogenesis and help to maintain cardiac homeostasis¹³⁸. Homozygous deficiency of one of the most prominent pericyte/CP markers PDGFR β is embryonically lethal in mice, due to vascular malformations and hemorrhaging¹³⁹. Similarly, deficiency of the ligand, such as in PDGFB KO murine models, causes cardiovascular defects such as pericyte/CP loss and cardiac deficits including dilated myocardial hypotrophy with thinning of the myocardial wall, myocardial hypertrabeculation and septal abnormalities⁴⁹.

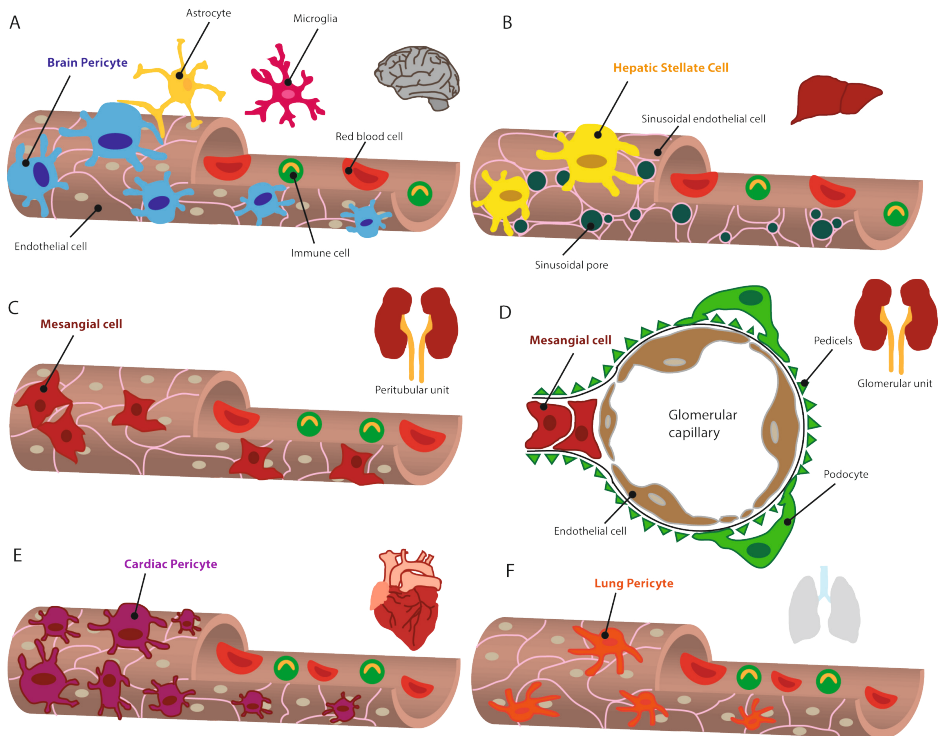


Figure 2. Vascular interaction of pericyte subtypes in different tissues.

The microvascular unit of the brain (A) consists of endothelial cells (ECs), brain pericytes, astrocytes and microglia. Red blood cells and immune cells flow through the capillaries. The microvascular unit of the liver (B) consists of sinusoidal ECs, sinusoidal pores and hepatic stellate cells (HSCs). The perivascular capillaries (C) are composed of ECs and mesangial cells. Capillaries in the glomerulus (D) are composed of ECs, podocytes and pedicels and mesangial cells. The microvascular unit in the heart (E) consists of ECs and cardiac pericytes in close contact with cardiomyocytes (not shown). The microvascular unit in the lung (F) consists of ECs and lung pericytes in close contact with lung epithelial cells (not shown).

Potential use of pericytes in pre-vascularization strategies

TE aims to create an artificial and functional replacement of damaged organs and tissues. Although it is a rapidly developing research field, clinical implementation of TE is still limited¹⁴⁰. Current techniques are still largely incapable to fully mimic natural circulation during *ex vivo* and *in vivo* tissue graft creation. This subsequently limits graft size and graft functionality, and hampers tissue graft survival during the initial phase after implantation¹⁷. Successful pre-vascularization of tissue grafts before grafting and strategies to enable immediate surgical anastomosis of the graft vasculature with the host's circulation would greatly enhance the clinical applicability of TE. Pre-vascularization of a construct is based on a top-down strategy¹⁴¹, with predesigned geometry and architecture of the vascular bed and pre-fabricated

supporting material before or while cells are introduced to the scaffold; or a bottom-up approach, in which cells are stimulated to recapitulate the bio-physiological mechanisms for native new vessel formation such as during embryonic development or wound healing¹⁴¹. In addition, hybrid approaches have been developed which implement useful characteristics of both top-down and bottom-up approaches and have a huge potential in TE strategies. A detailed overview of frequently used techniques has been described by many excellent reviews¹⁴²⁻¹⁴⁴. In this paragraph we highlight some of these techniques.

Top-down approach for pre-vascularization

The architecture of top-down scaffold designs, e.g. porosity, pore structure and pore size, influences the vascularization rate after implantation¹⁴⁵. Most scaffolds are composed of synthetic material due to the ease and flexibility of tailoring their mechanical properties. The generation of hollow channels in 3D hydrogel is commonly used to create vascular like structures *in vitro*. Vascular cells are seeded and adhere to the inner wall of the micro channels and the resulting vessels are guided by the pre-designed geometry of these channels. The drawback of using fully synthetic hydrogel is the limitation in cell-matrix interaction. As discussed above, neovessel sprouting from a pre-existing vessel requires breakdown of the BM and surrounding bio-matrix during the invasion phase. Most synthetic hydrogels, including sodium alginate, pectin, chitosan, or synthetic water-soluble hydrophilic polymers such as poly(vinyl alcohol) and poly(ethylene oxide) (PEO), are relatively impermeable for living cells, as they lack target sites for the proteinases that the vascular cells secrete¹⁴⁶. Therefore, sprouting of new vascular structures from EC-seeded pre-patterned channels is limited. The use of bioactive hydrogels, e.g. gelatin methacrylate (GelMA) and fibrinogen based-gels, containing biologically active molecules such as bioactive peptides segments (in addition to growth factors and enzymes), would allow ECs to invade from EC-covered pre-patterned channels into the bio-matrix to create a more complex interconnected vascular network¹⁴⁰.

Different ways to create hollow channels have been reported. These include for example, the casting of bioactive hydrogels in a silicone (polydimethylsiloxane (PDMS)) mold with microneedles as space occupiers. When the needles are extracted from the mold and hydrogel, tunnel shaped structures remain which can then be seeded with vascular cell types^{147, 148}. Based on the same principle, 3D printed sacrificial materials could be used instead of microneedles to pre-define the vascular pattern. After casting and crosslinking of the hydrogel, the sacrificial material is flushed out to leave the microfluidic tunnels for vascular cell seeding behind (Figure 3A). Homan *et al.* used this method to mimic the proximal tubule of the kidney in a

3D chip ¹⁴⁹. In their protocol, a fugitive ink (Pluronic® F127) is printed on a gelatin-fibrinogen ECM. Additional ECM will then be casted around the printed tubule and the fugitive ink is evacuated to create an open channel ready for cell seeding. Miller *et al.* used carbohydrate glass as sacrificial material to create interconnected orthogonal microvascular networks in fibrin hydrogels. The seeded ECs formed both single and multicellular sprouts from the pre-patterned vasculature in the ECM ¹⁵⁰.

In addition, nano- or microfibrillar scaffolds created by electrospinning, are used in both *in vitro* as *in vivo* TE scaffolds (Figure 3B). Electrospinning is a technique that uses electrostatic forces to produce fibrous scaffolds from biocompatible polymers, such as PCL. The microfibers are 3D porous and fiber thickness, orientation and density can be controlled to improve cell adherence, survival and expansion, while supporting tissue structure and function. Parameters can also be adapted to the mechanical and functional characteristics of the different types of tissues to create a more tailored scaffold. Depending on their pore size, electrospun fibers in nanoscale have been shown to provide an efficient exchange of nutrients and oxygen within the structure ¹⁵¹. Electrospun fibers have been used to improve endothelial differentiation of induced pluripotent stem cells (iPSCs), promoting an elongated vascular-like cell morphology to improve the healing response. Seeding of stem cell derived ECs on these fibers also resulted in improved survival and endothelial phenotype preservation, as well as improved blood perfusion after transplantation *in vivo* ¹⁵².

Furthermore, there are light- or laser based vascular TE techniques. Two-photon lithography (Figure 3C) is used to generate complex 3D microstructures in a single processing step from a photosensitive polymeric material ¹⁵³. Over the past years, this technique has been increasingly used in bio-engineering applications, including the fabrication of perfusable vascular networks ¹⁵⁴. In addition, this technique was also used to create micro-pores in the walls of a branched network of polyacrylate vessels. This facilitated the successful lining of vessels with ECs, as well as cell migration and medium exchange across the vessel wall ¹⁵⁵. However, this technique has some limitations, including limited choice of biocompatible photo initiators and high costs.

Another technique to create free-form channels in a cellularized hydrogel is the use of subtractive fabrication by laser ablation (Figure 3D) ¹⁵⁶. Multiphoton absorption of light generates small voids within the hydrogel which can be seeded with cells. For example, laser ablation was performed in a collagen-based hydrogel and

the obtained channels were seeded with endothelial cells ¹⁵⁷. The channels were perfused in a microfluidic chamber and the ECs successfully formed a monolayer lining the channel.

Digital micro-mirror devices (DMD) are, similar to two-photon lithography, based on photon polymerization of cell-laden liquid precursors (Figure 3E) ¹⁵⁸. In DMD, polymerization is selectively induced in regions exposed to UV-light in a 2D pattern generated by the projection of an image bitmap. Layer by layer 3D structures are formed by repetitive light exposure of serial projected patterns, alternated by washing steps to get rid of the unexposed un-polymerized gel precursor. This approach was used to create a complex network in GelMA gel seeded with ECs. The gel was subjected to patterned UV illumination to create a hollow structure, which was casted with another gel containing supporting cells. The ECs were shown to spontaneously form vessel-like structures *in vitro*. Upon implantation in immune deficient mice, the construct demonstrated a maturing endothelial network and anastomosis with the host circulation ¹⁵⁹. However, pre-seeding with ECs seems necessary, since implanted constructs without ECs did not show any vascularization upon implantation.

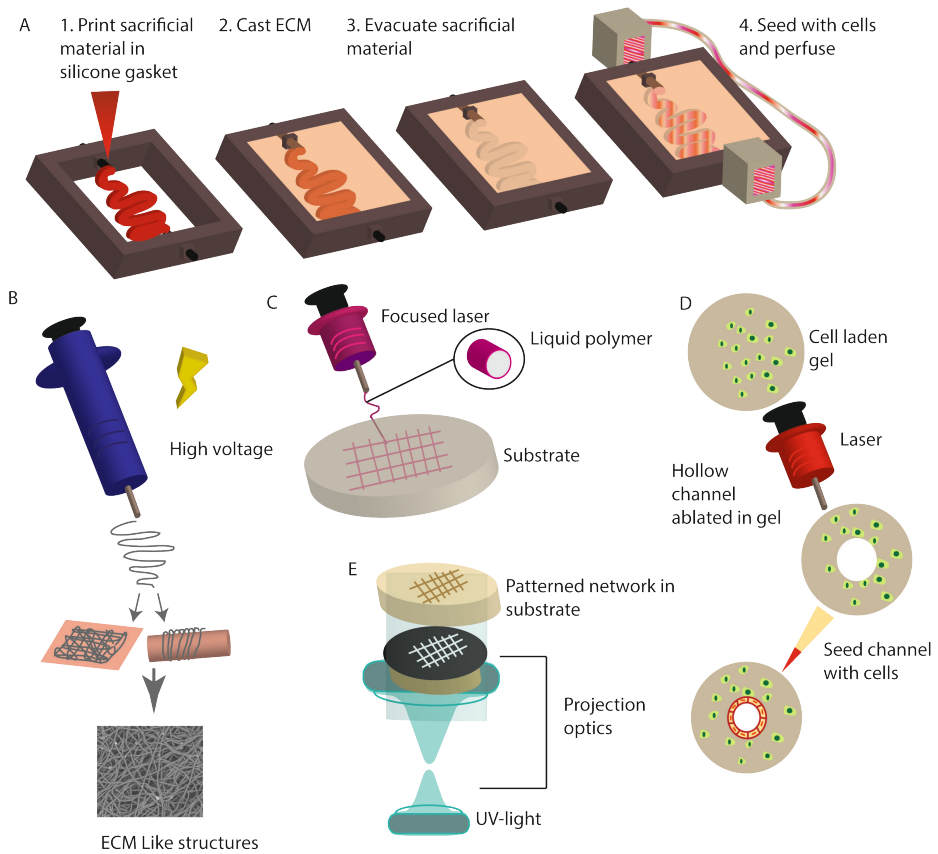


Figure 3. An overview of Top-down approaches.

(A) To create hollow channels in a silicone gasket, sacrificial material is printed in the gasket and cast with extracellular matrix. The sacrificial material is evacuated, creating an open channel for cell seeding and perfusion. Electrospinning (B) is a technique that uses electrostatic forces to produce fibrous scaffolds from biocompatible polymers. Tissue-specific vascular cells can be incorporated in or on top of these scaffolds. Two-photon polymerization (C) directly fabricates hollow tubular networks which can be printed in a hydrogel. Microchannels created in a cell-laden gel (D) by laser ablation can be directly seeded with cells of interest. In photolithography (E) UV-light is used to transfer a geometric pattern from an optical mask to a light-sensitive photoresist on the substrate.

Bottom-up approach for pre-vascularization

When considering bottom-up techniques to create self-assembled vascular structures, most standard protocols involve mixing of the required vascular cells (e.g. ECs and pericytes) in a bio-matrix environment, supplemented with growth factors to initiate angiogenesis¹⁶⁰. Another, more sophisticated approach is the use of vascularized spheroids. Extensively studied¹⁶¹, spheroids are 3D cultured cellular aggregates that are often cultured imbedded in a 3D matrix environment (Figure

4A). The relative quiescent state of cells on the surface of endothelial spheroids enhances the sensitivity to angiogenic stimulation compared to 2D cultures ¹⁶². HUVEC-based spheroids were shown to develop lumenized sprouts in the hydrogel in a high throughput drug screening platform ¹⁶¹. Recently, Wimmer *et al.* showed that it is possible to create blood vessel organoids derived from human iPSCs ¹⁶³. These 3D cultures differ from EC spheroids as they are composed of not only ECs but also mural cells including pericytes and smooth muscle cells and that the vascular cells self-organize into complex microvascular structures. After transplantation into mice, these vascular organoids successfully recapitulated the structure of a stable, perfused vascular bed. In general, vascular spheroids /organoids may serve as individual vascular units to pre-vascularize engineered organ tissue grafts. Due to the ease and versatility of 3D spheroid studies, strategies based on this bottom-up approach could be developed in which mixing of vascular spheroids/organoids with e.g. cardiac or liver spheroids in a bioreactor environment potentially generate a complex microenvironment such as cardiac and liver tissue in a bottom-up manner ^{164, 165}.

Recently, a hybrid strategy of a top down and bottom up approach has been developed and used for cardiac regeneration. Redd *et al.* (2019) demonstrated a new strategy for vascular remodeling and anastomosis *in vitro*. They combined pre-patterned, perfusable vascular channels (top-down) and self-assembling vessels in the bulk matrix (bottom-up) into a complex network with stem cell derived ECs as a cell source ¹⁶⁶. The perfused, pre-patterned vessels provided mechanical and biological cues for rapid anastomosis and host integration, giving a new insight into possible future tissue regeneration approaches. Another hybrid strategy could be to mix either iPSC derived vascular organoids or MVFs with a pre-defined 3D printed vascular structure. Separating the desired vascular cell pools (pericytes and ECs) from the vascular organoids or the MVFs provides control over the ratio of vascular cells needed in the TE construct and could improve viability and function of the vascular network upon implantation.

Over the past years, (pre-)vascularization techniques are shifting from single cell-based techniques towards more complex approaches. An example is a pre-vascularization strategy focused on the use of adipose tissue-derived microvascular fragments (MVFs) (Figure 4C). The MVFs exhibit a functional vascular morphology ¹⁶⁷. In-depth analysis confirmed that these fragments exhibit the structural features of microcirculatory blood vessel segments with a lumen and vessel wall-stabilizing pericytes on their outer surface ¹⁶⁸. In addition, they contain multipotent MSCs, which, preserve their self-renewal, proliferation, mobilization and proliferation

capacity in the recipient host. Various studies have shown that these fragments reassemble into new, microvascular networks and connect to the host vasculature after implantation ¹⁶⁹⁻¹⁷². To make the translation towards clinical approaches, patient derived cell sources might improve functionality. As MVFs can be easily harvested from adipose tissue, they offer an interesting option for *ex vivo* (graft) pre-vascularization and *in situ* vascular regeneration strategies ¹⁷³. It has been shown that MVFs can be cryopreserved without affecting their functionality and shape, which gives an opportunity for long-time storage in biobanks for later use ¹⁶⁷. MVFs already have been used as vascularization units to generate pre-vascularized tissue substitutes to improve the (blood) flow in e.g. epicardial patches and dermal skin-substitutes ^{172, 174}. Their ability to resemble into microvascular networks, connect to the host vasculature, easy harvesting and long-term storage options make MVFs a promising building block for (pre-) vascularization applications in regenerative medicine.

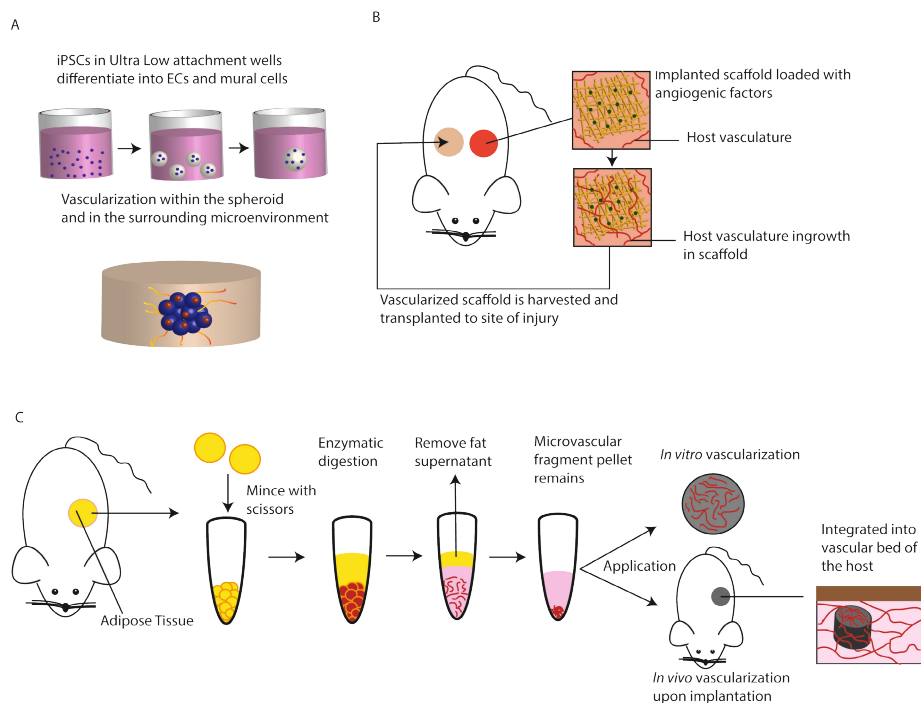


Figure 4. Bottom-up approaches.

iPSC derived vascular spheroids (A) are embedded in a 3D matrix environment. Vascular spheroids may serve as individual vascular units to pre-vascularize engineered organ tissue grafts. Organ scaffolds with pre-defined vascular structures (B) can be implanted in a vascularization site (e.g. subcutaneous pockets) to be cellularized and vascularized *in vivo* through cell invasion or vessel ingrowth by host cells. These can be harvested and implanted in the site of injury. Microvascular fragments (MVs) (C) can be harvested from various sources of adipose tissue. After enzymatic digestion, a pellet of MVFs remains, which can be used for different applications such as the testing of vascular response to different compounds in *in vitro* models or seeding the MVFs on scaffolds before implantation for pre-vascularization purposes.

In vivo TE organ graft (pre)vascularization

Vascular scaffolds with predesigned blood vessel morphology or organ scaffolds with pre-defined vascular structures can be implanted in a vascularization site (e.g. subcutaneous pockets) to be cellularized and vascularized *in vivo* through host cell invasion or vessel ingrowth (Figure 4B). These can then be later harvested and implanted at the site of injury. A major advantage of *in vivo* pre-vascularization is that the cellularization process takes place under the native physiological conditions of the host rather than *in vitro* in a bioreactor environment. In addition, strategies for *in situ* vascularization, in which an organ specific scaffold is implanted and vascularized directly at the injured site, have been investigated more recently

^{175, 176}. A disadvantage of these approaches is that underlying comorbidities such as obesity and diabetes in patients could impact vascularization efficiency. For example, vascular grafts can be implanted as vascular access for dialysis, but will mature under uremic conditions in patients with chronic kidney disease, while it is well-known that uremic toxins have a degenerative effect on the endothelium, limiting its regenerative capacity ^{177, 178}. In addition, *in vivo* vascularization in patients requires an extra invasive surgical procedure. *In vivo* approaches also have limited control over the cellularization process. As a result, *in vitro* pre-vascularization and pre-maturation of TE constructs before implantation have been investigated as a more viable approach. For example, Kusuma *et al.* used human iPSC-derived early vascular cells (VE-cadherin+ for early ECs and PDGFR β + cells for early pericytes) in a hyaluronic acid based hydrogel to promote pre-vascularization in hydrogel grafts ¹⁶⁰. Within three days, lumenized microvessels developed, enwrapped by pericytes. These scaffolds were then implanted in a murine model in which the transplanted vascular network was successfully anastomosed to the host circulatory system ¹⁶⁰. Abaci *et al.*, seeded hollow channels with iPSC derived ECs in an alginate scaffold embedded in collagen gel together with human dermal fibroblasts [174]. The seeded skin constructs established endothelial barrier function, but the vascular permeability remained significantly higher compared to native microvessels, which could be due to the absence of pericytes as supporting cells in this particular approach [147].

Implementing pericytes in bone and skeletal muscle grafts have been shown to be beneficial for bone formation. For example, studies in which intravascular dyes were used to label mural cells demonstrated that pericytes could contribute to bone repair ¹⁷⁹. Indeed subsequent pericyte-lineage-tracing studies in mice showed that endogenous pericytes can differentiate into osteoblasts and osteocytes and contribute to bone fracture healing as a source for osteogenic cells ¹⁸⁰. In addition, human perivascular stem cells have been used in the thigh muscle pouch model to promote ectopic bone formation due to their osteogenic capacity ¹⁸¹. Additional studies have demonstrated that, in order to establish a functional vascular network in bone grafts, EC interaction with mural cells including vSMCs and pericytes is essential ^{182, 183}. However, the application of pericytes in soft TE overall remains limited ^{184, 185}. The use of MSCs has been more extensively explored. For example, different groups have investigated the use of endothelial progenitor cells (EPCs) and MSCs in pre-vascularization of microvessel scaffolds *in vitro* before implantation in animal models. Subcutaneous injection of human blood-derived EPCs and MSCs into mice resulted in numerous lumenized vessels in the implantation area ¹⁸⁶. Others achieved a lumenized capillary network after combining EPC- derived vessel-like

structures and mural cells together in a hydrogel¹⁸⁷. In addition, human EPCs in a spheroid co-culture setting with undifferentiated MSCs formed an organized vascular-like network *in vivo*, in contrast to a HUVEC only culture¹⁸⁸. The same study concluded that *in vitro* pre-vascularization enhances graft survival in mice *in vivo*. Although these three research groups achieved similar successes in terms of vascularization, they drew different conclusions concerning the EC to MSC ratio, suggesting that the optimal EC to mural-cell ratio depends on the model, tissue type and the culture strategy. Overall most studies do not make a distinction between MSCs and pericytes, and do not use tissue-specific pericytes in their models. As highlighted in the previous section, pericytes from different tissues express different markers and exert different functions. The use of a tissue-specific pericyte pool for pre-vascularized TE constructs could be more beneficial for the vascularization process and improve functionality after implantation in general.

The use of pericytes in vascular tissue engineering

Without dispute, the pericyte is an essential cell type involved in vascular biology processes. In recent years, various research groups worked on the improvement of pericyte isolation techniques. Pericytes can be obtained from iPSCs by a differentiation protocol in combination with other iPSCs derived tissue-specific cells. Using this method, a tissue-specific pericyte with the desired functionality can be produced and used for tissue specific TE applications. These protocols are extensively reported by multiple research groups¹⁸⁹⁻¹⁹¹. In addition, pericytes can be purified from MVF cultures^{192,193}. However, the most common method for tissue-specific pericyte isolation is enzymatic digestion and mechanical dissociation of the targeted tissue, followed by fluorescence activated cell sorting (FACS) or magnetic activated cell sorting (MACS) of the obtained cell pool by using pericyte markers¹⁹⁴. This is done one for example cardiac tissue¹⁹⁵ renal tissue [118] and brain tissue¹⁹⁶. Retinal pericytes can be isolated by accurate dissection of the retina as described in the method of Bryan *et al.* where pericyte selection is based on size and culture medium¹⁹⁷. This paragraph describes the (putative) advantage of using pericytes and other perivascular cells in tissue graft pre-vascularization for different organs. An overview is provided in Table 2.

Table 2. Benefits of pericytes in tissue engineering

Target tissue	Experimental set-up	Outcome
Liver (Ahmed <i>et al.</i> 2017) [197]	3D liver membrane system <i>in vitro</i> using: (1) hepatic stellate cells in co-culture with (2) sinusoidal ECs and (3) hepatocytes.	Sinusoidal ECs formed vessel-like structures supported by stellate cells , established the structural architecture of the scaffold and improved hepatocyte-specific functions compared to hepatocyte monoculture.
Liver (Hussein <i>et al.</i> 2016) [199]	Heparin coated, acellular pig liver lobe cellularized by injecting human ECs in the de-cellularized vessels for re-population of the vasculature.	Perfusion with porcine blood for 10 days, resulted in equal EC distribution throughout the scaffold with no signs of thrombosis. Leakage of ECs outside the vascular structures into parenchyma remains problematic. The effect of supporting cells in this approach was not tested.
Kidney (Homan <i>et al.</i> 2016) [149]	Bio-printed proximal tubule seeded with proximal tubular cells.	The tubules were perfusable and promoted the formation of an epithelium with improved phenotypic and functional properties relative to the same cells grown on 2D. There was no microvasculature created in this approach.
Kidney (Homan <i>et al.</i> 2019) [208]	An <i>in vitro</i> method to vascularize kidney organoids under flow on a chip.	After subjection to high flow, they observed maturation of the tubular and podocyte compartments and formation of a perfusable vascular network within the organoids. Additional functionality of the podocyte compartment was not tested.
Lung (Petersen <i>et al.</i> 2010) [211]	Decellularized rat lungs, seeded with (1) vascular ECs and (2) epithelium for culture in a bioreactor.	The <i>in vitro</i> re-cellularized lungs tissues retained much of the microarchitecture of the native lung, however the alveolar barrier function showed leakage of blood components into the airways. This could be due to the lack of pericytes.
Lung (Ren <i>et al.</i> 2014) [29]	Decellularized rat lungs, co-seeded with (1) iPSC-derived ECs and (2) hMSCs, transplanted in rats. The same approach was adapted for human lung lobes in a bioreactor setting.	In the human lung lobe was efficient cell delivery, maintenance of cell viability and establishment of perfusable vascular lumens reported. <i>In vitro</i> preformed human capillaries in the pre-vascularized constructs anastomosed with the host vasculature to form functional blood vessels . Co-seeded constructs formed a large number of blood vessels <i>in vivo</i> , whereas hMSCs seeded constructs only formed a few. This suggests that hMSCs play a critical role in the network formation and vascularization process.

Table 2. Benefits of pericytes in tissue engineering (continued)

Target tissue	Experimental set-up	Outcome
Heart (Alvino <i>et al.</i> 2020) [216]	The isolation and expansion of pericytes from piglet hearts to produce an ECM scaffold with (1) cardiac pericytes and (2) swine pulmonary artery ECs. Seeded- and unseeded matrix constructs were used to replace the left pulmonary artery of piglets.	These findings showed the feasibility of using neonatal cardiac pericytes in combination with artery ECs for reconstruction of small-size branch pulmonary arteries in a large animal model. The CPs in combination with ECs established a leak-tight barrier in this model.
Heart (Schaeffer <i>et al.</i> 2018) [212]	The development of a bilayered patch composed of a (1) cardiomyocyte layer and a microvessel layer composed of (2) ECs and (3) CPs, which was implanted in a nude rat infarct model.	The bilayered graft produces substantially greater twitch force, greater CM survival, and enhanced CM maturation compared to a CM only control patch after two weeks of <i>in vitro</i> culture. After four weeks of implantation, the bilayered patches were invaded by the host's microvessels that align with the CMs and show blood perfusion as desired. Without the microvessel layer, there was no anastomosis to the host vasculature.

Liver

There are different strategies for TE liver grafts. Both stem cell derived- and patient derived mature liver hepatocytes can be used for replacement strategies in liver injury^{198,199}. The function and viability of these cells are enhanced when cultured in aggregates, which upon expansion towards large sized grafts, will require a vascular network for nutrients and oxygen transport. This can be achieved by mimicking the microenvironment of the liver, in a co-culture with other non-parenchymal cells including sinusoidal endothelial cells and HSCs. The group of Ahmed *et al.* successfully created a 3D liver membrane system *in vitro*, by co-culturing primary human sinusoidal ECs, HSCs and hepatocytes that were seeded sequentially on hollow fiber membranes to mimic the layers in the native liver²⁰⁰. The sinusoidal endothelial cells formed vessel-like structures surrounded by HSCs, established the structural architecture of the scaffold and improved hepatocyte-specific functions including higher urea and albumin synthesis rates, with respect to the hepatocyte monoculture. In addition, since HSCs are vitamin A storing cells, the inclusion of HSCs in TE liver graft is hypothesized to maintain this function and thus improve graft performance²⁰¹. The group of Hussein *et al.* performed portal-vein perfusion with detergents to decellularize the right lobe of a pig liver. They then cellularized the heparin coated, acellular pig liver lobe by injecting human ECs in the de-cellularized vessels for repopulation of the vasculature²⁰². This was followed by perfusion with porcine blood of the culture for 10 days, eventually resulting in equal EC distribution throughout the scaffold with no signs of thrombosis. Leakage of ECs outside the vascular structures into parenchyma remained problematic in their approach. However, the effect of including supporting cells such as hepatocytes and HSCs was not tested in this experiment, which could improve the barrier function of the vasculature. Despite these results, long term blood perfusion *in vivo* without heparin protection still remains a big hurdle in liver TE and patency over a long period should be improved to deliver a hepatic graft with clinically relevant performance.

Kidney

Vasculature in a renal scaffold is not only important for survival of the graft, but also essential to enable renal filtration and reabsorption function. Mature kidneys are prone to fibrosis after injury. Since not all donor kidneys are suitable for transplantation, it has been opted that rejected donor kidneys might be used for renal bio-engineering and regeneration strategies²⁰³. Studies showed that detergent-based de-cellularization of human kidneys preserved their ECM framework, biochemical properties, and angiogenic capacity²⁰⁴, and can be used as a starting point for re-cellularization with renal and vascular (progenitor) cell populations in future research.

In 2019, Lih *et al.* provided an optimized artificial scaffold for kidney regeneration in which they used a polylactic-co-glycolic acid (PGLA) scaffold with magnesium hydroxide combined with renal ECM to facilitate kidney reconstruction (histological structure and biological function) by neutralizing the acidic microenvironment and improving biocompatibility²⁰⁵. Magnesium hydroxide served as neutralization compound for the PGLA degradation byproducts and the ECM supplied growth factors to promote regeneration, which together seems possibly a good overall strategy for renal regeneration, although putative *in vivo* side effects of the addition of magnesium hydroxide and porcine EMC remains to be elucidated. Repopulation with healthy kidney tissue remains an issue, since the formation of new nephrons (the functional units of the kidney) only happens before or shortly after birth in mammals and is an extremely complex process, which is difficult to trigger in mature renal cells even in a pre-patterned scaffold environment. It also remains to be evaluated if these scaffolds can be successfully seeded with regenerative cell populations, such as iPSC-derived nephron progenitor cells. At the moment, no bio-fabrication methods are available to construct fully functional complex kidney tissues. Recent advances in regenerative medicine have created iPSC derived renal organoids. Different protocols describe the formation of these 3D aggregates, which contain all components of a human kidney, be it in a relatively immature state²⁰⁶⁻²⁰⁸. So far, renal organoids have not been successful in fully recapitulating a functional renal unit, and in part, this is due to immaturity and lack of interaction and/or formation of the vascular elements of the nephron²⁰⁹. The organization structure of even a single nephron unit is very complex and therefore a big challenge to recreate with the current limitations in scaffold fabrication and 3D printing techniques. Homan *et al.* bioprinted a renal channel that mimics a proximal tubule with diameters ranging from 400 μm to 550 μm , which they successfully seeded with proximal tubular epithelial cells (PTECs). These proximal tubules were perfusable and promoted the formation of an epithelium with improved phenotypic and functional properties relative to the same cells grown on 2D controls¹⁴⁹. However, to be able to print the small caliber structures of microcirculation (with average lumen diameter of $<10 \mu\text{M}$), technical limitations for such a top down approach, including low resolution and long printing time should be first amended to enable fabrication of renal units with a relevant anatomy that sufficiently mimic the native condition²¹⁰. To compensate for the lack of microvasculature in the renal units, the use of vascularized renal organoids could be an option. In 2019, the same group developed an *in vitro* method to vascularize kidney organoids under flow on a chip²¹¹. These kidney organoids were cultured in a fluidic chip and subjected to controlled wall shear stress. After 10 days in the chip under high flow (0.008–0.035 dyn/cm^2), they observed maturation of the tubular and podocyte compartments and formation

of a perfusable vascular network within the organoids [208]. The possible use of these organoids and the functionality of the vascular network for TE should be further investigated.

Lung

Since the functionality of the lungs is highly dependent on vascularization to achieve optimal gas exchange, lung TE has been mostly focused on (micro) vascular engineering. The most common approach is re-cellularization of de-cellularized lung scaffolds^{29, 212, 213}. Petersen *et al.* treated rat lungs with detergents to remove cellular components to create ECM scaffolds which were seeded with vascular endothelium and epithelium for culture in a bioreactor to mimic physiological pressures²¹⁴. These *in vitro* re-cellularized lung tissues retained much of the microarchitecture of the native lung, however the alveolar barrier function showed leakage of blood components into the airways, which could be improved by adding perivascular cells. Indeed the group of Ren *et al.* co-seeded iPSC-derived ECs together with hMSCs on de-cellularized lung scaffolds and transplanted them successfully into rats for three days. This approach was later adapted for TE of human lung lobes in a bioreactor setup, and the authors reported efficient cell delivery, maintenance of cell viability and establishment of perfusable vascular lumens²⁹. In particular, the *in vitro* grown lung tissues analyzed by immunohistochemistry after 7 days in culture showed that the density of blood vessels in the pre-vascularized constructs was higher compared to the non-pre-vascularized constructs.

Heart

Multiple studies have shown that cardiac pericytes promote the formation of microvessels and vascularization of cardiac tissue both *in vitro* or *in vivo*, and they are therefore considered a promising contributor in combination with ECs for building more organized microvessels for new cardiac tissue^{215, 216}. Additionally, pericytes are also used in cardiac TE strategies to help create macrovessels^{217, 218}. Alvino *et al.* successfully isolated pericytes from the hearts of piglets and expanded these to produce clinical-grade ECM scaffold. In addition, they provided evidence for the feasibility of using a pericyte and EC cellularized scaffold for reconstruction of the pulmonary artery in a piglet model²¹⁹. However, in TE approaches of the cardiac microvasculature, often MSCs are used as supporting cells in the scaffold²²⁰⁻²²². A unique approach was presented by Schaefer *et al.* who developed a bilayer patch composed of a human iPSC derived cardiomyocyte (CM) layer and a microvessel layer composed of ECs and CPs, which was implanted in a nude rat infarct model²¹⁵. The bilayered graft produces substantially greater twitch force, greater CM survival, and enhanced CM maturation compared to a CM-only control patch after only two

weeks of *in vitro* culture. After four weeks of implantation, the bilayered patches were invaded by the host's microvessels that align with the CMs and show blood perfusion ²¹⁵. However, based on findings from most implanted cell constructs in the heart, clinically significant scaffold prepositions are still quite rare. Poor electrochemical and vascular integration of the constructs remain common reasons for low functionality, and it remains important to further optimize cardiac graft vascularization techniques.

Conclusion

Research in regenerative medicine focused on TE organ graft creation has accelerated in recent years and has started to move closer towards complex tissues that exceed the mm-scale in dimensions. This development has highlighted the need to develop protocols to promote graft vascularization to safeguard long term tissue survival and function. As showcased in this review, the creation of a micro-capillary bed for nutrients and oxygen exchange based on both top-down and bottom strategies should consider the use of tissue-specific pericytes. This will not only warrant ideal microvascular behavior in each stage of new vessel formation, but also aid to establish optimal organ function that will benefit general clinical performance.

Conflict of interest

There are no conflicts of interest to declare.

Acknowledgements

This work was supported by Netherlands Foundation for Cardiovascular Excellence [C.C.], Netherlands Organization for Scientific Research Vidi grant [no. 91714302 to C.C.] and Material Driven Regeneration Consortium [Gravitation program to C.C., M.V.], the Erasmus MC fellowship grant [C.C.], the Regenerative Medicine Fellowship grant of the University Medical Center Utrecht [C.C.], the Netherlands Cardiovascular Research Initiative: An initiative with support of the Dutch Heart Foundation [CVON2014-11 RECONNECT to C.C. and M.V.], and the RECONNECT young talent grant [CVON2014-11 RECONNECT to C.v.D].

References

1. Rouget C. Mémoire sur le développement, la structure et les propriétés physiologiques des capillaires sanguins et lymphatiques. *Arch. Physiol. norm, et Path.* 5, 603–663 (1873).-Roux, W.:(a) Gesammelte Abhandlungen über Entwicklungsmechanik. Leipzig 1895.(b) Theorie der Gestaltung der Blutgefäße einschl. des Kollateralkreislaufes. *A Oppel: Über die gestaltliche Anpassung der Blutgefäße usw Leipzig.* 1910.
2. Zimmermann KW. Der feinere bau der blutcapillaren. *Zeitschrift für Anatomie und Entwicklungsgeschichte.* 1923;68(1):29-109.
3. Hirschi KK, D'Amore PA. Pericytes in the microvasculature. *Cardiovasc Res.* 1996;32(4):687-98.
4. Foster K, Sheridan J, Veiga-Fernandes H, et al. Contribution of neural crest-derived cells in the embryonic and adult thymus. *J Immunol.* 2008;180(5):3183-9.
5. Reyahi A, Nik AM, Ghiami M, et al. Foxf2 Is Required for Brain Pericyte Differentiation and Development and Maintenance of the Blood-Brain Barrier. *Dev Cell.* 2015;34(1):19-32.
6. Muller SM, Stolt CC, Terszowski G, et al. Neural crest origin of perivascular mesenchyme in the adult thymus. *J Immunol.* 2008;180(8):5344-51.
7. Wilm B, Ipenberg A, Hastie ND, et al. The serosal mesothelium is a major source of smooth muscle cells of the gut vasculature. *Development.* 2005;132(23):5317-28.
8. Asahina K, Zhou B, Pu WT, et al. Septum transversum-derived mesothelium gives rise to hepatic stellate cells and perivascular mesenchymal cells in developing mouse liver. *Hepatology.* 2011;53(3):983-95.
9. Que J, Wilm B, Hasegawa H, et al. Mesothelium contributes to vascular smooth muscle and mesenchyme during lung development. *Proc Natl Acad Sci U S A.* 2008;105(43):16626-30.
10. Armulik A, Genove G, Mae M, et al. Pericytes regulate the blood-brain barrier. *Nature.* 2010;468(7323):557-61.
11. Armulik A, Genove G, Betsholtz C. Pericytes: developmental, physiological, and pathological perspectives, problems, and promises. *Dev Cell.* 2011;21(2):193-215.
12. Yamazaki T, Mukoyama YS. Tissue Specific Origin, Development, and Pathological Perspectives of Pericytes. *Front Cardiovasc Med.* 2018;5:78.
13. Harrell CR, Simovic Markovic B, Fellabaum C, et al. Molecular mechanisms underlying therapeutic potential of pericytes. *J Biomed Sci.* 2018;25(1):21.
14. Crisan M, Yap S, Casteilla L, et al. A perivascular origin for mesenchymal stem cells in multiple human organs. *Cell Stem Cell.* 2008;3(3):301-13.
15. Caporarello N, D'Angeli F, Cambria MT, et al. Pericytes in Microvessels: From "Mural" Function to Brain and Retina Regeneration. *Int J Mol Sci.* 2019;20(24).
16. Diaz-Flores L, Gutierrez R, Madrid JF, et al. Pericytes. Morphofunction, interactions and pathology in a quiescent and activated mesenchymal cell niche. *Histol Histopathol.* 2009;24(7):909-69.
17. Rouwkema J, Rivron NC, van Blitterswijk CA. Vascularization in tissue engineering. *Trends Biotechnol.* 2008;26(8):434-41.
18. Pellegata AF, Tedeschi AM, De Coppi P. Whole Organ Tissue Vascularization: Engineering the Tree to Develop the Fruits. *Front Bioeng Biotechnol.* 2018;6:56.

19. Liu J, Hilderink J, Groothuis TA, et al. Monitoring nutrient transport in tissue-engineered grafts. *J Tissue Eng Regen Med*. 2015;9(8):952-60.
20. Folkman J, Hochberg M. Self-regulation of growth in three dimensions. *J Exp Med*. 1973;138(4):745-53.
21. Haruguchi H, Teraoka S. Intimal hyperplasia and hemodynamic factors in arterial bypass and arteriovenous grafts: a review. *J Artif Organs*. 2003;6(4):227-35.
22. Gui L, Niklason LE. Vascular Tissue Engineering: Building Perfusable Vasculature for Implantation. *Curr Opin Chem Eng*. 2014;3:68-74.
23. Catto V, Farè S, Freddi G, et al. Vascular Tissue Engineering: Recent Advances in Small Diameter Blood Vessel Regeneration. *ISRN Vascular Medicine*. 2014;2014:1-27.
24. Scott EC, Glickman MH. Conduits for hemodialysis access. *Semin Vasc Surg*. 2007;20(3):158-63.
25. Muylaert DE, van Almen GC, Talacua H, et al. Early in-situ cellularization of a supramolecular vascular graft is modified by synthetic stromal cell-derived factor-1alpha derived peptides. *Biomaterials*. 2016;76:187-95.
26. Duijvelshoff R, van Engeland NCA, Gabriels KMR, et al. Host Response and Neo-Tissue Development during Resorption of a Fast Degrading Supramolecular Electrospun Arterial Scaffold. *Bioengineering (Basel)*. 2018;5(3).
27. Kim TH, Kim SH, Leong KW, et al. Nanografted Substrata and Triculture of Human Pericytes, Fibroblasts, and Endothelial Cells for Studying the Effects on Angiogenesis. *Tissue Eng Part A*. 2016;22(7-8):698-706.
28. Damanik FFR, Spadolini G, Rotmans J, et al. Biological activity of human mesenchymal stromal cells on polymeric electrospun scaffolds. *Biomater Sci*. 2019;7(3):1088-100.
29. Ren L, Ma D, Liu B, et al. Preparation of three-dimensional vascularized MSC cell sheet constructs for tissue regeneration. *Biomed Res Int*. 2014;2014:301279.
30. Zhang L, Qian Z, Tahtinen M, et al. Prevascularization of natural nanofibrous extracellular matrix for engineering completely biological three-dimensional prevascularized tissues for diverse applications. *J Tissue Eng Regen Med*. 2018;12(3):e1325-e36.
31. Tian X, Brookes O, Battaglia G. Pericytes from Mesenchymal Stem Cells as a model for the blood-brain barrier. *Sci Rep*. 2017;7:39676.
32. Blocki A, Wang Y, Koch M, et al. Not all MSCs can act as pericytes: functional in vitro assays to distinguish pericytes from other mesenchymal stem cells in angiogenesis. *Stem Cells Dev*. 2013;22(17):2347-55.
33. Corselli M, Chen CW, Sun B, et al. The tunica adventitia of human arteries and veins as a source of mesenchymal stem cells. *Stem Cells Dev*. 2012;21(8):1299-308.
34. Armulik A, Abramsson A, Betsholtz C. Endothelial/pericyte interactions. *Circ Res*. 2005;97(6):512-23.
35. Mills SJ, Cowin AJ, Kaur P. Pericytes, mesenchymal stem cells and the wound healing process. *Cells*. 2013;2(3):621-34.
36. Lemos DR, Marsh G, Huang A, et al. Maintenance of vascular integrity by pericytes is essential for normal kidney function. *Am J Physiol Renal Physiol*. 2016;311(6):F1230-F42.
37. Morin KT, Dries-Devlin JL, Tranquillo RT. Engineered microvessels with strong alignment and high lumen density via cell-induced fibrin gel compaction and interstitial flow. *Tissue Eng Part A*. 2014;20(3-4):553-65.

38. Eglinger J, Karsjens H, Lammert E. Quantitative assessment of angiogenesis and pericyte coverage in human cell-derived vascular sprouts. *Inflamm Regen*. 2017;37:2.
39. Lindahl P, Johansson BR, Leveen P, et al. Pericyte loss and microaneurysm formation in PDGF-B-deficient mice. *Science*. 1997;277(5323):242-5.
40. Chen Z, Xu XH, Hu J. Role of pericytes in angiogenesis: focus on cancer angiogenesis and anti-angiogenic therapy. *Neoplasma*. 2016;63(2):173-82.
41. Blanco R, Gerhardt H. VEGF and Notch in tip and stalk cell selection. *Cold Spring Harb Perspect Med*. 2013;3(1):a006569.
42. Gaengel K, Genove G, Armulik A, et al. Endothelial-mural cell signaling in vascular development and angiogenesis. *Arterioscler Thromb Vasc Biol*. 2009;29(5):630-8.
43. Draoui N, de Zeeuw P, Carmeliet P. Angiogenesis revisited from a metabolic perspective: role and therapeutic implications of endothelial cell metabolism. *Open Biol*. 2017;7(12).
44. Carmeliet P. Mechanisms of angiogenesis and arteriogenesis. *Nat Med*. 2000;6(4):389-95.
45. Nehls V, Denzer K, Drenckhahn D. Pericyte involvement in capillary sprouting during angiogenesis in situ. *Cell Tissue Res*. 1992;270(3):469-74.
46. Amselgruber WM, Schafer M, Sinowatz F. Angiogenesis in the bovine corpus luteum: an immunocytochemical and ultrastructural study. *Anat Histol Embryol*. 1999;28(3):157-66.
47. Enge M, Bjarnegard M, Gerhardt H, et al. Endothelium-specific platelet-derived growth factor-B ablation mimics diabetic retinopathy. *EMBO J*. 2002;21(16):4307-16.
48. Benjamin LE, Hemo I, Keshet E. A plasticity window for blood vessel remodelling is defined by pericyte coverage of the preformed endothelial network and is regulated by PDGF-B and VEGF. *Development*. 1998;125(9):1591-8.
49. Bjarnegard M, Enge M, Norlin J, et al. Endothelium-specific ablation of PDGFB leads to pericyte loss and glomerular, cardiac and placental abnormalities. *Development*. 2004;131(8):1847-57.
50. Antonelli-Orlidge A, Saunders KB, Smith SR, et al. An activated form of transforming growth factor beta is produced by cocultures of endothelial cells and pericytes. *Proc Natl Acad Sci U S A*. 1989;86(12):4544-8.
51. Akhurst RJ, Lehnert SA, Faissner A, et al. TGF beta in murine morphogenetic processes: the early embryo and cardiogenesis. *Development*. 1990;108(4):645-56.
52. Shull MM, Ormsby I, Kier AB, et al. Targeted disruption of the mouse transforming growth factor-beta 1 gene results in multifocal inflammatory disease. *Nature*. 1992;359(6397):693-9.
53. Augustin HG, Koh GY, Thurston G, et al. Control of vascular morphogenesis and homeostasis through the angiopoietin-Tie system. *Nat Rev Mol Cell Biol*. 2009;10(3):165-77.
54. Fuxe J, Tabruyn S, Colton K, et al. Pericyte requirement for anti-leak action of angiopoietin-1 and vascular remodeling in sustained inflammation. *Am J Pathol*. 2011;178(6):2897-909.
55. Schuchardt M, Tolle M, Prufer J, et al. Pharmacological relevance and potential of sphingosine 1-phosphate in the vascular system. *Br J Pharmacol*. 2011;163(6):1140-62.
56. Bobbie MW, Roy S, Trudeau K, et al. Reduced connexin 43 expression and its effect on the development of vascular lesions in retinas of diabetic mice. *Invest Ophthalmol Vis Sci*. 2010;51(7):3758-63.

57. Diaz-Flores L, Gutierrez R, Varela H, et al. Microvascular pericytes: a review of their morphological and functional characteristics. *Histol Histopathol*. 1991;6(2):269-86.
58. Okamoto T, Usuda H, Tanaka T, et al. The Functional Implications of Endothelial Gap Junctions and Cellular Mechanics in Vascular Angiogenesis. *Cancers (Basel)*. 2019;11(2).
59. Potente M, Gerhardt H, Carmeliet P. Basic and therapeutic aspects of angiogenesis. *Cell*. 2011;146(6):873-87.
60. Gerhardt H, Betsholtz C. Endothelial-pericyte interactions in angiogenesis. *Cell Tissue Res*. 2003;314(1):15-23.
61. Herndon JM, Tome ME, Davis TP. Chapter 9 - Development and Maintenance of the Blood-Brain Barrier. In: Caplan LR, Biller J, Leary MC, Lo EH, Thomas AJ, Yenari M, Zhang JH, editors. *Primer on Cerebrovascular Diseases (Second Edition)*. San Diego: Academic Press; 2017. p. 51-6.
62. Shepro D, Morel NM. Pericyte physiology. *FASEB J*. 1993;7(11):1031-8.
63. Epling GP. Electron microscopic observations of pericytes of small blood vessels in the lungs and hearts of normal cattle and swine. *The Anatomical Record*. 1966;155(4):513-29.
64. Dore-Duffy P, Cleary K. Morphology and properties of pericytes. *Methods Mol Biol*. 2011;686:49-68.
65. Bergwerff M, Verberne ME, DeRuiter MC, et al. Neural crest cell contribution to the developing circulatory system: implications for vascular morphology? *Circulation research*. 1998;82(2):221-31.
66. Etchevers HC, Vincent C, Le Douarin NM, et al. The cephalic neural crest provides pericytes and smooth muscle cells to all blood vessels of the face and forebrain. *Development*. 2001;128(7):1059-68.
67. Sims DE. The pericyte--a review. *Tissue Cell*. 1986;18(2):153-74.
68. Smyth LCD, Rustenhoven J, Scotter EL, et al. Markers for human brain pericytes and smooth muscle cells. *J Chem Neuroanat*. 2018;92:48-60.
69. Crouch EE, Doetsch F. FACS isolation of endothelial cells and pericytes from mouse brain microregions. *Nat Protoc*. 2018;13(4):738-51.
70. Daneman R, Zhou L, Kebede AA, et al. Pericytes are required for blood-brain barrier integrity during embryogenesis. *Nature*. 2010;468(7323):562-6.
71. Kisler K, Nelson AR, Rege SV, et al. Pericyte degeneration leads to neurovascular uncoupling and limits oxygen supply to brain. *Nat Neurosci*. 2017;20(3):406-16.
72. Hall CN, Reynell C, Gesslein B, et al. Capillary pericytes regulate cerebral blood flow in health and disease. *Nature*. 2014;508(7494):55-60.
73. Rucker HK, Wynder HJ, Thomas WE. Cellular mechanisms of CNS pericytes. *Brain Res Bull*. 2000;51(5):363-9.
74. Bell RD, Winkler EA, Sagare AP, et al. Pericytes control key neurovascular functions and neuronal phenotype in the adult brain and during brain aging. *Neuron*. 2010;68(3):409-27.
75. Sengillo JD, Winkler EA, Walker CT, et al. Deficiency in mural vascular cells coincides with blood-brain barrier disruption in Alzheimer's disease. *Brain Pathol*. 2013;23(3):303-10.
76. Park TI, Feisst V, Brooks AE, et al. Cultured pericytes from human brain show phenotypic and functional differences associated with differential CD90 expression. *Sci Rep*. 2016;6:26587.

77. Kupffer Cv. Ueber Sternzellen der Leber. *Archiv für mikroskopische Anatomie*. 1876;12(1):353-8.
78. Zaret KS. Regulatory phases of early liver development: paradigms of organogenesis. *Nat Rev Genet*. 2002;3(7):499-512.
79. Loo CK, Wu XJ. Origin of stellate cells from submesothelial cells in a developing human liver. *Liver Int*. 2008;28(10):1437-45.
80. Gerlach JC, Over P, Turner ME, et al. Perivascular mesenchymal progenitors in human fetal and adult liver. *Stem Cells Dev*. 2012;21(18):3258-69.
81. Carotti S, Morini S, Corradini SG, et al. Glial fibrillary acidic protein as an early marker of hepatic stellate cell activation in chronic and posttransplant recurrent hepatitis C. *Liver Transpl*. 2008;14(6):806-14.
82. Geerts A. History, heterogeneity, developmental biology, and functions of quiescent hepatic stellate cells. *Semin Liver Dis*. 2001;21(3):311-35.
83. Shang L, Hosseini M, Liu X, et al. Human hepatic stellate cell isolation and characterization. *J Gastroenterol*. 2018;53(1):6-17.
84. Blaner WS, O'Byrne SM, Wongsiriroj N, et al. Hepatic stellate cell lipid droplets: a specialized lipid droplet for retinoid storage. *Biochim Biophys Acta*. 2009;1791(6):467-73.
85. Hellerbrand C. Hepatic stellate cells--the pericytes in the liver. *Pflugers Arch*. 2013;465(6):775-8.
86. Musso O, Theret N, Campion JP, et al. In situ detection of matrix metalloproteinase-2 (MMP2) and the metalloproteinase inhibitor TIMP2 transcripts in human primary hepatocellular carcinoma and in liver metastasis. *J Hepatol*. 1997;26(3):593-605.
87. Rockey DC. Characterization of endothelin receptors mediating rat hepatic stellate cell contraction. *Biochemical and biophysical research communications*. 1995;207(2):725-31.
88. Chen L, Zhang W, Zhou QD, et al. HSCs play a distinct role in different phases of oval cell-mediated liver regeneration. *Cell Biochem Funct*. 2012;30(7):588-96.
89. Reynaert H, Urbain D, Geerts A. Regulation of sinusoidal perfusion in portal hypertension. *The Anatomical Record: Advances in Integrative Anatomy and Evolutionary Biology: Advances in Integrative Anatomy and Evolutionary Biology*. 2008;291(6):693-8.
90. Reynaert H, Thompson MG, Thomas T, et al. Hepatic stellate cells: role in microcirculation and pathophysiology of portal hypertension. *Gut*. 2002;50(4):571-81.
91. Higashi T, Friedman SL, Hoshida Y. Hepatic stellate cells as key target in liver fibrosis. *Adv Drug Deliv Rev*. 2017;121:27-42.
92. Friedman SL. Molecular regulation of hepatic fibrosis, an integrated cellular response to tissue injury. *Journal of Biological Chemistry*. 2000;275(4):2247-50.
93. D'Ambrosio DN, Walewski JL, Clugston RD, et al. Distinct populations of hepatic stellate cells in the mouse liver have different capacities for retinoid and lipid storage. *PLoS one*. 2011;6(9).
94. Pannabecker TL. Renal vascular pericytes: long overlooked and poorly understood, but clearly important, and what about those regulatory pathways? *Am J Physiol Renal Physiol*. 2018;314(1):F67-F9.
95. Smith SW, Chand S, Savage CO. Biology of the renal pericyte. *Nephrol Dial Transplant*. 2012;27(6):2149-55.

96. Mugford JW, Sipila P, McMahon JA, et al. Osr1 expression demarcates a multi-potent population of intermediate mesoderm that undergoes progressive restriction to an Osr1-dependent nephron progenitor compartment within the mammalian kidney. *Dev Biol.* 2008;324(1):88-98.
97. Lin S-L, Kisseleva T, Brenner DA, et al. Pericytes and perivascular fibroblasts are the primary source of collagen-producing cells in obstructive fibrosis of the kidney. *The American journal of pathology.* 2008;173(6):1617-27.
98. Rojas A, Chang FC, Lin SL, et al. The role played by perivascular cells in kidney interstitial injury. *Clin Nephrol.* 2012;77(5):400-8.
99. Pan SY, Chang YT, Lin SL. Microvascular pericytes in healthy and diseased kidneys. *Int J Nephrol Renovasc Dis.* 2014;7:39-48.
100. Testagrossa L, Azevedo Neto R, Resende A, et al. Immunohistochemical expression of podocyte markers in the variants of focal segmental glomerulosclerosis. *Nephrol Dial Transplant.* 2013;28(1):91-8.
101. Brunskill EW, Georgas K, Rumballe B, et al. Defining the molecular character of the developing and adult kidney podocyte. *PLoS One.* 2011;6(9):e24640.
102. Ferland-McCollough D, Slater S, Richard J, et al. Pericytes, an overlooked player in vascular pathobiology. *Pharmacol Ther.* 2017;171:30-42.
103. Vaughan MR, Quaggin SE. How do mesangial and endothelial cells form the glomerular tuft? *J Am Soc Nephrol.* 2008;19(1):24-33.
104. Reiser J, Altintas MM. Podocytes. *F1000Res.* 2016;5.
105. Kurihara H, Anderson JM, Farquhar MG. Diversity among tight junctions in rat kidney: glomerular slit diaphragms and endothelial junctions express only one isoform of the tight junction protein ZO-1. *Proceedings of the National Academy of Sciences.* 1992;89(15):7075-9.
106. Kriz W, Hackenthal E, Nobiling R, et al. A role for podocytes to counteract capillary wall distension. *Kidney international.* 1994;45(2):369-76.
107. Schlondorff D, Banas B. The mesangial cell revisited: no cell is an island. *J Am Soc Nephrol.* 2009;20(6):1179-87.
108. Ausiello DA, Kreisberg JI, Roy C, et al. Contraction of cultured rat glomerular cells of apparent mesangial origin after stimulation with angiotensin II and arginine vasopressin. *The Journal of clinical investigation.* 1980;65(3):754-60.
109. Savin VJ. In vitro effects of angiotensin II on glomerular function. *American Journal of Physiology-Renal Physiology.* 1986;251(4):F627-F34.
110. Kennedy-Lydon TM, Crawford C, Wildman SS, et al. Renal pericytes: regulators of medullary blood flow. *Acta Physiol (Oxf).* 2013;207(2):212-25.
111. Pallone TL, Silldorff EP. Pericyte regulation of renal medullary blood flow. *Exp Nephrol.* 2001;9(3):165-70.
112. Park F, Mattson DL, Roberts LA, et al. Evidence for the presence of smooth muscle alpha-actin within pericytes of the renal medulla. *Am J Physiol.* 1997;273(5):R1742-8.
113. Stefanska A, Peault B, Mullins JJ. Renal pericytes: multifunctional cells of the kidneys. *Pflugers Arch.* 2013;465(6):767-73.
114. Kramann R, Wongboonsin J, Chang-Panesso M, et al. Gli1(+) Pericyte Loss Induces Capillary Rarefaction and Proximal Tubular Injury. *J Am Soc Nephrol.* 2017;28(3):776-84.

115. Kramann R, Schneider RK, DiRocco DP, et al. Perivascular Gli1+ progenitors are key contributors to injury-induced organ fibrosis. *Cell Stem Cell*. 2015;16(1):51-66.
116. Souma T, Yamazaki S, Moriguchi T, et al. Plasticity of renal erythropoietin-producing cells governs fibrosis. *J Am Soc Nephrol*. 2013;24(10):1599-616.
117. Asada N, Takase M, Nakamura J, et al. Dysfunction of fibroblasts of extrarenal origin underlies renal fibrosis and renal anemia in mice. *J Clin Invest*. 2011;121(10):3981-90.
118. Stefanska A, Kenyon C, Christian HC, et al. Human kidney pericytes produce renin. *Kidney Int*. 2016;90(6):1251-61.
119. Hung C, Linn G, Chow YH, et al. Role of lung pericytes and resident fibroblasts in the pathogenesis of pulmonary fibrosis. *Am J Respir Crit Care Med*. 2013;188(7):820-30.
120. Weibel ER. On pericytes, particularly their existence on lung capillaries. *Microvasc Res*. 1974;8(2):218-35.
121. Bagley RG, Weber W, Rouleau C, et al. Pericytes and endothelial precursor cells: cellular interactions and contributions to malignancy. *Cancer Res*. 2005;65(21):9741-50.
122. Hung CF, Mittelsteadt KL, Brauer R, et al. Lung pericyte-like cells are functional interstitial immune sentinel cells. *Am J Physiol Lung Cell Mol Physiol*. 2017;312(4):L556-L67.
123. Wilson CL, Stephenson SE, Higuero JP, et al. Characterization of human PDGFR-beta-positive pericytes from IPF and non-IPF lungs. *Am J Physiol Lung Cell Mol Physiol*. 2018;315(6):L991-L1002.
124. Yuan K, Orcholski ME, Panaroni C, et al. Activation of the Wnt/planar cell polarity pathway is required for pericyte recruitment during pulmonary angiogenesis. *Am J Pathol*. 2015;185(1):69-84.
125. Rock JR, Barkauskas CE, Cronce MJ, et al. Multiple stromal populations contribute to pulmonary fibrosis without evidence for epithelial to mesenchymal transition. *Proc Natl Acad Sci U S A*. 2011;108(52):E1475-83.
126. Ricard N, Tu L, Le Hires M, et al. Increased pericyte coverage mediated by endothelial-derived fibroblast growth factor-2 and interleukin-6 is a source of smooth muscle-like cells in pulmonary hypertension. *Circulation*. 2014;129(15):1586-97.
127. Ogura S, Kurata K, Hattori Y, et al. Sustained inflammation after pericyte depletion induces irreversible blood-retina barrier breakdown. *JCI Insight*. 2017;2(3):e90905.
128. Gaskill CF, Carrier EJ, Kropski JA, et al. Disruption of lineage specification in adult pulmonary mesenchymal progenitor cells promotes microvascular dysfunction. *J Clin Invest*. 2017;127(6):2262-76.
129. Rowley JE, Johnson JR. Pericytes in chronic lung disease. *Int Arch Allergy Immunol*. 2014;164(3):178-88.
130. Nees S, Weiss DR, Senftl A, et al. Isolation, bulk cultivation, and characterization of coronary microvascular pericytes: the second most frequent myocardial cell type in vitro. *American Journal of Physiology-Heart and Circulatory Physiology*. 2012;302(1):H69-H84.
131. Cai CL, Martin JC, Sun Y, et al. A myocardial lineage derives from Tbx18 epicardial cells. *Nature*. 2008;454(7200):104-8.
132. Al Haj CPCD, Zen A, Beltrami AP, Krankel N, Katare R, Angelini G, Emanuelli C, Madeddu P. Human adult vena saphena contains perivascular progenitor cells endowed with clonogenic and proangiogenic potential. *Circulation*. 2010;121:1735-45.

133. Nees S, Juchem G, Eberhorn N, et al. Wall structures of myocardial precapillary arterioles and postcapillary venules reexamined and reconstructed in vitro for studies on barrier functions. *American Journal of Physiology-Heart and Circulatory Physiology*. 2012;302(1):H51-H68.
134. Juchem G, Weiss DR, Gansera B, et al. Pericytes in the macrovascular intima: possible physiological and pathogenetic impact. *American Journal of Physiology-Heart and Circulatory Physiology*. 2010;298(3):H754-H70.
135. Tigges U, Komatsu M, Stallcup WB. Adventitial pericyte progenitor/mesenchymal stem cells participate in the restenotic response to arterial injury. *J Vasc Res*. 2013;50(2):134-44.
136. Chen WC, Baily JE, Corselli M, et al. Human myocardial pericytes: multipotent mesodermal precursors exhibiting cardiac specificity. *Stem Cells*. 2015;33(2):557-73.
137. Avolio E, Rodriguez-Arabaolaza I, Spencer HL, et al. Expansion and characterization of neonatal cardiac pericytes provides a novel cellular option for tissue engineering in congenital heart disease. *J Am Heart Assoc*. 2015;4(6):e002043.
138. Lee LL, Chintalgattu V. Pericytes in the Heart. *Pericyte Biology in Different Organs*: Springer; 2019. p. 187-210.
139. Hellstrom M, Gerhardt H, Kalen M, et al. Lack of pericytes leads to endothelial hyperplasia and abnormal vascular morphogenesis. *J Cell Biol*. 2001;153(3):543-53.
140. Yang G, Mahadik B, Choi JYJ, et al. Vascularization in tissue engineering: fundamentals and state-of-art. *Progress in Biomedical Engineering*. 2019;2.
141. Song HG, Rumma RT, Ozaki CK, et al. Vascular Tissue Engineering: Progress, Challenges, and Clinical Promise. *Cell Stem Cell*. 2018;22(3):340-54.
142. Nichol JW, Khademhosseini A. Modular Tissue Engineering: Engineering Biological Tissues from the Bottom Up. *Soft Matter*. 2009;5(7):1312-9.
143. Elbert DL. Bottom-up tissue engineering. *Curr Opin Biotechnol*. 2011;22(5):674-80.
144. Nemen-Guanzon JG, Lee S, Berg JR, et al. Trends in tissue engineering for blood vessels. *J Biomed Biotechnol*. 2012;2012:956345.
145. O'Brien FJ. Biomaterials & scaffolds for tissue engineering. *Materials Today*. 2011;14(3):88-95.
146. Wang WY, Lin D, Jarman EH, et al. Functional angiogenesis requires microenvironmental cues balancing endothelial cell migration and proliferation. *Lab Chip*. 2020;20(6):1153-66.
147. Nichol JW, Koshy ST, Bae H, et al. Cell-laden microengineered gelatin methacrylate hydrogels. *Biomaterials*. 2010;31(21):5536-44.
148. van Dijk CGM, Brandt MM, Poulis N, et al. A new microfluidic model that allows monitoring of complex vascular structures and cell interactions in a 3D biological matrix. *Lab Chip*. 2020.
149. Homan KA, Kolesky DB, Skylar-Scott MA, et al. Bioprinting of 3D Convulated Renal Proximal Tubules on Perfusable Chips. *Sci Rep*. 2016;6:34845.
150. Miller JS, Stevens KR, Yang MT, et al. Rapid casting of patterned vascular networks for perfusable engineered three-dimensional tissues. *Nature materials*. 2012;11(9):768-74.
151. Hong J, Yeo M, Yang GH, et al. Cell-Electrospinning and Its Application for Tissue Engineering. *Int J Mol Sci*. 2019;20(24).

152. Tan RP, Chan AH, Lennartsson K, et al. Integration of induced pluripotent stem cell-derived endothelial cells with polycaprolactone/gelatin-based electrospun scaffolds for enhanced therapeutic angiogenesis. *Stem cell research & therapy*. 2018;9(1):70.
153. Ovsianikov A, Schlie S, Ngezahayo A, et al. Two-photon polymerization technique for microfabrication of CAD-designed 3D scaffolds from commercially available photosensitive materials. *J Tissue Eng Regen Med*. 2007;1(6):443-9.
154. Meyer W, Engelhardt S, Novosel E, et al. Soft Polymers for Building up Small and Smallest Blood Supplying Systems by Stereolithography. *J Funct Biomater*. 2012;3(2):257-68.
155. Huber B, Engelhardt S, Meyer W, et al. Blood-Vessel Mimicking Structures by Stereolithographic Fabrication of Small Porous Tubes Using Cytocompatible Polyacrylate Elastomers, Biofunctionalization and Endothelialization. *J Funct Biomater*. 2016;7(2).
156. Applegate MB, Coburn J, Partlow BP, et al. Laser-based three-dimensional multiscale micropatterning of biocompatible hydrogels for customized tissue engineering scaffolds. *Proc Natl Acad Sci U S A*. 2015;112(39):12052-7.
157. Skylar-Scott MA, Liu MC, Wu Y, et al. Guided Homing of Cells in Multi-Photon Microfabricated Bioscaffolds. *Adv Healthc Mater*. 2016;5(10):1233-43.
158. Grebenyuk S, Ranga A. Engineering Organoid Vascularization. *Front Bioeng Biotechnol*. 2019;7:39.
159. Zhu W, Qu X, Zhu J, et al. Direct 3D bioprinting of prevascularized tissue constructs with complex microarchitecture. *Biomaterials*. 2017;124:106-15.
160. Kusuma S, Shen Y-I, Hanjaya-Putra D, et al. Self-organized vascular networks from human pluripotent stem cells in a synthetic matrix. *Proceedings of the National Academy of Sciences*. 2013;110(31):12601-6.
161. Heiss M, Hellström M, Kalén M, et al. Endothelial cell spheroids as a versatile tool to study angiogenesis in vitro. *The FASEB Journal*. 2015;29(7):3076-84.
162. Korff T, Augustin HG. Integration of endothelial cells in multicellular spheroids prevents apoptosis and induces differentiation. *The Journal of cell biology*. 1998;143(5):1341-52.
163. Wimmer RA, Leopoldi A, Aichinger M, et al. Human blood vessel organoids as a model of diabetic vasculopathy. *Nature*. 2019;565(7740):505-10.
164. Noguchi R, Nakayama K, Itoh M, et al. Development of a three-dimensional prevascularized scaffold-free contractile cardiac patch for treating heart disease. *The Journal of Heart and Lung Transplantation*. 2016;35(1):137-45.
165. Okudaira T, Amimoto N, Mizumoto H, et al. Formation of three-dimensional hepatic tissue by the bottom-up method using spheroids. *Journal of bioscience and bioengineering*. 2016;122(2):213-8.
166. Redd MA, Zeinstra N, Qin W, et al. Patterned human microvascular grafts enable rapid vascularization and increase perfusion in infarcted rat hearts. *Nat Commun*. 2019;10(1):584.
167. Laschke MW, Spater T, Menger MD. Microvascular Fragments: More Than Just Natural Vascularization Units. *Trends Biotechnol*. 2020.
168. Laschke MW, Karschnia P, Scheuer C, et al. Effects of cryopreservation on adipose tissue-derived microvascular fragments. *J Tissue Eng Regen Med*. 2018;12(4):1020-30.
169. Frueh FS, Spater T, Scheuer C, et al. Isolation of Murine Adipose Tissue-derived Microvascular Fragments as Vascularization Units for Tissue Engineering. *J Vis Exp*. 2017(122).

170. Laschke MW, Menger MD. Adipose tissue-derived microvascular fragments: natural vascularization units for regenerative medicine. *Trends Biotechnol.* 2015;33(8):442-8.
171. Laschke MW, Kleer S, Scheuer C, et al. Vascularisation of porous scaffolds is improved by incorporation of adipose tissue-derived microvascular fragments. *Eur Cell Mater.* 2012;24:266-77.
172. Frueh FS, Spater T, Lindenblatt N, et al. Adipose Tissue-Derived Microvascular Fragments Improve Vascularization, Lymphangiogenesis, and Integration of Dermal Skin Substitutes. *J Invest Dermatol.* 2017;137(1):217-27.
173. Nunes SS, Krishnan L, Gerard CS, et al. Angiogenic potential of microvessel fragments is independent of the tissue of origin and can be influenced by the cellular composition of the implants. *Microcirculation.* 2010;17(7):557-67.
174. Shepherd BR, Hoying JB, Williams SK. Microvascular transplantation after acute myocardial infarction. *Tissue Eng.* 2007;13(12):2871-9.
175. Fu J, Wang D-A. In Situ Organ-Specific Vascularization in Tissue Engineering. *Trends in Biotechnology.* 2018;36(8):834-49.
176. Mastrullo V, Cathery W, Velliou E, et al. Angiogenesis in Tissue Engineering: As Nature Intended? *Frontiers in Bioengineering and Biotechnology.* 2020;8.
177. Pei J, Harakalova M, den Ruijter H, et al. Cardiorenal disease connection during post-menopause: The protective role of estrogen in uremic toxins induced microvascular dysfunction. *Int J Cardiol.* 2017;238:22-30.
178. Jourde-Chiche N, Dou L, Cerini C, et al. Vascular incompetence in dialysis patients--protein-bound uremic toxins and endothelial dysfunction. *Semin Dial.* 2011;24(3):327-37.
179. Diaz-Flores L, Gutierrez R, Gonzalez P, et al. Inducible perivascular cells contribute to the neochondrogenesis in grafted perichondrium. *Anat Rec.* 1991;229(1):1-8.
180. Supakul S, Yao K, Ochi H, et al. Pericytes as a Source of Osteogenic Cells in Bone Fracture Healing. *Int J Mol Sci.* 2019;20(5).
181. James AW, Zara JN, Corselli M, et al. Use of human perivascular stem cells for bone regeneration. *J Vis Exp.* 2012(63):e2952.
182. Tsigkou O, Pomerantseva I, Spencer JA, et al. Engineered vascularized bone grafts. *Proc Natl Acad Sci U S A.* 2010;107(8):3311-6.
183. Xu J, Li D, Hsu CY, et al. Comparison of skeletal and soft tissue pericytes identifies CXCR4(+) bone forming mural cells in human tissues. *Bone Res.* 2020;8:22.
184. Gokcinar-Yagci B, Uckan-Cetinkaya D, Celebi-Saltik B. Pericytes: Properties, Functions and Applications in Tissue Engineering. *Stem Cell Rev Rep.* 2015;11(4):549-59.
185. Avolio E, Alvino VV, Ghorbel MT, et al. Perivascular cells and tissue engineering: Current applications and untapped potential. *Pharmacol Ther.* 2017;171:83-92.
186. Melero-Martin JM, De Obaldia ME, Kang S-Y, et al. Engineering robust and functional vascular networks in vivo with human adult and cord blood-derived progenitor cells. *Circulation research.* 2008;103(2):194-202.
187. Peters EB, Christoforou N, Leong KW, et al. Poly (ethylene glycol) hydrogel scaffolds containing cell-adhesive and protease-sensitive peptides support microvessel formation by endothelial progenitor cells. *Cellular and molecular bioengineering.* 2016;9(1):38-54.
188. Rouwkema J, Westerweel PE, de Boer J, et al. The use of endothelial progenitor cells for prevascularized bone tissue engineering. *Tissue Engineering Part A.* 2009;15(8):2015-27.

189. Faal T, Phan DTT, Davtyan H, et al. Induction of Mesoderm and Neural Crest-Derived Pericytes from Human Pluripotent Stem Cells to Study Blood-Brain Barrier Interactions. *Stem Cell Reports*. 2019;12(3):451-60.
190. Stebbins MJ, Gastfriend BD, Canfield SG, et al. Human pluripotent stem cell-derived brain pericyte-like cells induce blood-brain barrier properties. *Sci Adv*. 2019;5(3):eaau7375.
191. Jamieson JJ, Linville RM, Ding YY, et al. Role of iPSC-derived pericytes on barrier function of iPSC-derived brain microvascular endothelial cells in 2D and 3D. *Fluids Barriers CNS*. 2019;16(1):15.
192. McDaniel JS, Pilia M, Ward CL, et al. Characterization and multilineage potential of cells derived from isolated microvascular fragments. *J Surg Res*. 2014;192(1):214-22.
193. Sundberg C, Kowanetz M, Brown LF, et al. Stable expression of angiopoietin-1 and other markers by cultured pericytes: phenotypic similarities to a subpopulation of cells in maturing vessels during later stages of angiogenesis in vivo. *Lab Invest*. 2002;82(4):387-401.
194. Chasseigneaux S, Moraca Y, Cochois-Guegan V, et al. Isolation and differential transcriptome of vascular smooth muscle cells and mid-capillary pericytes from the rat brain. *Sci Rep*. 2018;8(1):12272.
195. Lee LL, Khakoo AY, Chintalgattu V. Isolation and Purification of Murine Cardiac Pericytes. *J Vis Exp*. 2019(150).
196. Crisan M, Deasy B, Gavina M, et al. Purification and long-term culture of multipotent progenitor cells affiliated with the walls of human blood vessels: myoendothelial cells and pericytes. *Methods Cell Biol*. 2008;86:295-309.
197. Bryan BA, D'Amore PA. Pericyte isolation and use in endothelial/pericyte coculture models. *Methods Enzymol*. 2008;443:315-31.
198. Mirdamadi ES, Kalhori D, Zakeri N, et al. Liver Tissue Engineering as an Emerging Alternative for Liver Disease Treatment. *Tissue Eng Part B Rev*. 2020;26(2):145-63.
199. Kazemnejad S. Hepatic tissue engineering using scaffolds: state of the art. *Avicenna J Med Biotechnol*. 2009;1(3):135-45.
200. Ahmed HMM, Salerno S, Morelli S, et al. 3D liver membrane system by co-culturing human hepatocytes, sinusoidal endothelial and stellate cells. *Biofabrication*. 2017;9(2):025022.
201. Senoo H, Kojima N, Sato M. Vitamin A-storing cells (stellate cells). *Vitam Horm*. 2007;75:131-59.
202. Hussein KH, Park KM, Kang KS, et al. Heparin-gelatin mixture improves vascular reconstruction efficiency and hepatic function in bioengineered livers. *Acta Biomater*. 2016;38:82-93.
203. Katari R, Peloso A, Zamboni JP, et al. Renal bioengineering with scaffolds generated from human kidneys. *Nephron Exp Nephrol*. 2014;126(2):119.
204. Orlando G, Booth C, Wang Z, et al. Discarded human kidneys as a source of ECM scaffold for kidney regeneration technologies. *Biomaterials*. 2013;34(24):5915-25.
205. Lih E, Park W, Park KW, et al. A Bioinspired Scaffold with Anti-Inflammatory Magnesium Hydroxide and Decellularized Extracellular Matrix for Renal Tissue Regeneration. *ACS Cent Sci*. 2019;5(3):458-67.
206. Takasato M, Pei XE, Chiu HS, et al. Kidney organoids from human iPS cells contain multiple lineages and model human nephrogenesis. *Nature*. 2015;526(7574):564-8.

207. Morizane R, Lam AQ, Freedman BS, et al. Nephron organoids derived from human pluripotent stem cells model kidney development and injury. *Nature biotechnology*. 2015;33(11):1193.
208. Takasato M, Er P, Becroft M, et al. Directing human embryonic stem cell differentiation towards a renal lineage generates a self-organizing kidney. *Nature cell biology*. 2014;16(1):118-26.
209. Geuens T, van Blitterswijk CA, LaPointe VLS. Overcoming kidney organoid challenges for regenerative medicine. *NPJ Regen Med*. 2020;5:8.
210. Jafarkhani M, Salehi Z, Aidun A, et al. Bioprinting in Vascularization Strategies. *Iran Biomed J*. 2019;23(1):9-20.
211. Homan KA, Gupta N, Kroll KT, et al. Flow-enhanced vascularization and maturation of kidney organoids in vitro. *Nat Methods*. 2019;16(3):255-62.
212. Maghsoudlou P, Georgiades F, Tyraskis A, et al. Preservation of micro-architecture and angiogenic potential in a pulmonary acellular matrix obtained using intermittent intra-tracheal flow of detergent enzymatic treatment. *Biomaterials*. 2013;34(28):6638-48.
213. Cortiella J, Niles J, Cantu A, et al. Influence of acellular natural lung matrix on murine embryonic stem cell differentiation and tissue formation. *Tissue Engineering Part A*. 2010;16(8):2565-80.
214. Petersen TH, Calle EA, Zhao L, et al. Tissue-engineered lungs for in vivo implantation. *Science*. 2010;329(5991):538-41.
215. Schaefer JA, Guzman PA, Riemenschneider SB, et al. A cardiac patch from aligned microvessel and cardiomyocyte patches. *J Tissue Eng Regen Med*. 2018;12(2):546-56.
216. Riemenschneider SB, Mattia DJ, Wendel JS, et al. Inosculation and perfusion of pre-vascularized tissue patches containing aligned human microvessels after myocardial infarction. *Biomaterials*. 2016;97:51-61.
217. Invernici G, Emanuelli C, Madeddu P, et al. Human fetal aorta contains vascular progenitor cells capable of inducing vasculogenesis, angiogenesis, and myogenesis in vitro and in a murine model of peripheral ischemia. *Am J Pathol*. 2007;170(6):1879-92.
218. Barcelos LS, Duplax C, Krankel N, et al. Human CD133+ progenitor cells promote the healing of diabetic ischemic ulcers by paracrine stimulation of angiogenesis and activation of Wnt signaling. *Circ Res*. 2009;104(9):1095-102.
219. Alvino VV, Kilcooley M, Thomas AC, et al. In Vitro and In Vivo Preclinical Testing of Pericyte-Engineered Grafts for the Correction of Congenital Heart Defects. *J Am Heart Assoc*. 2020;9(4):e014214.
220. Qian Z, Sharma D, Jia W, et al. Engineering stem cell cardiac patch with microvascular features representative of native myocardium. *Theranostics*. 2019;9(8):2143-57.
221. Wei H-J, Chen C-H, Lee W-Y, et al. Bioengineered cardiac patch constructed from multilayered mesenchymal stem cells for myocardial repair. *Biomaterials*. 2008;29(26):3547-56.
222. Ji ST, Kim H, Yun J, et al. Promising Therapeutic Strategies for Mesenchymal Stem Cell-Based Cardiovascular Regeneration: From Cell Priming to Tissue Engineering. *Stem Cells Int*. 2017;2017:3945403.

CHAPTER

3



3D Human iPSC Blood Vessel Organoids as a Source of Flow- Adaptive Vascular Cells for Creating a Human-Relevant 3D-Scaffold Based Macrovessel Model

Elana M. Meijer, Suzanne E. Koch, Christian G.M. van Dijk, Renee G.C. Maas, Ihsan Chrifi, Wojciech Szymczyk, Paul J. Besseling, Lisa Pomp, Vera J.C.H. Koomen, Jan Willem Buikema, Carlijn V.C. Bouten, Marianne C. Verhaar, Anthal I.P.M. Smits, Caroline Cheng

Advanced Biology, 7(1), 2200137.

Abstract

Background

3D-scaffold based *in vitro* human tissue models accelerate disease studies and screening of pharmaceuticals while improving clinical translation of findings. Here, we report the use of human iPSC (hiPSC)-derived vascular organoid cells as a new cell source for the creation of an electrospun polycaprolactone-bisurea (PCL-BU) 3D-scaffold based, perfused human macrovessel model.

Methods

A separation protocol to obtain monocultures of organoid-derived endothelial cells (ODECs) and-mural cells (ODMCs) from hiPSC vascular organoids was developed. Shear stress response of ODECs versus HUVECs and barrier function (by trans-endothelial electrical resistance) were measured. PCL-BU scaffolds were seeded with ODECs and ODMCs and tissue organization and flow adaptation were evaluated in a perfused bioreactor system.

Results

ODECs and ODMCs harvested from vascular organoids can be cryopreserved and expanded without loss of cell purity and proliferative capacity. ODECs are shear stress responsive and establish a functional barrier that self-restores after thrombin challenge. Static bioreactor culture of ODECs/ODMCs seeded scaffolds results in a biomimetic vascular bi-layer hierarchy, which is preserved under laminar flow similar to scaffolds seeded with primary vascular cells.

Conclusion

Human iPSC-derived vascular organoids can be used as a source of functional, flow-adaptive vascular cells for the creation of 3D-scaffold based human macrovascular models.

Introduction

Cardiovascular disease (CVD) is a leading cause of death and morbidity with rising prevalence in Western and Westernized countries¹. One of the principal disease mechanisms of CVD is the adverse, functional, and structural adaptation of the vascular tissue, leading to clinical complications including myocardial infarction, ischemia, stroke and aneurysms [1]. Studies based on human samples and animal experiments have contributed considerably to build our understanding of the pathways and mechanisms that drive pathological adaptation in CVD. Nevertheless, the involvement of multiple dynamic factors in CVD that interact in complex cross-cell type systems, as well as the fact that animal models are limited in their capacity to mimic the full human disease condition on a physiological and biological level²⁻⁴, considerably restrict the translatability of these findings to the clinic. Similarly, the growing demand for synthetic 3D vascular scaffolds for surgical replacement of diseased arteries in CVD patients, increasingly recognizes the value of the optimization of scaffold prototypes in *in vitro* bioreactor setups before testing the most improved design in animal studies. In particular, for the emerging field of scaffold based *in situ* tissue engineering, in which the material design is adapted to exploit the regenerative potential of autologous cells in the host's body to stimulate tissue formation, the step of *ex vivo* evaluation in high complexity bioreactor models could considerably reduce development costs associated with direct animal testing⁵⁻⁷. Human focussed *in vitro* vascular models could also aid in reducing the use of animals in research and improve the translational value of findings. Vascular models that combine cells with biomaterial scaffolds *in vitro* provide valuable simulates of the *in vivo* condition to study cell behaviour in disease and tissue generation, in a controlled manner that allows systematic evaluation of the impact of individual biological and mechanical cues. Although most *in vitro* models only rely on established 2D culture techniques, the introduction of biomaterials in combination with solution electrospinning (SES) that allows 3D-scaffold designs that mimic the properties of the ECM environment of the vessel wall, may provide improved models that better recapitulate native *in situ* cell behaviour. This, combined with advancement in the fluidics and bioreactor research field may enable perfused culture of 3D-scaffold based vessels and thus the introduction of fluid forces to the models, enabling the study of the role of haemodynamics in driving vascular disease as well as its impact on vascular regeneration.

To increase human relevance, human induced-pluripotent stem cells (hiPSCs) may be used as an autologous cell source for 3D-scaffold based vascular models. hiPSCs bypass the ethical dilemmas surrounding the use of embryonic stem cells

and can be differentiated in any specialized cell type including vascular cells^{8,9}, while the required dermal fibroblast or peripheral blood mononuclear cells for iPSC reprogramming can be easily sourced from healthy donors or CVD patients. The use of patient derived hiPSC in this setting also opens the door to complex human *in vitro* modeling of genetic vascular disease and offers a more direct translational alternative to mouse genetic disease models, as well as providing an *ex vivo* testing platform to adapt scaffold design for any negative impact of mutations on the patient's autologous regenerative capacity *in situ*. *In vitro* tissue engineered human vessels (TEHV) such as rolled cell-sheets based constructs in hydrogel¹⁰, or ePTFE, silicone or PGA scaffolds seeded with primary vascular cells have already demonstrated the feasibility of these systems in mimicking native cellular responses after exposure to mechanical and biological stimuli in bioreactor systems^{11,12}.

Different culture methods for the generation of only iPSC-derived endothelial cells (ECs) or only iPSC-derived mural cells (MCs) have been previously described^{8,9,13-20}, with each study reporting a different set of cell qualities and applications. It was previously shown that iPSC-derived ECs could display similar characteristics of primary endothelial cells in terms of morphology, junction formation, barrier function and shear stress response^{21,22}. For iPSC derived MCs, differentiation protocols typically generate smooth muscle-like cells that were similar to human aortic vascular smooth muscle cells (VSMCs) in terms of gene expression patterns, morphology, vascular cell marker expression and *in vitro* functional properties^{20,23}. Although iPSC derived vascular cells are now frequently used in 2D culture studies, only a very limited number of studies have tested their application creating hierarchically organized 3D-scaffold based blood vessels²⁴⁻²⁶. More importantly, reports that demonstrate the combined application of both hiPSC-ECs and hiPSC-MCs for the creation of a complex *in vitro* 3D-scaffold based human perfused blood vessel model, is currently lacking.

Here we aim to investigate the use of vascular cells from hiPSC-derived vascular organoids, as a cell source for the creation of 3D-scaffold based, biomimetic human blood vessel model in a perfused bioreactor system. Based on the protocol published by Wimmer *et al.*, these blood vessel organoids are composed of endothelial cells and mural cells that self-assemble into vascular networks enveloped by a basement membrane. Vascular differentiation from the mesoderm phase takes place in a 3D environment in which the EC and MC lineages can establish during natural interaction between the different cell types, instead of differentiation in cell type specific isolated cultures²⁷. Used in our pipeline this eliminates the need for establishing and maintaining two separate hiPSC-differentiation cultures. Pools of hiPSCs vascular

organoid derived ECs and VSMCs can be harvested and expanded in traditional 2D culture without reduction in cell survival and proliferation capacity or loss of cell phenotype. The capacity of organoid derived ECs (ODECs) to respond to shear stress and to establish and regulate endothelial barrier function was demonstrated in 2D assays. ODECs and organoid derived mural cells (ODMCs) were capable to grow and form native-like hierarchical vascular tissue in SES polycaprolactone-bisurea (PCL-BU) 3D-vascular scaffolds comparable to human primary vascular cells. ODECs and ODMCs derived human vessels preserved native-like tissue organization in response to hemodynamic exposure when tested in a previously published perfused bioreactor set-up²⁸.

Methods

Cell culture

Derivation and culture of human iPSCs

The hiPSCs (SCVI273) used in this study were kindly donated by the Joseph Wu Lab (Stanford Medicine, Department of Medicine and Radiology, Stanford CVI Biobank). Sendai viral reprogramming was used to generate all hiPSC lines from peripheral blood mononuclear cells obtained from individuals who gave informed consent under protocols approved by the Stanford University Human Subjects Research Institutional Review Board as described previously²⁹. The hiPSC were non-enzymatically passaged using 0.5 mM EDTA (Invitrogen) every 4 days. HiPSC clumps were passaged in a splitting ratio of 1:13 routinely at 80% confluence. Cells were plated in matrigel-coated 12-well plates and supplemented with E8 medium. Medium was changed every day. To improve cell survival, split ratio reliability and to reduce selective pressure, 1:2000 ROCK inhibitor (Calbiochem) was used in the first 24 h.

Vascular organoid differentiation

HiPSCs were harvested using EDTA and subsequently resuspended in differentiation medium (Dulbecco's modified Eagle's culture medium (DMEM): F12, 20% KnockOut Serum (KOSR), 1% Penicillin Streptomycin (PS), Glutamax and non-essential amino acids (NEAA; all Gibco), including 50 μM ROCK-inhibitor Y-27632 (Calbiochem). A schematic overview of the differentiation process is displayed in Figure 1a. Cells were plated into an ultra-low attachment six-well plate (Corning), in a final concentration of 2×10^5 cells per well. Cells were incubated on a shaker plate at 37°C for 2 h to form aggregates and subsequently transferred to hypoxic conditions (5% O₂). Cell aggregates were treated with 13 μM GSK-3 inhibitor CHIR99021 (Tocris) on

day 3. On day 5, 7 and 9, the aggregates were treated with bone morphogenetic protein 4 (BMP4) (30 ng/mL; Stemcell Technologies), vascular endothelial growth factor A (VEGF-A) (30 ng/mL; Peprotech) and fibroblast growth factor 2 (FGF-2) (30 ng/mL; Miltenyi Biotec) to promote the vascular lineage. On day 11, medium was supplemented with VEGF-A (30 ng/mL), FGF-2 (30 ng/mL) and transforming growth factor β (TGF β)-inhibitor SB43152 (10 μ M; Stemcell Technologies) to increase the yield of endothelial cells and suppress excessive differentiation into mesenchymal/mural like cells. The aggregates were collected on day 13, embedded in a 3:1 matrigel:collagen mixture (Atelocollagen Bovine Dermis 3 mg/mL, Bio-connect) and supplemented with differentiation medium containing 15% fetal bovine serum (FBS), VEGF-A (100 ng/mL) and FGF-2 (100 ng/mL). Medium was changed every other day. Vascular organoids were collected on day 18 and either disaggregated for further experiments or cultured in a 96-wells round bottom plate without ECM support to stimulate self-assemble into spheroid-shaped vascular organoids.

Organoid-derived cell culture

Organoid-derived mural cells (ODMCs) and organoid-derived endothelial cells (ODECs) were labeled P0 directly after sorting (described in section "MACS" below). ODMCs were cultured on SMGM2 medium (Lonza) and ODECs were cultured on EGM2 medium (Lonza) supplemented with TGF β -inhibitor SB43152 (10 μ M) and medium was changed every other day. Cells were passaged for expansion using Trypsin/EDTA (Gibco). Cells were harvested at P4 and stored in liquid nitrogen in medium supplemented with 10% FBS and 10% DMSO. Both ODMCs and ODECs were cultured in gelatin coated dishes at 37°C with 5% CO₂ after thawing and used in experiments till the 7th passage.

Primary cell culture

For control experiments, primary human umbilical vein endothelial cells (HUVECs) were purchased from Lonza and maintained in EGM2 medium with 1% PS. Primary human brain-derived vascular pericytes were purchased from ScienCell and maintained in DMEM (Gibco) + 10% FBS with 1% PS. Aortic vascular smooth muscle cells (VSMCs) were purchased from Lonza and maintained in SMGM2 medium supplemented with 1% PS. All cell types were cultured till passage 8 in gelatin coated dishes at 37°C with 5% CO₂.

Cell sorting and analysis

Flow cytometry

Vascular organoids were mechanically disrupted and disaggregated using 3 U/mL dispase (Gibco), 2 U/mL liberase (Roche) and 100 U DNase (Stemcell Technologies) in warm DMEM:F12 for 20 min at 37 °C while rotating. To remove excess gel and cell clumps from the suspension, the solution was filtered using a 70 µm cell strainer and spun down for 5 min at 400g. Cells were subsequently stained with anti-CD31 and anti-CD140b antibodies (Supplemental Table 1), together with Sytox blue (Invitrogen) to exclude dead cells. CytoFLEX flow cytometer (Beckman Coulter) was used for cell analysis and data analysis was performed using FlowJo software (Version 10.2).

Magnetic-activated cell sorting (MACS)

Vascular organoids were dissociated as described above. To ensure purity of the populations, cells were separated using a 2-step protocol. The cells were labeled with anti-CD140b antibody (PE) and subsequently with anti-PE magnetic beads. Cell pools were separated using the LS column (Miltenyi Biotec) on the MidiMACS™ (Miltenyi Biotec) separator according to manufacturer's instructions. Cells positive for CD140b were further cultured in a gelatin-coated six-well plate, supplemented with SMGM2 medium. Cells negative for CD140b were stained with anti-CD31 magnetic beads and cell pools were separated using the LS column on the MidiMACS™ separator again. Cells positive for CD31 were further cultured on a gelatin-coated six-well plate, supplemented with EGM2 medium. Single-step MACS protocol was performed after 2 passages, to ensure purity of the populations. Anti-CD31 labeling was used for ODECs and anti-CD140b was used for ODMCs.

qPCR analysis

Total RNA was isolated from cultures (ODECs, ODMCs, HUVECs, Pericytes and VSMCs) using RNA isolation kit (Bioline) according to the manufacturer's instructions. RNA from organoids and TEVGs was isolated using Trizol (Invitrogen) according to manufacturer's instructions. The purity and concentrations of RNA were quantified using spectrophotometry (DS-11; DeNovix) absorbance measurements at 260/280 nm. cDNA synthesis was performed according to the instructions from the Bioline cDNA synthesis kit. Gene expression was determined using FastStart SYBR-green (Roche) following the qPCR program: 8,5' 95 °C, 38 cycles (15" 95 °C; 45" 60 °C) 1' 95 °C, 1' 65 °C, 62 cycles (10" 65 °C + 0.5 °C) in the SYBR-Green-Cycler IQ5 detection protocol (Biorad CFX384), performed in 384-wells plates (Merck). The primer sequences used are listed in Supplemental Table 2. All results were normalized

for house-keeping gene β -actin, resulting in relative mRNA expression. In dynamic experiments, results were compared to static controls and represented as fold change ($\Delta\Delta Ct$).

***In vitro* assays**

PrestoBlue assay

Cells (N=5 different vials) were seeded on a gelatin coated six-well plate with a cell density of 5×10^4 cells per well. Cell viability was measured 24, 72 and 120 h post-seeding using PrestoBlue Cell Viability Reagent (ThermoScientific) according to manufacturer's protocol.

PicoGreen assay

Cells (N=5 different vials) were seeded on a gelatin coated six-well plate with a cell density of 5×10^4 cells per well. To quantify the amount of double stranded DNA, a Quant-iT™ PicoGreen™ dsDNA Assay (ThermoFisher) was performed 24, 72 and 120 h post-seeding according to manufacturer's protocol.

Transendothelial resistance measurements (TEER)

ODECs (9×10^4 , N=4 individual experiments) and HUVECs (5×10^4 , N=3 individual experiments) were seeded on a 0.1% gelatin permeable filter insert (0.4 μ m pore, Falcon). Before the experiment, the resistance (R_{blank}) was measured by placing unseeded inserts in an Endohm-SNAP chamber filled with 5 mL of EGM2 medium (World Precision Instruments). The chamber was coupled to an EVOMX resistance meter (World Precision Instruments). The transendothelial electrical resistance (TEER) was measured daily to monitor resistance buildup during growth towards full confluence. At day 4, confluent monolayers were treated with 1 U/mL thrombin (Sigma) for 30 min while the TEER was measured every 5 min. After 30 min, the thrombin solution was washed away and replaced with normal medium. TEER was measured every 15 min during the restoration phase for 2 h.

2D flow experiments

ECs (N=4 individual experiments) were seeded on collagen IV (HUVECs) or gelatin (ODECs) coated 6-channel μ -slides (VI 0.4, Ibidi) with a cell density of 1×10^6 cells/mL. The ECs were suspended in culture medium (40 μ L/channel) and 1% PS. After 1 h incubation (37°C, 5% CO₂), 100 μ L of EGM2 medium was added into each channel. The cells were cultured statically for 24 h before exposure to shear stress. Medium was changed after 24 h for the static control conditions. An overview of the applied incremental shear stress levels can be seen in Supplemental Table 3. For each Ibidi

system, the red perfusion set (Ibidi) in combination with a fluidic unit (Ibidi) and flow pump system (Ibidi) was used to create a unidirectional laminar flow. The μ -slides were connected in series. The μ -slides were subjected to wall shear stress for 48 h (1.5 Pa) after which two channels were fixed and used for immunostaining and four channels harvested and pooled for RNA isolation.

3D experiments

Scaffold preparation

Tubular scaffolds (\emptyset 3 mm, 25 mm, 250 μ m wall thickness, isotropic fiber orientation, 5 μ m fibers) were produced using electrospinning. The tubular scaffolds were electrospun from 23.3% (w/w) bis-urea (BU)-modified poly(ϵ -caprolactone) (PCL-BU, SyMO-Chem,) and 76.7% (w/w) chloroform (Sigma) polymer solutions, which were transferred (flow rate: 40 μ l/min) through a charged needle (18 kV) towards the negatively charged (-1 kV) rotating mandrel (400 rpm), which was placed at 17.5 cm distance in the climate controlled cabinet (23°C and 30% relative humidity, IME Technologies). To facilitate scaffold removal, the mandrel was coated prior to electrospinning with 5% (w/v) poly(ethylene oxide) (PEO, Sigma, M_w 900 kDa) aqueous solution. This electrospraying PEO solution was transferred (flow rate: 7.5 μ l min⁻¹) through a charged needle (15 kV) towards a negatively charged, rotating 3 mm \emptyset mandrel (-1kV, 1000 rpm, needle-mandrel distance: 16.5 cm). After electrospinning, the scaffolds were removed from the mandrels, cut to size (25 mm in length) and placed in a vacuum oven at 37°C overnight to remove residual solvent.

Before cell seeding, the scaffolds were sterilized by UV-light exposure with wavelength of 253.7 nm (30 min/side), incubated in phosphate buffered saline (PBS) and 2% PS (Lonza) for 24 h and afterwards coated in a collagen I/fibronectin solution (30 μ g/mL rat tail collagen I; Corning, 50 μ g/mL fibronectin from bovine plasma; Sigma-Aldrich) for 1 h at 37°C to enhance cell adhesion and retention to the graft. Thereafter, the scaffolds were incubated in culture medium with 10% FBS for 24 h.

Cell seeding

ODMCs and ODECs were seeded separately to obtain a bi-layered structure of the vascular graft (N=4 individual experiments). Prior to cell seeding, culture medium was removed and 3.8×10^6 ODMCs/graft were seeded using fibrin as a cell carrier as described before³⁰. In short, cells were suspended in a mixture of fibrinogen (bovine, 10 mg/mL, Sigma) and thrombin (bovine, 10 IU/mL, Sigma) and homogeneously dripped over both the lumen and adventitial side of the graft. To promote a uniform distribution of cells, the cell-loaded constructs were rotated by 180° every 15 min in

a general incubator (37°C, 5% CO₂) for 1 h. After 1 h polymerization at 37°C, SMGM2 medium with 0.25 mg/mL ascorbic acid was added to induce ECM production and ODMCs were further cultured in static conditions for 48 h.

After 48 h, the same procedure was repeated with ODECs (3.8*10⁶ ODEC's/graft) which were only seeded on the luminal side of the graft. The ODMCs- and ODECs-seeded graft was cultured statically for another 5 days in 1:1 SMGM2 with ascorbic acid and EGM2 media.

Hemodynamic loading of vascular graft

After 7 days of static culture, the grafts were mounted into a previously developed vascular flow bioreactor²⁸ and connected to the flow loop to start the 48 h perfusion period. The flow bioreactor is designed to allow for culturing of vascular constructs with separated luminal and adventitial media to support vascular co-cultures, as previously described in detail²⁸. The seeded tubular grafts were connected to a Luer Lock Connector Male (Ibidi) and a Luer Connector Male (Ibidi) on each side of the graft and mounted in the custom-made culture chamber with surgical prolene sutures (4-0 Ethicon, Johnson&Johnson), connecting the luminal side of the graft to the flow loop for unidirectional flow application, controlled by a flow pump system (Ibidi) with two medium reservoirs with EGM2 medium (total volume 8 mL medium/reservoir). Subsequently, the bioreactor was closed and the outer compartment was filled with SMGM2 medium supplemented with ascorbic acid. The bioreactor was placed in a general incubator (37°C, 5% CO₂). Gradually increased shear stress was applied towards 0.08 Pa with a flow rate towards 18 mL/min (Supplemental table 3). Static controls were connected to the pump system, and subjected to the minimum amount of flow (0.01 Pa) to allow for medium exchange. An overview of the shear stress levels applied on the TEVG, can be seen in Supplemental Table 3. Grafts seeded with HUVECs and VSMCs were used as control, and coupled to the same flow pump in parallel to the organoid seeded grafts.

Scanning Electron Microscopy (SEM)

The microstructure and surface coverage of the electrospun PCL-BU graft was analyzed using SEM (Quanta 600F; Thermo Fisher). The cell-laden samples were dehydrated by ethanol washing steps on a shaker (2x 10 min PBS, 15 min 50% ethanol/MiliQ, 10 min 70% ethanol/MiliQ, 10 min 80% ethanol/MiliQ, 10 min 90% ethanol/MiliQ, 10 min 95% ethanol/MiliQ, 3x 10 min 100% ethanol). The samples were dried with the critical point dryer (EM CPD300, Leica) and were gold sputtered. Samples were visualized with SEM in low vacuum, using an electron beam of 10 kV

and LFD and BSED (backscatter) detectors, visualized with a yellow and blue filter respectively. Images were taken at different representative locations at multiple magnifications (100x, 1000x).

(Immuno)histochemistry

All samples were fixed in 4% paraformaldehyde solution for 20 min at room temperature (RT) and subsequently washed with PBS. All samples were stored at 4°C until further staining.

2D cell cultures

Cell cultures on coverslips were blocked using a 2% PBS/BSA solution for 30 min. The cells were stained with anti-CD31, anti-VE-Cadherin, anti- α -SMA, anti-PDGFr β , anti- γ H2AX and anti-Ki67 overnight at 4°C (Supplemental Table 4). Thereafter, the staining solution was removed and the coverslips were washed with PBS. Secondary antibody incubation was performed for 1 h at RT (Supplemental Table 4). The coverslips were washed with PBS and counterstained with DAPI for 5 min. Coverslips were mounted on microscope glass with Mowiol 4-88. Samples were stored at 4°C prior to imaging.

2D hemodynamically loaded slides

Cells were blocked using 2% BSA/PBS for 30 min at RT. Cells were stained for anti-CD31 and anti-VE-cadherin (Supplemental Table 4) overnight 4°C. Thereafter, the cells were washed with PBS and secondary antibody incubation (Supplemental Table 4) was performed for 1 h at RT. DAPI was used as counterstaining and channels were filled with Mowiol 4-88. Samples were stored at 4°C.

3D organoid cultures

Cells were blocked and permeabilized using 3% FBS, 1% BSA, 0.5% Triton x-100 and 0.5% Tween in PBS for 2 h at RT. 3D cell cultures were stained with anti-CD31 and anti-PDGFr β antibodies (Supplemental Table 4) for 2 h at RT. The cells were washed with PBS-/Tween and secondary antibody incubation was performed for 2 h at RT. DAPI was used as counterstaining and 3D cell cultures were mounted with Mowiol4-88. Samples were stored at 4°C prior to imaging.

Paraffin sectioning of 3D grafts

Grafts were embedded into 25% agarose gel to protect the graft material during tissue processing steps. Grafts were processed (Leica EM tissue processor, overnight without formalin) and subsequently embedded in paraffin. Sections (7 μ M thickness) were deparaffinized and citrate buffer was used for antigen retrieval for 20 min.

Sections were subsequently blocked in 2% BSA/PBS and stained with anti-CD31, anti-PDGFR β , anti-collagen IV and anti- α -SMA (Supplemental Table 4) overnight at 4°C. Constructs were washed with PBS and secondary antibody staining (Supplemental Table 4) was performed for 1h at RT. DAPI was used as counterstaining and constructs were mounted with Mowiol 4-88. In addition, paraffin sections were stained for hematoxylin and eosin (H&E). Samples were stored at 4°C prior to imaging.

Whole mount staining of 3D grafts

Grafts were blocked using a 2% PBS/BSA solution for 30 min. The grafts were stained with anti-CD31, anti-VE-Cadherin anti-collagen IV and anti- α -SMA (Supplemental Table 4) overnight at 4°C. The staining solution was removed, and the coverslips were washed with PBS. Secondary antibody incubation (Supplemental Table 4) was performed for 1 h at RT. The constructs were washed with PBS and counterstained with DAPI. Constructs were mounted on microscope glass with Mowiol 4-88. Samples were stored at 4°C prior to imaging.

Imaging and analysis

Imaging was performed using the Leica Confocal SP8x (10x, 20x magnifications), the Leica Thunder microscope (10x, 20x and 40x magnifications for 3D organoid cultures, paraffin sections, Ibidi slides and 3D grafts) and the Olympus BX51 microscope (4x and 10x magnifications for 2D cell cultures). Images were analyzed using ImageJ software (V1.47). 3D images were composed in LASX (version 3.5.7.23225).

Statistics

The statistical analyses were performed using Graphpad Prism (version 8.3). The unpaired t-test and the ordinary one-way ANOVA test with Tukey post hoc test were used for statistics and $P \leq 0.05$ was accepted as statistically significant. Values are shown as individual data points with mean \pm SEM.

Results

Generation and characterization of human iPSC-derived blood vessel organoids

Vascular organoids were generated according to the hiPSCs differentiation protocol described by Wimmer *et al.*²⁷. Gene expression profiling (Supplemental Figure 1c) showed steady increase in the expression of EC markers CD31 and VE-cadherin, as well as an increase in expression of MC markers PDGFR β and ACTA2 over time during the differentiation process. In addition, EC progenitor marker CD34 increased during vascular lineage promotion and decreased during maturation of

the vascular networks. In line with these differentiation steps, iPSC specific marker expression decreased over time (NANOG and OCT4) while expression of mesoderm markers (SLUG, SNAIL and TWIST) showed a positive parabolic curve with a peak expression at day 11 (Supplemental Figure 2b). The presence of ECs and MCs was further supported by whole-mount staining of the vascular organoids at day 21; ECs and MCs were visualized by CD31 and PDGFR β staining, respectively, forming a dense vascular network (Supplemental Figure 1d-e). Cross-section images of the vascular networks confirm lumenization of the vascular networks and close proximity between ECs and MCs within the vessel structures, despite the absence of flow (Supplemental Figure 1f-g). These findings indicate that the iPSC to vascular organoid differentiation protocol as described by Wimmer *et al.* was successfully reproduced. At day 21, vascular organoids contained the highest relative numbers of vascular cells with a mature phenotype that could be used for isolation to generate pure EC and MC pools for further use.

Vascular organoid-derived, cell type-specific populations can be isolated, cryopreserved, and cultured in 2D culture without significant loss in cell phenotype, viability, or proliferative capacity

To investigate if both ECs and MCs populations can be isolated and cultured separately in 2D culture, fully differentiated organoids from day 18 till day 21 in 3D culture were chemically dissociated into a single-cell solution prior to cell sorting. Magnetic activated cell sorting (MACS) was used to isolate EC and MC populations from other cell types. To ensure purity of the EC and MC populations, the sorting process was repeated after expansion for two passages in 2D single culture. Cell populations were further expanded prior to cryopreservation and freezing, resulting in a biobank of pure organoid derived EC (ODEC) or organoid derived MC (ODMC) populations for further use (Figure 1a). To evaluate if EC and MC purity and phenotypes were maintained after cell sorting, cryopreservation, and prolonged 2D culture, batches of ODECs and ODMCs were thawed, followed by use in analysis and dynamic experiments up to passage 7.

Morphologically, ODECs formed a squamous-shaped, cobblestone-like single layer of cells when cultured on a gelatin coated 2D surface, similar to static 2D culture of primary human ECs (Figure 1b-c). ODMCs became elongated and were randomly distributed throughout the plate with the ability to form multilayers, similar to primary human VSMCs (Figure 1d-e). Immunofluorescent staining for EC marker VE-cadherin (Figure 1f-g) and MC marker α SMA (Figure 1h-i) confirmed the EC and MC phenotypes of ODECs and ODMCs and showed the ability of ODECs to form

adherent junctions comparably to control cell lines. Flow cytometry analysis using EC marker CD31 and MC marker CD140b showed limited to no cross-contamination and high purity of the ODEC and ODMC populations (Figure 1j-k).

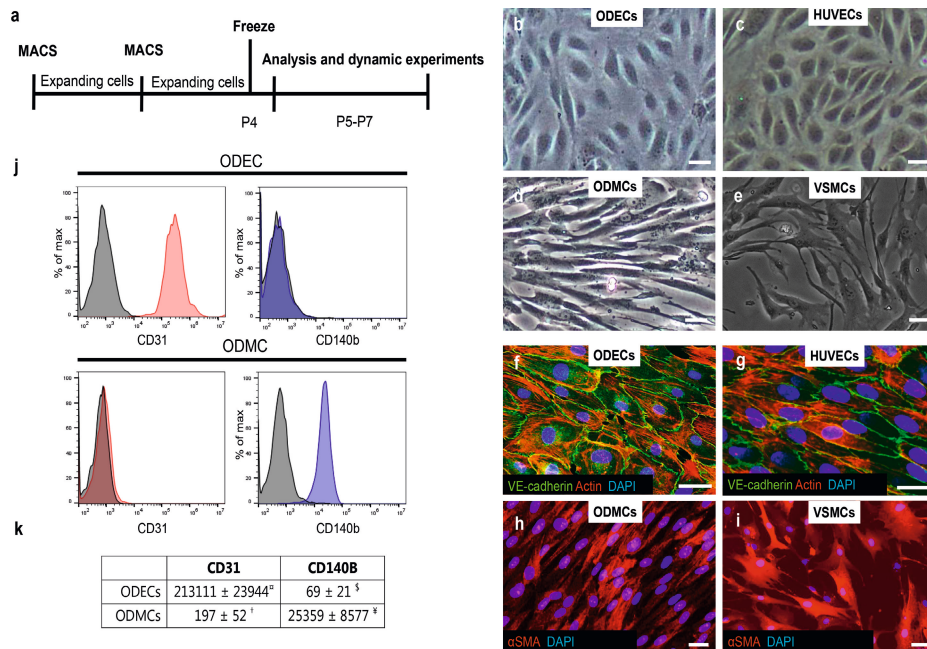


Figure 1. Validation of ODEC and ODMC populations.

a. Schematic overview of the cell culture regime, in which MACS is performed to obtain pure ODEC and ODMC populations. Isolated ODEC and ODMC pools were expanded and stored in liquid nitrogen at P4 prior to further experiments. Validation experiments including FACS analysis were performed after thawing and P5 or P6 cells were used in the dynamic experiments. **b-d.** Bright field pictures of the ODECs (**b**), HUVECs (**c**), ODMCs (**d**) and VSMCs (**e**). Scale bars represents 20 μ m. **f-i.** Immunofluorescent staining of ODECs (**f**) and HUVECs (**g**) for F-actin and EC marker VE-Cadherin and ODMCs (**h**) and VSMCs (**i**) for MC marker α SMA. Scale bars represents 20 μ m. **j.** Representative flow cytometry histograms of ODECs and ODMCs stained for both CD31 and CD140b. **k.** Mean fluorescent intensity (MFI) of ODEC and ODMC. Shown are mean \pm SEM, n=4, Paired t-test; ^ap<0.001 compared to CD140b. [†]p<0.05 compared to CD140b. [§]p<0.0001 compared to ODMCs. [‡]p<0.05 compared to ODECs. Abbreviations: passage (P), magnetic activated cell sorting (MACS), organoid derived endothelial cells (ODECs), organoid derived mural cells (ODMCs).

Both ODECs and ODMCs show persistent high viability (Figure 2a-b) and high proliferative capacity (based on DNA content assessment and Ki67 nucleus staining, Fig 2c) over different passages (5-7) in prolonged 2D single culture. Both ODECs and ODMCs showed no DNA damage, based on γ H2AX nucleus staining quantification that was comparable to HUVECs and VSMCs at passage 4 (Figure 2d). Doxorubicin treated pericytes were used as a negative control. In addition, qPCR analysis (Figure

2e) showed increased expression of EC markers (VE-cadherin and CD31) in ODECs similar to HUVECs compared to ODMCs and pericytes. *Visa versa*, expression of both pericyte marker PDGFr β and VSMC marker ACTA2 were increased in ODMCs similar to primary human control cell lines, compared to HUVECs and ODECs.

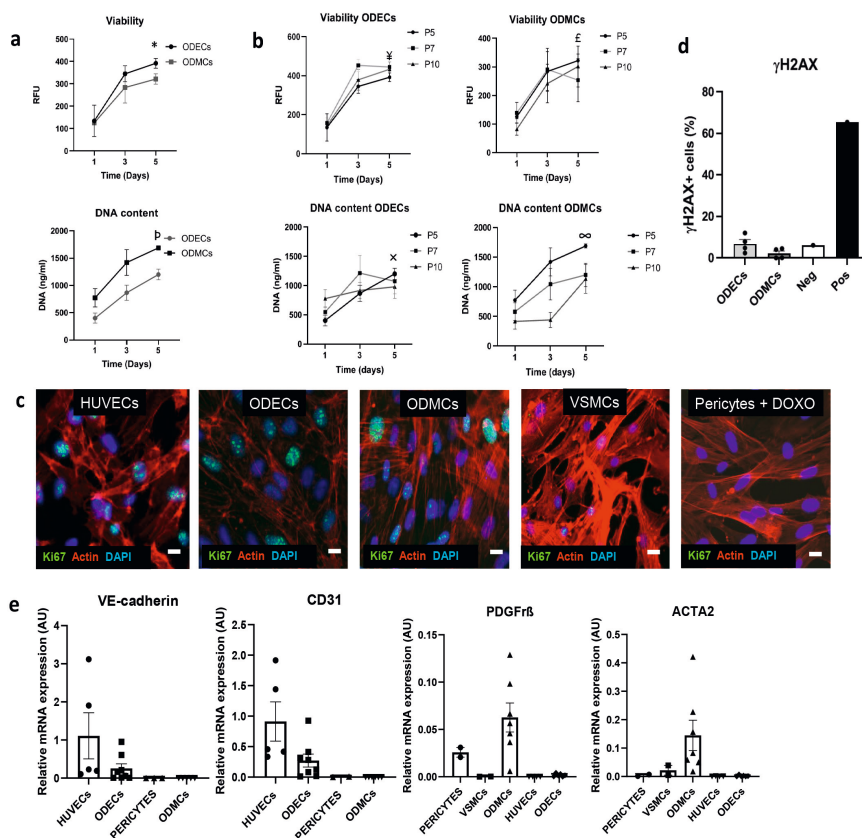


Figure 2. Organoid derived vascular cell populations preserve specific vascular cell type markers, viability and proliferative capacity.

a. Results of PrestoBlue viability assay and PicoGreen proliferation assay for passage 5. Results are presented as mean \pm SEM, $n=6$, one-way ANOVA with Tukey post hoc test. * $P<0.01$ for ODECs compared to day 1 and $P<0.05$ for ODMCs compared to day 1. $^{\#}P<0.01$ for both ODECs and ODMCs compared to day 1. **b.** Results of PrestoBlue viability assay and PicoGreen proliferation assay for multiple passages of ODECs and ODMCs. Results are presented as mean \pm SEM, $n=6$, one-way ANOVA with Tukey post hoc test $^{\#}p<0.001$ for P5 and P7 compared to day 1. $p<0.0001$ for P10 compared to day 1. $^{\$}P<0.05$ for P5 and P10 compared to day 1. $\times P<0.01$ for P5 compared to D1. $^{\circ}P<0.01$ for P5 compared to day 1 and $P<0.05$ for P10 compared to day 1. **c.** Immunofluorescent stainings for proliferation marker Ki67 (green), counterstained with phalloidin (red) and DAPI (blue). HUVECs and VSMCs were used as positive control and pericytes + 0.1 μ M doxorubicin (DOXO) were used as a negative control. Scale bar represents 20 μ m. **d.** Quantification of γ H2AX positive cells. Pericytes cultured in absence (neg) or presence (pos) 0.1 μ M doxorubicin for 72 h are used as positive control for DNA damage (γ H2AX). Results are presented as mean \pm SEM, $n=4$ (ODECs and ODMCs) and $n=1$ (control cells). **e.** qPCR results of ODECs, ODMCs with commercially available ECs and MCs as comparison (referred to as control; HUVECs, VSMCs and pericytes). Results are presented as mean \pm SEM, $n=5$ for control cell lines and $n=8$ for organoid-derived cells. Abbreviations: vascular endothelial cadherin (VE-cadherin), alpha smooth muscle actin (α SMA), relative fluorescent units (RFU), Vascular endothelial cadherin (VE-cad) cluster of differentiation (CD), platelet derived growth factor receptor β (PDGFR β), actin alpha 2 (ACTA2), organoid derived endothelial cells (ODECs), organoid derived mural cells (ODMCs), human umbilical vein endothelial cells (HUVEC), vascular smooth muscle cells (VSMCs).

Endothelium formed by ODECs is shear stress responsive and can actively maintain endothelial barrier function in 2D assay evaluation

To evaluate the shear stress responsiveness of ODECs, the Ibidi pump/slide system was used to expose ODEC monolayers to shear stress (1.5 Pa) for 48 h. A static condition was included as control. Bright field microscopy evaluation (Figure 3a-b) showed that ODECs subjected to shear stress become elongated and actively aligned in the direction of the flow, whereas static ODECs retained their cobblestone morphology. This was further confirmed by immunofluorescent staining (Figure 3c-d) of EC marker CD31 (green) and cytoskeleton fibers (f-actin; red) demonstrating cell alignment and orientation parallel to the direction of the flow. Similarly, qPCR results show upregulation of shear stress responsive genes KLF2, COX2 and eNOS in ODEC 2D cultures exposed to shear stress compared to static controls (Figure 3e, dotted line). Significant downregulation of pro-inflammatory genes VCAM and IL-8 were observed in ODECs exposed to shear stress compared to static controls, whereas MCP1 expression was not significantly affected (Supplemental Figure 3a). Exposure to shear stress did not significantly affect expression of EC specific markers VE-cadherin and CD31 (Supplemental Figure 3b).

Next, the ability of ODECs to form an endothelial barrier was studied using a trans-endothelial electrical resistance (TEER) assay. Endothelial barrier integrity of ODECs increased over 4 days and stabilized after reaching confluency (Figure 3f). HUVECs were used as a positive control and showed similar results to ODECs. To evaluate the potential of ODECs to regulate and maintain resistance and barrier function, we challenged ODEC and HUVEC monolayers with thrombin. Thrombin treatment (Figure 3g, grey area) for 30 min resulted in a significant decrease of barrier resistance in both ODECs and HUVECs. Removal of thrombin triggered barrier function restoration, resulting in complete recovery of both ODEC and HUVEC endothelial electrical resistance after 150 min (Figure 3g). These data indicate that similar to primary human ECs, ODECs can form an endothelium monolayer that is shear stress responsive and establish an endothelial barrier that is actively preserved.

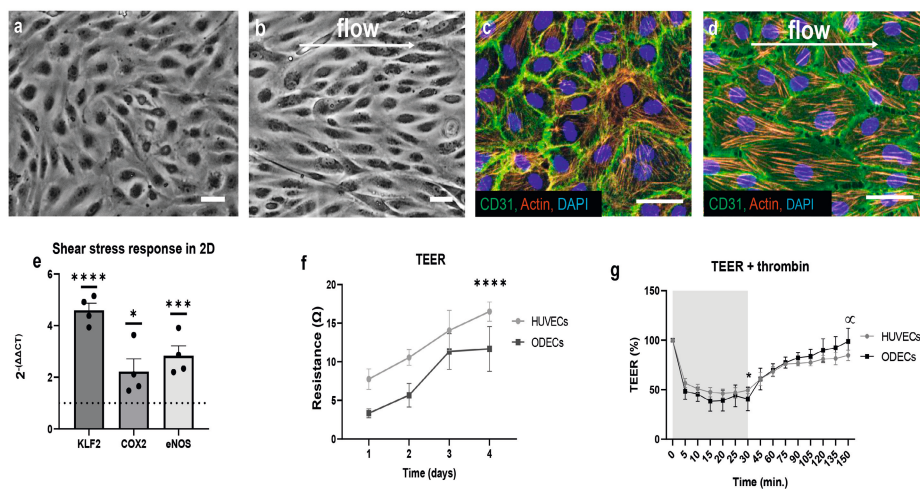


Figure 3. Functional analysis of ODECs.

a-b. Bright field image of ODECs on Ibidi slide after 48 h of static (a) and dynamic (b) culture (1.5 Pa). Scale bar represents 50 μm . **c-d.** Immunofluorescent staining of ODECs for F-actin (red) and EC marker CD31 (green) after 48 h of static (c) and dynamic (d) culture. DAPI (blue) was used as counterstaining. **e.** qPCR analysis of shear stress responsive genes KLF2, COX2 and eNOS after 48 h static and dynamic culture. Dashed line represents baseline expression levels of the static culture. Data are presented as mean \pm SEM, $n=4$. One-way ANOVA with Tukey post hoc test; * $P<0.05$, *** $P<0.001$, **** $P<0.0001$. **f.** Trans-endothelial electrical resistance (TEER) of ODECs and HUVECs over time. Data are presented as mean \pm SEM, $n=4$ (HUVECs), $n=3$ (ODECs). Paired t-test; **** $p<0.0001$ for both HUVECs and ODECs compared to day 1. **g.** TEER of ODECs and HUVECs over time during 30 min thrombin treatment (grey area) and subsequent recovery. Data are presented as mean \pm SEM, $n=4$ (HUVECs), $n=3$ (ODECs) Paired t-test; * $P<0.001$ for HUVECs compared to 0 min and $P<0.01$ for ODECs compared to 0 min. * $P<0.05$ for both HUVECs and ODECs compared to 30 min. Abbreviations, Krüppel-like factor 2 (KLF2), Prostaglandin-endoperoxide synthase 2 (COX2), endothelial nitric oxide synthase (eNOS)

Organoid-derived vascular cells can be used to populate small human artery sized 3D-vascular scaffolds to generate biomimetic bi-layered human blood vessels

To evaluate if organoid derived vascular cells can be used to create a 3D-scaffold based biomimetic human blood vessel with dimensions relevant for human sized small arteries (2-4 mm range), ODECs and ODMCs were seeded in a layered fashion onto PCL-BU scaffolds by using fibrin as a cell carrier and cultured for 48 h in static conditions. For the control group, a combination of HUVECs and VSMCs was seeded onto similar PCL-BU scaffolds using the same protocol. Scaffolds were processed according to a predefined scheme (Supplemental Figure 3c.)

Whole-mount staining revealed monolayer formation, with VE-cadherin expression and cell-cell junction formation on the luminal side of both 3D-vascular scaffolds seeded with control cells and organoid-derived cells (Figure 4a-b). Paraffin sectioning and subsequent H&E staining showed cell distribution throughout the scaffolds (Figure 4c-d, Supplemental Figure 3d), and the formation of MC and EC layers by immunofluorescent staining of PDGFR β and CD31, respectively, in both control and organoid-derived blood vessels (Figure 4e-f. 3D reconstruction of the lumen area of whole-mount stained samples revealed a bi-layered configuration consisting of a monolayer of VE-cadherin positive ECs and a thicker multicellular, subendothelial layer composed of actin positive MCs, in both vascular organoid derived and control blood vessels (Figure 4g-h).

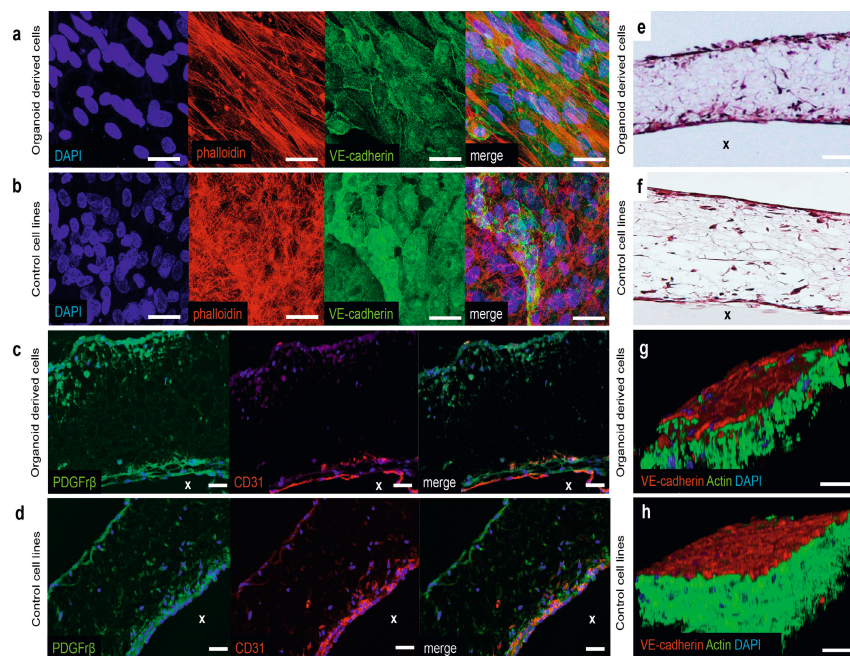


Figure 4. Evaluation of vascular grafts in static culture.

a-b. En-face Immunofluorescent whole-mount staining of a vascular graft seeded with organoid-derived cells (**a**) and control cell lines (**b**) with actin phalloidin (red) and EC marker VE-cadherin (green) signal after 48 h of static culture. DAPI (blue) was used to identify cell nuclei. Scale bar represents 50 μ m. **c-d.** H&E staining of vascular graft seeded with ODECs and ODMCs (**c**) and control cell lines (**d**) after 48 h of static culture. Scale bar represents 50 μ m. **e-f.** Cross-sectional immunofluorescent staining of vascular grafts, seeded with ODECs and ODMCs (**e**) and control cell lines (**f**) after 48 h of static culture. Stained with anti-PDGFR β (green), anti-CD31 (red) and DAPI (blue). X indicates the lumen area and scale bar represents 50 μ m. **g-h.** 3D images of whole mount staining of vascular graft seeded with ODECs and ODMCs (**g**) and control cell lines (**h**) after 48 h of static culture immunostained for VE-cadherin (red), actin (green) and DAPI (blue). Scale bar represents 50 μ m. Abbreviations: platelet derived growth factor receptor β (PDGFR β), vascular endothelial cadherin (VE-cad), cluster of differentiation (CD).

Organoid-derived human blood vessels exposed to flow in a perfused bioreactor system preserve intact endothelium and bi-layer configuration

Organoid- or control vascular cells seeded 3D-vascular scaffolds were mounted in a previously established bioreactor system that allows for vessel perfusion (Supplemental Figure 3e) ²⁸. Luminal flow generating a gradual increase in laminar shear stress of 0.08 Pa was applied and maintained for 48 h (Supplemental Table 3). Immunofluorescent whole mount staining of both organoid and control vascular cells derived human blood vessels showed preserved adherent junctions (VE-cadherin) and bi-layer configuration (VE-cadherin positive endothelial monolayer, and a multicellular subendothelial layer visualized by actin staining) after 48 h of flow exposure (Figure 5a-b and g-h). H&E staining of cross-sections of organoid-derived and control blood vessels showed the cell distribution throughout the scaffold (Figure 5c-d and Supplemental Figure 3d) after 48 h of flow. the MC and EC layers were preserved after flow exposure, as shown by immunofluorescent staining of ECs (CD31) and MCs (PDGFR β) in both control and organoid-derived human blood vessels (Figure 5e-f). PCL-BU grafts were analyzed before seeding using SEM (Figure 6a-b).

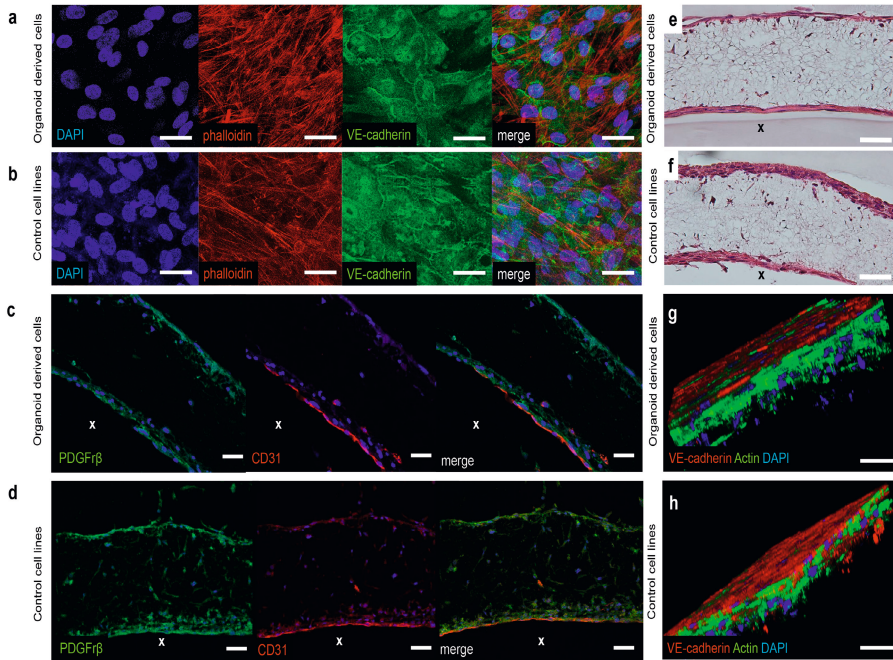


Figure 5. Evaluation of vascular grafts exposed to 48 hours of flow.

a-b. En-face Immunofluorescent whole-mount stainings of a vascular graft seeded with organoid-derived cells (**a**) and control cell lines (**b**) with phalloidin (red) and EC marker VE-cadherin (green) after 48 h of dynamic culture (gradually increased up to 0.08 Pa, Supplemental Table 3). DAPI (blue) was used to identify cell nuclei. Scale bar represents 50 μm . **c-d.** H&E staining of vascular graft seeded with ODECs and ODMCs (**c**) and control cell lines (**d**) after 48 h of dynamic culture (0.08 Pa). Scale bar represents 50 μm . **e-f.** Cross-sectional immunofluorescent staining of vascular graft, seeded with ODECs and ODMCs (**e**) and control cell lines (**f**) after 48 h of dynamic culture (0.08 Pa). Stained with anti-PDGFR β (green), anti-CD31 (red) and DAPI (blue). X indicates the lumen area and the scale bar represents 50 μm . **g-h.** 3D images of whole mount staining of vascular graft seeded with ODECs and ODMCs (**g**) and control cell lines (**h**) after 48 h of dynamic culture immunostained for VE-cadherin (red), actin (green) and DAPI (blue). Scale bar represents 50 μm . Abbreviations: platelet derived growth factor receptor β (PDGFR β), vascular endothelial cadherin (VE-cad), cluster of differentiation (CD).

SEM analysis of vascular organoid blood vessels showed a continuous lining of the luminal side of the scaffold in static culture (Figure 6c), which was preserved after 48 h of dynamic culture (Supplemental Figure 3f). Increased collagen IV deposition in dynamic conditions was shown by immunofluorescent staining in both organoid-derived and control human blood vessels (Figure 6d-g). mRNA analysis of shear stress responsive genes including KLF2, COX2 and eNOS showed no significant increase in expression in both organoid derived and control blood vessels in response to flow (Figure 6h). However, flow increased the expression of calponin in organoid-derived human blood vessels, whereas calponin levels in control human

vessels remained unchanged (Figure 6h). Expression levels of cell specific markers were preserved in both organoid derived and control human vessels after 48 h of flow (Supplemental Figure 3g). Similarly, dynamic culture did not affect the mRNA level of multiple ECM components in both organoid derived and vascular control human vessels (Figure 6i).

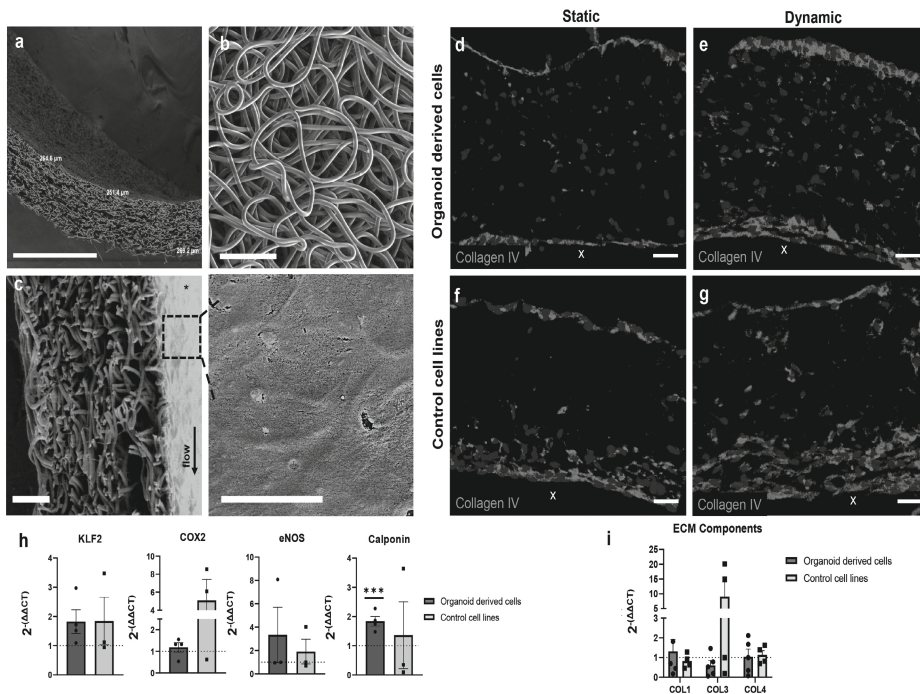


Figure 6. Flow response of vascular grafts.

a. A representative SEM picture of a scaffold prior cell seeding showing an average wall thickness of $268 \pm 8 \mu\text{m}$. **b.** SEM picture of a scaffold prior seeding showing an isotropic fiber orientation with an average fiber diameter of $4.1 \pm 0.2 \mu\text{m}$ at the luminal side of the scaffold. **c.** The left SEM picture of a scaffold seeded with ODECs and ODMCs demonstrates a confluent layer of cells at the luminal side of the scaffold. Detailed end-face SEM picture of the graft's endothelium at the right. **d-g.** Cross-sectional immunofluorescent staining of a vascular graft, either seeded with ODECs and ODMCs (**d,e**) or HUVECS and VSMCs (**f,g**) after 48 h of static and dynamic culture, stained with anti-collagen IV (green) and DAPI (blue). X Indicates lumen and scale bar represents $50 \mu\text{m}$. **h,i.** qPCR analysis of shear stress responsive genes KLF2, COX2, eNOS and calponin (**h**) and of ECM component genes Collagen I, Collagen II and Collagen IV (**i**) after 48 h static and dynamic culture. Dotted lines represent gene expression at static culture levels. Data are presented as mean \pm SEM, $n=4$ (organoid-derived graft), $n=4$ (control graft). Paired t-test; *** $p < 0.001$. Abbreviations: Krüppel-like factor 2 (KLF2), Prostaglandin-endoperoxide synthase 2 (COX2), endothelial nitric oxide synthase (eNOS), collagen (Col)

Discussion

The new method developed in this study uses hiPSC-organoid derived vascular cells to create for 3D-scaffold based tissue engineering to create a perfusable human blood vessel model that recapitulates the bi-layer architecture of native vessels. The hiPSC vascular organoid-derived pipeline eliminates the need for establishing and maintaining two separate hiPSC-differentiation cultures. The resulting system offers a complex bioreactor model to meet the growing demand for *in vitro* testing of different scaffold prototypes for the emerging field of *in situ* tissue engineering^{5, 6}. This model may be used in combination with patient-derived hiPSCs to enable to study the role of hemodynamics in driving genetic vascular disease and its impact on vascular regeneration.

Perfused 3D-scaffold based human blood vessel model

Multiple human 2D and 3D-scaffold based vascular platforms have been described in literature, most of these use primary vascular cells (e.g. aorta derived VSMCs, HUVECs) as a cell source³¹⁻³³ and are mainly focused on assessment of a single cell type in response to an isolated hemodynamic aspect without fully recapitulating the vessel architecture^{34, 35}. This limits the biological relevance of these systems as they lack the native bi-layer architecture with the natural paracrine, ion channel-based and receptor-ligand interactions between ECs and VSMCs³⁶, which have been shown to play critical roles in vasomotion, homeostasis, tissue adaptation in disease condition and vessel regenerative and hemodynamic response. However, in 2015, Nakayama et al. successfully produced bilayered aligned nanofibrillar collagen graft, using iPSC-derived vascular cells as cell source. They concluded that EC-seeded aligned scaffolds had significant reduced inflammatory response, based on adhesivity to monocytes and thus an atheroprotective function³⁷. In addition, recent work shows the possibility of using iPSC-derived vascular cells to create a bilayered TEVG, mimicking the native vessel architecture, opening up new possibilities for tissue engineering of patient-specific vascular grafts³⁸. The 3D-scaffold based model presented in this study offers a human blood vessel analogue that mimics the native vessel's bi-layer tissue organization, which is successfully preserved under flow. It would therefore enable studies that require the natural cross talk between the endothelium and medial layer to closely represent the human *in vivo* condition.

Various designs, fabrication methods and materials have been previously used to generate the vascular tubular scaffold backbone³⁹⁻⁴¹. In our experiments, the suitability of ODECs and ODMCs for vascular TE was tested on a small-diameter electrospun PCL-BU based scaffold with collagen I and fibronectin coating similar

to Pennings *et al.*²⁸, while cells were seeded in an additional fibrin carrier solution. The addition of fibrin was chosen because fibrin matrix support has been shown to improve vascular stability upon implantation and enhance EC retention under flow⁴²⁻⁴⁴. The use of fibrin as a cell carrier prevents loss of cell solution and ensures homogeneous cell distribution^{45, 46}. The selection of the PCL-BU material and fiber diameter as well as the random fiber orientation and scaffold thickness are based on findings of the successful application of this particular design in vascular tissue engineering by our group previously⁴⁷⁻⁴⁹. Furthermore, PCL-BU is an easy to functionalize polymer, which has been proven to be biocompatible and biodegradable in the local environment of the vascular system⁵⁰.

We observed that ODECs, similar to HUVECs in the control grafts, maintained CD31 EC marker expression, VE-cadherin expression in cell-cell junctions, and form a consistent monolayer when seeded into the 3D scaffolds. ODMCs, similar to VSMCs in control grafts, form tissue layers at the basal side of the endothelium, and are located dispersed throughout the scaffold wall. The resulting bi-layered (confluent endothelium and basal medial layer) configuration is in line with what was previously observed in static studies using the same bioreactor setup and PCL grafts seeded with endothelial colony forming cells (ECFCs) and VSMCs derived from mesenchymal stem cells (MSCs)²⁸. The bi-layered configuration with an intact endothelial monolayer on the luminal side of the scaffold on top of ODMCs or VSMCs was sustained when exposed to flow conditions (0.08 Pa). VE-cadherin signal remained localized in cell-cell junctions, and confluent luminal side coverage was confirmed by SEM analysis, indicating that the endothelium and the media was not disrupted after 48 h of flow exposure in both the organoid derived and control grafts. However, no flow-induced alignment was observed for both ODECs and HUVECs in the 3D culture, despite the observed shear stress sensitivity in 2D. The current shear stress levels of 0.08 Pa as applied in the bioreactor may not have been sufficient to provoke EC re-orientation. Furthermore, the high ODECs or HUVECs seeding density that was used may also have impeded the flow induced alignment, as was observed previously⁵¹.

Mural cells are considered the main contributor to the vascular ECM, with VSMCs with a synthetic phenotype in particular exhibiting a high proliferative and ECM production rate of mostly fibronectin and collagen I, whereas VSMCs with a contractile phenotype only produce small amounts of ECM, mainly collagen IV^{52, 53}. ECs are known to regulate phenotype switching of VSMCs⁵⁴⁻⁵⁶. In our experiments a significant upregulation of the contractile marker calponin was observed, implying a transition towards a contractile phenotype of the ODMCs in response to shear

stress exposure. In contrast, no upregulation in calponin expression was observed after hemodynamic loading of control graft. This lack of response may be due to differences in basal expression levels. Basal (non-flowed) Calponin mRNA levels were significantly lower in HUVECs/VSMCs grafts versus organoid-derived grafts (mean \pm stdev = 0.00023 \pm 0.00031 versus 0.0019 \pm 0.0011, for cell-line versus organoid derived respectively, $P=0.02$), implying that Calponin was hardly transcribed in the aorta derived VSMCs compared with ODMCs. The plasticity of graft seeded cells to *in vivo* adapt to local hemodynamic forces is critical for long term graft function and survival. In future studies, we will further assess the capacity of scaffold seeded ODECs to regulate phenotype transition of ODMCs in response to shear stress exposure.

Vascular organoid derived ODECs and ODMCs as a cell source for model building

Differentiation protocols for iPSC-derived ECs and iPSC-derived MCs have been previously reported^{8, 9, 13-20}. Although hiPSC-derived vascular cells are used for *in vitro* studies, only a select number of studies report their application in hierarchical vascular tissue engineering. Gui *et al.*, developed hiPSC-TE vascular constructs under static culture conditions by seeding hiPSC-VSMCs on polyglycolic acid (PGA) scaffolds followed by eight weeks of culture under static conditions. Scaffold-seeded hiPSC-VSMCs retained expression of VSMC contractile markers and collagen was deposited on scaffold fibers²⁶. Similarly, Sundaram *et al.* differentiated hiPSCs into mesenchymal progenitors and seeded these on PGA polymer scaffolds to develop tissue engineered vessels in a bioreactor that could provide pulsatile cyclic stretch. The use of PDGF-BB in the culture medium secured VSMC lineage specification of hiPSC-derived mesenchymal progenitors. This together with eight weeks of cyclic stretch exposure, promoted expression of typical VSMC markers and increased collagen deposition²⁴. However, no introduction of hiPSC-ECs and subsequent endothelialization of the 3D scaffold was reportedly achieved in these studies. Studies that investigate the application of hiPSC-EC in tissue engineered vessel is limited to a report by Tan *et al.* who demonstrated that PCL-gelatin scaffolds supported hiPSC-EC growth, phenotype retention and function *in vitro*²⁵. Nevertheless, reports that demonstrate the combined application of both hiPSC-ECs and hiPSC-MCs for tissue engineering of vascular structures for the creation of perfused human blood vessel models, are currently lacking.

Our perfused hiPSC human blood vessel model from organoid-derived vascular cells offers a 3D-scaffold based bi-layer vessel mimic in a perfusable bioreactor system that could be particularly useful as a patient-specific *in vitro* disease model. For

example hiPSCs derived from CVD patients with familiar genetic mutations or SNPs linked to early onset of coronary artery disease and endothelial dysfunction, may be used to model disease arteries to study their impact of on disease mechanisms or regenerative capacity. In relation to the latter, patient-cell derived vascular disease models are particularly relevant in combination with the emerging treatment strategy of *in situ* vascular tissue engineering, which is heavily reliant on the healing capacity of the recipient's cells⁵⁷. In this study, we investigated if pools of hiPSCs vascular organoid derived ECs and MCs can be harvested and used as a cell source for *in vitro* tissue engineering of small-diameter (3 mm) vascular constructs with native-like tissue hierarchy. In the native condition, the process of vascular cell differentiation from a progenitor state involves continuous guidance via cell contact and paracrine interaction between different cell types in the direct environment of the developing vasculature. Indeed multiple studies have also demonstrated that ECs and mural cells (MCs, or pericytes and VSMCs) interactions are critical for EC differentiation and function, and vice versa⁵⁸⁻⁶¹. The culture protocol used in this study for hiPSC-derived blood vessel organoids was first described in a recent paper by Wimmer *et al.*²⁷. Vascular differentiation from the mesoderm phase in this system takes place in a 3D environment in which the EC and MC lineages can establish with natural cross cell type interactions and eventually forms 3D structures that resemble a vascular network after 18-21 days of culture. Similar to previously reported hiPSC-derived EC and hiPSC-derived MCs, ODECs and ODMCs isolated from these vascular organoids recapitulate the morphology of human primary ECs (HUVECs) and MCs (aorta derived VSMCs) in 2D culture and express the corresponding characteristic markers^{22,23}. For the *in situ* vascular tissue engineering strategy, the capacity for fast *in situ* formation of the endothelial monolayer barrier after scaffold implantation and subsequent active preservation is crucial for the prevention of blood clotting and uncontrolled, adverse interactions of circulating immune cells and blood components with polymer structures^{62,63}, and thus is essential for protection against loss of patency. Similarly, the endothelial barrier is critical for the function of healthy vessels and is often compromised in CVD. Our experiments indicate that the ODECs can form confluent endothelial monolayers with well-established VE-cadherin adherens junctions and cobblestone morphology similar to HUVECs. Gradual increase of TEER signal indicates effective buildup of the endothelial barrier by ODECs over several days post seeding, also similar to HUVECs. More strikingly, confluent ODEC monolayers have the capacity to restore the endothelial barrier resistance actively and completely after thrombin challenge, similar to HUVEC monolayers. This innate restorative capacity of ODECs mimics the *in vivo* condition of healthy vessels.

Although cell seeding on scaffolds produced vascular grafts with a media composed of multiple layers of ODMCs, the scaffold's central core remained sparse of cells. This was also observed for grafts seeded with primary VSMCs, indicating that the observed lack of cells was not due to the iPSC origin of ODMCs. In our current seeding procedure, ODMCs and VSMCs were seeded on the scaffold's luminal and adventitial surface. Penetration of cells was feasible by design, as the scaffold's pores were on average $>15\ \mu\text{m}$ in diameter. Indeed, ODMCs and VSMCs tissue formation was observed inside the scaffold, expanding from the luminal and adventitial sides. The current protocol includes a step of 7 days of static culture after seeding before hemodynamic loading. More time may be required for ODMC and VSMC expansion to reach the core region. Although the scaffold's thickness (250 μm) does not exceed the hypothetical maximal diffusion distance for cell survival (1 mm), nutrients and oxygen may become less available at the centre once tissue structures are established in the border regions, thus reducing further expansion efficacy. To promote core cellularization, a protocol may be adapted in which only the luminal side is seeded with ODMCs/VSMCs, leaving an adventitial route of entry for the medium, followed by a prolonged static culture step.

The ODMCs/ODECs grafts were exposed 0.08 Pa of shear stress. This is only slightly lower than the levels found in veins (0.1-0.6 Pa)⁶⁴, which makes the model with the current flowing protocol suitable to study for example, venous disease. The current model can be further adapted to achieve a higher range of shear stresses by increasing viscosity of the flow medium⁶⁵ or by application of higher flow rates. The latter will require a prolonged culture step after scaffold seeding, to allow more time for the deposition of the basement membrane structures that are essential for the strengthening of the vessel wall. Our data indicate, that challenging ODECs/ODMCs or HUVECs/VSMCs grafts with 0.08 Pa shear stress can accelerate the build-up of collagen IV, a vascular basement membrane component vital for cell adhesion and stabilization (Fig. 6d-g). This observation is in line with previous publications, which have shown that shear stress stimulation during graft culture enhances several important aspects of graft maturation relevant for enhancing vascular strength⁶⁶⁻⁶⁸. Future studies will further explore prolonged static culture in combination with and without prolonged 0.08 Pa of shear stress exposure for the improvement of ODECs/ODMCs vascular graft strength to achieve higher shear stress ranges with this model.

In vivo, ECs in 3D-scaffold based grafts are required to adapt to local hemodynamic conditions, such as local shear stress levels to preserve vascular and endothelial integrity and barrier function. Depending on the location on the vascular tree,

shear stress levels vary between 0.2-1.6 Pa⁶⁹, and deviation in shear stress leads to onset and progression of CVD. In our experiments, ODECs subjected to relatively high shear stress (1.5 Pa) for 48 h responded like HUVECs, with actin stress fiber formation and cell alignment with the flow direction, whereas the integrity of the monolayer and adherens junctions was maintained. These findings are supported by the detected upregulation of shear stress responsive genes KLF2, COX2 and eNOS, upon subjection to flow. Increased expression of the KLF2 transcription factor expression is a key mechanism of the endothelium to mediate a protective anti-inflammatory response to shear stress via downregulation of (secreted) inflammation associated factors such as the cytokines IL8, MCP1 and membrane VCAM that facilitates immune cell adhesion^{70,71}. In ODECs, like in HUVECs, shear stress was previously shown to indeed reduce IL8, MCP1 and VCAM expression compared to static conditions⁷². Together, our data indicate that ODECs have the capacity to adequately adapt to shear stress conditions, similar to primary human endothelial cells.

Combined, these findings show that the use of ODECs in the perfused human blood vessel model, could therefore make the platform suitable for testing endothelialization and EC response to shear stress of different 3D-scaffold designs, and could be used for the creation of vascular disease models in which endothelial barrier function and shear stress adaptation are used as vital assay readouts.

In conclusion, the hiPSC derived vascular organoid cells can be successfully used as a source of functional, flow-adaptive vascular cells for tissue engineering of a perfused human blood vessel model. The methods may be used to establish an *in vitro* model for (cardio)vascular diseases for personalized drug treatment research, using hiPSCs from patients with genetic CVD. In addition, it may also be used as a platform for testing new scaffold designs for the *in situ* TE strategy in which the impact of genetic disease on the regeneration capacity of CVD patients can be evaluated.

Acknowledgements

The authors would like to thank Rob Driessen for his help with the flow pump system and the critical point dryer. In addition, the authors would like to thank Krista den Ouden for her help with sectioning and staining of the 3D samples.

Funding

This work is funded by the REGMEDXB cardiovascular moonshot consortium, the NWO vidi grant (no. 91714302 to CC), the TKI Health Holland BIORAB project (no. LSHM19032), and the InSiTeVx project (436001003), which is financially supported by ZonMw within the LSH 2Treat Program and the Dutch Kidney Foundation. We gratefully acknowledge the Gravitation Program “Materials Driven Regeneration”, funded by the Netherlands Organization for Scientific Research (024.003.013).

Conflicts of interest

The authors declare no conflict of interest for this study.

Author Contributions

K.L.C, A.I.P.M.S., M.C.V and C.V.C.B. devised the project and the main conceptual ideas. R.G.C.M and E.M.M. performed iPSC differentiation protocols, supervised by J.W.B. W.S. performed the electrospinning and provided the scaffolds. Static cell culture experiments were performed by E.M.M., I.C, C.G.M.D, P.J.B and S.E.K., L.P. and V.J.C.H.K performed dynamic cell culture experiments. E.M.M. S.E.K. and C.G.M.D analyzed the data and wrote the manuscript, with the help of K.L.C.. All the authors reviewed the final manuscript. The project was equally supervised by K.L.C. and A.I.P.M.S..

Data availability

The datasets generated during and/or analyzed during the current study are available from the corresponding author on reasonable request.

References

1. Mozaffarian D, Benjamin EJ, Go AS, Arnett DK, Blaha MJ, Cushman M, de Ferranti S, Despres JP, Fullerton HJ, Howard VJ, Huffman MD, Judd SE, Kissela BM, Lackland DT, Lichtman JH, Lisabeth LD, Liu S, Mackey RH, Matchar DB, McGuire DK, Mohler ER, 3rd, Moy CS, Muntner P, Mussolino ME, Nasir K, Neumar RW, Nichol G, Palaniappan L, Pandey DK, Reeves MJ, Rodriguez CJ, Sorlie PD, Stein J, Towfighi A, Turan TN, Virani SS, Willey JZ, Woo D, Yeh RW, Turner MB, American Heart Association Statistics C, Stroke Statistics S. Heart disease and stroke statistics--2015 update: a report from the American Heart Association. *Circulation* 2015;**131**:e29-322.
2. Mak IW, Evaniew N, Ghert M. Lost in translation: animal models and clinical trials in cancer treatment. *Am J Transl Res* 2014;**6**:114-118.
3. Pound P, Ram R. Are researchers moving away from animal models as a result of poor clinical translation in the field of stroke? An analysis of opinion papers. *BMJ Open Sci* 2020;**4**:e100041.
4. Lal S, Li A, Dos Remedios C. Limitations in Translating Animal Studies to Humans in Cardiovascular Disease. *J Cardiovasc Transl Res* 2016;**9**:165-166.
5. Duran-Rey D, Crisostomo V, Sanchez-Margallo JA, Sanchez-Margallo FM. Systematic Review of Tissue-Engineered Vascular Grafts. *Front Bioeng Biotechnol* 2021;**9**:771400.
6. Talacua H, Smits AI, Muylaert DE, van Rijswijk JW, Vink A, Verhaar MC, Driessen-Mol A, van Herwerden LA, Bouten CV, Kluin J, Baaijens FP. In Situ Tissue Engineering of Functional Small-Diameter Blood Vessels by Host Circulating Cells Only. *Tissue Eng Part A* 2015;**21**:2583-2594.
7. Abdulghani S, Mitchell GR. Biomaterials for In Situ Tissue Regeneration: A Review. *Biomolecules* 2019;**9**.
8. Orlova VV, van den Hil FE, Petrus-Reurer S, Drabsch Y, Ten Dijke P, Mummery CL. Generation, expansion and functional analysis of endothelial cells and pericytes derived from human pluripotent stem cells. *Nat Protoc* 2014;**9**:1514-1531.
9. Shen M, Quertermous T, Fischbein MP, Wu JC. Generation of Vascular Smooth Muscle Cells From Induced Pluripotent Stem Cells: Methods, Applications, and Considerations. *Circ Res* 2021;**128**:670-686.
10. L'Heureux N, Paquet S, Labbe R, Germain L, Auger FA. A completely biological tissue-engineered human blood vessel. *FASEB J* 1998;**12**:47-56.
11. Chavez RD, Walls SL, Cardinal KO. Tissue-engineered blood vessel mimics in complex geometries for intravascular device testing. *PLoS One* 2019;**14**:e0217709.
12. Gibbons MC, Foley MA, Cardinal KO. Thinking inside the box: keeping tissue-engineered constructs in vitro for use as preclinical models. *Tissue Eng Part B Rev* 2013;**19**:14-30.
13. Rufaihah AJ, Huang NF, Kim J, Herold J, Volz KS, Park TS, Lee JC, Zambidis ET, Reijo-Pera R, Cooke JP. Human induced pluripotent stem cell-derived endothelial cells exhibit functional heterogeneity. *Am J Transl Res* 2013;**5**:21-35.
14. Choi KD, Yu J, Smuga-Otto K, Salvagiotto G, Rehrauer W, Vodyanik M, Thomson J, Slukvin I. Hematopoietic and endothelial differentiation of human induced pluripotent stem cells. *Stem Cells* 2009;**27**:559-567.
15. Wang L, Xiang M, Liu Y, Sun N, Lu M, Shi Y, Wang X, Meng D, Chen S, Qin J. Human induced pluripotent stem cells derived endothelial cells mimicking vascular inflammatory response under flow. *Biomicrofluidics* 2016;**10**:014106.

16. Adams WJ, Zhang Y, Cloutier J, Kuchimanchi P, Newton G, Sehwat S, Aird WC, Mayadas TN, Lusinskas FW, Garcia-Cardena G. Functional vascular endothelium derived from human induced pluripotent stem cells. *Stem Cell Reports* 2013;**1**:105-113.
17. White MP, Rufaihah AJ, Liu L, Ghebremariam YT, Ivey KN, Cooke JP, Srivastava D. Limited gene expression variation in human embryonic stem cell and induced pluripotent stem cell-derived endothelial cells. *Stem Cells* 2013;**31**:92-103.
18. Orlova VV, Drabsch Y, Freund C, Petrus-Reurer S, van den Hil FE, Muenthaisong S, Dijke PT, Mummery CL. Functionality of endothelial cells and pericytes from human pluripotent stem cells demonstrated in cultured vascular plexus and zebrafish xenografts. *Arterioscler Thromb Vasc Biol* 2014;**34**:177-186.
19. Taura D, Sone M, Homma K, Oyamada N, Takahashi K, Tamura N, Yamanaka S, Nakao K. Induction and isolation of vascular cells from human induced pluripotent stem cells—brief report. *Arterioscler Thromb Vasc Biol* 2009;**29**:1100-1103.
20. Stephenson M, Reich DH, Boheler KR. Induced pluripotent stem cell-derived vascular smooth muscle cells. *Vasc Biol* 2020;**2**:R1-R15.
21. Kurokawa YK, Yin RT, Shang MR, Shirure VS, Moya ML, George SC. Human Induced Pluripotent Stem Cell-Derived Endothelial Cells for Three-Dimensional Microphysiological Systems. *Tissue Eng Part C Methods* 2017;**23**:474-484.
22. Jang S, Collin de l'Hortet A, Soto-Gutierrez A. Induced Pluripotent Stem Cell-Derived Endothelial Cells: Overview, Current Advances, Applications, and Future Directions. *Am J Pathol* 2019;**189**:502-512.
23. Dash BC, Jiang Z, Suh C, Qyang Y. Induced pluripotent stem cell-derived vascular smooth muscle cells: methods and application. *Biochem J* 2015;**465**:185-194.
24. Sundaram S, One J, Siewert J, Teodosescu S, Zhao L, Dimitrievska S, Qian H, Huang AH, Niklason L. Tissue-engineered vascular grafts created from human induced pluripotent stem cells. *Stem Cells Transl Med* 2014;**3**:1535-1543.
25. Tan RP, Chan AHP, Lennartsson K, Miravet MM, Lee BSL, Rnjak-Kovacina J, Clayton ZE, Cooke JP, Ng MKC, Patel S, Wise SG. Integration of induced pluripotent stem cell-derived endothelial cells with polycaprolactone/gelatin-based electrospun scaffolds for enhanced therapeutic angiogenesis. *Stem Cell Res Ther* 2018;**9**:70.
26. Gui L, Dash BC, Luo J, Qin L, Zhao L, Yamamoto K, Hashimoto T, Wu H, Dardik A, Tellides G, Niklason LE, Qyang Y. Implantable tissue-engineered blood vessels from human induced pluripotent stem cells. *Biomaterials* 2016;**102**:120-129.
27. Wimmer RA, Leopoldi A, Aichinger M, Wick N, Hantusch B, Novatchkova M, Taubenschmid J, Hammerle M, Esk C, Bagley JA, Lindenhofer D, Chen G, Boehm M, Agu CA, Yang F, Fu B, Zuber J, Knoblich JA, Kerjaschki D, Penninger JM. Human blood vessel organoids as a model of diabetic vasculopathy. *Nature* 2019;**565**:505-510.
28. Pennings I, van Haften EE, Jungst T, Bulsink JA, Rosenberg A, Groll J, Bouten CVC, Kurniawan NA, Smits A, Gawlitta D. Layer-specific cell differentiation in bi-layered vascular grafts under flow perfusion. *Biofabrication* 2019;**12**:015009.
29. Kitani T, Ong SG, Lam CK, Rhee JW, Zhang JZ, Oikonomopoulos A, Ma N, Tian L, Lee J, Telli ML, Witteles RM, Sharma A, Sayed N, Wu JC. Human-Induced Pluripotent Stem Cell Model of Trastuzumab-Induced Cardiac Dysfunction in Patients With Breast Cancer. *Circulation* 2019;**139**:2451-2465.
30. Koch SE, van Haften EE, Wissing TB, Cuypers LAB, Bulsink JA, Bouten CVC, Kurniawan NA, Smits A. A Multi-Cue Bioreactor to Evaluate the Inflammatory and Regenerative Capacity of Biomaterials under Flow and Stretch. *J Vis Exp* 2020.

31. Miyachi H, Reinhardt JW, Otsuru S, Tara S, Nakayama H, Yi T, Lee YU, Miyamoto S, Shoji T, Sugiura T, Breuer CK, Shinoka T. Bone marrow-derived mononuclear cell seeded bioresorbable vascular graft improves acute graft patency by inhibiting thrombus formation via platelet adhesion. *Int J Cardiol* 2018;**266**:61-66.
32. Fukunishi T, Best CA, Ong CS, Groehl T, Reinhardt J, Yi T, Miyachi H, Zhang H, Shinoka T, Breuer CK, Johnson J, Hibino N. Role of Bone Marrow Mononuclear Cell Seeding for Nanofiber Vascular Grafts. *Tissue Eng Part A* 2018;**24**:135-144.
33. Mirensky TL, Hibino N, Sawh-Martinez RF, Yi T, Villalona G, Shinoka T, Breuer CK. Tissue-engineered vascular grafts: does cell seeding matter? *J Pediatr Surg* 2010;**45**:1299-1305.
34. Hibino N, McGillicuddy E, Matsumura G, Ichihara Y, Naito Y, Breuer C, Shinoka T. Late-term results of tissue-engineered vascular grafts in humans. *J Thorac Cardiovasc Surg* 2010;**139**:431-436, 436 e431-432.
35. Sugiura T, Matsumura G, Miyamoto S, Miyachi H, Breuer CK, Shinoka T. Tissue-engineered Vascular Grafts in Children With Congenital Heart Disease: Intermediate Term Follow-up. *Semin Thorac Cardiovasc Surg* 2018;**30**:175-179.
36. Mendez-Barbero N, Gutierrez-Munoz C, Blanco-Colio LM. Cellular Crosstalk between Endothelial and Smooth Muscle Cells in Vascular Wall Remodeling. *Int J Mol Sci* 2021;**22**.
37. Nakayama KH, Joshi PA, Lai ES, Gujar P, Joubert LM, Chen B, Huang NF. Bilayered vascular graft derived from human induced pluripotent stem cells with biomimetic structure and function. *Regen Med* 2015;**10**:745-755.
38. Generali M, Casanova EA, Kehl D, Wanner D, Hoerstrup SP, Cinelli P, Weber B. Autologous endothelialized small-caliber vascular grafts engineered from blood-derived induced pluripotent stem cells. *Acta Biomater* 2019;**97**:333-343.
39. Ong CS, Zhou X, Huang CY, Fukunishi T, Zhang H, Hibino N. Tissue engineered vascular grafts: current state of the field. *Expert Rev Med Devices* 2017;**14**:383-392.
40. Liu Y, Nelson T, Chakroff J, Cromeens B, Johnson J, Lannutti J, Besner GE. Comparison of polyglycolic acid, polycaprolactone, and collagen as scaffolds for the production of tissue engineered intestine. *J Biomed Mater Res B Appl Biomater* 2019;**107**:750-760.
41. Rathore A, Cleary M, Naito Y, Rocco K, Breuer C. Development of tissue engineered vascular grafts and application of nanomedicine. *Wiley Interdiscip Rev Nanomed Nanobiotechnol* 2012;**4**:257-272.
42. Isenberg BC, Williams C, Tranquillo RT. Endothelialization and flow conditioning of fibrin-based media-equivalents. *Ann Biomed Eng* 2006;**34**:971-985.
43. Grassl ED, Oegema TR, Tranquillo RT. Fibrin as an alternative biopolymer to type-I collagen for the fabrication of a media equivalent. *J Biomed Mater Res* 2002;**60**:607-612.
44. Gosselin C, Vorp DA, Warty V, Severyn DA, Dick EK, Borovetz HS, Greisler HP. ePTFE coating with fibrin glue, FGF-1, and heparin: effect on retention of seeded endothelial cells. *J Surg Res* 1996;**60**:327-332.
45. Stekelenburg M, Rutten MC, Snoeckx LH, Baaijens FP. Dynamic straining combined with fibrin gel cell seeding improves strength of tissue-engineered small-diameter vascular grafts. *Tissue Eng Part A* 2009;**15**:1081-1089.
46. Mol A, van Lieshout MI, Dam-de Veen CG, Neuenschwander S, Hoerstrup SP, Baaijens FP, Bouten CV. Fibrin as a cell carrier in cardiovascular tissue engineering applications. *Biomaterials* 2005;**26**:3113-3121.

47. Wissing TB, Bonito V, van Haaften EE, van Doeselaar M, Brugmans M, Janssen HM, Bouten CVC, Smits A. Macrophage-Driven Biomaterial Degradation Depends on Scaffold Microarchitecture. *Front Bioeng Biotechnol* 2019;**7**:87.
48. Wu DJ, van Dongen K, Szymczyk W, Besseling PJ, Cardinaels RM, Marchioli G, van Genderen MHP, Bouten CVC, Smits AIPM, Dankers PYW. Optimization of Anti-kinking Designs for Vascular Grafts Based on Supramolecular Materials. *Frontiers in Materials* 2020;**7**.
49. Wissing TB, van Haaften EE, Koch SE, Ippel BD, Kurniawan NA, Bouten CVC, Smits A. Hemodynamic loads distinctively impact the secretory profile of biomaterial-activated macrophages - implications for in situ vascular tissue engineering. *Biomater Sci* 2019;**8**:132-147.
50. van Haaften EE, Duijvelshoff R, Ippel BD, Sontjens SHM, van Houtem M, Janssen HM, Smits A, Kurniawan NA, Dankers PYW, Bouten CVC. The degradation and performance of electrospun supramolecular vascular scaffolds examined upon in vitro enzymatic exposure. *Acta Biomater* 2019;**92**:48-59.
51. Ohta S, Inasawa S, Yamaguchi Y. Alignment of vascular endothelial cells as a collective response to shear flow. *Journal of Physics D: Applied Physics* 2015;**48**:245401.
52. Wang G, Jacquet L, Karamariti E, Xu Q. Origin and differentiation of vascular smooth muscle cells. *J Physiol* 2015;**593**:3013-3030.
53. Rzczudlo EM, Martin KA, Powell RJ. Regulation of vascular smooth muscle cell differentiation. *J Vasc Surg* 2007;**45 Suppl A**:A25-32.
54. Powell RJ, Cronenwett JL, Fillinger MF, Wagner RJ, Sampson LN. Endothelial cell modulation of smooth muscle cell morphology and organizational growth pattern. *Ann Vasc Surg* 1996;**10**:4-10.
55. Powell RJ, Hydowski J, Frank O, Bhargava J, Sumpio BE. Endothelial cell effect on smooth muscle cell collagen synthesis. *J Surg Res* 1997;**69**:113-118.
56. Powell R, Bhargava J, Sumpio B. Regulation of smooth muscle cell differentiation and expression of nonmuscle myosin by endothelial cells in coculture. SURGICAL FORUM-CHICAGO-: AMERICAN COLLEGE OF SURGEONS, 1997:408-410.
57. de Kort BJ, Koch SE, Wissing TB, Krebber MM, Bouten CVC, Smits A. Immuno-regenerative biomaterials for in situ cardiovascular tissue engineering - Do patient characteristics warrant precision engineering? *Adv Drug Deliv Rev* 2021;**178**:113960.
58. Brandt MM, van Dijk CGM, Maringanti R, Chrifi I, Kramann R, Verhaar MC, Duncker DJ, Mokry M, Cheng C. Transcriptome analysis reveals microvascular endothelial cell-dependent pericyte differentiation. *Sci Rep* 2019;**9**:15586.
59. Chiaverina G, di Blasio L, Monica V, Accardo M, Palmiero M, Peracino B, Vara-Messler M, Puliafito A, Primo L. Dynamic Interplay between Pericytes and Endothelial Cells during Sprouting Angiogenesis. *Cells* 2019;**8**.
60. Gerhardt H, Betsholtz C. Endothelial-pericyte interactions in angiogenesis. *Cell Tissue Res* 2003;**314**:15-23.
61. Lilly B. We have contact: endothelial cell-smooth muscle cell interactions. *Physiology (Bethesda)* 2014;**29**:234-241.
62. Cines DB, Pollak ES, Buck CA, Loscalzo J, Zimmerman GA, McEver RP, Pober JS, Wick TM, Konkle BA, Schwartz BS, Barnathan ES, McCrae KR, Hug BA, Schmidt AM, Stern DM. Endothelial cells in physiology and in the pathophysiology of vascular disorders. *Blood* 1998;**91**:3527-3561.

63. Rodrigues SF, Granger DN. Blood cells and endothelial barrier function. *Tissue Barriers* 2015;**3**:e978720.
64. Malek AM, Alper SL, Izumo S. Hemodynamic shear stress and its role in atherosclerosis. *JAMA* 1999;**282**:2035-2042.
65. Cho YI, Cho DJ, Rosenson RS. Endothelial shear stress and blood viscosity in peripheral arterial disease. *Curr Atheroscler Rep* 2014;**16**:404.
66. Resnick N, Yahav H, Shay-Salit A, Shushy M, Schubert S, Zilberman LC, Wofovitz E. Fluid shear stress and the vascular endothelium: for better and for worse. *Prog Biophys Mol Biol* 2003;**81**:177-199.
67. Dardik A, Liu A, Ballermann BJ. Chronic in vitro shear stress stimulates endothelial cell retention on prosthetic vascular grafts and reduces subsequent in vivo neointimal thickness. *J Vasc Surg* 1999;**29**:157-167.
68. Ott MJ, Ballermann BJ. Shear stress-conditioned, endothelial cell-seeded vascular grafts: improved cell adherence in response to in vitro shear stress. *Surgery* 1995;**117**:334-339.
69. Cheng C, Helderma F, Tempel D, Segers D, Hierck B, Poelmann R, van Tol A, Duncker DJ, Robbers-Visser D, Ursem NT, van Haperen R, Wentzel JJ, Gijzen F, van der Steen AF, de Crom R, Krams R. Large variations in absolute wall shear stress levels within one species and between species. *Atherosclerosis* 2007;**195**:225-235.
70. SenBanerjee S, Lin Z, Atkins GB, Greif DM, Rao RM, Kumar A, Feinberg MW, Chen Z, Simon DI, Lusinskas FW, Michel TM, Gimbrone MA, Jr., Garcia-Cardena G, Jain MK. KLF2 is a novel transcriptional regulator of endothelial proinflammatory activation. *J Exp Med* 2004;**199**:1305-1315.
71. Atkins GB, Jain MK. Role of Kruppel-like transcription factors in endothelial biology. *Circ Res* 2007;**100**:1686-1695.
72. Nayak L, Lin Z, Jain MK. "Go with the flow": how Kruppel-like factor 2 regulates the vasoprotective effects of shear stress. *Antioxid Redox Signal* 2011;**15**:1449-1461.

Supplemental information



CHAPTER

4



Induction of Fenestrae in hiPSC-Derived Endothelial Cells for Disease Modeling

Elana M. Meijer, Christian G.M. van Dijk, Rachel Giles, Karlijn Gijsen, Ihsan Chrifi, Marianne C. Verhaar, Caroline Cheng

Tissue Eng Part A. 2023 Dec 21. doi: 10.1089

Abstract

The endothelial linings of capillaries, such as those in the kidney and small intestines, possess fenestrae that facilitate fluid and exchange of small molecules. Alterations in the size and number of endothelial fenestrae have been implicated in the pathogenesis of various diseases. The re-creation of fenestrated endothelium using human induced pluripotent stem cells (hiPSCs) provides a promising avenue to investigate the involvement of fenestrae in disease mechanisms and pharmacodynamics. In this project, we aim to induce the formation of fenestrae in non-fenestrated hiPSCs-derived endothelial cells (hiPSC-ECs). Vascular endothelial growth factor A (VEGFA) and phorbol myristate acetate (PMA) were employed as inducers of fenestrae in hiPSC-ECs. The assessment of fenestrae formation included gene-expression analysis, scanning electron microscopy (SEM), transmission electron microscopy (TEM), and immunofluorescent staining. Endothelial monolayer functionality was evaluated by dextran permeability assays. Stimulation with VEGFA and PMA significantly induced expression of the diaphragmed fenestrae-associated marker, PLVAP, in hiPSC-ECs at the mRNA and protein levels. SEM analysis revealed VEGFA and PMA induced fenestrae structures on the cell membrane of hiPSC-ECs. The increased membrane localization of PLVAP visualized by TEM and immunofluorescent staining supported these findings. The induced fenestrated endothelium in hiPSC-ECs demonstrated selective passage of small solutes across a confluent monolayer with intact cell junctions, confirming functional competence. In conclusion, we present a novel methodology for inducing and regulating fenestrated endothelium in hiPSC-ECs. This innovative approach paves the way for the development of fenestrated microvasculature in human organ-on-a-chip systems, enabling complex disease modeling and physiologically relevant investigations of pharmacodynamics.

Impact statement

In this study, a novel approach is devised to induce fenestrae in non-fenestrated human ECs derived from hiPSCs obtained from vascular organoids (ODECs). Both VEGFA or PMA stimulation of ODECs successfully promotes fenestrae formation to a level comparable to the baseline of human glomerular endothelium, which naturally forms fenestrae *in vivo* and *in vitro*. The strategy described here for inducing fenestrae in hiPSC-derived endothelium has potential applications in complex modelling of human disease and pharmacodynamics *in vitro*.

Introduction

In theory, human induced pluripotent stem cells (hiPSCs) derived from somatic cell types have the potential to provide an unlimited supply of human cells for clinical and scientific applications. Specifically, patient-specific hiPSCs could be utilized to study the molecular and genetic basis of disease. The development and improvement of protocols for directing hiPSC differentiation into functional adult cell types that closely mimic *in vivo* conditions is crucial to explore this potential. Advancements in microfluidics, 3D printing techniques, and co-culture systems are gradually replacing simple 2D culture assays with more complex human tissue models that can more accurately replicate interactions between cell type compartments in conjunction with exposure to hemodynamic forces, circulating cells and solutes. Further improvements in hiPSC strategies have aided in this transition, creating systems that are even more sophisticated and representative of the human condition. One of the essential steps required to closely replicate physiological and disease tissue conditions *in vitro* is to model vascularization.

A number of strategies have been reported in recent years for the conversion of hiPSCs into vascular cell types^{1,2}, and some have demonstrated successful integration of hiPSCs derived endothelial and mural cells into sophisticated blood vessel and vascularized tissue on-a-chip models^{3,4}. However, full replication of the *in situ* function of hiPSCs derived vessels remains challenging due to the considerable heterogeneity in EC morphology, which strongly correlates to blood vessel function and location in the vascular tree⁵.

In all organs, the endothelium lining the microvasculature is responsible for the transvascular solute and gas exchange between blood and the underlying tissue interstitial space. Three main structures of the endothelium are classically identified as; continuous non-fenestrated, continuous fenestrated and sinusoidal endothelium⁶.

Continuous non-fenestrated endothelium, present in arteries, veins and the capillaries of the brain, heart, skin and lung, contain aqueous pores including aqua(glycerol) porins, which allow passing of only small molecules such as water, glucose and hormones, due to the relatively narrow channel size (<0.5 nm wide). Continuous fenestrated endothelium, present in the kidney, small intestines, and endocrine glands, supports larger transcellular pores called fenestrae which allow passage of molecules typically in the 6-12 nm range. The sinusoidal endothelium is characterized by the absence of a basement membrane underlying large open

fenestrae (>50 nm diameter, depending on the species), which facilitates passages of macromolecules. This type of endothelium is found primarily in the capillaries of the liver and the spleen ⁷.

Changes in endothelial fenestrae size and number are associated with the onset and progression of disease. For example, the loss of glomerular capillary endothelial fenestrae is a feature of type 1 and 2 diabetic nephropathy in patients ⁸. A progressive loss of fenestrae in the peritubular capillaries was also observed in chronic kidney disease (CKD) patient biopsy samples and in various murine CKD models ⁹. Similar decline in fenestrae was reported for liver sinusoidal ECs in liver fibrosis occurring in humans and animal models ¹⁰, whereas the reversal of fenestrae loss was associated with fibrosis regression via interaction of the sinusoidal ECs with hepatic stellate cells ¹⁰. An improved understanding of the impact of disease conditions on vascular fenestrae stability and their contribution to disease mechanisms and pharmacodynamics during treatment, could thus result in more effective therapies for a large variety of conditions, including CKD, diabetes, and liver fibrosis. Although *in vitro* studies often use 2D monocultures of fenestrated human EC types like glomerular capillary ECs and liver sinusoidal ECs, fenestrated ECs are reported to typically quickly lose trans-endothelial structures when brought into culture ¹¹. For hiPSC derived vascular cells, subcapsular implantation of hiPSC derived kidney organoids were shown to be able to promote tissue maturation and as a result, successful endothelial fenestrae ¹². Nevertheless, a strategy in which fenestrae of hiPSC derived endothelium can reliably be achieved *in vitro* is currently lacking.

Endothelial cell fenestrae are circular openings, approximately 70-100 nm in diameter, situated on the luminal side. These fenestrae are grouped in clusters called sieve plates, which are located away from the cell body and typically contain 10-100 fenestrae^{13, 14}. Individual fenestra are mechanically supported by a surrounding cytoskeletal lattice at the ultrastructural level ¹⁵. Membrane spanning plasmalemmal vesicle associated protein (PLVAP) is frequently present in endothelial fenestrae, creating spoke wheel-like structures that span the fenestrae near the base. These structures, known as diaphragms, are found in most but not all fenestrated ECs. Studies *in vitro* using PLVAP silencing and findings in PLVAP deficient mice identified this molecular component to be involved in endothelial fenestrae formation ^{13, 15-19}. Similarly, structural proteins like spectrin and moesin, known to interact with the actin cytoskeleton, have been reported to also contribute to fenestrae formation ^{20, 21}, whereas annexin A2 plays an inhibitory role ²¹. A select number of compounds were also reported to regulate the fenestrae process. This includes the

use of vascular endothelial growth factor A (VEGFA) to induce fenestrae formation and phorbol myristate acetate (PMA) to induce fenestrae and upregulate PLVAP expression²¹⁻²³. In addition, treatment with actin disruptor cytochalasin B is known to increase the amount of fenestrae with up to 300%²⁰, whereas diamide decreases the number of fenestrae by oxidising the spectrin filaments in liver sinusoidal ECs²⁴.

The presence and function of fenestrated endothelium have been widely acknowledged. However, only a limited number of studies have investigated fenestrae induction and control for complex disease modeling or regenerative medicine strategies, especially using relevant endothelial cells derived from hiPSCs. In this study, a novel approach is devised to induce fenestrae in non-fenestrated human ECs derived from hiPSCs obtained from vascular organoids. The resulting strategy described in this study facilitates the creation of fenestrated microvasculature for complex disease modelling. The integration with patient-specific hiPSCs holds potential for constructing disease models tailored to individual patients, thereby advancing personalized medicine. Furthermore, this approach has the potential to enhance the functionality of vascularized organ grafts using hiPSC derived ECs towards a more physiological state for regenerative purposes.

4

Methods

Cell Culture and Fenestrae Induction

Organoid derived ECs (ODECs) are derived from hiPSC-induced organoids and are cultured according to the protocol described by Meijer et al.²⁵. A schematic representation of the workflow for the generation of ODECs is shown in Fig. 1a. Human umbilical vein ECs (HUVECs) and human renal glomerular ECs (HRGECs) were purchased from Lonza and used as positive control. All ECs were cultured in EBM-2 medium (Lonza) supplemented EGM-2 bullet kit (Lonza) and 100 µg/mL Penicillin/Streptomycin (Thermo Fisher). Cells were cultured under standard growth conditions (37°C, 5% CO₂). Once thawed, cells were seeded at a density equivalent to 1 x 10⁶ cells per mL medium on 0.1% gelatin-coated coverslips or culture dishes for 48 h prior to fenestrae induction. Cells were treated with 50 nM of PMA (Thermo Fisher) or 100 ng/mL VEGF-A (PeproTech) for 48 h to induce fenestrae. Thirty min before the readouts, 21 µM of cytochalasin B (Sigma) or 500 µM of diamide (Sigma) was added to control the size and frequency of the fenestrae in both ODECs and HRGECs. Growth-factors were diluted according to manufacturer's instructions.

RNA isolation and Real-Time Quantitative Polymerase Chain Reaction (RT-qPCR).

After treatment, total RNA was extracted from the cells with ISOLATE II RNA mini kit (Bioline). To address initial gene-expression levels of PLVAP in primary cell lines, $n = 4$ biological replicates. The other gene-expression analysis experiments include $n = 6$ biological replicates for both HRGECs and ODECs. Every sample is measured in duplo. Equal amounts of 500 ng RNA were reverse transcribed into complementary DNA (cDNA) using the cDNA synthesis kit (Bioline). RNA expression levels were determined by RT-qPCR reactions using FastStart Universal SYBR Green Master (Roche). Primers used are shown in supplemental Table 1. All measurements were performed in duplicate on a Bio-Rad CFX384 qPCR System. Gene expression levels were normalized to the housekeeping genes β -actin and RPLP0. The cycle threshold values were converted into relative gene expression levels using the $\Delta\Delta C_t$ control method and transformed into a log scale.

Immunofluorescent staining

Human- iPSC-derived blood vessel organoids were stained according to the protocol described by Meijer et al.²⁵. Cells were cultured on gelatin-coated coverslips (18 mm \varnothing , $n = 5$ biological replicates, 3 pictures per sample). The cells were fixed with warm 4% paraformaldehyde (PFA) for 30 min at room temperature. The fixed cells were blocked with 2% PBS/bovine serum albumin (BSA) for 30 min to prevent non-specific binding of the primary antibody. Staining was performed with the rabbit anti-PLVAP (Atlas, 1:250) in 1% BSA/PBS overnight at 4°C. After a triple washing step with 1% BSA/PBS, the cells were incubated with the secondary antibody Alexafluor™ 488 goat anti-rabbit (Invitrogen, 1:500), and Phalloidin-rhodamine (Thermo Fisher, 1:40) for counterstaining of actin filaments for 1 h at room temperature (RT). The coverslips were washed with PBS and counterstained with DAPI (1:5000) for 10 min at RT. Coverslips were mounted on a microscope glass with Mowiol 4–88. Samples were stored at 4°C prior to imaging. The samples were imaged using confocal microscopy (Leica TCS SP8X) with a 63x magnification (63x apo oil 1.4). The following excitation-emission spectra were used: DAPI (exc. 359, em. 461), Alexa Fluor 488 (Green, exc. 499, em. 520) and Rhodamine red (exc. 573, em. 591). The used Z-step size was 0.2 μm and samples were analyzed within 48 h after staining with random selection of imaging location. ImageJ was used to quantify the area per cell. Both microscope and ImageJ (threshold) settings were kept the same for all images within one experiment.

Immuno-Electron microscopy: (Cryo) fixation, preparation and imaging

Cells cultured in gelatine coated wells ($n = 3$ biological replicates) were fixed for immuno-electron microscopy by adding freshly prepared 4% formaldehyde (441244, Sigma-Aldrich) in 0.1 M phosphate buffer (pH 7.4) to an equal volume of culture medium. After 10 min, refreshed to continue fixation O/N. Cells were stored in 1% formaldehyde at 4°C until further processing. Embedding, ultrathin cryosectioning and immunogold labelling were performed as described²⁶. In brief, the fixed cells were washed with 0.05 M glycine in PBS, embedded in 12% gelatin in PBS, 37°C, solidified on ice and cut into small blocks. Cryoprotection was performed by infiltrating blocks overnight in 2.3 M sucrose at 4°C. Blocks were mounted on aluminum pins and frozen in liquid nitrogen. Ultrathin cryosections (60 nm) were cut (Leica EM UC7), transferred on TEM grids with a 1:1 mixture of 2.3 M sucrose and 1.8% methylcellulose, and immunolabelled using primary antibodies Rabbit α -PLVAP (Atlas 1:10). Primary antibodies were detected by Protein A conjugated to 15 nm gold particles (Cell Microscopy Core, Utrecht, The Netherlands). Pictures (4 per sample) were collected on a JEM1010 (JEOL) equipped with a Veleta 2k \times 2k CCD camera (EMSIS, Munster, Germany).

Scanning Electron Microscopy Imaging and Quantification

Cells grown on 10 mm coverslips were fixated overnight in 1/2 Karnovsky 0.1M PHEM (Karnovsky, 1965). Samples were rinsed with 0.1M PHEM buffer, followed by dehydration in a series of ethanol concentrations, each for 10 min (70%, 80%, 90%, 3 \times 100%). For further dehydration, the samples were incubated in hexamethyldisilane (HMDS) for 3 min and fully dried in a desiccator for 25 min. Coverslips were mounted on stubs and coated with 6 nm of gold using a rotary pumped coater (Q150R). Imaging was performed using the Scanning Electron Microscope (SEM) (FEI Scios). From each sample, five cells were imaged at a magnitude of 44.000. ImageJ was used to measure the diameter and frequency of fenestrae. Per condition, 3 locations per sample were imaged from $n = 5$ samples.

Statistical analysis

All data are represented as mean \pm standard error of the mean (SEM). Outlier tests were performed (Grubb's test) and significant outliers ($P < 0.05$) were removed before further statistical analysis. For statistical analysis, differences between groups were evaluated with either one-way or two-way ANOVA test with Tukey post hoc tests. The number of both technical and biological replicates is described in corresponding sections and figure legends. All statistical evaluations were carried out using GraphPad prism software. A value of $P < 0.05$ was considered statistically significant.

Experiments

VEGFA or PMA induces fenestrae formation in vascular organoid derived human iPSC endothelial cells.

Previous studies reported that VEGFA, PMA, cytochalasin B and diamide can be used to induce and manipulate fenestrae formation. In this study, we combined a regime of VEGFA or PMA stimulation for fenestrae induction with cytochalasin B and diamide treatment for structure control to regulate the fenestrae process in hiPSC vascular organoid derived ECs (ODECs). HRGECs are included as a positive control. A schematic representation of the workflow for the generation of ODECs is shown in Fig. 1a. HiPSC derived vascular organoids, which express vascular cell markers CD31 and CD140b and present a microvascular network on D18 (Fig. 1b, d) are harvested and processed to obtain an ODEC population of cells that express endothelial markers CD31 and VE-cadherin and display a typical endothelial monolayer morphology in 2D culture, with limited expression of mural cell marker CD140b (Fig. 1c, e, f). For fenestrae induction, a schematic representation of the workplan is presented in Fig. 2a.

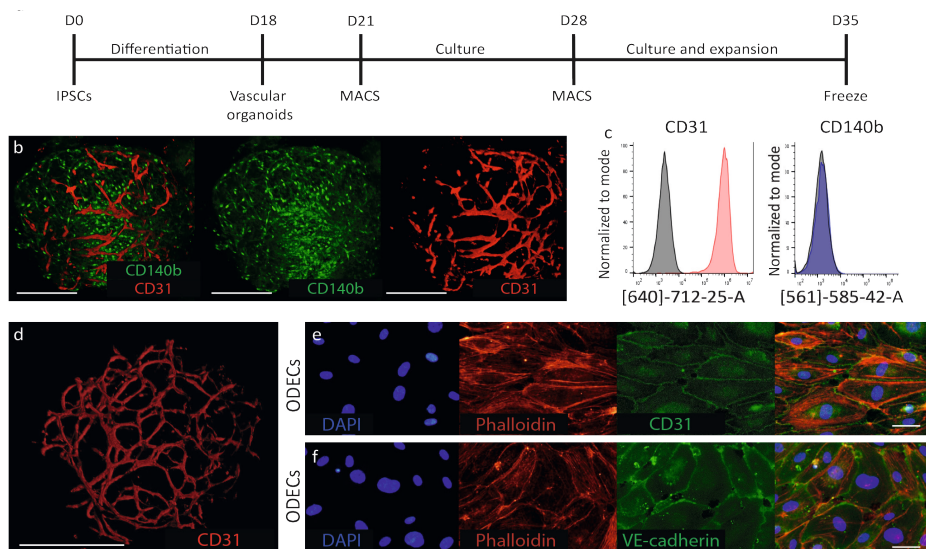


Figure 1. Vascular Organoid-derived Endothelial Cells.

a. Schematic timeline of the experimental set-up. **b.** Whole mount double staining of a vascular organoid. Mural cells are stained for CD140b (green) and endothelial cells are stained for CD31 (red). Scale bar depicts 500 μ m. **c.** FACS analysis of sorted ODECs labeled with CD31 (positive) and CD140b (negative) compared to the isotype control. **d.** Whole mount staining of a vascular organoid for CD31 (red). Scale bar depicts 500 μ m. **e.** IF staining of a 2D ODEC culture, stained for endothelial marker CD31 (green), Phalloidin (red) and counterstained with DAPI (blue). Scale bar depicts 20 μ m. **f.** IF staining of a 2D ODEC culture, stained for endothelial tight junction marker VE-cadherin (green), Phalloidin (red) and counterstained with DAPI (blue). Scale bar depicts 20 μ m.

Expression of PLVAP was first monitored by qPCR analysis as a marker for fenestrae. Analysis of the basic mRNA levels of PLVAP in HRGECs, ODECs, and HUVECs demonstrated that in line with previous reports of high level of fenestrae, HRGECs show significant higher expression of PLVAP compared to the other cell types (Fig. 2b). After, 48 h of treatment with 100 ng/mL VEGFA, VEGFA significantly enhanced PLVAP marker expression in ODECs, but not in HRGECs (Fig. 2c). In contrast, treatment for 48 h with 50 nM PMA enhanced PLVAP expression in both ODECs and HRGECs (Fig. 2c). In line with these observations, SEM evaluation of untreated cells reveal the presence of multiple fenestrae in sieve plate like locations in HRGECs, whereas hardly any fenestrae structures can be detected in ODECs (Fig. 2d, upper two panels). Following 48 h of VEGFA or PMA treatment, multiple fenestrae can be observed by SEM in ODECs (Fig. 2d, lower two panels), but had limited effect in HRGECs (Fig. 3b-c). The quantification of the SEM data using Imagej showed a significant increase in fenestrae numbers of ODECs in response to VEGFA or PMA stimulation, whereas fenestrae numbers in HRGECs remained unaffected (Fig.

2e, left graph). VEGFA or PMA treatment did not affect the average diameter of individual fenestrae (Fig. 2e, right graph). Likewise, immunofluorescent staining for fenestrae structures using the PLVAP marker reveal a higher basal PLVAP signal in untreated HRGECs compared to untreated ODECs (Fig. 2f, first two columns). The PLVAP signal is dramatically increased in ODECs treated with VEGFA or PMA (Fig. 2f, last two columns).

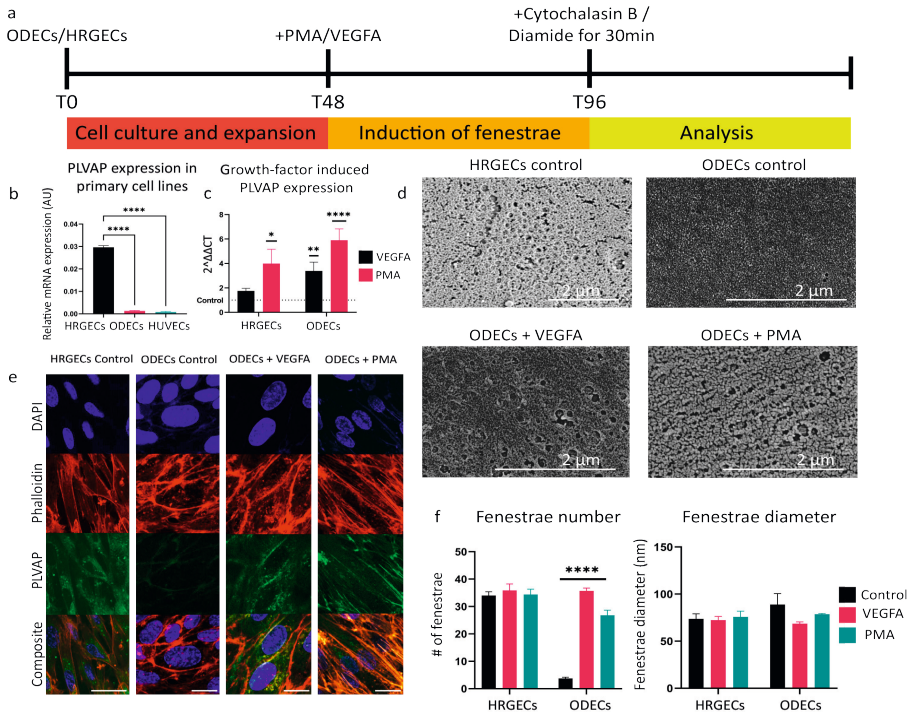


Figure 2. VEGFA or PMA induces fenestrae formation in Vascular Organoid-Derived human iPSC Endothelial Cells.

a. Schematic timeline of experimental set-up. **b.** Gene expression analysis of PLVAP basic levels in primary human cell lines HUVECs and HRGECs compared to ODECs. One-way ANOVA with Tukey post hoc test, **** $p < 0.0001$. Data represented as mean \pm SEM, $n = 4$ biological replicates. All samples were measured in duplo. **c.** PLVAP expression in HRGECs and ODECs after supplementation with VEGFA or PMA, compared to control conditions (dashed line). Two-way ANOVA with Tukey post hoc test, * $p < 0.05$, ** $p < 0.01$, **** $p < 0.0001$. Data represented as mean \pm SEM, $n = 6$ biological replicates. All samples were measured in duplo. **d.** SEM images of untreated fenestrated HRGECs compared to untreated ODECs and ODECs after supplementation with VEGFA or PMA. Scale bar depicts 2 μm. **e.** Immunofluorescent imaging of untreated HRGECs and ODECs supplemented with VEGFA or PMA. PLVAP is stained in green, phalloidin in red and DAPI is used as counterstaining in blue. Scale bar depicts 20 μm. **f.** SEM fenestrae quantification of treated HRGECs and ODECs after supplementation with VEGFA or PMA compared to control conditions. Two-way ANOVA with Tukey post hoc test, **** $P < 0.0001$. Data represented as mean \pm SEM, $n = 5$ biological replicates. Per sample, 3 pictures were used for analysis.

Regulation of fenestrae numbers and diameter in response to cytochalasin B or diamide following fenestrae induction.

Next, we evaluated if subsequent treatment with cytochalasin B or diamide could be used to regulate fenestrae number and structural characteristics. After 48 h of VEGFA treatment followed by 30 min of stimulation with cytochalasin B, we observed significantly increased fenestrae numbers in HRGECs but not ODECs, as shown by quantification of SEM data (Fig. 3a-d). Diamide treatment after VEGFA did not affect fenestrae number in HRGECs. However, it significantly decreased structure numbers in ODECs. After 48 h of PMA treatment followed by 30 min of stimulation with cytochalasin B or diamide, the number of fenestrae in HRGECs increased. In ODECs, only PMA + cytochalasin B increased fenestrae numbers (Fig. 3a-c and d). For the fenestrae diameter, VEGFA in combination with cytochalasin B treatment enhanced the average fenestrae diameter size in HRGECs, whereas PMA followed by diamide treatment caused a decline in diameter size in ODECs (Fig. 3a-c and d). qPCR analysis of the fenestrae structural proteins moesin, PLVAP and the fenestrae inhibitor annexin 2A, show upregulation of moesin expression in both HRGECs and ODECs following PMA with subsequent diamide stimulation (Fig. 3e). PLVAP expression was significantly enhanced in ODECs following PMA + cytochalasin B treatment, whereas annexin 2A remained unaffected after this regime in both cell types (Fig. 3e).

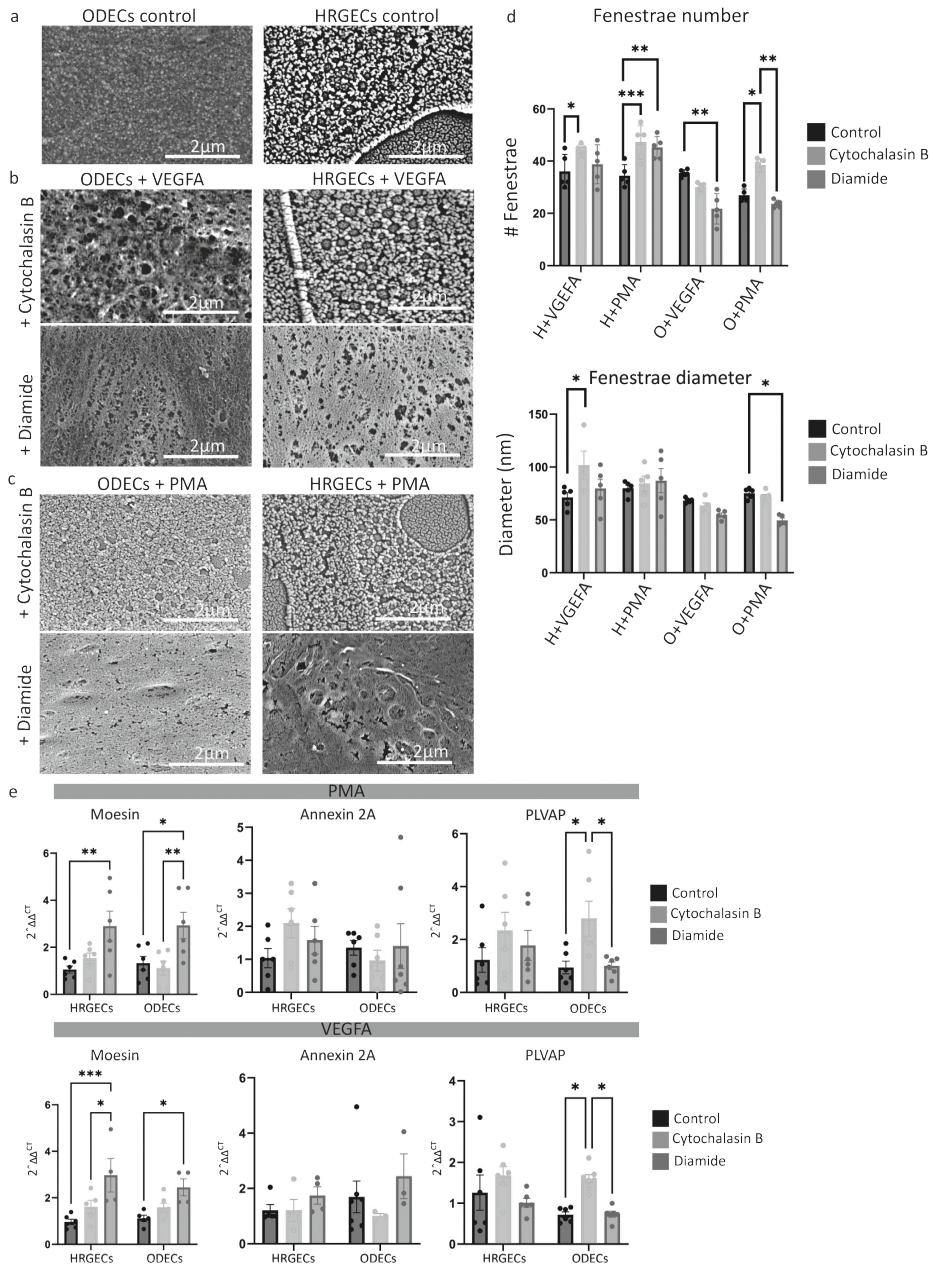


Figure 3. Effect of supplementation of Cytochalasin B and Diamide in fenestrated cells. **a.** SEM imaging of ODECs and HRGECs untreated (control). Scale bar depicts 2µm. **b.** SEM imaging of ODECs and HRGECs stimulated with VEGFA with and without supplementation with Cytochalasin B and Diamide. **c.** SEM imaging of ODECs and HRGECs stimulated with PMA with and without supplementation with Cytochalasin B and Diamide. Scale bar depicts 2µm. **d.** Fenestrae quantification

without (control) and with supplementation with Cytochalasin B and Diamide. Two-way ANOVA with Tukey post hoc test, * $p < 0.05$, ** $p < 0.01$, *** $p < 0.001$. Data represented as mean \pm SEM $n = 5$ biological replicates. Per sample, 3 pictures were used for analysis. **e.** Gene-expression analysis of fenestrated (PMA or VEGFA induced) HRGECs and ODECs with and without supplementation with Cytochalasin B and Diamide. Two-way ANOVA with Tukey post hoc test, * $p < 0.05$, ** $p < 0.01$. Data represented as mean \pm SEM, $n = 6$ biological replicates. All samples were tested in duplo.

Cellular localization of PLVAP

To evaluate the localization of the PLVAP protein, PLVAP gold labeling followed by TEM analysis was conducted on cell samples. Untreated ODECs showed little to no PLVAP signal (Fig. 4a). Analysis of HRGECs showed PLVAP signal localization in round membrane structures with 50-60 nm in diameter. ODECs following PMA treatment showed enhanced PLVAP signal in these membrane structures (Fig. 4a).

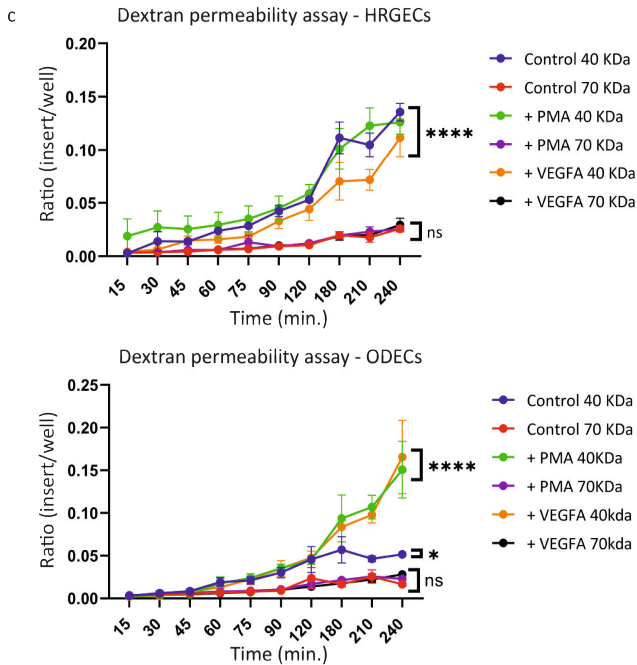
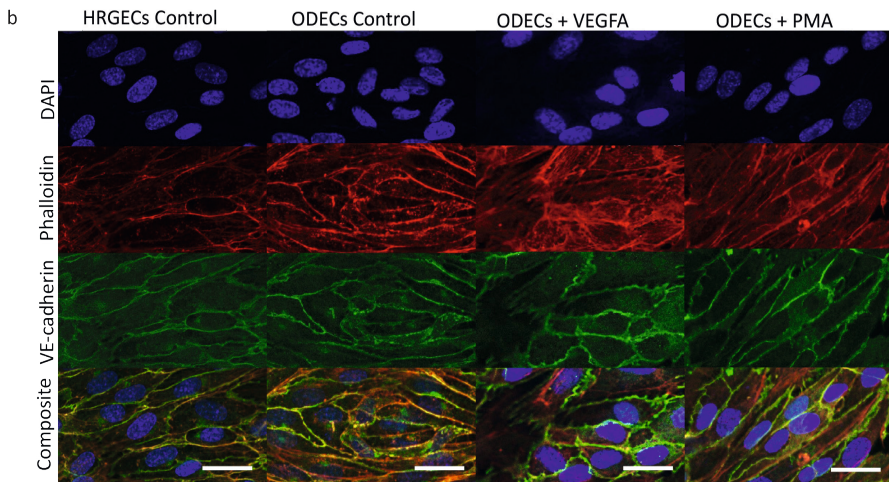
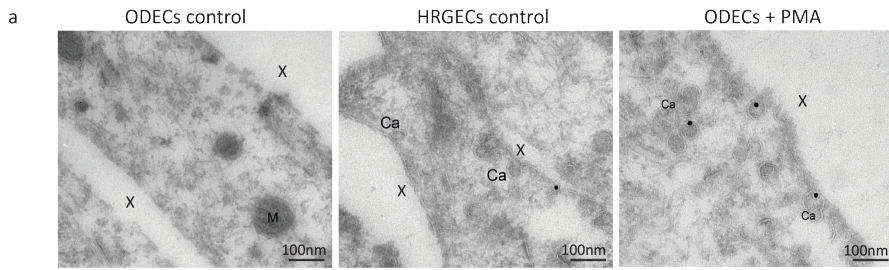


Figure 4. Selective permeability in fenestrated cells.

a. TEM imaging of PLVAP-labeled control HRGECs and ODECs compared to PMA-treated HRGECs. Ca: Caveolae, M: Mitochondria, X: lumen. PLVAP is labeled in black. Scale bar depicts 100nm. **b.** Immunofluorescent imaging of the adherent junctions of HRGECs and ODECs treated with and without VEGFA or PMA. Stained with VE-cadherin (green), Phalloidin (red) and counterstained with DAPI (blue). Scale bar depicts 20µm. **c.** Dextran permeability assay of control conditions and cells supplemented with VEGFA and PMA. Results are displayed as insert/well ratio. Two-way ANOVA with Tukey post hoc test, * $p < 0.05$, **** $p < 0.0001$, compared to 15 min. timepoint. Data represented as mean \pm SEM, $n = 3$ biological replicates. All samples were measured in triplo.

Selective permeability in fenestrated cells

To validate that fenestrae induction did not impact cell junction formation, confluent HRGEC and ODEC monolayers were evaluated for junction impairments using immunofluorescent VE-cadherin staining. Untreated HRGECs and ODECs form VE-cadherin cell junctions (Fig. 4b, first and second column). Treatment of ODECs with VEGFA or PMA did not induce disruptions in VE-cadherin cell junctions (Fig. 4b, third and fourth column).

Next, the functionality of the induced fenestrae was evaluated. Although fenestrated capillaries have on average 60 nm diameter openings, permeability is restricted to small hydrophilic solutes by PLVAP diaphragms that only allow passage of molecules up to 5 nm²⁷. Here passage efficacy of 40kDa (<5.77 nm) and 70kDa dextran (~5.77 nm) over a confluent endothelial layer of HRGECs and ODECs was evaluated¹⁸. HRGECs, naturally exhibiting elevated fenestrae numbers and PLVAP levels in the untreated state, demonstrated increased passage of 40kDa dextran across the monolayer over a 4-hour period compared to ODECs. (Fig. 4c). Passage of the 70kDa dextran was lower compared to that of the 40kDa dextran in both HRGECs and ODECs. Treatment with PMA or VEGFA, which had a limited effect in HRGECs on the level of fenestrae and PLVAP, similarly did not improve passage of the 40kDa dextran. In contrast, in ODECs, PMA and VEGFA stimulation significantly improved the 40kDa dextran passage, indicating transport via the induced fenestrae. Passage of the 70kDa dextran was not improved by PMA or VEGFA treatment in neither HRGECs nor ODECs, indicating a functional endothelial barrier. VE-cadherin (junctional) and actin (cytoskeletal) distribution was quantified using immunofluorescent microscopy and ImageJ analysis (Supplemental Fig. 1a-b). The results show no significant differences in VE-cadherin or actin area per cell, further indicative of a limited effect of the treatment regimes on barrier function.

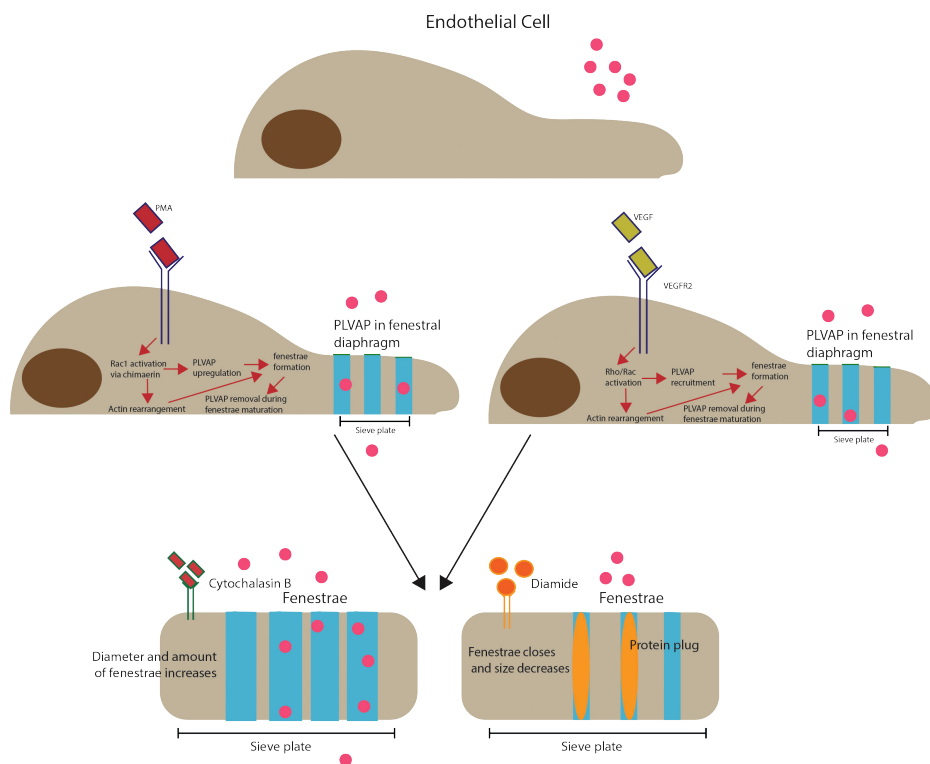


Figure 5. Schematic representation of fenestrae formation.

Binding of PMA causes (1) PLVAP upregulation and (2) Rac1 activation via Chimaerin, resulting in actin rearrangement and fenestrae formation. Binding of VEGFA to VEGFR2 results in (1) Rho/Rac activation resulting in actin rearrangement and (2) PLVAP recruitment. Both mechanisms induce fenestrae formation and facilitate molecule transport. PLVAP is located in the fenestral diaphragms and is removed during fenestrae maturation via an unknown mechanism. Binding of Cytochalasin B to fenestrated endothelium increases frequency and size of fenestrae on the endothelial membrane. Binding of Diamide results in the formation of protein plugs, closing the fenestrae and decreasing the size.

Discussion

Although the presence and critical function of fenestrae in the endothelium in select sections of the vascular tree has been long widely acknowledged and the most important steps in the fenestration process have been described, only a limited number of studies have investigated the factors that trigger fenestrae induction. This study demonstrates the successful induction and regulation of fenestrae formation in endothelial cells derived from vascular organoids of hiPSC source. The main findings are: (1) VEGFA or PMA stimulation of ODECs successfully promotes fenestrae formation to a level comparable to the baseline of HRGECs,

which naturally form fenestrae *in vivo* and *in vitro*. (2) A combination of VEGFA/PMA induction and cytochalasin B and diamide treatment can be used to further control fenestrae formation, although the response to the optimal doses of the secondary treatments differs considerably between HRGECs and ODECs. (3) Fenestrae induction in ODECs improved passage of small solutes over a confluent monolayer of ODECs without affecting passage of larger solutes, providing evidence of function for the induced fenestrae in ODECs. In contrast, additional fenestrae induction by VEGFA or PMA in HRGECs does not improve passage of small solutes over a confluent HRGEC monolayer. An overview of these findings are presented in figure 5. Overall, this study provides a new strategy for the induction and control of fenestrated endothelium in hiPSCs (organoid derived) endothelial cells. It also provides some insight into the regulation of fenestrae and has potential implication for human disease model building, drug delivery strategies, and vascularized tissue engineering applications.

Although the presence and critical function of fenestrae in the endothelium in select sections of the vascular tree has been widely acknowledged and the critical steps in the fenestrae process have been described, only a limited number of studies have investigated the factors that trigger fenestrae induction. Pro-angiogenic factor VEGFA was first primarily known for its ability to increase the permeability of blood vessels for plasma proteins. Although VEGFA is highly produced during embryonic vasculogenesis and angiogenesis, in adult conditions, in most organ tissues, VEGFA is downregulated once the endothelium transitions away from expansion and reaches quiescence²⁸. However, in some tissue types with highly fenestrated microvasculature, such as the choroid plexus in the brain and kidney glomeruli, VEGFA levels remain relatively high throughout adult life²⁹, which is coincided by continuous high expression of the VEGF receptors in the ECs³⁰. Combined, these findings are indicative that a consistent high level of VEGFA signaling is involved in the induction or maintenance of endothelial fenestrae in specific adult tissues. Indeed, Roberts *et al.* first confirmed that topical application or injection of VEGFA *in vivo* leads to the induction of fenestrae together with increased permeability of the otherwise typically continuous non-fenestrated endothelium of the venules and capillaries in skeletal muscle and skin²². Esser *et al.* validated the capacity of VEGFA by inducing fenestrae *in vitro*. They achieved this by coculturing bovine adrenal cortex ECs with mammary epithelial cells transiently overexpressing VEGFA splice variants VEGF120 and VEGF164, whereas coculture with cells lacking VEGFA overexpression did not induce a similar effect.³¹

Other *in vitro* studies have also identified a number of other extracellular signalling molecules, including TGF β , retinoic acid, serotonin, and a select group of extracellular matrix (ECM) components, that could impact fenestrae formation. **Lombardi *et al.* demonstrated the use of** phorbol 12-myristate 13-acetate (PMA), a diester of phorbol, could induce a five-fold increase in diaphragmed fenestrae in microvascular ECs in culture³². The same group also demonstrated that ECs derived from large vessels such as the umbilical vein and pulmonary artery, which are typically continuous and non-fenestrated *in vivo* and *in vitro*, can adapt a fenestrated phenotype in response to PMA stimulation³³. Although these observations have been made decades ago, and the use of VEGFA, PMA and other extracellular factors have been implemented in studies to improve our understanding of the mechanistic pathways of the fenestration process, none of these methods have thus far been explored to induce and control fenestrae in regenerative medicine.

Our findings show, for the first time, that both PMA or VEGFA can be used to trigger fenestrae formation in otherwise non-fenestrated ODECs from a hiPSC source. SEM analyses revealed a significant increase in fenestrae structures to a level that is comparable to the basic fenestrae level of HRGECs in culture. Several different methods for hiPSC differentiation of ECs have been reported. The ODECs used in this study are derived from hiPSC vascular organoids, cultured according to method reported by Wimmer *et al.*³⁴. We have previously described a new strategy for harvesting and isolating ECs from these organoids for guided (top down) vascular engineering purposes, including cell seeding of synthetic grafts²⁵. ODECs express several typical EC markers as CD31 and VE-cadherin, are shear stress responsive, and demonstrate endothelial barrier function with regenerative capacity after thrombin challenge. Furthermore, the ODECs in their initial vascular organoid structure show angiogenic and sprouting behaviour. In these aspects, they are thus comparable to primary ECs in culture, such as HUVECs and (skin derived) microvascular ECs²⁵. In line with this, previous studies conducted with hiPSC derived ECs derived from single cell type differentiation protocols, also report that they exhibit pro-angiogenic capacity, either by providing paracrine support to existing vessels *in vivo* or by actual physical contribution to neo-vessel formation *in vivo* and *in vitro*^{1,4,35,36}. In addition, some of these cells can adapt to shear stress on a morphological and molecular level³⁷. However, although these findings indicate that hiPSC derived ECs can perform basic EC function, it remained to be investigated whether hiPSC-derived ECs can adapt to organ-specific phenotypes and transform into fenestrated endothelium in particular.

Our study demonstrates that endothelium derived from vascular organoids of hiPSC origin can differentiate using PMA or VEGFA stimulation into a continuous fenestrated phenotype. Although fenestrae induction by PMA and VEGFA has been shown to be feasible in human primary ECs, this has not been demonstrated before for ECs of hiPSC origin. Remarkably, fenestrae number could not be further increased in HRGECs, a cell phenotype that is naturally fenestrated *in vivo* and *in vitro*, by PMA and VEGFA. Fenestrae induction by both compounds lead to comparable number of fenestrae density in ODECs, implying that at least via these pathways of induction, the optimal density of fenestrae may be reached.

Previous mechanistic studies often used cytoskeleton modulators to study fenestrae formation. For example, reduction of cytoskeleton and cell stiffness by actin depolymerization using cytochalasin B, has been reported to increase fenestrae density in primary liver sinusoid ECs (LSECs) ²⁴. In contrast, diamide, a compound that increases cell and cytoskeleton stiffness by oxidizing spectrin, thereby interfering with its function as a structural actin-crosslinking protein that is part of a scaffold complex providing cell membrane support, decreases fenestrae number and the diameter of the remaining pores ²⁰.

These previous observations in LSECs are partially in line with the observations in our study, in which HRGECs treated with VEGFA or PMA, and ODECs with PMA treatment showed a significant further increase in fenestrae density. In addition, an increase in fenestrae diameter was observed in HRGECs treated with VEGFA. However, further increase in fenestrae density in ODECs with VEGFA treatment was not observed. Similarly, diamide either had no effect or unexpectedly further increased fenestrae numbers, in HRGECs treated with VEGFA or PMA, respectively. In ODECs, diamide decreased fenestrae number in the VEGFA treated condition as expected, but it had no further effect on fenestrae diameter. In ODECs preconditioned with PMA, a decline in diameter size was observed, but no significant decline in fenestrae number.

As most of the reported studies with the cytoskeleton modulators were conducted in LSECs, whereas here we compared ODEC performance to that of HRGECs, the difference in response may be attributed to differences in EC phenotype on an epigenetic level and may be linked to the basic stiffness level of the cells. As cell stiffness is known to be impacted by mechanical stimulation in correlation to the degree and type of ECM contact ³⁸⁻⁴⁰, it would be of interest to further explore the induction in fenestrae in hiPSC-derived ODECs as well as primary EC types under

hemodynamic exposure and in different hydrogel and ECM environments. The findings of such studies may lead to new strategies to further promote fenestrae in ECs by also considering local *in situ* haemodynamic and ECM parameters.

The use of PLVAP as a marker for fenestrae components provides a limited interpretation of the degree of fenestrae. PLVAP encodes a structural protein that forms spoke-wheel-like diaphragms spanning small to medium-sized diameter fenestrae. As fenestrae mature and the pore diameter increases, the PLVAP structures disappear. The transient nature of the PLVAP diaphragms suggests that PLVAP and the related structure may be critical for the initial phase of fenestrae development. However, this hypothesis was later refuted by data provided by genetic murine PLVAP models^{17,18}. However, the PLVAP protein is proven essential for diaphragm formation. Furthermore, PLVAP is also present in caveola, invaginations in the plasma membrane that is enriched with caveolin^{13,16,41,42}. Nevertheless, as PLVAP expression correlates with fenestrae initiation, it may be used to identify small to midsized diaphragmed fenestrae, but this data should be supplemented and verified by SEM, as demonstrated in this study.

Functional evaluation of fenestrae induction using a trans-endothelium dextran assay reveals the passage of dextran with a size of 40kDa (<5.77 nm) in HRGECs and ODECs after fenestrae induction, but not 70kDa (~5.77nm). We chose these specific sizes because typically, solutes that can pass through fenestration structures have a diameter limit of 5 nm⁴³. Above this size, intracellular passage via this route becomes difficult and instead may only occur through active transport or intercellular junction leakage. Analysis of the cell junctions demonstrate no impact on endothelial barrier integrity by either VEGFA or PMA treatment, suggesting that the 40kDa dextran passed through fenestrae pores, thereby indicating that the induced fenestrae are functional.

The strategy described here for inducing fenestrae in hiPSC-derived endothelium has potential applications in complex disease modelling *in vitro* and tissue vascularization strategies in regenerative medicine. Incorporating fenestrated vasculature is critical for the physiological function of organ tissue from a regenerative medicine perspective. The strategy presented here represents a useful tool for building a functional vascularized tissue unit that recreates structures such as the peritubular network, which facilitates solute re-absorption in the nephrons, or the villous capillary network in small intestinal villi, which aid in nutrients uptake. Regarding disease modelling, including fenestrated vasculature in relevant tissue-on-a-chip platforms, such as those representing the kidney, small intestine, endocrine glands,

and adipose systems, could greatly enhance their biological relevance by mimicking natural solute exchange ⁴⁴. The presence of fenestrated vasculature can influence not only the local permeability of naturally secreted biological compounds but also impact the delivery of external compounds. Therefore, relevant tissue models that incorporate fenestrated vascularization may be more suitable for candidate drug screening than their counterparts that ignore this aspect of the vascular biology. Without incorporating fenestrae, the efficacy of drug delivery to tissue cells and its subsequent effects may not be relevant *in vivo* in tissues where continuous endothelium with limited drug passage does not accurately represent real-life scenarios. In the context of human disease modelling, the new protocol can also enhance our comprehension of how fenestrae structures are influenced by systemic and local factors associated with disease, ultimately contributing to disease progression. For example, elevated levels of local or circulating cytokines such as IL-6 in CKD ⁴⁵ may disrupt the balance of local VEGFA levels ⁴⁶, which are crucial for maintaining peritubular fenestrae structures ⁴⁷. Exposure to disease-related elements may cause a similar condition in other organs with fenestrated vasculature, as inhibition of VEGFA-VEGFR signaling in mice (partially) results in significant capillary regression, with surviving capillaries displaying fewer fenestrae ⁴⁸.

In conclusion, we present a novel strategy to induce fenestrae formation in human induced pluripotent stem cell (hiPSC)-derived endothelium of vascular organoids. Our approach has promising implications for the generation of physiologically relevant *in vitro* models of human diseases, particularly for organs that rely on fenestrated microvasculature for their physiological function. Additionally, our method could enable the development of a fenestrated microcapillary network for regenerative medicine applications. The use of hiPSCs in this context also holds potential for advancing the field of personalized medicine.

Acknowledgements

The authors would like to thank Tineke Veenendaal for performing the TEM preparation and analysis at the Core Microscopy Center in the UMCU.

Author contributions

EMM wrote the manuscript together with CC and performed experiments. EMM, CC and CVD were responsible for experimental design. CC and MCV supervised the project. IC, KG and RG performed experiments.

Conflict of Interest

The authors declare no conflict of interest.

Funding statement

This work was funded by the REGMEDXB cardiovascular moonshot consortium and the NWO Vidi grant (no. 91714302 to CC). The authors gratefully acknowledge the Gravitation Program “Materials Driven Regeneration”, funded by the Netherlands Organization for Scientific Research (024.003.013).

References

1. Rufaihah AJ, Huang NF, Jame S, et al. Endothelial cells derived from human iPSCs increase capillary density and improve perfusion in a mouse model of peripheral arterial disease. *Arterioscler Thromb Vasc Biol.* 2011;31(11):e72-9.
2. Lee SJ, Sohn YD, Andukuri A, et al. Enhanced Therapeutic and Long-Term Dynamic Vascularization Effects of Human Pluripotent Stem Cell-Derived Endothelial Cells Encapsulated in a Nanomatrix Gel. *Circulation.* 2017;136(20):1939-54.
3. Campisi M, Shin Y, Osaki T, et al. 3D self-organized microvascular model of the human blood-brain barrier with endothelial cells, pericytes and astrocytes. *Biomaterials.* 2018;180:117-29.
4. Vila Cuenca M, Cochrane A, van den Hil FE, et al. Engineered 3D vessel-on-chip using hiPSC-derived endothelial- and vascular smooth muscle cells. *Stem Cell Reports.* 2021;16(9):2159-68.
5. Kibria G, Heath D, Smith P, et al. Pulmonary endothelial pavement patterns. *Thorax.* 1980;35(3):186-91.
6. Risau W. Development and differentiation of endothelium. *Kidney Int Suppl.* 1998;67:S3-6.
7. Sarin H. Physiologic upper limits of pore size of different blood capillary types and another perspective on the dual pore theory of microvascular permeability. *J Angiogenesis Res.* 2010;2:14.
8. Toyoda M, Najafian B, Kim Y, et al. Podocyte detachment and reduced glomerular capillary endothelial fenestration in human type 1 diabetic nephropathy. *Diabetes.* 2007;56(8):2155-60.
9. Babickova J, Klinkhammer BM, Buhl EM, et al. Regardless of etiology, progressive renal disease causes ultrastructural and functional alterations of peritubular capillaries. *Kidney Int.* 2017;91(1):70-85.
10. Xie G, Wang X, Wang L, et al. Role of differentiation of liver sinusoidal endothelial cells in progression and regression of hepatic fibrosis in rats. *Gastroenterology.* 2012;142(4):918-27 e6.
11. Milici AJ, Furie MB, Carley WW. The formation of fenestrations and channels by capillary endothelium in vitro. *Proc Natl Acad Sci U S A.* 1985;82(18):6181-5.
12. van den Berg CW, Ritsma L, Avramut MC, et al. Renal Subcapsular Transplantation of PSC-Derived Kidney Organoids Induces Neo-vasculogenesis and Significant Glomerular and Tubular Maturation In Vivo. *Stem Cell Reports.* 2018;10(3):751-65.
13. Stan RV. Multiple PV1 dimers reside in the same stomatal or fenestral diaphragm. *Am J Physiol Heart Circ Physiol.* 2004;286(4):H1347-53.
14. Satchell SC, Braet F. Glomerular endothelial cell fenestrations: an integral component of the glomerular filtration barrier. *Am J Physiol Renal Physiol.* 2009;296(5):F947-56.
15. Ioannidou S, Deinhardt K, Miotla J, et al. An in vitro assay reveals a role for the diaphragm protein PV-1 in endothelial fenestra morphogenesis. *Proc Natl Acad Sci U S A.* 2006;103(45):16770-5.
16. Stan RV. Endothelial stomatal and fenestral diaphragms in normal vessels and angiogenesis. *J Cell Mol Med.* 2007;11(4):621-43.

17. Herrnberger L, Seitz R, Kuespert S, et al. Lack of endothelial diaphragms in fenestrae and caveolae of mutant Plvap-deficient mice. *Histochem Cell Biol.* 2012;138(5):709-24.
18. Stan RV, Tse D, Deharvengt SJ, et al. The diaphragms of fenestrated endothelia: gatekeepers of vascular permeability and blood composition. *Dev Cell.* 2012;23(6):1203-18.
19. van der Wijk AE, Wisniewska-Kruk J, Vogels IMC, et al. Expression patterns of endothelial permeability pathways in the development of the blood-retinal barrier in mice. *FASEB J.* 2019;33(4):5320-33.
20. Zapotoczny B, Braet F, Kus E, et al. Actin-spectrin scaffold supports open fenestrae in liver sinusoidal endothelial cells. *Traffic.* 2019;20(12):932-42.
21. Ju M, Ioannidou S, Munro P, et al. A Na,K-ATPase-Fodrin-Actin Membrane Cytoskeleton Complex is Required for Endothelial Fenestra Biogenesis. *Cells.* 2020;9(6).
22. Roberts WG, Palade GE. Increased microvascular permeability and endothelial fenestration induced by vascular endothelial growth factor. *J Cell Sci.* 1995;108 (Pt 6):2369-79.
23. Roberts WG, Palade GE. Neovasculature induced by vascular endothelial growth factor is fenestrated. *Cancer Res.* 1997;57(4):765-72.
24. Zapotoczny B, Szafranska K, Owczarczyk K, et al. Atomic Force Microscopy Reveals the Dynamic Morphology of Fenestrations in Live Liver Sinusoidal Endothelial Cells. *Sci Rep.* 2017;7(1):7994.
25. Meijer EM, Koch SE, van Dijk CGM, et al. 3D Human iPSC Blood Vessel Organoids as a Source of Flow-Adaptive Vascular Cells for Creating a Human-Relevant 3D-Scaffold Based Macrovascular Model. *Adv Biol (Weinh).* 2022:e2200137.
26. Slot JW, Geuze HJ. Cryosectioning and immunolabeling. *Nat Protoc.* 2007;2(10):2480-91.
27. Claesson-Welsh L, Dejana E, McDonald DM. Permeability of the Endothelial Barrier: Identifying and Reconciling Controversies. *Trends Mol Med.* 2021;27(4):314-31.
28. Carmeliet P, Jain RK. Molecular mechanisms and clinical applications of angiogenesis. *Nature.* 2011;473(7347):298-307.
29. Breier G, Albrecht U, Sterrer S, et al. Expression of vascular endothelial growth factor during embryonic angiogenesis and endothelial cell differentiation. *Development.* 1992;114(2):521-32.
30. Millauer B, Wizigmann-Voos S, Schnurch H, et al. High affinity VEGF binding and developmental expression suggest Flk-1 as a major regulator of vasculogenesis and angiogenesis. *Cell.* 1993;72(6):835-46.
31. Esser S, Wolburg K, Wolburg H, et al. Vascular endothelial growth factor induces endothelial fenestrations in vitro. *J Cell Biol.* 1998;140(4):947-59.
32. Lombardi T, Montesano R, Furie MB, et al. Endothelial diaphragmed fenestrae: in vitro modulation by phorbol myristate acetate. *J Cell Biol.* 1986;102(5):1965-70.
33. Lombardi T, Montesano R, Orci L. Phorbol ester induces diaphragmed fenestrae in large vessel endothelium in vitro. *Eur J Cell Biol.* 1987;44(1):86-9.
34. Wimmer RA, Leopoldi A, Aichinger M, et al. Human blood vessel organoids as a model of diabetic vasculopathy. *Nature.* 2019;565(7740):505-10.
35. Orlova VV, van den Hil FE, Petrus-Reurer S, et al. Generation, expansion and functional analysis of endothelial cells and pericytes derived from human pluripotent stem cells. *Nat Protoc.* 2014;9(6):1514-31.

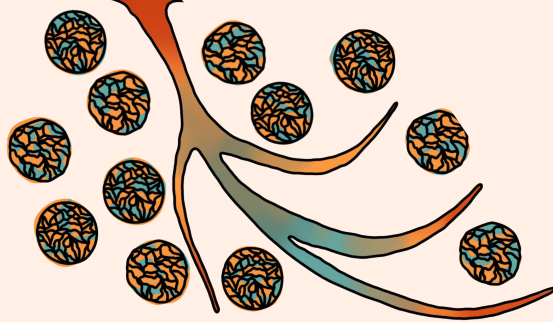
36. Gara E, Zucchelli E, Nemes A, et al. 3D culturing of human pluripotent stem cells-derived endothelial cells for vascular regeneration. *Theranostics*. 2022;12(10):4684-702.
37. Helle E, Ampuja M, Antola L, et al. Flow-Induced Transcriptomic Remodeling of Endothelial Cells Derived From Human Induced Pluripotent Stem Cells. *Front Physiol*. 2020;11:591450.
38. Janmey PA, Fletcher DA, Reinhart-King CA. Stiffness Sensing by Cells. *Physiol Rev*. 2020;100(2):695-724.
39. d'Angelo M, Benedetti E, Tupone MG, et al. The Role of Stiffness in Cell Reprogramming: A Potential Role for Biomaterials in Inducing Tissue Regeneration. *Cells*. 2019;8(9).
40. Yi B, Xu Q, Liu W. An overview of substrate stiffness guided cellular response and its applications in tissue regeneration. *Bioact Mater*. 2022;15:82-102.
41. Hamilton BJ, Tse D, Stan RV. Phorbol esters induce PLVAP expression via VEGF and additional secreted molecules in MEK1-dependent and p38, JNK and PI3K/Akt-independent manner. *J Cell Mol Med*. 2019;23(2):920-33.
42. Milici AJ, Peters KR, Palade GE. The endothelial pocket. A new structure in fenestrated endothelia. *Cell Tissue Res*. 1986;244(3):493-9.
43. Herrnberger L, Hennig R, Kremer W, et al. Formation of fenestrae in murine liver sinusoids depends on plasmalemma vesicle-associated protein and is required for lipoprotein passage. *PLoS One*. 2014;9(12):e115005.
44. Aird WC. Phenotypic heterogeneity of the endothelium: I. Structure, function, and mechanisms. *Circ Res*. 2007;100(2):158-73.
45. Pecoits-Filho R, Heimbürger O, Barany P, et al. Associations between circulating inflammatory markers and residual renal function in CRF patients. *Am J Kidney Dis*. 2003;41(6):1212-8.
46. Cohen T, Nahari D, Cerem LW, et al. Interleukin 6 induces the expression of vascular endothelial growth factor. *J Biol Chem*. 1996;271(2):736-41.
47. Kuppe C, Rohlfes W, Greppl M, et al. Inverse correlation between vascular endothelial growth factor back-filtration and capillary filtration pressures. *Nephrol Dial Transplant*. 2018;33(9):1514-25.
48. Kamba T, Tam BY, Hashizume H, et al. VEGF-dependent plasticity of fenestrated capillaries in the normal adult microvasculature. *Am J Physiol Heart Circ Physiol*. 2006;290(2):H560-76.

Supplemental information



CHAPTER

5



The Effect of Mechanical Stimuli on the Phenotypic Plasticity of Induced Pluripotent Stem Cell-Derived Vascular Smooth Muscle Cells in a 3D Hydrogel

Elana M. Meijer, Rachel Giles, Christian G.M. van Dijk, Ranganath Maringanti, Tamar B. Wissing, Ymke Appels, Ihsan Chrifi, Hanneke Crielaard, Marianne C. Verhaar, Anthal I.P.M. Smits, Caroline Cheng

ACS Appl Bio Mater. 2023 Dec 18;6(12):5716-5729. doi: 10.1021

Abstract

Introduction

Vascular smooth muscle cells (VSMCs) play a pivotal role in vascular homeostasis, with dysregulation leading to vascular complications. Human induced pluripotent stem cell (hiPSC)-derived VSMCs offer prospects for personalized disease modeling and regenerative strategies. Current research lacks comparative studies on the impact of 3D substrate properties under cyclic strain on phenotypic adaptation in hiPSC-derived VSMCs. Here we aim to investigate the impact of intrinsic substrate properties, such as the hydrogel's elastic modulus and crosslinking density in a 3D static and dynamic environment, on the phenotypical adaptation of human mural cells derived from hiPSC-derived organoids (ODMCs), compared to aortic VSMCs.

Methods and results

ODMCs were cultured in 2D conditions with synthetic or contractile differentiation medium, or in 3D Gelatin Methacryloyl (GelMa) substrates with varying degrees of functionalization and percentages to modulate Young's modulus and crosslinking density. Cells in 3D substrates were exposed to cyclic, unidirectional strain. Phenotype characterization was conducted using specific markers through immunofluorescence and gene expression analysis. Under static 2D culture, ODMCs derived from hiPSCs exhibited a VSMC phenotype, expressing key mural markers, and demonstrated a level of phenotypic plasticity similar to primary human VSMCs. In static 3D culture, a substrate with a higher Young's modulus and crosslinking density promoted a contractile phenotype in ODMCs and VSMCs. Dynamic stimulation in the 3D substrate promoted a switch towards a contractile phenotype in both cell types.

Conclusion

Our study demonstrates a phenotypic plasticity of human ODMCs in response to 2D biological and 3D mechanical stimuli that equals that of primary human VSMCs. These findings may contribute to the advancement of tailored approaches for vascular disease modeling and regenerative strategies.

Keywords

vascular smooth muscle cells, blood vessels, iPSCs, organoids, vasculature, GelMa, tissue engineering, hydrogels

Introduction

Vascular smooth muscle cells (VSMCs) provide structural vascular support and stability, regulate blood flow, contribute to immune responses and participate in tissue repair mechanisms¹⁻³. VSMC dysfunction leads to vascular complications with a significant impact on morbidity and mortality, including (non-)obstructive coronary artery disease (CAD), carotid artery and aortic aneurysms, and pulmonary arterial hypertension⁴⁻⁸. Understanding the cellular processes that contribute to disease etiology is essential for developing dedicated *in vitro* disease models, targeted therapies as well as regenerative strategies for the treatment of vascular diseases.

Following differentiation during vascular development, VSMCs retain a considerable degree of plasticity, manifesting a spectrum of phenotypic variations. This spectrum encompasses synthetic characteristics, including proliferation, extracellular matrix (ECM) synthesis, and tissue repair, as well as contractile properties involving force generation^{6,9,10}. During neovascularization, VSMCs exhibit a synthetic phenotype characterized by high rates of proliferation, cell migration, and deposition of ECM^{3,4}. In mature functional blood vessels, VSMCs typically assume a contractile phenotype to fulfil an essential role in vessel stabilization and vasomotion, displaying a quiescent state with an elongated, spindle-shaped morphology⁴. Phenotypic switching between contractile to synthetic occurs during adulthood in response to e.g. vessel injury and represents a critical step in the repair process⁵.

Although animal models and primary VSMC culture systems have provided valuable insights into vascular biology and disease, there are substantial disparities in the vascular physiology between rodents and humans. Additionally, limited availability of patient-derived VSMCs and the absence of well-characterized patient-specific three-dimensional (3D) tissue models that aim to closely mimic the dynamic *in vivo* environment, currently impede advancements in research. Human-induced pluripotent stem cell (iPSC)-derived VSMCs offer an alternative platform for studying human vascular biology¹¹⁻¹⁷. Generated from healthy donor or patient-derived somatic cells, iPSC derived tissue cells represent an abundant source for disease modeling, drug screening, and tissue engineering. Concerning VSMCs derived from iPSCs, several significant challenges remain to be addressed. One key issue is the phenotypic and developmental heterogeneity observed in many culture protocols, resulting in a mixed population of VSMCs with varying levels of synthetic and contractile phenotypes, as well as a degree of "contamination" of the cell pool with non-VSMCs. Several strategies have been developed for the enrichment of lineage-

or phenotype-specific VSMCs while excluding non-VSMCs^{18, 19}. However, most published studies have still relied on differentiated VSMCs with unclear embryonic origin, purity, or functional phenotype. This phenotypic heterogeneity in particular poses a significant challenge in their application for human disease modeling as well as regenerative medicine. The successful replication of physiological function relies on the presence of contractile VSMCs, whereas in vascular diseases as well as tissue (re)generation, synthetic VSMCs play critical roles. This duality becomes particularly problematic as iPSC-derived VSMCs need to effectively mimic either contractile or synthetic phenotypes to accurately represent various disease conditions *in vitro* or achieve the desired cellular phenotypes in different phases of vascular tissue engineering. An improved understanding of how environmental factors define (h) iPSC-derived VSMC phenotypes could provide leads to possible solutions.

Various biological growth factors are known to induce the phenotypic switch in VSMCs *in vitro*, including Platelet Derived Growth factor B (PDGFB), which can be used to induce synthetic characteristics in primary VSMCs^{18, 20}, and transforming growth factor beta (TGF- β), which is reported to reverse synthetic VSMCs into a contractile phenotype¹⁹. In addition, phenotype transformation of VSMCs is known to be modulated by mechanical cyclic strain, as shown in various *in vitro* studies, mimicking *in vivo* vascular dynamics. VSMC responses are variable, depending on the applied strain frequencies, elongation, and orientation (e.g. uni or bidirectional, on a flat or circumferential surface)²¹⁻²³. Phenotype determination in primary VSMCs may also be controlled by intrinsic matrix properties^{24, 25}, where cell responses appear to significantly differ between 2D (cells grown on top of a matrix substrate) versus 3D (grown in a matrix substrate) culture conditions²⁶⁻²⁸.

For (h)iPSC-derived VSMCs, previous studies have demonstrated that both biological growth factors and dynamic strain can initiate phenotypic adaptation, resembling the response of primary VSMCs^{14, 22}. Nevertheless, the influence of intrinsic matrix substrate properties, such as the hydrogel's elastic modulus, and crosslinking density (degree of functionalization, or DOF) on (h)iPSC-derived VSMCs, especially in 3D instead of 2D structures, where the 3D environment closely mimics the physiological conditions, has not yet been investigated. Moreover, the phenotypic adaptation of (h)iPSC-derived VSMCs in response to these factors in 3D environments under cyclic strain, remains unexplored.

In this study, we evaluated the potential of human mural cells derived from hiPSCs obtained from vascular organoids (organoid derived mural cells, or ODMCs) to adapt into VSMCs with a contractile or synthetic phenotype. In particular, their response

to various phenotype differentiation inducers, such as biological growth factors (TGF- β and PDGFB) were evaluated. Additionally, we assessed their phenotypic responses to differences in elastic modulus and crosslinking density of the matrix in a 3D environment, using Gelatin Methacryloyl (GelMa) with weight percentages and DOFs respectively, in the presence and absence of cyclic unidirectional strain. By investigating the impact of these environmental components on the phenotypic switch in ODMCs, the optimal conditions can be defined to grow and maintain a hiPSC-derived VSMC pool with the desired phenotype. The findings from this study thus provide valuable strategies for complex *in vitro* modeling of vascular diseases and have implications for regenerative approaches.

Methods

2D Growth factor experiments

2D Cell Culture

ODMCs were differentiated and harvested from hiPSC-derived blood vessel organoids as described previously²⁹. Aortic VSMCs were purchased from Lonza. Both ODMCs and VSMCs were cultured on 1% gelatin coated cell culture plates in SMGM-2 medium (Lonza) at 5% CO₂. Medium was changed every other day. Cells were passaged for expansion or harvesting using Trypsin/EDTA (Gibco). Cells were used until passage 7.

Growth factor induced phenotypic switch

Cells were plated onto gelatin-coated 18mm coverslips (staining) or gelatin coated 6-well plates (PrestoBlue and gene expression analysis). They were serum-starved (0.5% Fetal Bovine Serum (FBS) in DMEM) for 24 h before inducing the phenotypic switch. Control groups were cultured in DMEM with 10% FBS and 1% Pen/Strep (P/S). Synthetic groups were cultured in DMEM with 10% FBS, 1% P/S, 10ng/ml PDGF and 1ng/ml TGF β . Contractile groups were cultured in DMEM with 0.5% FBS, 1% P/S and 1ng/ml TGF β . All were kept at 37°C with 5% CO₂.

PrestoBlue viability assay

Cells ($n=6$ different vials per cell type) were seeded on a gelatin coated six-well plate with a cell density of 50 000 cells per well. Cell viability was measured 24, 72 and 144 h after growth factor treatment using PrestoBlue Cell Viability Reagent (ThermoScientific) according to the manufacturer's protocol.

FACS analysis of ODMCs

ODMCs were cultured and harvested using Trypsin/EDTA as described above. Cells were distributed in a 96-well plate (25 000 cells per well) and subsequently stained with anti-CD31 and anti-CD140b antibodies (Table S1), together with Sytox blue (Invitrogen) to exclude dead cells. The CytoFLEX flow cytometer (Beckman Coulter) was used for cell analysis and data analysis was performed using FlowJo software (Version 10.2).

3D Static GelMa experiments

GelMa hydrogel preparation

Two GelMa stocks with different Degree of Functionalization (DOF) were prepared. For both, 10g type A gelatin from porcine skin (Sigma Aldrich) was dissolved in 100mL PBS at 60°C to obtain a 10% gelatin solution. The DOF is defined by the percentage of modified lysin residues as described and validated previously^{30,31}. After 3 h, 400mL PBS was added and the solution was dialyzed against distilled water to remove salts and methacrylic acid for 7 consecutive days. Finally, the solution was lyophilized and stored at -80°C until further use.

To prepare hydrogels, GelMa dissolved in PBS was subjected to radical crosslinking in the presence of a photo-initiator. For this, a 0.1% 2-Hydroxy-2-methylpropiophenone photo-initiator (PI) (Irgacure, Sigma Aldrich®) was prepared using PBS. Lyophilized GelMa (5 or 10% w/v) was mixed with 0.1% PBS-PI and incubated for 15 minutes at 80°C to dissolve. This protocol is executed according to a previously described protocol by Bracco Gartner et al.³².

GelMa swelling assay

30µL of pre-polymer solution with both 80 DOF and 50 DOF (5% and 10%) was pipetted onto a 10 cm petri dish between two spacers with a height of 0.45mm and was covered with a sterile glass slide. The pre-polymer solution was placed under a 450mW UV-light (OmniCure Series 2000, Excelitas) for 50 seconds. The hydrogel was removed from the glass slide and washed with PBS. Empty hydrogels were incubated in PBS at 37°C for 24 h before mechanical testing and hydrogel swelling analysis.

Swollen GelMa hydrogels (3 per experiment for 5 different experiments) were weighed (ww) and subsequently dried by lyophilization. After that, dried weight (wd) of GelMa hydrogels were obtained and the mass-swelling ratio (q) was calculated as $q = ww/wd$.

Dynamic mechanical analysis - DMA

The Q800 Dynamic Mechanical Analyzer (DMA) (TA Instruments, Inc.) was used to test the hydrogel mechanical properties through a controlled force. The hydrogels were placed between the parallel-plate compression. A ramp force was applied at 0.010N/minute to 0.500N with a preload force of 0.0010N for 10 minutes. The Young's Modulus was calculated by the slope of the most linear part (8 datapoints) of the stress-strain curve.

Cell-laden 3D static GelMa hydrogels

The ODMCs/VSMCs were added to the GelMa-PI solution to achieve a cell density of 75,000 cells per 30 μ L. The cell containing GelMa solution (30 μ L) was pipetted on a 10cm petri dish between two spacers covered with a sterile microscope slide and placed under a 450mW UV-light (OmniCure Series 2000, Excelitas) for 50 seconds. The hydrogels were subjected to serum starvation (0.5% DMEM) for 24 h after which 10% DMEM was added. $N=6$ per condition.

Live/dead cell viability assay

A live/dead assay on the cell-laden GelMa constructs ($n=6$ per condition) was performed using a LIVE/DEAD™ Cell Imaging kit (Invitrogen, Waltham, Massachusetts, United States) 144 h after GelMa synthesis. The fluorescent dyes were diluted according to the manufacturer's protocol, in DMEM supplemented with 10% FBS and 1% P/S and added to the hydrogels to incubate for 10 minutes at room temperature in the dark. The constructs were analyzed with fluorescence imaging on 470nm and 550nm wavelengths for the green and the red signal respectively.

3D Dynamic experiments

Cell-laden 3D GelMa hydrogels exposed to dynamic loading

Two 5 x 20mm Velcro strips were glued in parallel, 5mm apart, to the bottom of each well of 6-well Bioflex culture plates (untreated, Flexcell Int) using medical adhesive silicone (Silastic MDX4-4210, Dow Corning, Midland, MI). Each pair of Velcro strips served as a mold to attach a hydrogel to the Flexcell membrane. Cell-GelMa suspensions (750 000 cells per 300 μ L each) were pipetted within these molds and placed under a 450mW UV-light for 100 seconds. The hydrogels were covered with SMGM-2 medium and cultured for two days before dynamic loading was applied. On day 3, cell-laden GelMa hydrogels were placed on the Flexcell FX-5000T (Flexcell Int, McKeesport, PA) and exposed to 2 days of 10% strain (0.5 Hz). $N=3$ per condition. Schematic representation of the strain experiments are displayed in Supplemental figure S2A.

Strain validation

To validate the intra- and inter-experimental variations in dynamic loading, 3 x 3 dotted patterns were created on the membranes of a 6-well Bioflex culture plate (untreated, Flexcell Int). Videos were captured on day 3 (the first day of straining) and day 5. Subsequently, the maximum strain in the y direction ($\epsilon_{yy,max}$) was calculated (Supplemental fig. S3) by tracking the displacements of the previously applied dotted patterns over time using the open source software Tracker (<https://physlets.org/tracker>). Schematic representation of the strain validation is displayed in Supplemental figure S2D.

To validate whether hydrogel intrinsic properties affected the strain of cell-laden 3D GelMa hydrogels, 50-5 and 80-10 hydrogels (n=6/group) without cells were created, covered with graphite particles, and imaged while being exposed to the 10% strain protocol. To assess whether cell remodeling activities would affect the strain pattern in the hydrogels, strain patterns of cell-laden 3D GelMa hydrogels were also assessed on day 5 in a similar fashion.

The captured videos were converted to images at 30Hz in MATLAB (Mathworks, Massachusetts, USA). Subsequently, the maximum strain in the y direction ($\epsilon_{yy,max}$) per loading regime group were calculated (Supplemental fig. S3) using the open source 2D DIC software Ncorr (v1.2, www.ncorr.com).

Analysis and Immunohistochemistry

Quantitative Polymerase Chain Reaction Analysis

Total RNA was isolated from cultures (ODMCs and VSMCs) using the RNA isolation kit (Bioline) according to the manufacturer's protocol. Cells from 3D GelMa constructs were extracted using the QIAshredder columns according to the manufacturer's protocol. The supernatant was subsequently used for RNA extraction with the RNA isolation kit from Bioline as described above. The purity and concentrations of RNA were quantified using spectrophotometry (DS-11; DeNovix), absorbance measurements at 260/280nm. cDNA synthesis was performed according to the protocol from the Bioline cDNA synthesis kit. Gene expression was determined using FastStart SYBR-green (Roche) following the quantitative polymerase chain reaction (qPCR) program: 8,5' 95°C, 38 cycles (15" 95°C; 45" 60°C) 1' 95 °C, 1' 65°C, 62 cycles (10" 65°C + 0.5°C) in the SYBR-Green-Cycler IQ5 detection protocol (Biorad CFX384), performed in 384-well plates (Merck). The primer sequences used are listed in Table

S2. All results were normalized for house-keeping genes ROPL and RPLP0, resulting in relative mRNA expression. In the dynamic experiments, results were compared to the static controls and represented as fold change ($\Delta\Delta Ct$).

2D Immunohistochemistry

Phenotypic switch was induced in cells cultured on 18mm coverslips as described in 1.2. Cells were fixated after 24 h and 72 h using 4% PFA for 20 minutes. Cells were blocked using a 2% PBS/bovine serum albumin (BSA) solution for 30 minutes. The cells were stained with anti-Calponin overnight at 4°C (Table **S3**). Thereafter, the staining solution was removed, and the coverslips were washed three times with PBS. Secondary antibody incubation together with phalloidin was performed for 1 h at RT (Table **S3**). The coverslips were washed with PBS and counterstained with DAPI for 5 minutes. Coverslips were mounted on microscope glass slides using Mowiol 4-88. Samples were stored at 4°C prior to imaging.

3D immunohistochemistry

Cell-laden GelMa constructs were fixated using 4% PFA for 1 h at RT. Constructs were blocked and permeabilized using 3% FBS, 1% BSA, 0.5% Triton x-100 and 0.5% Tween in PBS for 2 h at RT. GelMa constructs were stained with anti-Smooth Muscle Actin α and anti-Calponin (Table **S3**) for 2 h at RT. The cells were washed three times with PBS-/Tween and stained with secondary antibodies (Table **S3**) and incubated for 2 h at RT. DAPI was used as a counterstain and GelMa constructs were mounted using Mowiol4-88. Samples were stored at 4°C prior to imaging.

Imaging and Analysis

Imaging was performed using the Leica Confocal SP8 \times (2D cultures; 63 \times magnifications) and the Leica Thunder microscope (10 \times , 20 \times and 40 \times magnifications for 3D GelMa constructs). Images were analyzed using ImageJ software (Version 1.47). 3D images were composed in LASX (Version 3.5.7.23225).

Statistical Analysis

The statistical analyses were performed using Graphpad Prism (Version 8.3). Values are shown as individual data points with mean \pm SEM. Prior to statistical testing, outliers were removed from the results when detected using a Grubbs' test ($\alpha=0.05$). The paired, two-sided t-test and the ordinary one-way ANOVA test with Tukey post hoc test were used when appropriate. Experiments were performed at least in triplicate. The detailed sample size for each result is listed in the legend of the figures. A p-value of $p\leq 0.05$ was accepted as statistically significant. Significance is further described in the figure legends and results section.

Results

ODMCs are capable of growth factor induced phenotype switching similar to primary human aorta derived VSMCs.

ODMCs were harvested from human iPSC-derived blood vessel organoids following a previously described protocol summarized in figure 1A. Blood vessel organoids, were cultured following the adapted Wimmer lab protocol,^{29, 33} and contain both endothelial (CD31+) and mural (CD140b+) cells in a vasculature-like organization (fig. 1B). Extracted ODMCs brought into a single culture express both α SMA and CD140b (fig. 1C-E) and were devoid of endothelial cell contamination as confirmed by FACS analysis (fig. 1E).

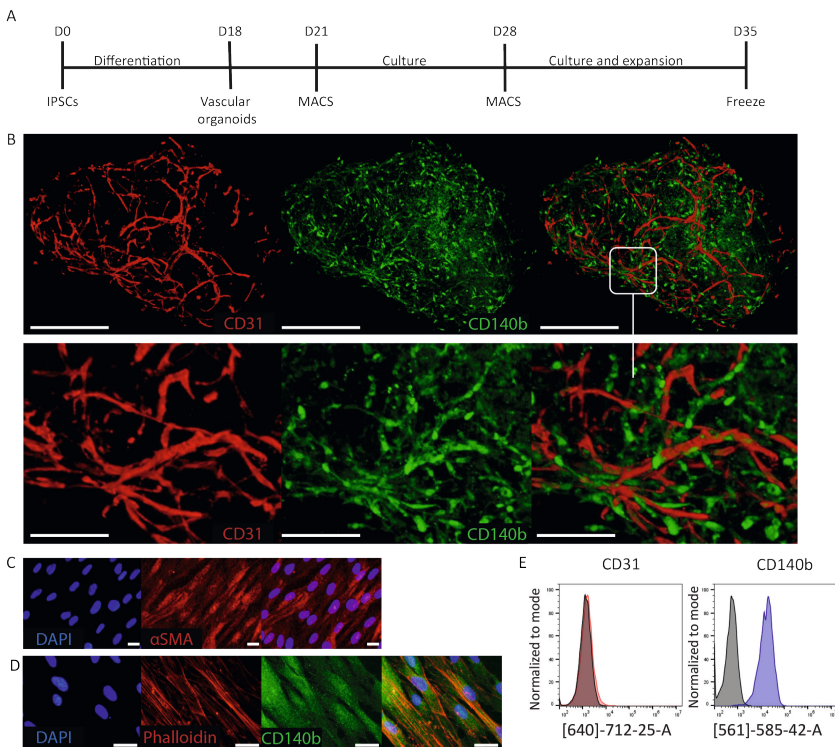


Figure 1. Differentiation of Organoid Derived Mural Cells (ODMCs).

A. Schematic overview of the experimental timeline. **B.** Whole mount staining analysis of a vascular organoid stained for both CD31 (red) and PDGFr β (CD140b; green). Scale bar depicts 500 μ m (complete organoid) and 100 μ m (zoomed-in structure). **C.** Immunofluorescent staining of ODMCs with anti-Smooth Muscle Actin- α (ACTA2; red), counterstained with DAPI (blue). Scale bar depicts 20 μ m. **D.** Immunofluorescent staining of ODMCs with anti-PDGFr β (green), counterstained with phalloidin (red) and DAPI (blue). Scale bar depicts 20 μ m. **E.** FACS analysis of sorted ODMCs, stained for CD31 (red histogram) and CD140b (blue histogram) and compared to isotype control (gray).

Throughout the study, human aortic VSMCs were used as a control. The phenotypic switch towards a contractile phenotype in 2D culture was induced in VSMCs and ODMCs by a combination of low serum and TGF β for 48 h (T=72 h in culture, see schematics in fig. 2A). Full DMEM (with 10% serum) supplemented with both PDGFB and TGF β was used for the synthetic phenotype, and the control groups were maintained on full DMEM (10% serum). Cell viability, as measured by PrestoBlue, remained unchanged in the contractile population. Whereas in the control and synthetic groups, this number increased significantly over time for both VSMCs and ODMCs (fig. 2B). In addition, gene expression analysis of contractile markers ACTA2 and Calponin shows significant upregulation of both genes after inducing the phenotypic switch towards a contractile population, both in ODMCs and VSMCs (fig. 2C). Immunofluorescent staining of synthetic and contractile populations (fig. 2D-E) shows similar changes in morphology and expression of Calponin protein levels in ODMCs and VSMCs in response to phenotype induction. The synthetic cells displayed a more rhomboid shape, while the contractile cells demonstrated cell elongation, as indicated by the quantification of the aspect ratio (major axis/minor axis) (fig. 2F). Cell expression of Calponin protein was quantified by assessment of the Calponin+ area per cell (fig. 2G). The contractile populations of ODMCs and VSMCs show comparable high levels of Calponin+ cells, compared to their respective synthetic populations. This data indicates that ODMCs are capable of adapting to a synthetic or contractile phenotype induced by different growth factor regimes, similar to primary VSMCs.

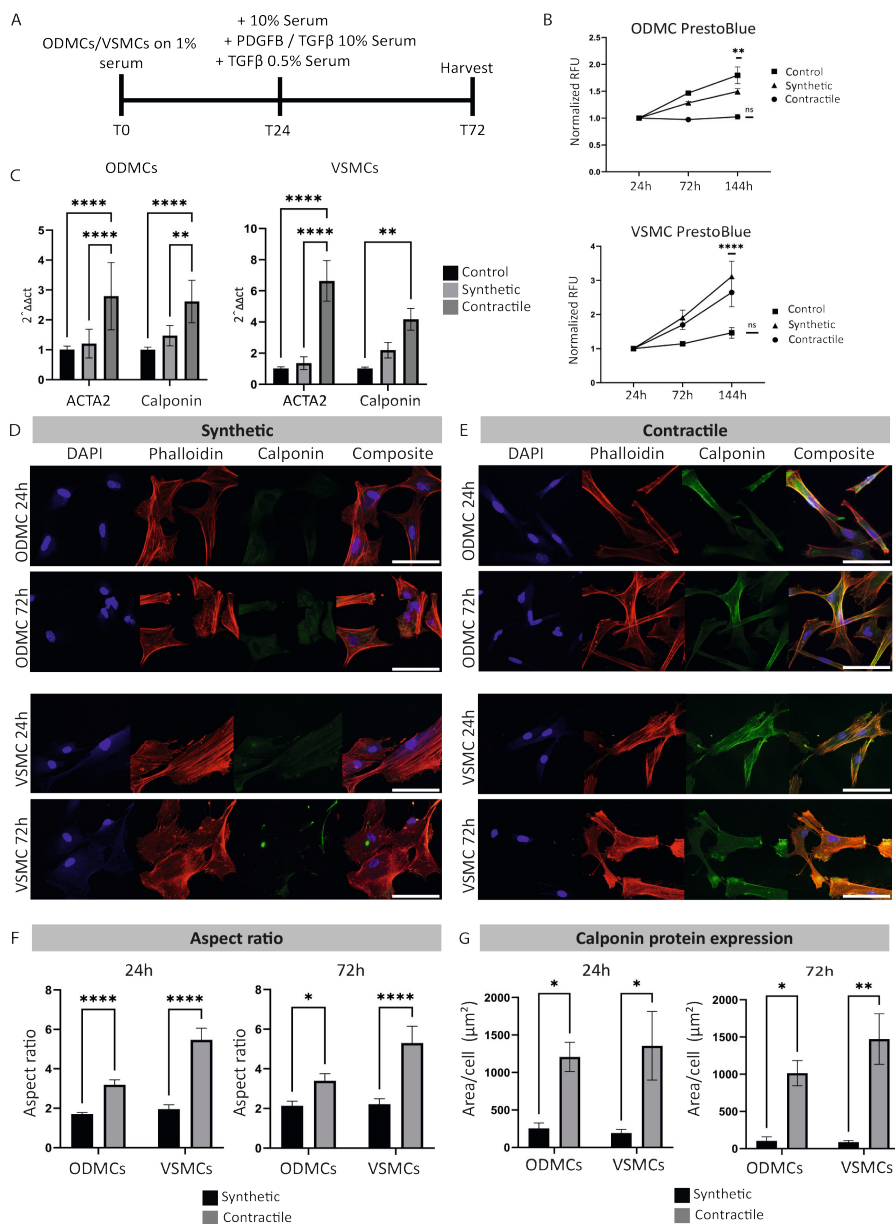


Figure 2. Growth factor induced phenotypic switch in 2D.

A. Schematic overview of the experimental timeline. **B.** PrestoBlue viability assay. Data represented as mean \pm SEM, $n=6$, one-way ANOVA with Tukey post hoc test. $**p<0.01$ for ODMCs compared to 24 h and $****p<0.0001$ for VSMCs compared to 24 h. Data is normalized to the 24 h timepoint. **C.** Gene expression analysis of the ODMCs and VSMCs 24 h after treatment, normalized to the control conditions. Data represented as mean \pm SEM, $n=6$ for both cell types. One-way ANOVA with Tukey post hoc test, $**p<0.01$, $****p<0.0001$. **D.** 2D Immunofluorescent staining of synthetic ODMCs and VSMCs after 24 h and 72 h,

stained for contractile marker calponin (green), counterstained for phalloidin (red) and DAPI (blue). Scale bar depicts 20 μ m. **E.** 2D Immunofluorescent staining of contractile ODMCs and VSMCs after 24 h and 72 h, stained for contractile marker calponin (green), counterstained for phalloidin (red) and DAPI (blue). Scale bar depicts 20 μ m. **F.** Aspect ratio of contractile and synthetic VSMC and ODMC populations after 24 h and 72 h. Aspect ratio is calculated as major axis divided by the minor axis. $N=4$ samples, 8 cells per sample. One-way ANOVA with Tukey post hoc test, * $p<0.05$, **** $p<0.0001$. **G.** Calponin protein expression levels by immunofluorescent quantification. Expression levels were calculated by the signal area divided by the number of nuclei. $N=6$, one-way ANOVA with Tukey post hoc test, * $p<0.05$, ** $p<0.01$.

ODMC and VSMC static culture in 3D in different GelMa hydrogel conditions with specific intrinsic matrix characteristics has limited impact on cell survival.

Cells were seeded and statically cultured in 3D in GelMa hydrogels for a total of 72 h before harvesting (fig. 3E). Bare GelMa hydrogel characteristics were first analyzed, starting with the water absorption capacity using a swelling assay (fig. 3A). This assay tests the DOF, with higher DOF hydrogels accommodating higher degree of crosslinking, resulting in a lower mass/swelling ratio (q). The q was higher for the 5% compared to the 10% hydrogels for both DOFs ($p<0.001$ for 50 DOF, $p<0.0001$ for 80 DOF). All the 80 DOF hydrogels show significantly higher ratios versus 50 DOF when compared to their respective percentage counterparts.

The hydrogel mechanical characteristics were assessed by dynamic mechanical analysis (DMA), generating stress strain curves from which the Young's modulus was calculated and displayed as kPa (fig. 3B, C). The Young's modulus reflects the material's viscoelastic response, with higher values representing higher material resistance to deformation when subjected to mechanical forces. The 10% hydrogels demonstrate a significantly higher Young's modulus compared to the 5% hydrogels for all DOFs ($p<0.0001$ for 80 DOF, $p<0.01$ for 50 DOF).

Calculation of the Live/dead cell ratio of ODMCs and VSMCs in the different hydrogels after a maximum of 144 h of static culture show no effect of hydrogel conditions in ODMCs, and only a significant decline in the 5% 50 DOF versus the 10% 80 DOF condition in VSMCs (Fig. 3D). Combined, this data validates the differences in intrinsic matrix properties between hydrogel conditions. The higher water absorption capacity in the 50 DOF compared to the 80 DOF indicates a higher crosslinking density in the 80 DOF. Additionally, there was a higher Young's modulus in the 10% versus the 5% compositions. These conditions have no significant impact on cell survival of ODMCs in static culture.

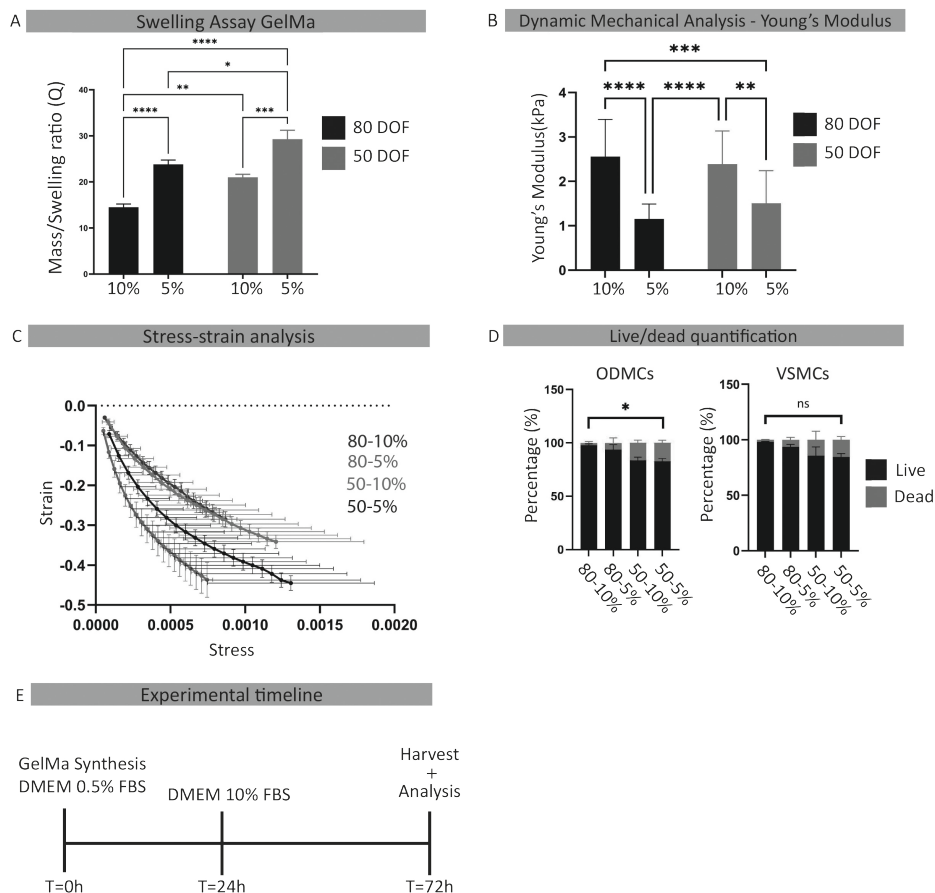


Figure 3. ODMCs and VSMCs in 3D GelMa hydrogels.

A. Swelling assay; displayed as mass/swelling ratio (Q) for both 5% and 10% gels of 80 DOF and 50 DOF. Data represented as mean \pm SEM, $n=5$, one-way ANOVA with Tukey post hoc test, $*p<0.05$, $**p<0.01$, $***p<0.001$, $****p<0.0001$. **B.** Young's modulus of the GelMa hydrogels, displayed in kPa. Data represented as mean \pm SEM, $n=5$, one-way ANOVA with Tukey post hoc test, $**p<0.01$, $***p<0.001$. **C.** Stress-strain curves of GelMa hydrogels. $N=20$ gels per condition. **D.** Live-dead assay of the vascular cells in the GelMa hydrogels. Data represented as percentage live or dead cells, and displayed as mean \pm SEM, $n=5$, one-way ANOVA with Tukey post hoc test, $*p<0.05$. **E.** Schematic overview of the experimental timeline.

3D GelMa hydrogel with higher DOF combined with lower Young's modulus promotes a contractile phenotype in ODMCs and VSMCs under static conditions.

After 72 h of static 3D culture in the GelMa hydrogels, cells were harvested for analysis. Expression of contractile markers ACTA2, Calponin and Collagen I were assessed using qPCR to evaluate the impact on cell phenotype. Relative mRNA

expression levels are shown in figure 4A. In ODMCs, in 5% hydrogels, 80 DOF had significantly increased expression of contractile markers compared to 50 DOF ($p < 0.05$ for ACTA, $p < 0.0001$ for Calponin and $p < 0.01$ for Collagen I). In 10% hydrogels, a similar trend was observed, where ACTA2 expression was significantly increased in 80 DOF versus 50 DOF ($p < 0.05$) (fig. 4A). This indicates the GelMa hydrogels with a similar Young's modulus, but higher crosslinking densities (DOF) promoted more adaptation to a contractile phenotype under static culture in ODMCs. For VSMCs, a similar trend was observed with increased expression of Calponin, but also a decrease in Collagen I, in the 80 DOF compared to 50 DOF in the 5% hydrogels ($p < 0.05$ for Calponin, $p < 0.01$ for Collagen I). In the 10% hydrogels, both ACTA2 and Calponin were upregulated in the 80 DOF versus 50 DOF ($p < 0.05$ for ACTA, $p < 0.01$ for Calponin).

When the weight percentages of the same DOFs were compared, a significant ($p < 0.05$) increased expression was observed in the ODMCs of both Calponin and Collagen I in the 10% hydrogels compared to the 5% hydrogels of the same DOFs (Supplemental Fig S1A). For VSMCs, there were no significant differences in expression of contractile genes in the 50 DOF conditions. In the 80 DOF, the 10% hydrogels caused significant ($p < 0.05$) upregulation of Calponin and Collagen I. These findings indicate that 3D culture in GelMa hydrogels with the same DOF and a higher Young's modulus promotes a contractile phenotype in ODMCs and VSMCs.

The addition of growth factors in the different static 3D GelMa conditions did not significantly alter gene expression of contractile markers of ODMCs or VSMCs (Supplemental figure S1B). Protein levels of ACTA2, quantified by the assessment of the ACTA2⁺ area per cell (fig. 4B) showed significant increase in 80 versus 50 DOF in 5% hydrogels for ODMCs and an increase in 80 versus 50 DOF, similarly in 5% hydrogels for VSMCs. Examples of the ACTA2 staining of the 50 and 80 DOF in 5% hydrogel for ODMCs are shown in figure 4C. Examples of ACTA2 staining for all conditions for both ODMCs and VSMCs are displayed in Supplemental figure S1C. For 80 DOF in 10% hydrogel, both ODMCs and VSMCs exhibited a rounded cell morphology with limited elongation, suggesting minimal interaction with the hydrogel.

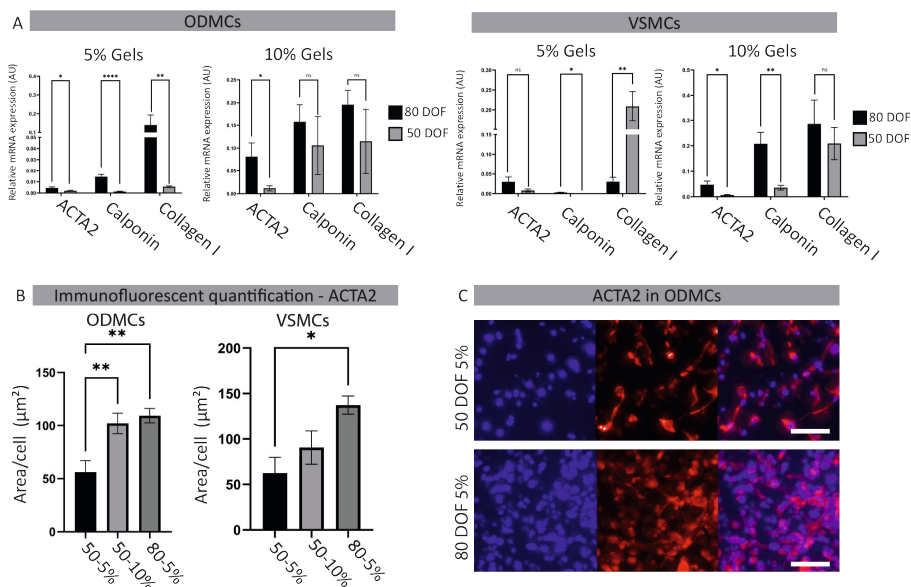


Figure 4. The effect of GelMa properties on smooth muscle cell phenotype in static conditions.

A. Gene expression analysis of the ODMCs and VSMCs 48 h after seeding. Data represented as mean \pm SEM, $n=6$ for ODMCs, $n=5$ for VSMCs. One-way ANOVA with Tukey post hoc test, * $p<0.05$, ** $p<0.01$, *** $p<0.001$. **B.** ACTA2 protein levels based on immunofluorescent quantification. Expression levels were calculated by the signal area divided by the number of nuclei. $N=5$ gels, 3 locations per gel, one-way ANOVA with Tukey post hoc test, * $p<0.05$, ** $p<0.01$, *** $p<0.0001$. **C.** Immunofluorescent whole mount staining of ACTA2 (red). Stained GelMa gels 48 h after seeding. DAPI (blue) was used as a counterstain. Scale bar depicts $50\mu\text{m}$.

Uniaxial strain induces a switch towards a contractile phenotype in 3D GelMa cultured ODMCs and VSMCs

Using the Flexcell© Tissue train system, 10% uniaxial strain was applied for 48 h on (72 h old) seeded hydrogels, as displayed in the timeline in figure 5A. The effect of hydrogel characteristics on strain patterns was assessed by comparing strain levels between the strongest (80 DOF in 10%) and weakest (50 DOF in 5%) hydrogels. No significant differences in strain patterns were detected (Supplemental fig. S2B). Strain analysis also reveals no significant differences in strain levels between day 0 and day 2 timepoints or between the different experiments (Supplemental fig. S2C). Gene expression levels of contractile markers in dynamic conditions were compared to the static controls, displayed in figure 5B. After 48 h of strain, the expression of contractile markers increased in GelMa hydrogels for multiple conditions. In ODMCs, 80 DOF in 5% and 10%, and 50 DOF in 10% GelMa hydrogels show significantly increased expression of ACTA2 ($p<0.01$ for 80 DOF in 10%, $p<0.05$ for 80 DOF in 5%

and $p < 0.01$ for 50 DOF in 10% hydrogel) and Calponin ($p < 0.01$ for 80 DOF in 10%, $p < 0.05$ for 80 DOF in 5% and $p < 0.05$ for 50 DOF in 10% hydrogel) after exposure to strain. For VSMCs, all conditions except the 80 DOF in 5% hydrogel showed significantly increased expression of ACTA2 ($p < 0.001$ for 80 DOF in 10%, $p < 0.05$ for 50 DOF in 10% and $p < 0.001$ for 50 DOF for 5% hydrogel). For Calponin, only the cells in the 50 DOF in 5% ($p < 0.05$) and 80 DOF in 10% hydrogels ($p < 0.01$) showed significant upregulation. For Collagen I, the exposure to strain did not significantly affect gene expression levels in both cell types. ACTA2 protein levels were assessed by quantification of the ACTA2+ area per cell (Fig. 5C). Strain significantly increased ACTA2+ levels in the 50 DOF hydrogels for both cell types ($p < 0.05$ for 5% hydrogels in ODMCs, $p < 0.001$ for 5% hydrogels in VSMCs and for 10% hydrogels in VSMCs and ODMCs).

In the 80 DOF hydrogels, there was only a significant increase in the 5% hydrogels in both cell types ($p < 0.05$ for ODMCs, $p < 0.01$ for VSMCs). Examples of the ACTA2 staining of both 50 DOF in 10% and 80 DOF in 5% hydrogels are shown in figure 5D. Increased elongation of both ODMCs and VSMCs after exposure to strain is clearly visible, indicating morphological adaptation to strain. ACTA2 staining for all conditions for both cell types are displayed in Supplemental figure S3A-B.

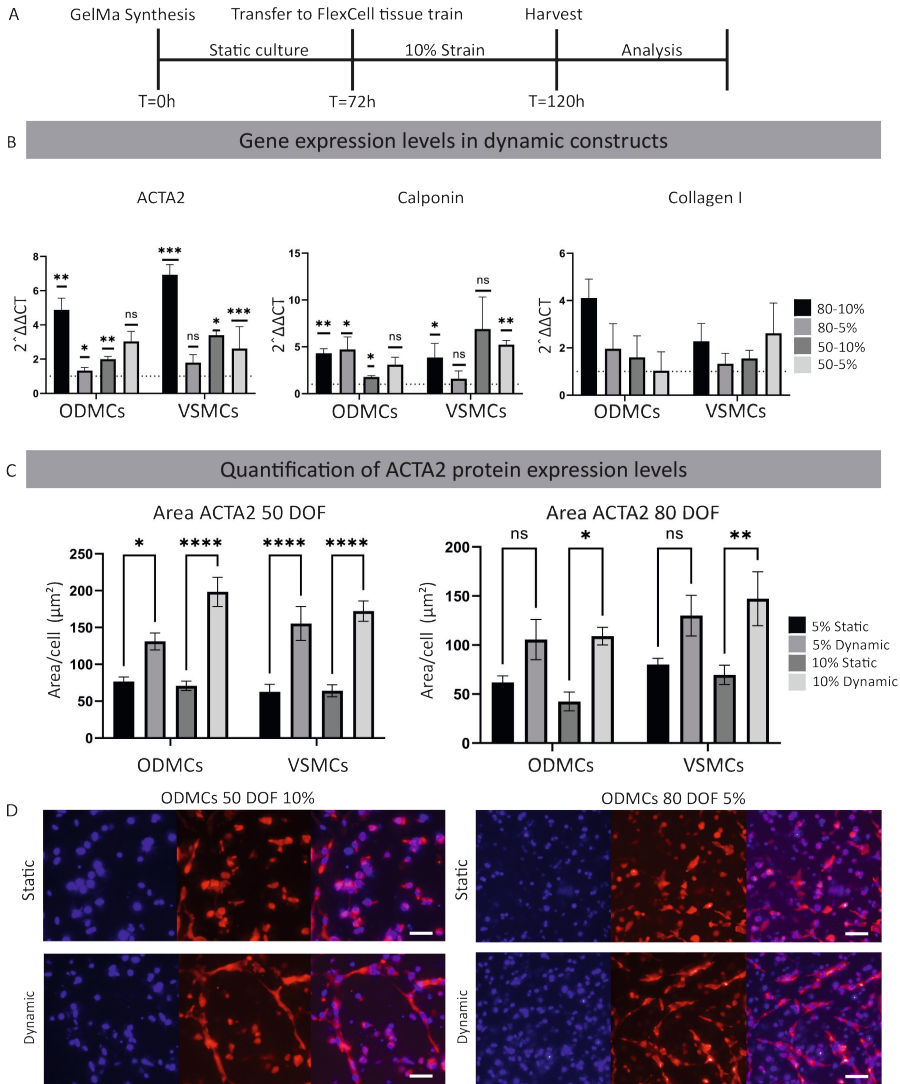


Figure 5. The effect of cyclic strain on the smooth muscle cell phenotype in 3D GelMa hydrogels.

A. Schematic overview of the experimental timeline. **B.** Gene expression analysis of the ODMCs and VSMCs after 48 h of 10% strain. Results are compared to the static controls (dotted line). Data represented as mean \pm SEM, $n=3$ for both conditions. One-way ANOVA with Tukey post hoc test, $*p<0.05$, $**p<0.01$, $***p<0.001$. **C.** ACTA2 protein levels based on immunofluorescent quantification. Expression levels were calculated by the signal area divided by the number of nuclei. $N=3$ gels, 3 locations per gel, one-way ANOVA with Tukey post hoc test, $*p<0.05$, $**p<0.01$, $****p<0.0001$. **D.** Immunofluorescent whole mount staining of the static and dynamic (48 h of 10% strain) GelMa gels. Cells were stained for ACTA2 (red) and DAPI (blue) was used as a counterstain. Scale bar depicts $50\mu\text{m}$.

Discussion

Within the vascular research field, there is a notable gap in comparative studies regarding the impact of intrinsic matrix substrate properties, such as elastic modulus and degree of crosslinking, on the cell behaviour of (h) iPSC-derived VSMCs, particularly when cultured in 3D structures. Additionally, the phenotypic adaptation of (h) iPSC-derived VSMCs in response to these factors in 3D environments under cyclic strain is largely unexplored. Here, we demonstrated the ability of hiPSC ODMCs to undergo phenotype switching under different culture and 3D GelMa hydrogel conditions, similar to primary VSMCs, illustrating their suitability of use in modeling of complex disease and potential for therapeutic interventions. The main findings are: (1) ODMCs derived from hiPSCs exhibited a VSMC phenotype, expressing key mural markers such as α -smooth muscle actin (α SMA) and CD140b. (2) ODMCs demonstrated phenotypic plasticity in response to specific culture conditions and can adopt a contractile phenotype similar to primary human VSMCs. (3) The mechanical properties in a 3D hydrogel substrate, including elastic modulus and degree of crosslinking had profound impact on both ODMCs and VSMCs under static culture, where hydrogels with a higher Young's modulus and a higher crosslinking density induced a contractile phenotype. (4) Dynamic stimulation in a 3D substrate using uniaxial strain further promotes a switch towards a contractile phenotype in both ODMCs and VSMCs. Our research enhances knowledge of human iPSC-derived VSMCs, particularly ODMCs, by elucidating the influence of culture medium composition, intrinsic matrix properties, and dynamic stimuli on phenotypic changes. These findings have practical implications for tissue engineering and regenerative medicine, especially in vascular disease treatment and modeling.

ODMCs are capable of growth factor induced phenotype switching similar to primary human aorta derived VSMCs.

ODMCs derived from vascular organoids³³ typically exhibit pericyte-like coverage of microcapillaries. However, when isolated and purified through CD140b sorting and cultured in VSMC medium, they undergo a morphological transition towards VSMC-like cells. When seeded on solution electrospun vascular scaffolds, these ODMCs can form tissue structures resembling the tunica media²⁹. Notably, they form a distinct multicellular layer separate from the endothelium and contribute to the stability of these vascular grafts under flow conditions. The phenotypic characteristics of these ODMCs have not been comprehensively evaluated. Here, we demonstrated, for the first time, the phenotypic plasticity of ODMCs derived from vascular organoids.

In healthy adult vasculature, VSMCs exhibit a contractile phenotype with limited proliferation and low synthetic activity. Following vascular injury, VSMCs undergo phenotypic changes, increasing migratory, synthetic, and proliferative capacities, contributing to vascular repair but also to diseases such as atherosclerosis, cancer, and hypertension^{9, 34, 35}. Notably, PDGFB induces the synthetic VSMC phenotype by downregulating contractile gene expression and promoting proliferation and migration^{1, 36}. In contrast, TGF- β and Bone Morphogenetic Protein 4 (BMP4) inhibit VSMC proliferation and migration while inducing contractile gene expression^{19, 37-39}. Serum deprivation enhances contractile gene expression, which can be reversed upon restoring a serum-rich medium, resulting in decreased contractile gene expression and a morphological transition of VSMCs. Notably, serum and PDGFB deprivation of human pluripotent stem cell (hPSC)-derived VSMCs have been observed to induce maturation towards a contractile phenotype¹⁴, whereas the use of a high-serum medium in conjunction with PDGFB treatment has been found to induce the synthetic phenotype in these hPSCs.

Based on these previous reports, we used serum and PDGFB starvation, along with TGF- β treatment in our experiments to assess the capacity of ODMCs to acquire a contractile phenotype. Our results demonstrated that ODMCs, like VSMCs, successfully acquired a contractile phenotype when exposed to the “contractile” culture conditions. This was evidenced by the upregulation of contractile markers, a reduction in cell proliferation rate, and elongation of cells, as compared to the control conditions (ODMCs and VSMCs in 10% serum) and the synthetic conditions (ODMCs and VSMCs in 10% serum, with PDGFB and TGF- β). Stimulation with the synthetic culture medium did not elicit any differences in marker expression, cell proliferation rate, or morphology in ODMCs or VSMCs, compared to the control conditions. It has been observed that (prolonged) *in vitro* expansion of VSMCs can lead to a gradual loss of the contractile phenotype⁴⁰. The lack of response to the “synthetic” culture medium could indicate that the control conditions utilized in our experiments already maintained a more synthetic population of ODMCs and VSMCs. Nevertheless, our findings demonstrate that ODMCs exhibit a level of phenotype plasticity that is comparable to that of VSMCs.

Higher Young's modulus and crosslinking density in a static 3D GelMa environment promotes a contractile phenotype in ODMCs and VSMCs.

Based on gelatin modified with methacryloyl groups, GelMa is biocompatible and biodegradable and is widely used in various tissue engineering strategies, including 3D cell printing to recapitulate blood vessels or vascularized tissues⁴¹. The

mechanical properties of GelMa are tunable by altering its crosslinking conditions, including polymer concentration, degree of methacrylation, light wavelength and intensity, and light exposure time^{42,43}. The viability, function and survival of GelMa loaded cells is highly dependent on the resulting crosslinking density. Here, we used two different degrees of methacrylation (or degree of functionalization, DOF), 50% and 80%. Of these two DOFs, we used two different hydrogel weight percentages, 5% and 10%, to create four different hydrogels, each with distinct intrinsic matrix properties: (1) High crosslinking density, high Young's modulus (80 DOF in 10% hydrogel), (2) high crosslinking density, low Young's modulus (80 DOF in 5% hydrogel), (3) low crosslinking density, high Young's modulus (50 DOF in 10% hydrogel), (4) low crosslinking density, low Young's modulus (50 DOF in 5% hydrogel). For vascular cells, high crosslinking density in GelMa was previously shown to be detrimental to vascular network formation *in vitro* and *in vivo*, resulting in less and shorter neovessels with fewer branchpoints^{44,45}. Although the impact of a high degree of GelMa crosslinking on VSMCs was not investigated, the mesenchymal stem cells that were used for vascular support in these studies showed significant reduction in perivascular recruitment by neovessels and *in situ* impairment of differentiation into mural cells. A higher degree of crosslinking has also been associated with reduced cell spreading capacity by increasing the physical matrix barrier and reduction in pore size⁴⁶. In line with these observations, ODMCs and VSMCs in 80 DOF in 10% hydrogels showed limited elongation in cell morphology compared to cells in 50 DOF (in 10% and 5%) or 80 DOF in 5% hydrogel under static conditions, indicative of impairment in cell spreading. Dynamic stimulation of the 80 DOF in 10% hydrogel condition only induced limited morphological adaptation in VSMCs but not ODMCs, and strained VSMCs displayed non-typical cell thinning or enlargement instead of elongation (Supplemental figure S3). A higher degree of crosslinking in GelMa was previously reported to reduce expression of mural cell markers in mesenchymal stem cells⁴⁴, but the impact on VSMC phenotype switching in hiPSC-derived mural cells remained to be investigated. Here we observed under static conditions a significantly higher expression of contractile markers in 80 DOF versus 50 DOF, in 5% and to a lesser extent in 10% hydrogels, with ODMCs performing better than VSMCs (Fig 4A, B), demonstrating that higher crosslinking density of 3D hydrogels promotes a contractile phenotype.

Phenotype determination in primary VSMCs may also be controlled by the elastic modulus of the hydrogels. The limited data available on the effect of these parameters on VSMC behavior is derived from 2D experiments. 2D studies have also highlighted the impact of different ECM components. For example, Collagen type I coating on substrates with an increasingly higher Young's modulus

reduced (synthetic phenotype associated) VSMC migration, whereas under similar conditions, a fibronectin coating promoted migratory behaviour²⁴. Notably, it has been indicated that the migratory response to substrates within a range of 1.0 to 308kPa (Young's modulus) is biphasic, implying that there is an optimum for maximal migration²⁵. Another interesting observation is that substrates with a higher Young's modulus require lower density of ECM (fibronectin) coating to achieve a similar migratory response in VSMCs than substrates with a lower modulus²⁵. **These findings indicate that the response of VSMCs to the mechanical substrate properties in 2D is highly dependent on the assessed Young's modulus range and ECM component type and density. How these findings will translate in a more physiologically relevant 3D environment, in particular for hiPSC-derived VSMCs, remains largely underexplored.** A recent comparative investigation focusing on the cyclic stretching stimulation of human VSMCs showed contrasting outcomes between 2D and 3D models, with contractile protein expression remaining unaltered under 2D stretching conditions, and exhibiting a notable increase within 3D collagen matrix conditions²⁸. These disparities underscore the possible critical influence of extracellular dimensionality (2D or 3D) on cellular responses to mechanical stimulation, emphasizing the urgent need to broaden the scope of current investigations in this domain. By comparing 5% with 10% hydrogels, our data showed that 3D GelMa hydrogels with a higher Young's modulus in a static environment increased the expression of contractile markers in ODMCs in both 80 and 50 DOF conditions. The same effect was observed to a lesser extent for VSMCs for 80 DOF hydrogels (Supplemental figure S1C, figure 4B). These results are partially in line with previous findings. **Peyton et al. showed that adjusting the modulus within the range of 0.45 to 5.8kPa resulted in the modulation of cytoskeletal assembly in human primary VSMCs in a 3D PEG-fibrinogen based static hydrogel, with stiff matrices exhibiting a slightly elevated level of F-actin bundling⁴⁷. However, the expression of contractile markers in Peyton's study was only increased in matrices with a higher Young's modulus after** constitutive RhoA activation, which may be attributed to the use of different hydrogels (GelMa versus PEG-fibrinogen). Similar to Peyton's findings, static 3D culture with different matrix properties (5% versus 10% hydrogels) had no effect on cell survival of ODMCs and VSMCs. Crosslinking density also had no impact on the survival of ODMCs (figure 3D). Combined, these findings demonstrate, for the first time, that increasing the Young's modulus in GelMa based hydrogels promotes a viable contractile phenotype in hiPSC-derived VSMCs.

Increasing the strength of GelMa as a bioink for 3D printing may not only offer mechanical stability to aid during the fabrication, but also ultimately create vessel grafts with higher vessel wall strength to better withstand physiological flow ranges. A new dual crosslinking method was recently reported for vascular 3D printing, which combines photo-cross-linking with enzymatic cross-linking facilitated by glucose peroxidase and horseradish peroxidase, which resulted in a construct with higher substrate strength⁴⁸. However, biological performance was investigated with endothelial cells seeded on top of the gel in the lumen of the channels created by sacrificial printing. Although this showed adequate cell adhesion and viability for the endothelium, similar parameters were not tested in a condition in which vascular (mural) cells were suspended in the dual cross-linked gel in 3D⁴⁸.

Uniaxial strain induces a phenotypic switch towards a contractile population of smooth muscle cells in ODMCs and VSMCs

The effect of cyclic strain on the morphology and function of VSMCs has been described predominantly in 2D setups. The use of cyclic strain in 2D within the pathologically relevant range (>15%) has been shown to induce DNA synthesis through increased reactive oxygen species (ROS) production and NF- κ B pathway activation⁴⁹. Conversely, physiological strain levels (10%) inhibit VSMC proliferation by upregulating p21 expression and promoting apoptosis^{50,51}. For human iPSC-derived VSMCs, data on cyclic strain is very limited, with findings that indicate an ability for cytoskeletal remodeling in response to 2D strain similar to primary VSMCs in a progeria-on-a-chip model⁵². In relation to expression of phenotypic markers, up and down regulation of contractile markers have been reported following VSMC exposure to cyclic strain⁵³⁻⁵⁷. Most notably, Bono et al. (2016) compared the impact of cyclic strain on VSMCs cultured in type I Collagen substrate in both 2D and 3D environments²⁸. In the 2D model, they reported a downregulation of contractile proteins (α SMA and Calponin) in the strained versus static samples. In contrast, a twofold increase in α SMA and 14-fold increase in Calponin expression was observed in the 3D conditions when exposed to cyclic strain. This coincided with a difference in morphological adaptation with a perpendicular (80-90 degrees) alignment in the 2D cultured versus parallel (0-10 degrees) alignment in 3D cultured VSMCs, in relation to the strain direction. These findings imply that VSMC adaptation to cyclic strain is profoundly different in 2D versus 3D conditions. In line with these 3D findings from Bono's study, we observed that cyclic strain significantly increased the expression of contractile markers and caused elongation of ODMCs and VSMCs in the direction of the applied strain in all our four 3D hydrogel conditions. Crosslinking density (comparing the 80 DOF and 50 DOF hydrogels) and matrix Young's modulus (comparing 10% and 5% hydrogels) did not affect this contractile switch in both cell

types. Strain pattern comparison of the 80 DOF in 10% versus the 50 DOF in 5% hydrogels did not show any significant differences, indicating variations within this range may have limited impact on the local strain levels of what the cells experience on an individual level. Future research should investigate hydrogels with a higher range in crosslinking density and elastic modulus to assess the impact of hydrogel properties on the conveyance of strain from the tissue to the cellular level.

Conclusion

In this study, we demonstrated the phenotypic plasticity of hiPSC-derived ODMCs, which have the capacity to adopt a contractile phenotype in response to growth factor stimulation in 2D. In addition, 3D culture in GelMa hydrogels under static conditions showed that properties like a higher Young's modulus and higher crosslinking density induced a contractile phenotype in these cells, similar to VSMCs. Dynamic stimulation in the 3D substrate using uniaxial strain further promoted a switch towards a contractile phenotype in both ODMCs and primary VSMCs.

These findings underscore the significance of optimizing matrix properties within a (dynamic) 3D environment and contribute to the advancement of sophisticated human disease models and vascular tissue engineering strategies.

Supporting information

Comparative gene-expression analysis in different DOFs, gene-expression analysis of the effect of growth factors in 3D, immunofluorescent hydrogel staining, strain analysis without cells, immunofluorescent staining of strained gels.

Acknowledgements

This work was funded by the REGMEDXB cardiovascular moonshot consortium and the NWO Vidi grant (no. 91714302 to CC). The authors gratefully acknowledge the Gravitation Program "Materials Driven Regeneration", funded by the Netherlands Organization for Scientific Research (024.003.013).

Author Contributions

EMM wrote the manuscript together with **RG** and **CC**. Experiments were executed by **EMM, RG, CVD, RM, IC, TBW** and **YA**. **HC** performed strain analysis. **AIPMS, MCV** and **CC** supervised the project. All authors read, revised and accepted the manuscript.

Conflict of Interest

The authors declare no conflict of interest.

References

1. Owens, G. K. Regulation of differentiation of vascular smooth muscle cells. *Physiol Rev* **1995**, *75* (3), 487-517. DOI: 10.1152/physrev.1995.75.3.487.
2. Jones, B. A.; Aly, H. M.; Forsyth, E. A.; Sidawy, A. N. Phenotypic characterization of human smooth muscle cells derived from atherosclerotic tibial and peroneal arteries. *J Vasc Surg* **1996**, *24* (5), 883-891. DOI: 10.1016/s0741-5214(96)70027-7.
3. Campbell, J. H.; Campbell, G. R. Smooth muscle phenotypic modulation--a personal experience. *Arterioscler Thromb Vasc Biol* **2012**, *32* (8), 1784-1789. DOI: 10.1161/ATVBAHA.111.243212.
4. Chakraborty, R.; Chatterjee, P.; Dave, J. M.; Ostriker, A. C.; Greif, D. M.; Rzucidlo, E. M.; Martin, K. A. Targeting smooth muscle cell phenotypic switching in vascular disease. *JVS Vasc Sci* **2021**, *2*, 79-94. DOI: 10.1016/j.jvssci.2021.04.001.
5. Worssam, M. D.; Jorgensen, H. F. Mechanisms of vascular smooth muscle cell investment and phenotypic diversification in vascular diseases. *Biochem Soc Trans* **2021**, *49* (5), 2101-2111. DOI: 10.1042/BST20210138.
6. Bennett, M. R.; Sinha, S.; Owens, G. K. Vascular Smooth Muscle Cells in Atherosclerosis. *Circ Res* **2016**, *118* (4), 692-702. DOI: 10.1161/CIRCRESAHA.115.306361.
7. Harman, J. L.; Jorgensen, H. F. The role of smooth muscle cells in plaque stability: Therapeutic targeting potential. *Br J Pharmacol* **2019**, *176* (19), 3741-3753. DOI: 10.1111/bph.14779.
8. Lyle, M. A.; Davis, J. P.; Brozovich, F. V. Regulation of Pulmonary Vascular Smooth Muscle Contractility in Pulmonary Arterial Hypertension: Implications for Therapy. *Front Physiol* **2017**, *8*, 614. DOI: 10.3389/fphys.2017.00614.
9. Owens, G. K.; Kumar, M. S.; Wamhoff, B. R. Molecular regulation of vascular smooth muscle cell differentiation in development and disease. *Physiol Rev* **2004**, *84* (3), 767-801. DOI: 10.1152/physrev.00041.2003.
10. Alexander, M. R.; Owens, G. K. Epigenetic control of smooth muscle cell differentiation and phenotypic switching in vascular development and disease. *Annu Rev Physiol* **2012**, *74*, 13-40. DOI: 10.1146/annurev-physiol-012110-142315.
11. Lee, T. H.; Song, S. H.; Kim, K. L.; Yi, J. Y.; Shin, G. H.; Kim, J. Y.; Kim, J.; Han, Y. M.; Lee, S. H.; Lee, S. H.; et al. Functional recapitulation of smooth muscle cells via induced pluripotent stem cells from human aortic smooth muscle cells. *Circ Res* **2010**, *106* (1), 120-128. DOI: 10.1161/CIRCRESAHA.109.207902.
12. Ge, X.; Ren, Y.; Bartulos, O.; Lee, M. Y.; Yue, Z.; Kim, K. Y.; Li, W.; Amos, P. J.; Bozkulak, E. C.; Iyer, A.; et al. Modeling supravalvular aortic stenosis syndrome with human induced pluripotent stem cells. *Circulation* **2012**, *126* (14), 1695-1704. DOI: 10.1161/CIRCULATIONAHA.112.116996.
13. Lin, B.; Kim, J.; Li, Y.; Pan, H.; Carvajal-Vergara, X.; Salama, G.; Cheng, T.; Li, Y.; Lo, C. W.; Yang, L. High-purity enrichment of functional cardiovascular cells from human iPS cells. *Cardiovasc Res* **2012**, *95* (3), 327-335. DOI: 10.1093/cvr/cvs185.
14. Wanjare, M.; Kuo, F.; Gerecht, S. Derivation and maturation of synthetic and contractile vascular smooth muscle cells from human pluripotent stem cells. *Cardiovasc Res* **2013**, *97* (2), 321-330. DOI: 10.1093/cvr/cvs315.

15. Cheung, C.; Bernardo, A. S.; Trotter, M. W.; Pedersen, R. A.; Sinha, S. Generation of human vascular smooth muscle subtypes provides insight into embryological origin-dependent disease susceptibility. *Nat Biotechnol* **2012**, *30* (2), 165-173. DOI: 10.1038/nbt.2107.
16. Orlova, V. V.; van den Hil, F. E.; Petrus-Reurer, S.; Drabsch, Y.; Ten Dijke, P.; Mummery, C. L. Generation, expansion and functional analysis of endothelial cells and pericytes derived from human pluripotent stem cells. *Nat Protoc* **2014**, *9* (6), 1514-1531. DOI: 10.1038/nprot.2014.102.
17. Shen, M.; Quertermous, T.; Fischbein, M. P.; Wu, J. C. Generation of Vascular Smooth Muscle Cells From Induced Pluripotent Stem Cells: Methods, Applications, and Considerations. *Circ Res* **2021**, *128* (5), 670-686. DOI: 10.1161/CIRCRESAHA.120.318049.
18. Papetti, M.; Shujath, J.; Riley, K. N.; Herman, I. M. FGF-2 antagonizes the TGF-beta1-mediated induction of pericyte alpha-smooth muscle actin expression: a role for myf-5 and Smad-mediated signaling pathways. *Invest Ophthalmol Vis Sci* **2003**, *44* (11), 4994-5005. DOI: 10.1167/iovs.03-0291.
19. Tang, Y.; Urs, S.; Boucher, J.; Bernaiche, T.; Venkatesh, D.; Spicer, D. B.; Vary, C. P.; Liaw, L. Notch and transforming growth factor-beta (TGFbeta) signaling pathways cooperatively regulate vascular smooth muscle cell differentiation. *J Biol Chem* **2010**, *285* (23), 17556-17563. DOI: 10.1074/jbc.M109.076414.
20. Han, J. H.; Park, H. S.; Lee, D. H.; Jo, J. H.; Heo, K. S.; Myung, C. S. Regulation of autophagy by controlling Erk1/2 and mTOR for platelet-derived growth factor-BB-mediated vascular smooth muscle cell phenotype shift. *Life Sci* **2021**, *267*, 118978. DOI: 10.1016/j.lfs.2020.118978.
21. Qu, M. J.; Liu, B.; Wang, H. Q.; Yan, Z. Q.; Shen, B. R.; Jiang, Z. L. Frequency-dependent phenotype modulation of vascular smooth muscle cells under cyclic mechanical strain. *J Vasc Res* **2007**, *44* (5), 345-353. DOI: 10.1159/000102278.
22. Wanjare, M.; Agarwal, N.; Gerecht, S. Biomechanical strain induces elastin and collagen production in human pluripotent stem cell-derived vascular smooth muscle cells. *Am J Physiol Cell Physiol* **2015**, *309* (4), C271-281. DOI: 10.1152/ajpcell.00366.2014.
23. Yao, Q. P.; Zhang, P.; Qi, Y. X.; Chen, S. G.; Shen, B. R.; Han, Y.; Yan, Z. Q.; Jiang, Z. L. The role of SIRT6 in the differentiation of vascular smooth muscle cells in response to cyclic strain. *Int J Biochem Cell Biol* **2014**, *49*, 98-104. DOI: 10.1016/j.biocel.2014.01.016.
24. Rickel, A. P.; Sanyour, H. J.; Leyda, N. A.; Hong, Z. Extracellular Matrix Proteins and Substrate Stiffness Synergistically Regulate Vascular Smooth Muscle Cell Migration and Cortical Cytoskeleton Organization. *ACS Appl Bio Mater* **2020**, *3* (4), 2360-2369. DOI: 10.1021/acscabm.0c00100.
25. Peyton, S. R.; Putnam, A. J. Extracellular matrix rigidity governs smooth muscle cell motility in a biphasic fashion. *J Cell Physiol* **2005**, *204* (1), 198-209. DOI: 10.1002/jcp.20274.
26. Li, S.; Lao, J.; Chen, B. P.; Li, Y. S.; Zhao, Y.; Chu, J.; Chen, K. D.; Tsou, T. C.; Peck, K.; Chien, S. Genomic analysis of smooth muscle cells in 3-dimensional collagen matrix. *FASEB J* **2003**, *17* (1), 97-99. DOI: 10.1096/fj.02-0256fje.
27. Stegemann, J. P.; Nerem, R. M. Altered response of vascular smooth muscle cells to exogenous biochemical stimulation in two- and three-dimensional culture. *Exp Cell Res* **2003**, *283* (2), 146-155. DOI: 10.1016/s0014-4827(02)00041-1.

28. Bono, N.; Pezzoli, D.; Levesque, L.; Loy, C.; Candiani, G.; Fiore, G. B.; Mantovani, D. Unraveling the role of mechanical stimulation on smooth muscle cells: A comparative study between 2D and 3D models. *Biotechnol Bioeng* **2016**, *113* (10), 2254-2263. DOI: 10.1002/bit.25979.
29. Meijer, E. M.; Koch, S. E.; van Dijk, C. G. M.; Maas, R. G. C.; Chrifi, I.; Szymczyk, W.; Besseling, P. J.; Pomp, L.; Koomen, V.; Buikema, J. W.; et al. 3D Human iPSC Blood Vessel Organoids as a Source of Flow-Adaptive Vascular Cells for Creating a Human-Relevant 3D-Scaffold Based Macrovascular Model. *Adv Biol (Weinh)* **2023**, *7* (1), e2200137. DOI: 10.1002/adbi.202200137.
30. Klotz, B. J.; Lim, K. S.; Chang, Y. X.; Soliman, B. G.; Pennings, I.; Melchels, F. P. W.; Woodfield, T. B. F.; Rosenberg, A. J.; Malda, J.; Gawlitta, D. Engineering of a complex bone tissue model with endothelialised channels and capillary-like networks. *Eur Cell Mater* **2018**, *35*, 335-348. DOI: 10.22203/eCM.v035a23.
31. Van Den Bulcke, A. I.; Bogdanov, B.; De Rooze, N.; Schacht, E. H.; Cornelissen, M.; Berghmans, H. Structural and rheological properties of methacrylamide modified gelatin hydrogels. *Biomacromolecules* **2000**, *1* (1), 31-38. DOI: 10.1021/bm990017d.
32. Bracco Gartner, T. C. L.; Deddens, J. C.; Mol, E. A.; Magin Ferrer, M.; van Laake, L. W.; Bouten, C. V. C.; Khademhosseini, A.; Doevendans, P. A.; Suyker, W. J. L.; Sluijter, J. P. G.; Hjortnaes, J. Anti-fibrotic Effects of Cardiac Progenitor Cells in a 3D-Model of Human Cardiac Fibrosis. *Front Cardiovasc Med* **2019**, *6*, 52. DOI: 10.3389/fcvm.2019.00052.
33. Wimmer, R. A.; Leopoldi, A.; Aichinger, M.; Wick, N.; Hantusch, B.; Novatchkova, M.; Taubenschmid, J.; Hammerle, M.; Esk, C.; Bagley, J. A.; et al. Human blood vessel organoids as a model of diabetic vasculopathy. *Nature* **2019**, *565* (7740), 505-510. DOI: 10.1038/s41586-018-0858-8.
34. Carmeliet, P. Angiogenesis in life, disease and medicine. *Nature* **2005**, *438* (7070), 932-936. DOI: 10.1038/nature04478.
35. Frid, M. G.; Kale, V. A.; Stenmark, K. R. Mature vascular endothelium can give rise to smooth muscle cells via endothelial-mesenchymal transdifferentiation: in vitro analysis. *Circ Res* **2002**, *90* (11), 1189-1196. DOI: 10.1161/01.res.0000021432.70309.28.
36. Somlyo, A. P.; Somlyo, A. V. Ca²⁺ sensitivity of smooth muscle and nonmuscle myosin II: modulated by G proteins, kinases, and myosin phosphatase. *Physiol Rev* **2003**, *83* (4), 1325-1358. DOI: 10.1152/physrev.00023.2003.
37. ten Dijke, P.; Arthur, H. M. Extracellular control of TGFbeta signalling in vascular development and disease. *Nat Rev Mol Cell Biol* **2007**, *8* (11), 857-869. DOI: 10.1038/nrm2262.
38. Lagna, G.; Ku, M. M.; Nguyen, P. H.; Neuman, N. A.; Davis, B. N.; Hata, A. Control of phenotypic plasticity of smooth muscle cells by bone morphogenetic protein signaling through the myocardin-related transcription factors. *J Biol Chem* **2007**, *282* (51), 37244-37255. DOI: 10.1074/jbc.M708137200.
39. Kramann, R.; Goettsch, C.; Wongboonsin, J.; Iwata, H.; Schneider, R. K.; Kuppe, C.; Kaesler, N.; Chang-Panesso, M.; Machado, F. G.; Gratwohl, S.; et al. Adventitial MSC-like Cells Are Progenitors of Vascular Smooth Muscle Cells and Drive Vascular Calcification in Chronic Kidney Disease. *Cell Stem Cell* **2016**, *19* (5), 628-642. DOI: 10.1016/j.stem.2016.08.001.
40. Chamley, J. H.; Campbell, G. R.; McConnell, J. D.; Groschel-Stewart, U. Comparison of vascular smooth muscle cells from adult human, monkey and rabbit in primary culture and in subculture. *Cell Tissue Res* **1977**, *177* (4), 503-522. DOI: 10.1007/BF00220611.

41. Rawal, P.; Tripathi, D. M.; Ramakrishna, S.; Kaur, S. Prospects for 3D bioprinting of organoids. *Bio-Design and Manufacturing* **2021**, *4*, 627-640.
42. Im, G. B.; Lin, R. Z. Bioengineering for vascularization: Trends and directions of photocrosslinkable gelatin methacrylate hydrogels. *Front Bioeng Biotechnol* **2022**, *10*, 1053491. DOI: 10.3389/fbioe.2022.1053491.
43. Loessner, D.; Meinert, C.; Kaemmerer, E.; Martine, L. C.; Yue, K.; Levett, P. A.; Klein, T. J.; Melchels, F. P.; Khademhosseini, A.; Hutmacher, D. W. Functionalization, preparation and use of cell-laden gelatin methacryloyl-based hydrogels as modular tissue culture platforms. *Nat Protoc* **2016**, *11* (4), 727-746. DOI: 10.1038/nprot.2016.037.
44. Chen, Y. C.; Lin, R. Z.; Qi, H.; Yang, Y.; Bae, H.; Melero-Martin, J. M.; Khademhosseini, A. Functional Human Vascular Network Generated in Photocrosslinkable Gelatin Methacrylate Hydrogels. *Adv Funct Mater* **2012**, *22* (10), 2027-2039. DOI: 10.1002/adfm.201101662.
45. Lin, R. Z.; Chen, Y. C.; Moreno-Luna, R.; Khademhosseini, A.; Melero-Martin, J. M. Transdermal regulation of vascular network bioengineering using a photopolymerizable methacrylated gelatin hydrogel. *Biomaterials* **2013**, *34* (28), 6785-6796. DOI: 10.1016/j.biomaterials.2013.05.060.
46. Pepelanova, I.; Kruppa, K.; Scheper, T.; Lavrentieva, A. Gelatin-Methacryloyl (GelMA) Hydrogels with Defined Degree of Functionalization as a Versatile Toolkit for 3D Cell Culture and Extrusion Bioprinting. *Bioengineering (Basel)* **2018**, *5* (3). DOI: 10.3390/bioengineering5030055.
47. Peyton, S. R.; Kim, P. D.; Ghajar, C. M.; Seliktar, D.; Putnam, A. J. The effects of matrix stiffness and RhoA on the phenotypic plasticity of smooth muscle cells in a 3-D biosynthetic hydrogel system. *Biomaterials* **2008**, *29* (17), 2597-2607. DOI: 10.1016/j.biomaterials.2008.02.005.
48. Peng, K.; Liu, X.; Zhao, H.; Lu, H.; Lv, F.; Liu, L.; Huang, Y.; Wang, S.; Gu, Q. 3D Bioprinting of Reinforced Vessels by Dual-Cross-linked Biocompatible Hydrogels. *ACS Appl Bio Mater* **2021**, *4* (5), 4549-4556. DOI: 10.1021/acsbm.1c00283.
49. Hishikawa, K.; Oemar, B. S.; Yang, Z.; Luscher, T. F. Pulsatile stretch stimulates superoxide production and activates nuclear factor-kappa B in human coronary smooth muscle. *Circ Res* **1997**, *81* (5), 797-803. DOI: 10.1161/01.res.81.5.797.
50. Morrow, D.; Sweeney, C.; Birney, Y. A.; Cummins, P. M.; Walls, D.; Redmond, E. M.; Cahill, P. A. Cyclic strain inhibits Notch receptor signaling in vascular smooth muscle cells in vitro. *Circ Res* **2005**, *96* (5), 567-575. DOI: 10.1161/01.RES.0000159182.98874.43.
51. Chapman, G. B.; Durante, W.; Hellums, J. D.; Schafer, A. I. Physiological cyclic stretch causes cell cycle arrest in cultured vascular smooth muscle cells. *Am J Physiol Heart Circ Physiol* **2000**, *278* (3), H748-754. DOI: 10.1152/ajpheart.2000.278.3.H748.
52. Ribas, J.; Zhang, Y. S.; Pitrez, P. R.; Leijten, J.; Miscuglio, M.; Rouwkema, J.; Dokmeci, M. R.; Nissan, X.; Ferreira, L.; Khademhosseini, A. Biomechanical Strain Exacerbates Inflammation on a Progeria-on-a-Chip Model. *Small* **2017**, *13* (15). DOI: 10.1002/sml.201603737.
53. Hu, B.; Song, J. T.; Qu, H. Y.; Bi, C. L.; Huang, X. Z.; Liu, X. X.; Zhang, M. Mechanical stretch suppresses microRNA-145 expression by activating extracellular signal-regulated kinase 1/2 and upregulating angiotensin-converting enzyme to alter vascular smooth muscle cell phenotype. *PLoS One* **2014**, *9* (5), e96338. DOI: 10.1371/journal.pone.0096338.

54. Wan, X. J.; Zhao, H. C.; Zhang, P.; Huo, B.; Shen, B. R.; Yan, Z. Q.; Qi, Y. X.; Jiang, Z. L. Involvement of BK channel in differentiation of vascular smooth muscle cells induced by mechanical stretch. *Int J Biochem Cell Biol* **2015**, *59*, 21-29. DOI: 10.1016/j.biocel.2014.11.011.
55. Rodriguez, A. I.; Csanyi, G.; Ranayhossaini, D. J.; Feck, D. M.; Blose, K. J.; Assatourian, L.; Vorp, D. A.; Pagano, P. J. MEF2B-Nox1 signaling is critical for stretch-induced phenotypic modulation of vascular smooth muscle cells. *Arterioscler Thromb Vasc Biol* **2015**, *35* (2), 430-438. DOI: 10.1161/ATVBAHA.114.304936.
56. Kollros, P. R.; Bates, S. R.; Mathews, M. B.; Horwitz, A. L.; Glagov, S. Cyclic AMP inhibits increased collagen production by cyclically stretched smooth muscle cells. *Lab Invest* **1987**, *56* (4), 410-417.
57. Sumpio, B. E.; Banes, A. J.; Link, W. G.; Johnson, G., Jr. Enhanced collagen production by smooth muscle cells during repetitive mechanical stretching. *Arch Surg* **1988**, *123* (10), 1233-1236. DOI: 10.1001/archsurg.1988.01400340059010.

Supplemental information



PART 2

CHAPTER

6



Contributions of Wall Stretch and Shear Stress to Vascular Regulation: Molecular Mechanisms of Homeostasis and Expansion

**Elana M. Meijer, Ranganath Maringanti, Maarten M. Brandt, Dirk J. Duncker,
and Caroline Cheng**

Vascular Mechanobiology in Physiology and Disease, 21-46.

Abstract

Blood vessels are continuously exposed to hemodynamic forces due to the pulsatile nature of the blood flow. In normal physiological settings, these forces are essential in the maintenance of vascular cell function and structure, vascular growth, and in the regulation of vascular tone. However, when exceeding the physiological range these biomechanical forces become detrimental and may initiate pathological pathways. In this chapter, we discuss the types of vascular biomechanical forces, unravel cellular and molecular mechanisms underlying the physiological and pathophysiological response of the vascular cells to these biomechanical stimuli, and describe their role in triggering vascular growth.

Introduction

The main biomechanical stimuli that affect the vascular system are shear stress and wall stretch¹. The vascular wall, which is exposed to these forces, is comprised of three main cell types: endothelial cells (ECs), lining the tunica intima, vascular smooth muscle cells (VSMCs) in the tunica media, and fibroblasts within the adventitial layer². The endothelium, which covers the inner lining of blood vessels, mainly responds to shear stress due to its direct contact with the blood- stream. Shear stress is generated by the intraluminal blood flow, which exerts force in the longitudinal direction on the surface of the vessel wall³. Circumferential stress or wall stretch, generated by intraluminal pressure of blood flow that exerts forces in perpendicular direction, triggers a direct activation of both ECs and VSMCs^{4,5}.

Shear stress

An important biomechanical stimulus that influences endothelial behavior is shear stress. Shear stress is the force per unit area created when a tangential force (blood flow) acts on a surface (endothelium) (Fig. 2.1). Shear stress is expressed in dynes, where 1 dyne equals 0.1 N/m². Shear stress (τ) in a circular channel depends on volumetric flow (Q), fluid viscosity (μ), and lumen radius (r). The level of shear stress can be calculated according to the relationship: $\tau = \frac{4\mu Q}{\pi r^3}$, under the additional assumptions that the vessel is a circular tube with a constant diameter, and that the blood flow is fixed⁶. The level of shear stress is actively maintained within a certain range in the circulation as the vasculature responds to shear stress changes by adjusting vascular tone and diameter. The ability of the vasculature to respond is mediated by the conversion of mechanical stress to biochemical responses, the so-called process of mechanotransduction⁶. Throughout the vasculature, ECs experience various flow conditions. Shear stress levels are for instance low (between 0.76 and 7.6 dynes/cm²) in the venous system, whereas high shear levels are found in arteries and arterioles (between 11.4 and 30.4 dynes/cm² for large arteries, and between 19.0 and 60.8 dynes/cm² for arterioles)⁷ (Table 2.1). Non-uniform organization of the vascular network based on complex bifurcations, branch points, and curved regions greatly influence shear stress characteristics. In straight sections of the vasculature, both pulsatile and steady laminar flow occurs, resulting in the production of various biological factors by the endothelium for vascular support. In bifurcated regions, the blood flow patterns create oscillating shear stress, characterized by flow reversal, which can include occasional turbulence. Oscillatory shear stress, also referred to as disturbed shear stress, challenges the ECs to respond to the non-laminar changes in hemodynamic forces⁸. Low shear stress is typically associated with the venous system and the inner parts of the

arterial curvature. The bigger the angle of the curve, the lower the force on the inner part, which results in differences in shear force between the inner and outer parts of the curvature.

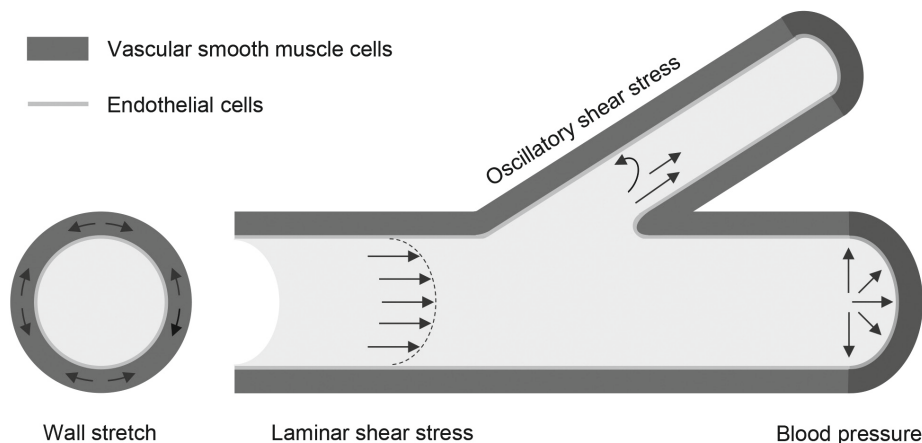


Figure. 2.1 Schematic representation of wall stretch on the left and shear stress on the right.

In wall stretch, distension pressure results in the radial forces exerted on the vessel which leads to the extension of the vascular wall and in turn vascular cell elongation in a direction perpendicular to the force applied. Shear stress depends on flow rate, fluid viscosity, and radial distance of the vessel lumen. In straight regions of the vasculature, endothelial cells experience unidirectional shear stress, while at branch points and vascular bifurcations, endothelial cells experience oscillatory or low shear stress

Table 2.1 Physiological ranges of biomechanical forces in the arterial and venous systems

	Arterial system	Venous system	References
Physiological shear stress (dynes/cm ²)	11.4–30.4 (19.0–60.8 for arterioles)	0.76–7.6	Kroll et al. ⁷
Pathophysiological shear stress (dynes/cm ²)	< 11.4	< 0.76	Kroll et al. ⁷
Physiological wall stretch (%)	5–10%	N.A.	Anwar et al. ⁴
Pathophysiological wall stretch (%)	>20%	N.A.	Anwar et al. ⁴

Wall Stretch

The pressure exerted by blood volume produces forces in perpendicular direction to the vessel wall that leads to stretch in circumferential manner, resulting in circumferential stress also termed as “wall stretch” (Fig. 2.1)⁵. This pressure ‘P’ is the force (F) per unit area (A) exerting in perpendicular direction to the vessel wall, and results in radial forces triggering elongation of the vessel wall, thus causing cellular elongation. This alteration of the vessel wall in response to the amount of stretch applied to it

is referred to as “wall strain” which is a measure of deformation^{9,10}. In the wall of macro- and microvascular structures, VSMCs and ECs are sensitive to wall stretch and undergo structural and functional adaptation in response to it⁴. Wall stretch is mainly studied as a force active in macrovascular vessels. Low magnitude stretches between 5–10% are considered as physiological stretch, which promotes vascular stability, control of vascular tone as well as proliferation, and may also contribute to angiogenesis (Table 2.1). Under these conditions, wall stretch also stimulates a contractile VSMC phenotype, which is characterized by elongated, spindle-shaped cells. On the other hand, high magnitude stretches of 20% and above, are considered as pathological stretch⁴ (Table 2.1). Under these conditions, VSMCs switch from the contractile to a “synthetic” phenotype, which shows poor contractility, pro-migratory, and pro-inflammatory behavior on a functional and structural level, and are characterized by a cobblestone morphology with a rhomboid shape and a reduction in length^{11,12}.

Mechanosensing

Mechanical forces affect ECs and VSMCs via mechanotransduction, which refers to the process through which cells sense and respond to biomechanical stimuli and translate these into the biochemical signals that elicit specific cellular responses^{4,13}. Any cellular structure that can detect these mechanical forces is called a mechanosensor. The receptors that are involved in sensing these mechanical forces are termed mechanoreceptors. Activation of mechanosensors by mechanical factors leads to the initiation of multiple complex intracellular signaling pathways, which affect cellular function and drive the expression of particular genes^{2,4}. Due to the direct contact of ECs with blood flow, shear stress predominantly activates ECs³. To date, many mechanosensors have been described in ECs and do not appear to be limited to adhesion molecules, integrins, and ion channels, but for instance also include the membrane lipid bilayer itself and the glycocalyx¹³. These structures enable the vascular wall to adapt to differences in shear forces, by, e.g., stimulating local cell proliferation, or by modulating the vessel diameter. Many of these endothelial mechanosensors are also involved in sensing wall stretch. In addition to ECs, wall stretch also directly activates VSMCs. Accumulating evidence indicates that various aspects of mechanosensing act in parallel and interact rather than operate individually. The mechanosensors and mechanosensing mechanisms of shear stress and wall stretch will be discussed in the following section in more detail.

Receptor Tyrosine Kinases

Receptor tyrosine kinases (RTKs) are high-affinity cell surface receptors that are activated either by mechanical or chemical factors. They undergo dimerization,

which allows tyrosine residues of the receptor in the cytoplasmic portion to undergo trans-phosphorylation by its partner receptor, followed by signal transmission through the plasma membrane¹⁴. This phosphorylation of tyrosine residues creates binding sites for intracellular downstream factors, such as tyrosine protein kinase “Src” and phospholipase-C γ (PLC- γ). A well-described RTK, vascular endothelial growth factor receptor-2 (VEGFR2), acts as a mechanosensor in association with platelet endothelial cell adhesion molecule 1 (PECAM-1) and vascular endothelial (VE)-cadherin, in response to both shear stress and wall stretch. Previous studies have shown that unidirectional shear stress induces increased tension on PECAM-1, which triggers recruitment and activation of Src family kinases. VE-cadherin links PECAM-1 to VEGFR2, which enables Src-dependent transactivation of VEGFR2 and subsequent activation of phosphoinositide 3-kinase (PI3-K) (Fig. 2.2). The Src-induced activation of VEGFRs does not necessarily require vascular endothelial growth factor (VEGF) stimulation, although it has previously been demonstrated that knockdown of VEGF results in attenuation of the protective effect of shear stress, implicating that VEGF signaling, via an alternative route, may be involved in maintaining a healthy vascular environment¹⁵.

In the early adaptive response to flow, PI3-K activation by VEGFR2 stimulates the serine/threonine kinase protein kinase-B (PKB), also known as Akt (Fig. 2.2). Stimulation of Akt not only stimulates endothelial survival, but also favors endothelial nitric oxide synthase (eNOS) induced production of nitric oxide (NO)¹⁶. In this mechanosensor complex, PECAM-1 is responsible for direct transmission of shear forces and Src activation; VEGFR2 is required for the activation of PI3-K, whereas VE-cadherin serves as an adaptor molecule. Disruption of any of these molecules leads to impaired activation and signaling¹⁷. Furthermore, this tri-molecular complex-mediated PI3-K signaling leads to upstream integrin activation, which exerts distinct cellular responses. In response to disturbed shear stress, PI3-K-induced activation of integrins stimulates focal adhesion kinase (FAK) followed by recruitment of a complex consisting of growth factor receptor-bound protein 2 (GRB2)/son of sevenless (SOS), stimulating activation of mitogen-activated protein kinases (MAPKs) and subsequent nuclear factor κ B (NF- κ B) and activating protein-1 (AP-1) mediated expression of pro-inflammatory genes (Fig. 2.2)¹⁸.

In addition to fluid shear stress, PECAM-1 has also been shown to be activated by a wide variety of additional mechanostimuli, including osmotic shock and wall stretch¹⁹. In response to physiological wall stretch, endothelial PECAM-1 undergoes phosphorylation and initiates protein tyrosine phosphatase-2 (SHP-2) binding, subsequently activating MAPK and extracellular regulated kinase (ERK) (Fig. 2.3).

The activation of MAPK and ERK promotes endothelial elongation and reorientation, ensuring that ECs are aligned in parallel to the direction of applied stretch^{20,21}. Under pathological stretch levels, PECAM-1 phosphorylation and subsequently ERK activation instead activate Ras and Raf²², stimulating the expression of pro-inflammatory genes, such as monocyte chemoattractant protein- 1 (MCP-1)² (Fig. 2.3). RTKs have also been reported to play a role in VSMCs exposed to wall stretch. In VSMCs, the stretch is involved in activating platelet- derived growth factor- β (PDGFR β). PDGFRs form a wide subclass of the RTKs family that regulate various cellular responses, such as cell proliferation, differentiation, growth, and development in response to different stimuli. It has been reported that upon the stretch, PDGFR β undergoes ligand-independent phosphorylation, thereby inducing VSMC proliferation²³.

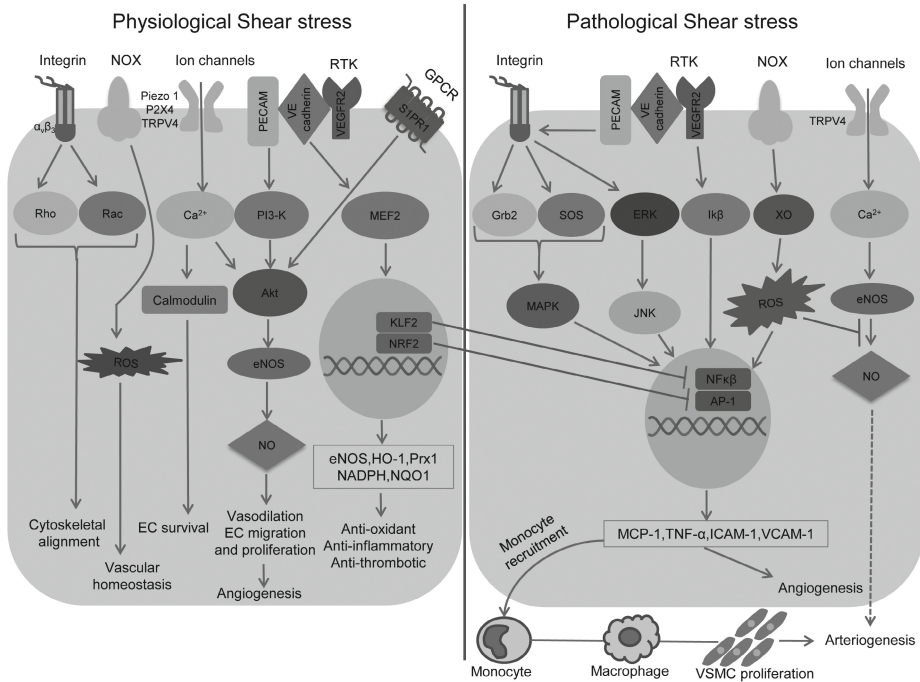


Fig. 2.2 Schematic representation of the mechanosensing and signaling in physiological (left) and pathological (right) shear stress.

Shear stress is sensed by various mechanoreceptors or mechanosensory complexes. These mechanosensors initiate various downstream signaling pathways, which at their turn activate transcription factors and co-factors to modulate endothelial cell (EC) function and phenotype. In physiological shear stress shown on the left, these pathways result in vascular homeostasis, vasodilation, EC migration and proliferation, cytoskeletal alignment, and angiogenesis. Physiological shear stress has also antioxidant, anti-inflammatory, and anti-thrombotic functions. Pathological shear stress, in contrast, triggers different pathways, resulting in monocyte recruitment and thereby inflammation, but also eventually in angiogenesis and arteriogenesis. Akt protein kinase B, AP-1 activator protein-1, eNOS endothelial nitric oxide synthase, ERK extracellular signal-regulated kinases, GPCR G-protein coupled receptor, GRB2 growth factor receptor-bound protein 2, HO-1 heme oxygenase 1, ICAM-1 intercellular adhesion molecule 1, JNK Jun N-terminal kinase, MAPK mitogen-activated protein kinases, MCP-1 mono-cyte chemoattractant protein-1, MEF2 myocyte enhancer factor-2, NF-κB nuclear factor kappa beta, NO nitric oxide, NOX NADPH oxidases, NQO1 NAD(P)H dehydrogenase quinone 1, PECAM-1 platelet endothelial cell adhesion molecule-1, Piezo 1 piezo protein 1, PI3K phosphoinositide-3 kinases, PRX1 paired related homeobox 1, P2X4 purinoceptor 4, ROS reactive oxygen species, RTK receptor tyrosine kinases, SOS son of seven less complex, SRPR1 sphingosine-1-phosphate receptor 1, TNF-α tumor necrosis factor-alpha TRPV4 transient receptor potential cation channel subfamily V member 4, VCAM-1 vascular cell adhesion molecule-1, VE-cadherin vascular endothelial cadherin, VEGF vascular endothelial growth factor, VEGFR2 vascular endothelial growth factor receptor-2, XO xanthine oxidase

Integrins

Integrins are transmembrane receptors that attach the cytoskeleton to the extracellular matrix (ECM) and are considered important mechanosensors²⁴. They are heterodimeric in structure, meaning that they contain two subunits (α and β), of which in mammals, 18 α - and 8 β -subunits are known²⁵. Integrins interact with focal adhesion (FA) proteins across the plasma membrane and contribute to adhesion between the cytoskeleton and ECM via these FA-complexes¹³. In response to physiological shear stress, subsequent conformational activation of integrin $\alpha_v\beta_3$, facilitates an increase in EC binding to ECM. This shear-induced $\alpha_v\beta_3$ integrin binding to ECM leads to transient inactivation of Rho (Fig. 2.2). The Rho family of GTPases is a family of small signaling G-proteins involved in organelle development and cell movement. Short-term inactivation of Rho via $\alpha_v\beta_3$ aids in cytoskeletal alignment to the direction of flow during the late adaptive response²⁶. In this process, the previously described tri-molecular complex (PECAM-1, VEGFR2 and VE-cadherin) activates integrins, forming a new integrin-matrix interaction which drives shear-induced adaptive responses in physiological conditions (cell alignment) via transient Rho inactivation²⁶, and pathological conditions (inflammation) via GRB2/SOS-MAPK- NF- κ B signaling¹⁸ (Fig. 2.2). Regulation of Rho in response to shear stress is complex. Rho-activation occurs quickly and spontaneously under shear stress and immediately induces cell contraction via Rho-kinase. Once Rho-kinase reaches basal levels, ECs elongate in the direction of flow, coinciding with the upregulation of Rac-1 and Cdc42. Rho and Rac activation are both involved in the regulation of the directionality of cell movement. Inhibition of Rho/Rho-kinase leads to increased cell displacement, indicating that EC reorientation occurs in two-step process which involves Rho-induced depolarization followed by Rho/Rac-mediated polarization and subsequent migration in the direction of flow. In general, transient inactivation of Rho via integrin and Rho/Rac regulation is required for EC reorientation, migration, and flow alignment in response to shear stress²⁷. Remarkably, responding to physiological stretch, integrin α_2 and β_1 subunits are known to activate p38 MAPK, which has also been shown to contribute to endothelial reorientation²⁸ (Fig. 2.3). In addition, integrin signaling via Rho induces adaptation of cell morphology and orientation and Rho-induced PI3-K activation leads to NO production via the Akt/eNOS pathway that facilitates vascular tone regulation². In contrast, under pathological stretch, integrins induce reactive oxygen species (ROS) production via the c-Jun-N-terminal Kinase (JNK) pathway, which results in the expression of pro-inflammatory genes (such as MCP-1) (Fig. 2.3)².

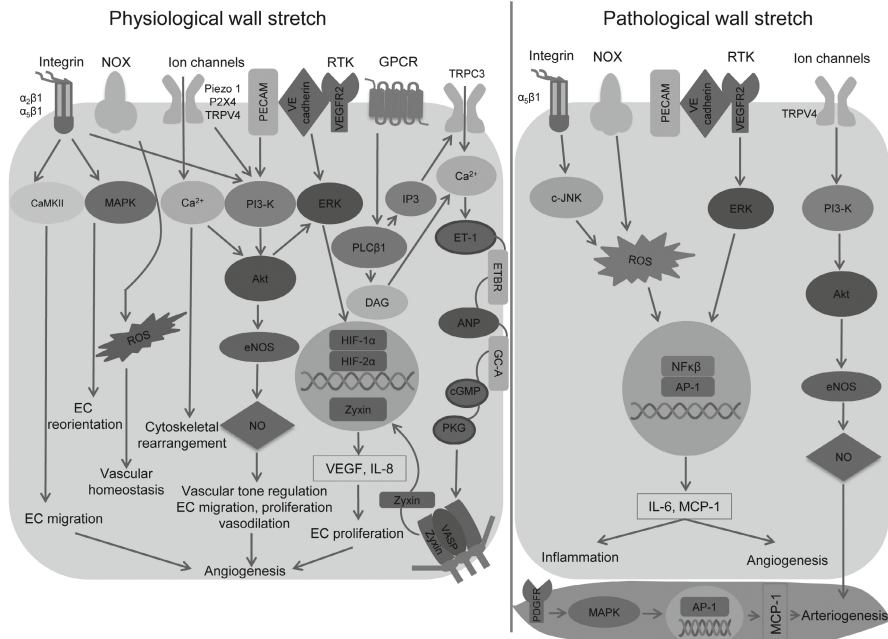


Fig. 2.3 Summary of the mechanosensing mechanisms induced by wall stretch.

Wall stretch stimuli are sensed by mechanosensors of both endothelial cells and vascular smooth muscle cells that transduce downstream signals. This results in the activation of transcription factors that regulates gene expression followed by increased protein synthesis which alters cell morphology and function. However, different mechanisms are activated upon different intensities, magnitude, and duration of stretch applied. Physiological wall stretch (left) is beneficial in maintaining healthy phenotype of endothelial and vascular smooth muscle cells and thus regulating vascular growth and function; Whereas pathological wall stretch (right), could activate pathways leading to disease progression or may induce arteriogenesis as a compensatory mechanism that could limit disease development. Thus, it is important to understand the signaling mechanisms that are triggered in response to wall stretch as this could aid in the identification of novel therapeutic targets that could stimulate vascular regeneration and restore vascular function aimed at treating vascular-related diseases. ANP atrial natriuretic peptide, AP-1 activator protein-1, CaMKII calmodulin-dependent protein kinase-II, cGMP cyclic guanosine monophosphate, c-JNK c-Jun N-terminal kinase, DAG diacyl glycerol, eNOS endothelial nitric oxide synthase, ERK extracellular signal-regulated kinases, ET-1 endothelin 1, ETBR endothelin-B receptor, GC-A guanylyl cyclase-A, GPCR G-protein coupled receptor, HIF-1α hypoxia-inducible factor-1α, HIF-2α hypoxia-inducible factor-2α, IL-6 interleukin-6, IL-8 interleukin-8, IP3 inositol triphosphate, MAPK mitogen-activated protein kinases, MCP-1 monocyte chemoattractant protein-1, NF-κ nuclear factor kappa beta, NO nitric oxide, NOX NADPH oxidases, PDGFRβ platelet cell-derived growth factor receptor-beta, PECAM- 1 platelet endothelial cell adhesion molecule-1, PI3K phosphoinositide-3 kinases, PKG protein kinase-G, PLCβ1 phospholipase-C β1, P2X4 purinoceptor 4, ROS reactive oxygen species, RTK receptor tyrosine kinases, TRPC3 transient receptor potential channel 3, TRPV4 transient receptor potential cation channel subfamily V member 4, VASP vasodilator stimulated phosphoprotein, VCAM-1 vascular cell adhesion molecule-1, VE-cadherin vascular endothelial cadherin, VEGF vascular endothelial growth factor, VEGFR2 vascular endothelial growth factor receptor-2

Ion Channels

Ion channels also represent important sensors for shear stress and wall stretch. Shear stress induces the activation of several non-specific cation channels, including Piezo Type Mechanosensitive Ion Channel Component 1 (Piezo1), Transient Receptor Potential Cation Channel Subfamily V Member 4 (TRPV4), and P2X Purinoceptor 4 (P2X4), all causing cellular depolarization and elevated cytoplasmic Ca^{2+} levels²⁹ (Fig. 2.2). Elevated Ca^{2+} levels stimulate the opening of Ca^{2+} -dependent K^+ channels, leading to K^+ influx and hyperpolarization. In response to shear stress-activated ion channels on ECs and via Calmodulin/ Ca^{2+} /eNOS/NO signaling, VSMCs neighboring ECs also hyperpolarize and (partially) through direct electrical coupling via gap junctions, cause vessel relaxation and vasodilation (Fig. 2.2)³⁰. The elevated cytoplasmic Ca^{2+} levels furthermore contribute to Akt-mediated activation of eNOS, as Ca^{2+} -activated calmodulin releases eNOS from its bound state in caveolae, which renders the enzyme inactive³¹. Similarly, stretch also causes a rise in cytoplasmic Ca^{2+} levels, as for instance observed in capillary ECs via TRPV4, which facilitated cytoskeletal rearrangements and capillary cell orientation³¹. This stretch-induced rise of Ca^{2+} levels similarly led to Akt-induced activation of eNOS³³ (Fig. 2.3).

G-Proteins and G-Protein-Coupled Receptors

Heterotrimeric G-protein complexes act as molecular switches capable of transmitting a variety of external stimuli into the cell. Their activity is regulated by their ability to bind and hydrolyze guanosine triphosphate (GTP) to guanosine diphosphate (GDP). It has previously been demonstrated that physiological levels of fluid shear stress cause dose-dependent activation of GTP hydrolysis by G-proteins that were reconstituted into phospholipid vesicles. Increasing or decreasing membrane fluidity by incorporation of lysophosphatidylcholine or cholesterol in the membrane, respectively, affected the activation of G-proteins by shear, indicating that physical properties of the phospholipid bilayer, rather than protein receptor-induced signaling, mediate this activation of G-proteins by shear³⁴. Nonetheless, G-protein-coupled receptors do in fact respond to shear stress and may play an important role in mechanosensing. It has for instance been demonstrated that applying shear, as well as a membrane-fluidizing agent, causes rapid and ligand-independent activation of the endothelial bradykinin B2 receptor.

Moreover, the G-protein-coupled receptor (GPCR) sphingosine-1 phosphate receptor 1 (S1P1) has also been demonstrated to be required for shear-induced activation of Akt and eNOS. Similar to bradykinin B2 receptor, activation of S1P1 was ligand-independent, as experiments with ligand binding-deficient mutants of S1P1 led to the functional rescue of the S1P1 knockout phenotype. Using pertussis toxin (PTX), a G-

protein inhibitor, it has also been demonstrated that applying physiological stretch for 24 h stimulates endothelial migration via activation of G_i - α subunits and GTPase activity³⁵. Applying stretch on ECs causes the activation of secondary messengers inositol trisphosphate (IP_3) and Diacylglycerol (DAG) through phospholipase-C- β 1 (PLC β 1). These secondary messengers in turn activate Ca^{2+} influx via transient receptor potential channel-3 (TRPC3), eventually leading to secretion of endothelin-1 (ET-1) and thus activating endothelin B-1 receptor (ETB1R). Activation of ET-1 receptor subsequently results in the secretion of pro atrial natriuretic peptide (pro-ANP) that binds to guanylyl cyclase-A (GC-A) receptor, followed by downstream effects such as cyclic guanosine monophosphate (cGMP)-induced protein kinase-G (PKG) activation. This complex stretch-induced autocrine-signaling loop in ECs leads to translocation of zyxin into the nucleus where it controls the expression of stretch-sensitive genes involved in cell cycle regulation and endothelial function³⁶. Compared with static ECs, stretch-induced translocation of zyxin also induced the expression of several pro-inflammatory genes, illustrating the various adaptive responses this stretch-responsive GPCR-mediated signaling axis may be involved in³⁶. In addition to ECs, stretch-mediated activation of GPCRs has also been demonstrated in VSMCs. Exposing primary renal rat VSMCs to osmotic stretch led to increased Ca^{2+} levels which could be inhibited with the angiotensin 1 receptor (AT_1R) blocker losartan^{37,38}.

NADPH Oxidases

The intensity and type of shear stress also directly affects the activity of NADPH oxidases (NOXs). NOXs belong to a family of membrane-bound protein complexes, of which NOX 1, 2, 4, and 5 isoforms are expressed in the vasculature. They facilitate the production of O_2^- , a free radical that is the precursor of most ROS. It has been observed that steady laminar flow leads to limited and transient induction of NOX, which in concert with mitochondrial oxidation contributes to low amounts of ROS (Fig. 2.2)³⁹. ROS and shear-induced NO could interact, forming reactive nitrogen species (RNS) that cause nitrosative damage³⁹. During physiological conditions, limited ROS production ensures that this interaction hardly occurs, and as a consequence, the availability of both factors suffices vascular homeostasis. In response to oscillatory shear or flow reversal, however, sustained NOX activity causes xanthine oxidase- (XO) dependent elevation of ROS production³⁹. The augmented production of ROS favors an oxidative state and not only causes an increase in RNS, but also lowers NO availability. This lowering of NO bioavailability blunts the vasodilatory capacities, and since NO also provides S-nitrosation of regulatory proteins involved in the suppression of AP-1 and NF- κ B activity, its lowering also results in elevated expression of pro-inflammatory cytokines and adhesion molecules (Fig. 2.2).

In addition to shear stress, wall stretch also affects the NOX activity in ECs. Several studies revealed that upon long-term physiological stretch in ECs, NOX4 was significantly downregulated, leading to reduced ROS formation (Fig. 2.3). This stretch-dependent downregulation of NOX4 expression and ROS formation was found to be abolished when eNOS was inhibited by N omega-nitro-L-arginine methyl ester hydrochloride (L-NAME), implicating that physiological stretch on ECs induces its vasoprotective activity by suppressing NOX4 and ROS via eNOS (Goettsch⁴⁰). On the other hand, pathological stretch leads to pro-inflammatory conditions in ECs. Pathological stretch causes excessive production of free radicals that can either react alone, or via superoxide dismutase, to generate hydrogen peroxide, which stimulates NF- κ B activity^{41,42}. In addition, phosphorylation of P66^{Shc} in response to pathological stretch leads to elevated superoxide anions and reduced NO levels, indicating that pathological stretch is associated with increased ROS production, promoting oxidative stress and endothelial dysfunction⁴³.

Glycocalyx

The glycocalyx is a thin apical layer (approximately 500 nm) composed of glycoproteins, glycolipids, and proteoglycans, such as Syndecan-1 and -4. The cytoplasmic domain of these Syndecans directly interacts with the cytoskeleton, providing a potential route of force transfer from shear stress towards the endothelium. Genetic ablation of syndecans results in dysregulation of Rho-induced structural adaptations required to align ECs to the direction of flow and causes elevated expression of inflammatory genes. Moreover, enzymatic removal of heparin sulfate and hyaluronic acid, both glycosaminoglycans bound to proteoglycans, was shown to attenuate shear-induced production of NO and vasodilation. Suppression of syndecan-4 expression in ECs did not affect shear-induced phosphorylation of VEGFR2, suggesting that Syndecans might signal independent from the PECAM-1/VE-Cadherin/VEGFR2 complex, although since Syndecans also act as Integrin co-receptor during adhesion, it could be argued as well that it signals downstream of this junctional complex. In addition to shear stress, endothelial glycocalyx was also found to respond to wall stretch. Recent studies have demonstrated that in response to physiological stretch, activated glycocalyx mediates NO production. Using atomic force and fluorescence microscopy techniques, the rapid production of NO was observed in the presence of heparin sulfate and hyaluronic acid which are present on the surface of glycocalyx indicating that glycocalyx mechanotransduction contributes to endothelial function in response to physiological stretch⁴⁴.

Transcriptional and Functional Response

Many aspects of vascular cell function are affected by mechanical stimuli. Endothelial growth, for instance, is highly dependent on the type of shear stress the endothelium is exposed to^{45,46}. In response to laminar flow, only limited numbers of ECs enter the cell cycle, rendering the majority of the cells arrested in G₀ or G₁ phase⁴⁷. This shear-induced growth arrest is mediated by a mechanism involving tumor suppressor protein 53 (p53). Upon p53 activation, cyclin-dependent kinase 4 (CDK4) activity is decreased and retinoblastoma protein (Rb) is not phosphorylated⁴⁷. Rb phosphorylation is required to release E2F transcription factors from the pRb/E2F complex to induce the expression of genes required for DNA replication. Consequently, this shear-induced inhibition of CDK4 limits proliferation⁴⁸. Simultaneously, laminar flow also serves a protective role by reducing EC turnover, preventing the occurrence of lesions^{49,50}. Besides this proliferative response, the inflammatory- and thrombotic state of vascular cells is highly related to shear stress and wall stretch. Depending on type and intensity of mechanical stimuli, particularly transcription factors, including Krüppel-like factors (KLFs) 2 and 4, nuclear factor erythroid 2-like (Nrf2), AP-1, hypoxia-inducible factor 1 α (HIF1 α), and zyxin are either activated or inactivated (Fig. 2.2).

Krüppel-Like Factors 2 and 4

KLF-2 and 4 are identified as laminar flow inducible factors that play an important role in the regulation of endothelial function. With respect to the vasculature, KLF2 is exclusively present in the endothelium, robustly expressed in straight parts of the vasculature, and notably lower expressed in branch points and bifurcated regions⁵¹. KLF2, together with Nrf2, modulates the expression of genes critical in regulating vascular tone, hemostasis/thrombosis, and inflammation, and regulates endothelial barrier function and its antioxidative capacity (Fig. 2.2)⁵². Shear stress-induced expression of KLF2 depends on myocyte enhancer-binding factor 2 (MEF2). Under static conditions, histone deacetylase 5 (HDAC5) is bound to MEF2 on the KLF2 promotor and inhibits its transcriptional activity. High unidirectional shear stress results in HDAC5 dissociation from MEF2, allowing increased flow-dependent KLF2 transcription. KLF2 directly binds to the promotor of eNOS, inducing its transcription. At the same time, KLF2 also downregulates Caveolin-1, a negative regulator of eNOS. *In vitro* studies also demonstrated that overexpression of KLF2, by inhibiting NF- κ B, lowers the production of inflammatory cytokines and adhesion molecules vascular cell adhesion molecule-1 (VCAM1) and E-selectin⁵².

Like KLF2, KLF4 increases the expression of eNOS and thrombomodulin, while reducing the expression of VCAM1 and pro-coagulant factors. Although similarities to the actions and effects of KLF2 exist, KLF4 differs in its expression in response to inflammatory stimuli. In response to inflammatory stimuli, such as tumor necrosis factor- α (TNF α), expression of KLF4 is heavily increased. In the context of inflammation, KLF4 may serve as a back-up to modulate endothelial inflammation when KLF2 levels are strongly attenuated⁵³. Compared to shear stress, the effect of wall stretch on KLF2 regulation is less well understood. However, recent evidence has shown that wall stretch also has an impact on KLF2 regulation. In microvascular ECs, pathological stretch halved the expression of KLF2 compared to cells under physiological stretch. This indicates that pathological wall stretch suppresses the functions of KLF2, which may lead to vasoconstriction, inflammation, coagulation, or thrombosis⁵⁴.

Nuclear Factor Erythroid 2-Like

Another important laminar flow-responsive transcription factor is Nrf2, which plays an important role in the protection of ECs from oxidative stress⁵⁵. Like KLF2, Nrf2 is activated by shear-induced activation of MAPK signaling which stimulates its release from Kelch-like ECH-associated protein 1 (keap1), resulting in Nrf2 translocation to the nucleus. In addition, the activity of Nrf2 is enhanced by KLF2 and PI3K/Akt signaling, which also enhances the nuclear localization of Nrf2 and stimulates expression of the majority of shear stress-regulated vasoprotective genes⁵⁶. Transcriptional activation of Nrf2 leads to induction of antioxidant response element- (ARE) related genes. These genes, including hemo oxygenase-1 (HO-1), peroxiredoxin 1 (Prx-1), nicotinamide adenine dinucleotide phosphate (NADPH), and quinone oxidoreductase-1 (NQO1) play key roles in the protection of vascular endothelium from oxidative stress during the development of vascular diseases.

Nuclear Factor Kappa Beta

Opposing many of the laminar flow-induced effects, disturbed flow is related to pro-oxidant and pro-inflammatory conditions in ECs, of which chronic activation is associated with the development of vascular disease. Important transcriptional events that reflect the pro-oxidant and pro-inflammatory condition of ECs in response to disturbed flow include the activation of NF- κ B (Fig. 2.2). NF- κ B is a transcription factor involved in both inflammation- and oxidative stress-mediated signaling⁵⁷. In the absence of inflammatory stimuli, the non-activated form of NF- κ B is maintained in the cytoplasm together with its inhibitory subunit I κ B, but when activated, proteolysis of I κ B results in the exposition of a nuclear recognition site in NF- κ B, which stimulates it to translocate into the nucleus. Disturbed flow both

attenuates KLF2-mediated inhibition of NF- κ B and simultaneously induces I κ B degradation, resulting in a pronounced increase of NF- κ B activity⁵⁸. There has been accumulating evidence that wall stretch also induces activation of NF- κ B in ECs by various signaling pathways. Depending on the magnitude of wall stretch, the adaptation of ECs through NF- κ B activation varies. For example, studies have shown that a 12% stretch in ECs leads to NF- κ B activation that results in increased MCP-1 expression, which is chemotactic to monocytes and macrophages⁵⁸. Based on the known role of MCP-1 in ECs, this increased MCP-1 expression via NF- κ B activation may promote capillary tube formation. Other studies demonstrated that in response to 25% stretch, NF- κ B was activated and was shown to significantly elevate levels of interleukin-6 (IL-6), which is involved in inflammatory processes. Mechanistically, NF- κ B activation requires outside-in signaling via integrin activation followed by PI3-K/PLC/PKC signaling, which is also observed in VSMCs upon exposure to stretch⁶⁰.

Activator protein 1

Like NF- κ B, AP-1 is also activated in response to disturbed flow. AP-1 is a heterodimer composed of members of the c-Jun, c-Fos, activating transcription factor (ATF), and Jun dimerization protein (JDP) families. In response to disturbed, or low oscillatory flow, impaired Nrf2 activation causes a reduced inhibition of JNK and p38 MAPK, whereas nuclear translocation of AP-1 subunits is promoted by downregulation of KLF2, eventually both contributing to a rapid activation of AP-1 (Fig. 2.2)^{56, 61}. Like NF- κ B, activation of AP-1 eventually results in enhanced expression of numerous adhesion molecules, such as VCAM-1, intercellular adhesion protein-1 (ICAM-1) and E-selectin, thus promoting mononuclear cell recruitment and extravasation, and enhances the transcription of a variety of cytokines, including TNF- α , MCP-1, and interleukins to stimulate an inflammatory response⁵⁷. Oscillatory flow-mediated activation of pro-inflammatory NF- κ B and AP-1 and counterbalancing activation of vasculoprotective KLF2 and Nrf2 thus helps to define the shear stress-dependent endothelial phenotype in atheroprone/atheroprotective arterial sites⁸. AP-1 activation has also been reported in response to pathological elevation of wall stretch in both ECs and VSMCs where it regulates many functions such as proliferation, inflammation, and vascular growth. In ECs, wall stretch-induced activation of AP-1 leads to transcription of MCP-1, which stimulates monocyte recruitment and inflammation^{59, 62}. Similarly, stretch-induced activation of AP-1 in VSMCs results in MCP-1 synthesis, which via its monocyte recruitment function also stimulates VSMC proliferation⁶³. Notably, despite its pro-inflammatory role, deletion of AP-1 family member Jun-D leads to oxidative stress, suggesting that AP-1 also plays a role in protecting ECs from dysfunction⁶⁴.

Hypoxia-Inducible Factor 1 α

It has previously been demonstrated that HIF1 α also is a prominent disturbed shear stress-responsive factor. HIFs are heterodimeric nuclear transcriptional factors consisting of two subunits that regulate the transcription of genes mediating cellular homeostatic responses to altered oxygenation. The expression of HIF1 α in many tissues increases exponentially as oxygen concentration declines⁶⁵. HIF1 α was found to be upregulated in atheroprone regions of arteries, and HIF1 α expression is increased in response to low shear stress in cultured ECs⁶⁵. It has also been demonstrated that disturbed shear activates HIF1 α via induction of NOX4 and ROS production. Activation of HIF1 α by disturbed shear results in metabolic reprogramming of the endothelium by promoting endothelial glycolytic metabolism and reduction in mitochondrial oxidative phosphorylation. In response to wall stretch, HIF1 α activation has not only been reported in ECs [66] but also in VSMCs⁶⁷. Transcriptional activation of HIF1 α was observed in skeletal muscle capillary beds and inferior vena cava under prolonged exposure to stretch⁶⁸. *In vitro* studies of arterial cells have also demonstrated that wall stretch-induced activation of HIF1 α promotes VSMC proliferation^{67, 69}. Furthermore, physiological stretch on skeletal muscle and capillary ECs promote transcription and DNA binding activity of both HIF1 α and HIF2 α , leading to transcription of vascular growth- and ECM modulation-associated factors (Fig. 2.3)⁶⁶ and matrix metalloproteinases (MMPs)⁶⁸.

Zyxin

Zyxin is yet another important transcription factor, recently described for its stretch-dependent activity. Zyxin is a LIM-domain containing protein that appears to be located at focal adhesion regions of ECs and VSMCs, in association with vasodilator adhesion protein (VASP). In ECs, zyxin was found to be activated and translocated directly into the nucleus in response to stretch, where it controls many stretch-sensitive genes, such as interleukin-8 (IL-8), Hairy/enhancer-of-split related with YRPW motif protein 1 (Hey-1) and VCAM. This translocation of zyxin occurs through a complex series of events, where initially GPCRs respond to wall stretch, thereby activating PLC β that lead to the release of secondary messengers IP₃ and DAG. These secondary messengers activate TRPC3 thereby enhancing Ca²⁺ influx, which leads to activation of ETBR via ET-1 binding. These events further lead to the release of pro-ANP that binds to GC-A leading to downstream cGMP-PKG signaling, finally inducing zyxin phosphorylation at Ser142. Pathway analysis revealed that the genes regulated by zyxin in ECs upon stretch mainly control cell cycle and inflammatory factor release, suggesting that zyxin-induced transcriptional regulation contributes to the maintenance of endothelial cell function³⁶. On the other hand, zyxin plays a different role in VSMCs upon stretch induction. Instead of inducing direct

translocation to the nucleus, upon its activation, zyxin activates RhoA and increases actin polymerization, transforming G-actin to F-actin, which leads to the expression of myocardin-related transcription factor-A (MRTF-A) and translocation of MRTF-A to the nucleus. Upon binding of MRTF-A to serum response factor (SRF) in the nucleus, it controls the expression of mechanosensitive genes that mediate the maintenance of the contractile phenotype of VSMCs. Combined, these data suggest that zyxin plays an important role in cellular adaptations in response to stretch⁷⁰.

Mechanical Stimuli in Vascular Growth

The development of the human vascular system starts already in the third week of embryonic development by a process called vasculogenesis. At this point in development, the mechanical factors described in previous sections are still absent. At later stages, however, vascular growth predominantly occurs via angiogenesis and arteriogenesis, two distinctly different processes, in which biomechanical stimuli are of critical importance.

Arteriogenesis

Arteriogenesis, or collateralization, refers to the process of developing pre-existing arterioles into functional muscular collateral arteries, thereby increasing the diameter of these vessels. Physiologically, this is of relevance, for instance, in microvascular remodeling upon exercise training, in which an increase in arteriole diameter leads to an elevation of the total flow a vascular bed can withstand. However, arteriogenesis is mostly known for its vitally important role in overcoming vascular stenosis, which is referred to as abnormal narrowing of blood vessels with subsequent reduction of the lumen. Growth and expansion of pre-existing arterioles to by-pass an occluded vessel provides the vascular system with the ability to compensate for stenosis-induced attenuation of tissue perfusion. Both under these physiological and patho-physiological circumstances, arteriogenesis involves proliferation and migration of ECs and VSMCs, as well as degradation and reorganization of extracellular structures. To facilitate these features, activated ECs express high levels of ICAM1, VCAM1, E-selectin, and MCP-1 to attract monocytes, which in turn secrete a local cocktail of growth factors, proteases, and chemokines, including fibroblast growth factors (FGFs) and MMPs (Fig. 2.2).

Remarkably, in zebrafish embryos, in which all cells can be supplied with oxygen via diffusion, it has been demonstrated that arteriogenesis does not depend on hypoxia, yet predominantly develops in response to altered biomechanical stimuli⁷¹. During progressive stenosis of an artery, altered hemodynamic patterns emerge. The pressure differs between the proximal and distal portions from the occlusion

site, creating a pressure gradient in the artery. The pressure drop distal to the occlusion drives the increase in blood flow and subsequently leads to increased collateral fluid shear stress⁷². This increased shear stress results, among others, in endothelial NO release causing vasodilation⁷³, subsequently causing an inevitable

rise in wall stretch too. Via the combined activation of various mechanosensors, this rise in biomechanical stimuli activates vascular growth-associated signaling in both ECs and VSMCs recruiting pre-existing arterioles spanning two neighboring arteries. Immunoprecipitation analysis illustrated that in response to pathological shear stress, integrin $\alpha_v\beta_3$, β_1 , and β_5 associate with Shc protein (contains Src homology-2 domain). These integrins are known to stimulate arteriogenesis by activation of ERK and JNK signaling, thereby activating the transcription complex AP-1⁷⁴, or via GRB2/SOS signaling, leading to the activation of NF- κ B (Fig. 2.2)¹⁸. Aided by the disturbed shear-induced loss of Nrf2 activity, which leads to attenuated inhibition of JNK-mediated AP-1 activation, this elevated shear stress-induced activation of integrins initiates the expression of inflammatory factors, such as ICAM1, VCAM1, and MCP-1⁵⁷. These factors are strongly involved in adhering and attracting monocytes which, upon binding to the vascular wall, trans-migrate and differentiate into macrophages, stimulating VSMC proliferation and collateral maturation, mostly in a paracrine manner⁷⁵.

Likewise, wall stretch also plays a fundamental role in collateral vessel growth through the activation of integrins. In response to pathological stretch, integrin activation, such as $\alpha_5\beta_1$ in ECs, via JNK signaling, phosphorylates p66^{Shc} and in parallel activates NADPH-oxidase that leads to ROS production⁴³. This ROS production leads to the expression of MCP-1 through transcriptional activation of NF- κ B or AP-1 and results in the development of collateral vessel growth^{2,74} (Fig. 2.2). Furthermore, elevated wall stretch leads to integrin β_3 and $\alpha_v\beta_5$ activation in VSMCs, which results in the secretion of platelet-derived growth factor-A (PDGFA), stimulating VSMC proliferation via an autocrine-signaling loop⁷⁶. Although the exact mechanism leading to stretch-induced secretion of PDGFA via integrins activation in VSMCs still needs to be elucidated, it was reported that upon induction of stretch, VSMCs undergo this mitogenic response only when grown on collagen type 1, vitronectin, or fibronectin, but not on elastin or laminin, indicating this response is matrix type-dependent⁷⁶.

In addition to integrins, signaling via the mechanosensor PECAM-1 also contributes to collateralization⁷⁷. PECAM-1 is a widely described vascular cell junction molecule, known for its role in endothelial function. In previous studies, it has been

demonstrated that shear stress-induced PECAM-1 activation enhances PI3-K/Akt signaling, which in turn may stimulate integrin-mediated inflammatory signaling (Fig. 2.2)¹⁶. In mice, loss of PECAM-1 causes poor perfusion of collaterals⁷⁷ due to impaired complex formation with VE-cadherin and VEGFR2, suggesting that PECAM-1 is essential for arteriogenic signaling¹⁶. Similar to shear stress, wall stretch also leads to PECAM-1-mediated signaling, stimulating Ras- and Raf-induced activation of ERK signaling, which in turn stimulates the production of MCP-1 and arteriogenesis^{19,77}. In VSMCs, wall stretch activates the RTKs PDGFR α and PDGFR β ²³. Wall stretch stimulates rapid phosphorylation of PDGFR α and PDGFR β , which in turn leads to MAPK activation and enhanced DNA binding of AP-1^{23,78}. Like in ECs, activation of AP-1 in VSMCs enhances the transcription of MCP-1, which via attraction of monocytes indirectly results in VSMC proliferation, but at the same time also directly stimulates VSMC proliferation and transcriptional activation of NF- κ B⁷⁹ (Fig. 2.2).

Although ion channels also serve an important role in sensing shear stress and wall stretch, it is poorly understood how these sensors respond and participate in vascular function and tone under pathophysiological levels of shear stress and stretch. Femoral artery ligation studies have shown that TRPV4 expression is increased in growing collaterals at both RNA and protein levels. The notion that expression was upregulated secondary to femoral ligation suggests that TRPV4 is not directly involved as a primary sensor, though in experiments with a specific TRPV4 activator (4 α PDD), it has been demonstrated that elevated TRPV4 levels could stimulate proliferation of both ECs and VSMCs, and thus be an essential factor in collateral vessel growth (Troidl⁸⁰) (Fig. 2.2). Stretch activated TRPV4 in ECs participates in eNOS and NO production via activation of PI3K and Akt. Blocking of TRPV4 was shown to attenuate eNOS expression, and since several studies have illustrated that lack of NO impairs collateral growth^{33,81}, this suggests that stretch-induced activation of TRPV4 may utilize this signaling route to stimulate arteriogenesis. In addition, previous studies have also shown that NO inhibits VE-cadherin, causing increased vascular permeability and allowing infiltration of monocytes, which may contribute to the pro-inflammatory environment required for arteriogenesis⁸².

Angiogenesis

Angiogenesis is defined as the formation of new vessels from pre-existing vessels, which either occurs via sprouting of ECs or via intussusception. In sprouting angiogenesis, ECs are activated upon exposure to angiogenic stimuli, such as FGFs and VEGFA. These factors are produced during hypoxia and nutritional stress, and initiate various signaling cascades in ECs. In addition to activating ECs, hypoxia

has also been demonstrated to stimulate pre-capillary sphincters⁸³, a band of contractile mural cells known to regulate blood flow in capillaries⁸⁴. During exercise, for instance, hypoxia in muscle tissue stimulates these pre-capillary sphincters to relax and induces vessel dilation. The subsequent rise in the flow not only provides the surrounding tissue with its oxygen demands, but also stimulates a variety of mechanosensors that may drive angiogenesis⁸⁵. In contrast to sprouting angiogenesis, intussusceptive angiogenesis contributes to vascular growth by the division of existing vessels into multiple smaller vessels. It is initiated by the formation of so-called pillar core structures between opposing ECs. Pericytes and myofibroblasts invade these pillar cores and stabilize them by deposition of extra-cellular matrix components, followed by expansion of the tissue pillars until eventually the capillary is split in two. Although the exact mechanisms driving intussusceptive angiogenesis are still not fully understood, mechanical forces are suspected to play a vital role⁸⁶.

In response to unidirectional shear stress, PECAM-1-induced activation of PI3K and Akt signaling results in eNOS-mediated NO production¹⁶ (Fig. 2.2). Besides its role in vasomotion, endothelial NO is involved in various responses, predominantly in endothelial survival, but also in EC migration and proliferation⁸⁷. These aspects facilitate normal vascular homeostasis of mature capillaries, but are also indispensable for angiogenesis. In addition, NO has also been shown to suppress Angiostatin, an endogenous antagonist of angiogenesis⁸⁸. Wall stretch-induced activation of PECAM-1 signaling, leading to MCP-1 expression has also been shown to promote endothelial migration and proliferation^{19,77}. Previous studies showed that MCP-1 via MCP-1-induced protein (MCP1-IP) stimulates capillary new growth, whereas silencing of MCP1-IP abrogated this angiogenic response⁸⁹. RTKs, facilitating the above-described production of NO and MCP-1 initiated by PECAM-1, were also reported to stimulate angiogenesis in alternative ways. For instance, in response to shear stress, enhanced I κ B kinase activity was observed, while this activity was abolished upon inhibition of VEGFR2⁹⁰. Although, this study has not demonstrated that this pathway promotes angiogenesis, enhanced I κ B kinase activity could mediate angiogenesis in ECs via NF- κ B activation which was supported by other reports, showing that NF- κ B activation promotes capillary tube formation⁹¹. Physiological stretch has been reported to stimulate angiogenesis via VEGFR2 (Fig. 2.2). Stretch-induced VEGFR2 activation is ligand-independent, though this activation of VEGFR2 stimulates Akt and ERK, which in turn remarkably increases endothelial VEGF sensitivity, resulting in endothelial proliferation⁹². This increased VEGF sensitivity may occur through the activation of HIF-1 α or HIF-2 α ⁶⁶.

Shear stress and wall stretch have also been found to regulate angiogenesis via integrins. Integrins such as $\alpha_v\beta_3$ and $\alpha_v\beta_5$ were shown to regulate cell survival and angiogenesis but via distinct ways. Antagonists of $\alpha_v\beta_3$ were shown to disrupt FGF-mediated angiogenesis, while $\alpha_v\beta_5$ antagonists on the other hand disrupted VEGF-mediated signaling⁹³. In response to physiological shear stress, studies have demonstrated $\alpha_v\beta_3$ activation with sustained Shc association⁹⁴. In ECs, activated $\alpha_v\beta_3$ along with FGF, leads to Ras-induced protection from apoptosis, whereas $\alpha_v\beta_5$ activation under shear stress, along with VEGF, utilizes Ras- and Raf-induced activation of ERK, promoting both endothelial survival and angiogenesis⁹³. In response to physiological stretch, a complex is formed by integrin $\alpha_v\beta_3$ and $\alpha_5\beta_1$, which eventually stimulates angiogenesis. $\alpha_5\beta_1$ mediates EC migration through calmodulin kinase-II (CaMKII) signaling, whereas inhibition of $\alpha_v\beta_3$ leads to the blockage of this signaling leading to attenuation of EC migration, indicating that both of these integrins are closely involved in this functional response⁹⁵.

Ion channels were also reported in the regulation of angiogenesis in response to shear stress and wall stretch. For instance, physiological shear activates various ion channels, including Piezo 1 and TRPV4, which causes cellular depolarization and elevated cytoplasmic Ca^{2+} levels²⁹ (Fig. 2.2). These elevated Ca^{2+} levels in turn activate K^+ channels leading to K^+ influx and membrane hyperpolarization. The elevated Ca^{2+} levels contribute to eNOS activation and NO production, the role of which in vascular growth had been mentioned before³³. Similarly, GPCRs such as SP1R1 also activate this eNOS and NO signaling route in response to shear stress and thereby participate in the formation of new blood vessels⁹⁶. As described earlier, physiological stretch also induces GPCR activation which finally leads to transcription of stretch-sensitive genes, such as IL-8, VCAM-1, and Hey-8 through zyxin translocation into the nucleus⁷⁰. Transcription of these genes may contribute to endothelial migration, survival, and angiogenesis (Li 2003). Moreover, G-proteins have been reported to contribute to stretch-mediated angiogenesis. In response to physiological stretch at 1 Hz frequency for 24 hours on ECs, the G_i - α subunit, which belongs to the heterotrimeric G-alpha subunit family, is activated. This G_i - α subunit is bound to GDP during the inactivated state, whereas in response to stretch, G_i - α releases GDP and binds to GTP, inducing downstream signaling. Despite of the unknown signaling pathway, the enhanced GTPase activity in response to physiological stretch is intimately involved in the regulation of the angiogenic signal to maintain an adequate vascular capacity, as the G_i -protein inhibitor pertussis toxin-induced attenuation of endothelial migration and tube formation in response to wall stretch³⁵.

Shear stress is also involved in the last phases of angiogenesis; vessel maturation upon onset of flow in the newly formed capillary. The development of a vascular network or vascular plexus is mostly not pre-patterned, leading to highly complex branched vascular networks that require the elimination of poorly flowed branches (pruning) and maintenance of well-flowed blood vessels (maturation)⁹⁷. It has for instance been shown that shear stress-induced downregulation of the pro-angiogenic C-X-C motif receptor 4a results in maturation and stabilization of newly formed vascular connections in the zebrafish trunk- and brain vasculature⁹⁸. Moreover, flow-induced modulation of S1PR1 expression stabilizes the primary vascular network by enhanced cell-to-cell adhesion and by inhibiting angiogenic sprout formation⁹⁹. Another example of shear stress-induced stabilization involves a particular member of the tissue inhibitors of matrix metalloproteinases (TIMPs) family. TIMPs have been shown to coregulate capillary tube stabilization by inhibition of MMPs responsible for ECM breakdown. In particular, TIMP3 has been shown to play a crucial role in vessel stabilization and maturation upon flow¹⁰⁰. TIMP3 is expressed by pericytes and both regulated by cell-cell contact and shear stress. Increased expression of TIMP3 results in downregulation of A disintegrin and metalloproteinase with thrombospondin motif 1 (ADAMTS-1)¹⁰¹. The microvascular stabilizing capacities of pericytes exposed to shear stress are also mediated by miR-27. Unidirectional shear stress in the vasculature of a murine uterus caused the enhanced expression of miR-27, resulting in increased pericyte coverage on the vessel, whereas inhibition of miR-27 resulted in reduced pericyte coverage and therefore reduced vessel stability¹⁰².

Conclusion

Vascular growth occurs through various processes such as vasculogenesis, angiogenesis, and arteriogenesis, which are essential for vessel homeostasis and vascular integrity. Receptors, chemokines, cytokines, and growth factors that regulate these processes have attracted much attention in the past decades due to their roles in vessel growth. However, the underlying complex mechanisms of vessel growth and

the lack of effectiveness of pro-angiogenic or pro-arteriogenic factors, for instance in regenerative medicine, are still not completely unraveled. Recently, much attention has been drawn to studying the role of biomechanical factors in stimulating vessel growth. It has become more evident that these factors stimulate vessel growth by activating mechanosensors, which transduce mechanical stimuli into a vascular growth regulatory response. Shear stress levels are maintained in the vasculature by diameter adaptations via vasoregulation that adjusts the vascular tone. Similarly,

wall stretch induces a physiological response and predominantly provides a stimuli to maintain a contractile VSMC phenotype. However, increased magnitude of these forces leads to pathological deviations in vascular wall adaptation and vascular remodeling. Vascular regenerative processes such as arteriogenesis and angiogenesis were initiated in response to deviations in biomechanical stimuli and serve as parallel compensatory mechanism to limit disease progression. As mentioned, there are still considerable gaps in understanding the mechanisms that transduce signals from vascular cell-mechanosensors to regulation of the factors involved in vascular growth. For instance, PDGF a known proliferative marker for VSMCs is upregulated via integrin activation in response to stretch. The signaling mechanism is not clearly understood but may be important for providing targets to combat undesired inflammatory responses or to promote desired arteriogenesis in occlusive artery diseases. Despite many of these mechanosensors have been reported to contribute to vascular diseases, stimulation of vascular growth in response to pathological levels of these forces may serve as an important functional aspect and there is a great need for further research to identify therapeutic targets that could stimulate vascular regeneration and restoration of blood flow thereby limiting disease progression.

Conflict of Interest

Authors declare that they have no conflict of interest.

Compliance with Ethical Standards Sources of Funding

This work was supported by the Netherlands Foundation for Cardiovascular Excellence [to CC], Netherlands Organization for Scientific Research Vidi grant [no. 91714302 to CC], the Erasmus MC fellowship grant [to CC], the Regenerative Medicine Fellowship grant of the University Medical Center Utrecht [to CC] and the Netherlands Cardiovascular Research Initiative: An initiative with the support of the Dutch Heart Foundation [CVON2014-11 RECONNECT to CC and DD].

References

1. Evans PC, Kwak BR (2013) Biomechanical factors in cardiovascular disease. *Cardiovasc Res* 99(2):229–231
2. Jufri NF, Mohamedali A, Avolio A, Baker MS (2015) Mechanical stretch: physiological and pathological implications for human vascular endothelial cells. *Vasc Cell* 7:8
3. Davies PF (2009) Hemodynamic shear stress and the endothelium in cardiovascular patho- physiology. *Nat Clin Pract Cardiovasc Med* 6(1):16–26
4. Anwar MA, Shalhoub J, Lim CS, Gohel MS, Davies AH (2012) The effect of pressure-induced mechanical stretch on vascular wall differential gene expression. *J Vasc Res* 49 (6):43–478
5. Kwak BR, Back M, Bochaton-Piallat ML, Caligiuri G, Daemen MJ, Davies PF, Hoefler IE, Holvoet P, Jo H, Krams R, Lehoux S, Monaco C, Steffens S, Virmani R, Weber C, Wentzel JJ, Evans PC (2014) Biomechanical factors in atherosclerosis: mechanisms and clinical implications. *Eur Heart J* 35(43):3013–3020. 3020a-3020d
6. Papaioannou TG, Stefanadis C (2005) Vascular wall shear stress: basic principles and methods. *Hell J Cardiol* 46(1):9–15
7. Kroll MH, Hellums JD, McIntire LV, Schafer AI, Moake JL (1996) Platelets and shear stress. *Blood* 88(5):1525–1541
8. Chistiakov DA, Orekhov AN, Bobryshev YV (2017) Effects of shear stress on endothelial cells: go with the flow. *Acta Physiol (Oxford)* 219(2):382–408
9. Huang L, Korhonen RK, Turunen MJ, Finnila MAJ (2019) Experimental mechanical strain measurement of tissues. *PeerJ* 7:e6545
10. Yang S, Gong X, Qi Y, Jiang Z (2020) Comparative study of variations in mechanical stress and strain of human blood vessels: mechanical reference for vascular cell mechanobiology. *Biomech Model Mechanobiol* 19(2):519–531
11. Chamley-Campbell J, Campbell GR, Ross R (1979) The smooth muscle cell in culture. *Physiol Rev* 59(1):1–61
12. Hao H, Gabbiani G, Bochaton-Piallat ML (2003) Arterial smooth muscle cell heterogeneity: implications for atherosclerosis and restenosis development. *Arterioscler Thromb Vasc Biol* 23(9):1510–1520
13. Fang Y, Wu D, Birukov KG (2019) Mechanosensing and Mechanoregulation of endothelial cell functions. *Compr Physiol* 9(2):873–904
14. Lemmon MA, Schlessinger J (2010) Cell signaling by receptor tyrosine kinases. *Cell* 141 (7):1117–1134
15. dela Paz NG, Walshe TE, Leach LL, Saint-Geniez M, D'Amore PA (2012) Role of shear-stress-induced VEGF expression in endothelial cell survival. *J Cell Sci* 125(Pt 4):831–843
16. Tzima E, Irani-Tehrani M, Kiosses WB, Dejana E, Schultz DA, Engelhardt B, Cao G, DeLisser H, Schwartz MA (2005) A mechanosensory complex that mediates the endothelial cell response to fluid shear stress. *Nature* 437(7057):426–431
17. Givens C, Tzima E (2016) Endothelial Mechanosignaling: does one sensor fit all? *Antioxid Redox Signal* 25(7):373–388
18. Zhou J, Li YS, Chien S (2014) Shear stress-initiated signaling and its regulation of endothelial function. *Arterioscler Thromb Vasc Biol* 34(10):2191–2198

19. Fujiwara K (2006) Platelet endothelial cell adhesion molecule-1 and mechanotransduction in vascular endothelial cells. *J Intern Med* 259(4):373–380
20. Fujiwara K (2003) Mechanical stresses keep endothelial cells healthy: beneficial effects of a physiological level of cyclic stretch on endothelial barrier function. *Am J Phys Lung Cell Mol Phys* 285(4):L782–L784
21. Steward R Jr, Tambe D, Hardin CC, Krishnan R, Fredberg JJ (2015) Fluid shear, intercellular stress, and endothelial cell alignment. *Am J Phys Cell Phys* 308(8):C657–C664
22. Ikeda M, Kito H, Sumpio BE (1999) Phosphatidylinositol-3 kinase dependent MAP kinase activation via p21ras in endothelial cells exposed to cyclic strain. *Biochem Biophys Res Commun* 257(3):668–671
23. Shimizu N, Yamamoto K, Obi S, Kumagaya S, Masumura T, Shimano Y, Naruse K, Yamashita JK, Igarashi T, Ando J (2008) Cyclic strain induces mouse embryonic stem cell differentiation into vascular smooth muscle cells by activating PDGF receptor beta. *J Appl Physiol* (1985) 104(3):766–772
24. Giancotti FG, Ruoslahti E (1999) Integrin signaling. *Science* 285(5430):1028–1032
25. Vicente-Manzanares M, Choi CK, Horwitz AR (2009) Integrins in cell migration--the actin connection. *J Cell Sci* 122(Pt 2):199–206
26. Tzima E, del Pozo MA, Shattil SJ, Chien S, Schwartz MA (2001) Activation of integrins in endothelial cells by fluid shear stress mediates Rho-dependent cytoskeletal alignment. *EMBO J* 20(17):4639–4647
27. Wojciak-Stothard B, Ridley AJ (2003) Shear stress-induced endothelial cell polarization is mediated by Rho and Rac but not Cdc42 or PI 3-kinases. *J Cell Biol* 161(2):429–439
28. Hirayama Y, Sumpio BE (2007) Role of ligand-specific integrins in endothelial cell alignment and elongation induced by cyclic strain. *Endothelium* 14(6):275–283
29. Gerhold KA, Schwartz MA (2016) Ion channels in endothelial responses to fluid shear stress. *Physiology (Bethesda)* 31(5):359–369
30. Billaud M, Lohman AW, Johnstone SR, Biber LA, Mutchler S, Isakson BE (2014) Regulation of cellular communication by signaling microdomains in the blood vessel wall. *Pharmacol Rev* 66(2):513–569
31. Rafikov R, Fonseca FV, Kumar S, Pardo D, Darragh C, Elms S, Fulton D, Black SM (2011) eNOS activation and NO function: structural motifs responsible for the posttranslational control of endothelial nitric oxide synthase activity. *J Endocrinol* 210(3):271–284
32. Ito S, Suki B, Kume H, Numaguchi Y, Ishii M, Iwaki M, Kondo M, Naruse K, Hasegawa Y, Sokabe M (2010) Actin cytoskeleton regulates stretch-activated Ca²⁺ influx in human pulmonary microvascular endothelial cells. *Am J Respir Cell Mol Biol* 43(1):26–34
33. Takeda H, Komori K, Nishikimi N, Nimura Y, Sokabe M, Naruse K (2006) Bi-phasic activation of eNOS in response to uni-axial cyclic stretch is mediated by differential mechanisms in BAECs. *Life Sci* 79(3):233–239
34. Gudi S, Nolan JP, Frangos JA (1998) Modulation of GTPase activity of G proteins by fluid shear stress and phospholipid composition. *Proc Natl Acad Sci U S A* 95(5):2515–2519
35. Von Offenbergsweeney N, Cummins PM, Cotter EJ, Fitzpatrick PA, Birney YA, Redmond EM, Cahill PA (2005) Cyclic strain-mediated regulation of vascular endothelial cell migration and tube formation. *Biochem Biophys Res Commun* 329(2):573–582
36. Wojtowicz A, Babu SS, Li L, Gretz N, Hecker M, Cattaruzza M (2010) Zyxin mediation of stretch-induced gene expression in human endothelial cells. *Circ Res* 107(7):898–902

37. Mederos y Schnitzler M, Storch U, Meibers S, Nurwakagari P, Breit A, Essin K, Gollasch M, Gudermann T (2008) Gq-coupled receptors as mechanosensors mediating myogenic vasoconstriction. *EMBO J* 27(23):3092–3103
38. Storch U, Mederos M, Schnitzler Y, Gudermann T (2012) G protein-mediated stretch reception. *Am J Physiol Heart Circ Physiol* 302(6):H1241–H1249
39. Brandes RP, Weissmann N, Schroder K (2014) Nox family NADPH oxidases in mechanotransduction: mechanisms and consequences. *Antioxid Redox Signal* 20(6):887–898
40. Goettsch C, Goettsch W, Arsov A, Hofbauer LC, Bornstein SR, Morawietz H (2009) Long-term cyclic strain downregulates endothelial Nox4. *Antioxid Redox Signal* 11(10):2385–2397
41. Ali MH, Pearlstein DP, Mathieu CE, Schumacker PT (2004) Mitochondrial requirement for endothelial responses to cyclic strain: implications for mechanotransduction. *Am J Phys Lung Cell Mol Phys* 287(3):L486–L496
42. Ross R (1999) Atherosclerosis--an inflammatory disease. *N Engl J Med* 340(2):115–126
43. Spescha RD, Glanzmann M, Simic B, Witassek F, Keller S, Akhmedov A, Tanner FC, Luscher TF, Camici GG (2014) Adaptor protein p66(Shc) mediates hypertension-associated, cyclic stretch-dependent, endothelial damage. *Hypertension* 64(2):347–353
44. Dragovich MA, Chester D, Fu BM, Wu C, Xu Y, Goligorsky MS, Zhang XF (2016) Mechanotransduction of the endothelial glycocalyx mediates nitric oxide production through activation of TRP channels. *Am J Phys Cell Phys* 311(6):C846–C853
45. Dewey CF Jr, Bussolari SR, Gimbrone MA Jr, Davies PF (1981) The dynamic response of vascular endothelial cells to fluid shear stress. *J Biomech Eng* 103(3):177–185
46. Levesque MJ, Nerem RM, Sprague EA (1990) Vascular endothelial cell proliferation in culture and the influence of flow. *Biomaterials* 11(9):702–707
47. Akimoto S, Mitsumata M, Sasaguri T, Yoshida Y (2000) Laminar shear stress inhibits vascular endothelial cell proliferation by inducing cyclin-dependent kinase inhibitor p21(Sdi1/Cip1/Waf1). *Circ Res* 86(2):185–190
48. Hermann C, Zeiher AM, Dimmeler S (1997) Shear stress inhibits H₂O₂-induced apoptosis of human endothelial cells by modulation of the glutathione redox cycle and nitric oxide synthase. *Arterioscler Thromb Vasc Biol* 17(12):3588–3592
49. Bell FP, Adamson IL, Schwartz CJ (1974) Aortic endothelial permeability to albumin: focal and regional patterns of uptake and transmural distribution of ¹³¹I-albumin in the young pig. *Exp Mol Pathol* 20(1):57–68
50. Stemerman MB, Morrel EM, Burke KR, Colton CK, Smith KA, Lees RS (1986) Local variation in arterial wall permeability to low density lipoprotein in normal rabbit aorta. *Arteriosclerosis* 6(1):64–69
51. Dekker RJ, van Soest S, Fontijn RD, Salamanca S, de Groot PG, VanBavel E, Pannekoek H, Horrevoets AJ (2002) Prolonged fluid shear stress induces a distinct set of endothelial cell genes, most specifically lung Kruppel-like factor (KLF2). *Blood* 100(5):1689–1698
52. Novodvorsky P, Chico TJ (2014) The role of the transcription factor KLF2 in vascular development and disease. *Prog Mol Biol Transl Sci* 124:155–188
53. Nayak L, Lin Z, Jain MK (2011) “Go with the flow”: how Kruppel-like factor 2 regulates the vasoprotective effects of shear stress. *Antioxid Redox Signal* 15(5):1449–1461

54. Huang RT, Wu D, Meliton A, Oh MJ, Krause M, Lloyd JA, Nigdelioglu R, Hamanaka RB, Jain MK, Birukova A, Kress JP, Birukov KG, Mutlu GM, Fang Y (2017) Experimental lung injury reduces Kruppel-like factor 2 to increase endothelial permeability via regulation of RAPGEF3-Rac1 signaling. *Am J Respir Crit Care Med* 195(5):639–651
55. McSweeney SR, Warabi E, Siow RC (2016) Nrf2 as an endothelial Mechanosensitive transcription factor: going with the flow. *Hypertension* 67(1):20–29
56. Boon RA, Horrevoets AJ (2009) Key transcriptional regulators of the vasoprotective effects of shear stress. *Hamostaseologie* 29(1):39–40. 41–33
57. Saito T, Hasegawa Y, Ishigaki Y, Yamada T, Gao J, Imai J, Uno K, Kaneko K, Ogihara T, Shimosawa T, Asano T, Fujita T, Oka Y, Katagiri H (2013) Importance of endothelial NF-kappaB signalling in vascular remodelling and aortic aneurysm formation. *Cardiovasc Res* 97(1):106–114
58. Nigro P, Abe J, Berk BC (2011) Flow shear stress and atherosclerosis: a matter of site specificity. *Antioxid Redox Signal* 15(5):1405–1414
59. Wung BS, Cheng JJ, Hsieh HJ, Shyy YJ, Wang DL (1997) Cyclic strain-induced monocyte chemotactic protein-1 gene expression in endothelial cells involves reactive oxygen species activation of activator protein 1. *Circ Res* 81(1):1–7
60. Kobayashi S, Nagino M, Komatsu S, Naruse K, Nimura Y, Nakanishi M, Sokabe M (2003) Stretch-induced IL-6 secretion from endothelial cells requires NF-kappaB activation. *Biochem Biophys Res Commun* 308(2):306–312
61. Boon RA, Fledderus JO, Volger OL, van Wanrooij EJ, Pardali E, Weesie F, Kuiper J, Pannekoek H, ten Dijke P, Horrevoets AJ (2007) KLF2 suppresses TGF-beta signaling in endothelium through induction of Smad7 and inhibition of AP-1. *Arterioscler Thromb Vasc Biol* 27(3):532–539
62. Wang BW, Chang H, Lin S, Kuan P, Shyu KG (2003) Induction of matrix metalloproteinases-14 and -2 by cyclical mechanical stretch is mediated by tumor necrosis factor-alpha in cultured human umbilical vein endothelial cells. *Cardiovasc Res* 59(2):460–469
63. Demicheva E, Hecker M, Korff T (2008) Stretch-induced activation of the transcription factor activator protein-1 controls monocyte chemoattractant protein-1 expression during arteriogenesis. *Circ Res* 103(5):477–484
64. Bakiri L, Matsuo K, Wisniewska M, Wagner EF, Yaniv M (2002) Promoter specificity and biological activity of tethered AP-1 dimers. *Mol Cell Biol* 22(13):4952–4964
65. Feng S, Bowden N, Fragiadaki M, Souilhol C, Hsiao S, Mahmoud M, Allen S, Pirri D, Ayllon BT, Akhtar S, Thompson AAR, Jo H, Weber C, Ridger V, Schober A, Evans PC (2017) Mechanical activation of hypoxia-inducible factor 1alpha drives endothelial dysfunction at Atheroprone sites. *Arterioscler Thromb Vasc Biol* 37(11):2087–2101
66. Milkiewicz M, Doyle JL, Fudalewski T, Ispanovic E, Aghasi M, Haas TL (2007) HIF-1alpha and HIF-2alpha play a central role in stretch-induced but not shear-stress-induced angiogenesis in rat skeletal muscle. *J Physiol* 583(Pt 2):753–766
67. Chang H, Shyu KG, Wang BW, Kuan P (2003) Regulation of hypoxia-inducible factor-1alpha by cyclical mechanical stretch in rat vascular smooth muscle cells. *Clin Sci (Lond)* 105 (4):447–456
68. Lim CS, Qiao X, Reslan OM, Xia Y, Raffetto JD, Paleolog E, Davies AH, Khalil RA (2011) Prolonged mechanical stretch is associated with upregulation of hypoxia-inducible factors and reduced contraction in rat inferior vena cava. *J Vasc Surg* 53(3):764–773

69. Mata-Greenwood E, Grobe A, Kumar S, Noskina Y, Black SM (2005) Cyclic stretch increases VEGF expression in pulmonary arterial smooth muscle cells via TGF-beta1 and reactive oxygen species: a requirement for NAD(P)H oxidase. *Am J Phys Lung Cell Mol Phys* 289 (2):L288–L289
70. Suresh Babu S, Wojtowicz A, Freichel M, Birnbaumer L, Hecker M, Cattaruzza M (2012) Mechanism of stretch-induced activation of the mechanotransducer zyxin in vascular cells. *Sci Signal* 5(254):ra91
71. Gray C, Packham IM, Wurmser F, Eastley NC, Hellewell PG, Ingham PW, Crossman DC, Chico TJ (2007) Ischemia is not required for arteriogenesis in zebrafish embryos. *Arterioscler Thromb Vasc Biol* 27(10):2135–2141
72. Heil M, Schaper W (2004) Influence of mechanical, cellular, and molecular factors on collateral artery growth (arteriogenesis). *Circ Res* 95(5):449–458
73. Lu D, Kassab GS (2011) Role of shear stress and stretch in vascular mechanobiology. *J R Soc Interface* 8(63):1379–1385
74. Wang Y, Miao H, Li S, Chen KD, Li YS, Yuan S, Shyy JY, Chien S (2002) Interplay between integrins and FLK-1 in shear stress-induced signaling. *Am J Phys Cell Phys* 283(5):C1540–C1547
75. Zimarino M, D'Andreamatteo M, Waksman R, Epstein SE, De Caterina R (2014) The dynamics of the coronary collateral circulation. *Nat Rev Cardiol* 11(4):191–197
76. Sasamoto A, Nagino M, Kobayashi S, Naruse K, Nimura Y, Sokabe M (2005) Mechanotransduction by integrin is essential for IL-6 secretion from endothelial cells in response to uniaxial continuous stretch. *Am J Phys Cell Phys* 288(5):C1012–C1022
77. Chen Z, Rubin J, Tzima E (2010) Role of PECAM-1 in arteriogenesis and specification of preexisting collaterals. *Circ Res* 107(11):1355–1363
78. Hu Y, Bock G, Wick G, Xu Q (1998) Activation of PDGF receptor alpha in vascular smooth muscle cells by mechanical stress. *FASEB J* 12(12):1135–1142
79. Selzman CH, Miller SA, Zimmerman MA, Gamboni-Robertson F, Harken AH, Banerjee A (2002) Monocyte chemotactic protein-1 directly induces human vascular smooth muscle proliferation. *Am J Physiol Heart Circ Physiol* 283(4):H1455–H1461
80. Troidl C, Troidl K, Schierling W, Cai WJ, Nef H, Mollmann H, Kostin S, Schimanski S, Hammer L, Elsasser A, Schmitz-Rixen T, Schaper W (2009) Trpv4 induces collateral vessel growth during regeneration of the arterial circulation. *J Cell Mol Med* 13(8B):2613–2621
81. Eitenmuller I, Volger O, Kluge A, Troidl K, Barancik M, Cai WJ, Heil M, Pipp F, Fischer S, Horrevoets AJ, Schmitz-Rixen T, Schaper W (2006) The range of adaptation by collateral vessels after femoral artery occlusion. *Circ Res* 99(6):656–662
82. Caicedo D, Devesa P, Arce VM, Requena J, Devesa J (2018) Chronic limb-threatening ischemia could benefit from growth hormone therapy for wound healing and limb salvage. *Ther Adv Cardiovasc Dis* 12(2):53–72
83. Lu W, Schroit AJ (2005) Vascularization of melanoma by mobilization and remodeling of preexisting latent vessels to patency. *Cancer Res* 65(3):913–918
84. Zweifach BW, Lee RE, Hyman C, Chambers R (1944) Omental circulation in Morphinized dogs subjected to graded hemorrhage. *Ann Surg* 120(2):232–250
85. Granger HJ, Goodman AH, Cook BH (1975) Metabolic models of microcirculatory regulation. *Fed Proc* 34(11):2025–2030
86. Mentzer SJ, Konerding MA (2014) Intussusceptive angiogenesis: expansion and remodeling of microvascular networks. *Angiogenesis* 17(3):499–509

87. Ziche M, Morbidelli L (2000) Nitric oxide and angiogenesis. *J Neuro-Oncol* 50(1-2):139–148
88. Matsunaga T, Weihrauch DW, Moniz MC, Tessmer J, Warltier DC, Chilian WM (2002) Angiostatin inhibits coronary angiogenesis during impaired production of nitric oxide. *Circulation* 105(18):2185–2191
89. Niu J, Azfer A, Zhelyabovska O, Fatma S, Kolattukudy PE (2008) Monocyte chemotactic protein (MCP)-1 promotes angiogenesis via a novel transcription factor, MCP-1-induced protein (MCPIP). *J Biol Chem* 283(21):14542–14551
90. Wang Y, Chang J, Li YC, Li YS, Shyy JY, Chien S (2004) Shear stress and VEGF activate IKK via the Flk-1/Cbl/Akt signaling pathway. *Am J Physiol Heart Circ Physiol* 286(2):H685–H692
91. Stoltz RA, Abraham NG, Laniado-Schwartzman M (1996) The role of NF-kappaB in the angiogenic response of coronary microvessel endothelial cells. *Proc Natl Acad Sci U S A* 93 (7):2832–2837
92. Zheng W, Christensen LP, Tomanek RJ (2004) Stretch induces upregulation of key tyrosine kinase receptors in microvascular endothelial cells. *Am J Physiol Heart Circ Physiol* 287(6): H2739–H2745
93. Friedlander M, Brooks PC, Shaffer RW, Kincaid CM, Varner JA, Cheresh DA (1995) Definition of two angiogenic pathways by distinct alpha v integrins. *Science* 270 (5241):1500–1502
94. Chen KD, Li YS, Kim M, Li S, Yuan S, Chien S, Shyy JY (1999) Mechanotransduction in response to shear stress. Roles of receptor tyrosine kinases, integrins, and Shc. *J Biol Chem* 274(26):18393–18400
95. Perdih A, Dolenc MS (2010) Small molecule antagonists of integrin receptors. *Curr Med Chem* 17(22):2371–2392
96. Chachisvilis M, Zhang YL, Frangos JA (2006) G protein-coupled receptors sense fluid shear stress in endothelial cells. *Proc Natl Acad Sci U S A* 103(42):15463–15468
97. Campinho P, Vilfan A, Vermot J (2020) Blood flow forces in shaping the vascular system: a focus on endothelial cell behavior. *Front Physiol* 11:552
98. Packham IM, Gray C, Heath PR, Hellewell PG, Ingham PW, Crossman DC, Milo M, Chico TJ (2009) Microarray profiling reveals CXCR4a is downregulated by blood flow in vivo and mediates collateral formation in zebrafish embryos. *Physiol Genomics* 38(3):319–327
99. Jung B, Obinata H, Galvani S, Mendelson K, Ding BS, Skoura A, Kinzel B, Brinkmann V, Rafii S, Evans T, Hla T (2012) Flow-regulated endothelial S1P receptor-1 signaling sustains vascular development. *Dev Cell* 23(3):600–610
100. Saunders WB, Bohnsack BL, Fasse JB, Anthis NJ, Bayless KJ, Hirschi KK, Davis GE (2006) Coregulation of vascular tube stabilization by endothelial cell TIMP-2 and pericyte TIMP-3. *J Cell Biol* 175(1):179–191
101. Schrimpf C, Koppen T, Duffield JS, Boer U, David S, Ziegler W, Haverich A, Teebken OE, Wilhelm M (2017) TIMP3 is regulated by Pericytes upon shear stress detection leading to a modified endothelial cell response. *Eur J Vasc Endovasc Surg* 54(4):524–533
102. Demolli S, Doddaballapur A, Devraj K, Stark K, Manavski Y, Eckart A, Zehendner CM, Lucas T, Korff T, Hecker M, Massberg S, Liebner S, Kaluza D, Boon RA, Dimmeler S (2017) Shear stress-

CHAPTER

7



A complex three-dimensional
microfluidic model that mimics the
early stage events in the human
atherosclerotic artery

Ranganath Maringanti, Christian G.M. van Dijk, Elana M. Meijer, Maarten M. Brandt, Vera P.C. Tiggeloven, Merle M. Krebber, Ihsan Chrifi, Dirk J. Duncker, Marianne C. Verhaar, Caroline Cheng.

In submission

Abstract

Background: Atherosclerosis is a complex inflammatory vascular disease characterized by lipid and immune cells accumulation in the vessel wall, leading to lumen narrowing. Although several 3D *in vitro* microfluidic systems were previously described, a realistic reconstruction of the *in vivo* human atherosclerotic environment requires co-culture of different cell types arranged in atherosclerotic vessel-like structures with exposure to flow and circulating cells, creating challenges for disease modelling.

In this study we developed a 3D tubular microfluidic model with quadruple coculture of human aortic smooth muscle cells (hAoSMCs), human umbilical cord vein endothelial cells (HUVECs) and foam cells to re-create a complex human atherosclerotic vessel *in vitro* to study the effect of flow and circulating immune cells. **Methods & Results:** Our new co-culture protocol with BFP-labelled hAoSMCs, GFP- labelled HUVECs and THP-1 macrophages-derived, Dil-labelled Oxidized Low- Density Lipoprotein (Dil-Ox-LDL) foam cells in a fibrinogen/collagen-I based 3D extracellular matrix (ECM) resulted in vessels with an early lesion morphology showing a layered vessel-like composition with an endothelium and media, with foam cells accumulating in the sub-endothelial space. Perfusion for 24 hours of atherosclerotic and “healthy” vessels (BFP hAoSMCs and GFP HUVECs without foam cells) showed that the layered wall composition remained stable. Perfusion with circulating THP-1 monocytes demonstrated cell extravasation into the atherosclerotic vessel wall and recruitment of THP-1 cells to the foam cell core. QPCR analysis revealed increased expression of atherosclerosis markers in the atherosclerotic vessels and adaptation in VSMCs migration to flow and the plaque microenvironment, compared to control vessels.

Conclusion: We present a 3D tubular microfluidic model of a complex early atherosclerotic human vessel that can be exposed to flow and circulating THP-1 monocytes to study hemodynamic changes and immune cell recruitment under live confocal imaging. This novel atherosclerosis-on-a-chip model offers a humanized platform for in-depth mechanistic *in vitro* studies and drug testing.

Introduction

Atherosclerosis is a chronic inflammatory disease of the arteries, marked by the accumulation of cholesterol-containing low-density lipoproteins (LDL) leading to plaque formation and lumen narrowing¹. As a leading cause of disease related death worldwide², the aetiology of atherosclerosis is widely studied and is hallmarked by several causal factors including dyslipidaemia with high blood LDL levels, resulting in chronic inflammation and foam cell accumulation in the arterial wall. On a cellular level, it involves the activation of disease pathways in several vascular and immune cell types that interact with each other to amplify inflammation while adapting to (changes in) local hemodynamical factors. Traditionally, rodent disease models are used to provide valuable insights into the disease mechanism, but these are also known to diverge on multiple immune and mechanical aspects from the human condition, imposing limitations to their translational value³⁻⁵. Two-dimensional (2D) and three-dimensional (3D) human cell culture systems are also often used, for example to study vascular and immune cell responses to LDL and flow dynamics (reviewed in ⁶). The most advanced of these 3D tools are based on tissue engineered (TE) vascular constructs, which can show a higher degree of complexity to mimic certain aspects of the atherosclerotic vessel, such as co-culture of multiple (vascular) cell types and organization of a layered wall structure⁷⁻⁹. Suitable for mechanistic studies and drug and toxicity testing in a controlled environment, they are cultured in static conditions^{7, 8}, or exposed to lumen flow by perfusion in macroscale bioreactors when combined with mechanical support provided by (synthetic) scaffolds⁹ or hydrogels¹⁰. In recent years, microfluidic technology has allowed the introduction of luminal perfusion in complex microtissues. This adds critical flow dynamics (i.e. shear stress) to these biological models and bridges the gap between perfused culture with large (centimetre scale) bioreactor-based platforms to smaller, (micrometre scale) chip-format assays that can be more cost-effective as a result of their suitability for upscaling^{11, 12}. In vascular research, multiple static models and perfused microfluidic devices have been developed to study endothelial function, angiogenesis, vasculogenesis, and inflammation¹³⁻¹⁵, but so far, only a handful of studies have presented an *in vitro* human cell microfluidic system for atherosclerosis⁶. In general, these studies demonstrated assays with co-cultures of vascular cells with immune cells that are organized in vascular-like structures, yet still lacked critical factors of atherogenesis, including physiologically relevant vessel anatomy and flow dynamics and vessel wall interaction with circulating immune cells¹⁶⁻¹⁹.

In this study, we created a complex, perfused human atherosclerosis on a chip (OAC) model that mirrors the atherosclerotic wall within a tubular arterial geometry in a full 3D extra cellular matrix (ECM) environment that allows physiological laminar flow patterns and natural interaction with circulating immune cells. This atherosclerosis model is based on a chip design that was recently published by our group²⁰ and involves a 5 micro-channel system which can be further scaled up for the creation of multiple atherosclerotic vessels per chip for high throughput screening. Co-culture of endothelial cells, vascular smooth muscle cells (VSMCs), and (oxLDL loaded) foam cells in this full 3D ECM environment recreates a layered lesion structure that mimics the human atherosclerotic lesion in the initial phase of the disease. Fluorescent labelling of each individual cell type allows spatio-temporal visualization of cell behaviour during the different stages of immune cell-lesion interaction under live confocal imaging under luminal flow. This new complex human atherosclerosis-OAC model is suitable for mechanistic studies of atherogenesis and drug testing that focusses on the contribution of circulating factors and immune cells on plaque progression. The system may also be further adapted to incorporate patient-derived cells (of induced pluripotent stem cell (iPSC) and/or PBMC origin), to create dedicated platforms for drug screening for patient populations with a genetic predisposition to coronary artery disease (CAD).

Materials and Methods

Detailed descriptions can be found in the supplemented data.

Cell culture (2D)

Primary cell culture

Human aortic smooth muscle cells (hAoSMC, Lonza) with a blue fluorescent protein (BFP)-tag were cultured in smooth muscle cell growth medium-2 (SMGM2) (Lonza). Human umbilical cord vein endothelial cells (HUVEC; Lonza) with a green fluorescent protein (GFP)-tag were cultured in endothelial growth medium-2 (EGM2).

Cell line /Suspension culture

THP-1 monocytes (ATCC TIB-202™) were cultured in RPMI 1640 medium + L Glutamine (Life Technologies, Grand Island, NY) supplemented with 10% FBS (Gibco).

Differentiation of THP-1 monocytes into macrophages and foam cells

THP-1 cell differentiation into macrophages was induced by phorbol myristate acetate (PMA) in 10% FCS/RPMI medium. Macrophages were differentiated into foam cells by treating with Dil-labelled Ox-LDL (Invitrogen) with a concentration of 20 µg/mL for 24 h in RPMI bare medium.

Cell culture (3D)*Co-culturing of vascular cells in a 3D microfluidic system*

BFP-labelled hAoSMCs at a 10×10^6 cells/mL concentration were seeded into the channels on day 1. The bioreactor was placed in 30 mm dish and rotated for 1-2 h on a MACSmix™ tube rotator (Miltenyl biotech) for uniform spreading and attachment of cells in the channel. After rotation, bioreactors were submerged in SMGM2 medium and incubated. 12×10^6 cells/mL GFP-labelled HUVECs were seeded in the same channels on day 2 and 3 and submerged in EGM2 and SMGM2 medium (ratio 1:1).

Labelling of monocytes or foam cells

THP-1 monocytes or foam cell suspensions were incubated with 1 µM Cell-tracker deep red solution for 30-45 min.

Co-culturing of circulating immune cells in a 3D microfluidic system

Cell-tracker deep red labelled THP-1 monocytes were perfused through the EC- VSMC co-cultured channels for 24 h in a cocktail medium (SMGM2: EGM2: RPMI- 1:1:1) via the Ibidi pump system (Ibidi, Germany), at 5×10^5 cells/mL circulating medium.

Co-culturing of vascular cells and foam cells in a 3D microfluidic system

To mimic atherosclerosis in the 3D microfluidic system, BFP-hAoSMCs were co-cultured with foam cells (pre-differentiated in 2D) and seeded in the channels. Foam cells and BFP-hAoSMCs were seeded in the ratio of 1:400, with foam cells and BFP-AoSMCs concentrated to 25000 and 10 million cells/mL respectively. To monitor if only macrophages have taken up Dil-ox-LDL in the experiments presented in Figure 4 and 5, foam cells were also stained with cell-tracker deep red before seeding. After seeding into the channels, the bioreactors were rotated and incubated followed by seeding of GFP-HUVECs on day 2 and 3. Finally, the bioreactors were incubated in cocktail medium (SMGM2:EGM2: RPMI, ratio 1:1:1).

Perfusion experiments (3D)

After 4 days of static co-culture, the microfluidic devices were subjected to flow using the Ibidi pump system. A selection of channels was connected to the perfusion

system via 26G needles (perfused group). The others were closed with PE-50 tubing (static group). To allow the cells to adjust to unidirectional flow, 20 $\mu\text{l}/\text{min}$ flow rate was first maintained for one hour before it was increased to 40 $\mu\text{l}/\text{min}$.

Confocal Imaging

Imaging was performed by Leica SP8 confocal microscope using 10x magnification for both z-stack mode (12 μm step size) and tile scan mode (3x2). Image analysis was performed with Leica Application Suite X software, (version 3.7.1.21655) and ImageJ.

Gel excision from 3D microfluidic device and qPCR analysis

Following confocal readout, the microfluidic devices were snap frozen on dry ice and the gel was excised from the bioreactor and dissolved in RNA lysis buffer. Total RNA was isolated from the channels using RNA isolation kit (Bioline) for gene expression analysis.

Statistics

Statistical analysis was performed using GraphPad Prism 9.0. Data were represented as means \pm SEM. Groups were compared using unpaired t-test or two-way or one-way ANOVA followed by Dunnett's multiple comparison test or Tukey post hoc test, when appropriate. If other statistical methods were used, it was stated separately in the legends. Statistical significance was accepted when $P \leq 0.05$.

Results

Medium optimization and creation of a human macrovessel mimic in a 3D microfluidic system for live confocal imaging

The human primary vascular cell types required for the creation of macrovessels were first assessed on cell survival and proliferation capacity in response to different growth medium conditions. hAoSMCs and HUVECs were cultured either in bare basal medium (SMBM2 bare, EBM2 bare or RPMI bare), their suitable full medium (SMGM2 or EGM2, for hAoSMCs and HUVECs respectively) and 2 cocktail media (SMGM2:EGM2 in 1:1 ratio or SMGM2:EGM2:RPMI in 1:1:1 ratio). The inclusion of RPMI in the second cocktail medium is for the final co-culture protocol with hAoSMCs, HUVECs and THP-1 cells. The cells were maintained for 7 days and cell viability was determined using PrestoBlue viability assay.

Both hAoSMCs and HUVECs cultured in full growth medium SMGM2 or EGM2 (respectively), and cocktail medium SMGM2:EGM2:RPMI showed significant increase in cell viability compared to bare medium (SMBM2 bare or EBM2 bare, and RPMI bare). Cell culture of hAoSMCs or HUVECS in cocktail medium SMGM:EGM2 or SMGM2:EGM2:RPMI showed comparable cell viability versus full growth mediums SMGM2 or EGM2 (Supplemental Fig. 1a & c). PicoGreen assay as a measurement for cell proliferation showed significant increase in DNA content in hAoSMCs and HUVECs cultured in their full growth medium SMGM2 and EGM2, and in the cocktail medium SMGM2:EGM2:RPMI versus their relevant bare medium conditions and RPMI bare. hAoSMCs or HUVECs cultured in cocktail medium SMGM2:EGM2 or SMGM2:EGM2:RPMI showed comparable DNA levels versus their relevant full medium conditions (Supplemental Fig. 1b & d). These observations indicate that the media SMGM2:EGM2 and SMGM2:EGM2:RPMI are suitable for coculture of hAoSMCs and HUVECs in the 3D microfluidic system as cell viability and growth are not negatively affected. For the use of THP-1 cells as circulating monocytes and differentiated macrophages, we tested the viability of THP-1 cells in full medium (RPMI 10% FCS), bare medium (RPMI), and cocktail medium (SMGM2:EGM2:RPMI, ratio 1:1:1). Both cell viability and DNA content showed a significant higher cell viability for THP-1 cells cultured in full growth medium versus bare medium (Supplemental Fig.1e & f). THP-1 cell viability was significantly increased in cocktail (SMGM2:EGM2:RPMI) versus bare and full medium conditions (Supplemental Fig. 1e & f). These data demonstrate that SMGM2:EGM2:RPMI is a suitable growth medium for the co-culture of human HUVECs and VSMCs with THP- 1 cells.

The human artery is composed of an inner endothelial monolayer surrounded by VSMCs in the media. To engineer a human macrovessel consisting of a confluent endothelium and sub-endothelial VSMCs layers that can be monitored live in the microfluidic device (Supplemental Fig. 2a), 500 μm diameter channels were created by casting of a mix of fibrinogen (20 mg/mL in SMGM2) and collagen-I (2 mg/mL in SMGM2) ECM gel in the chamber, followed by seeding of vascular cells and subsequent rotation for uniform distribution in the channel (as described in Supplemental Fig. 2b and d). After 4 days of static co-culture (Supplemental Fig. 2e, timeline a). Confocal analysis showed a human macrovascular-like structure composed of a uniform endothelial monolayer formed by GFP-HUVECs (green) and sub-endothelial BFP-AoSMCs layers (blue) (Fig. 1a, shown as merged maximum projection images of the vessel wall). The 3D composite cross-sectional display (Fig. 1b), 3D reconstruction of half of the macrovessel (Fig. 1c), as well as the longitudinal (Fig. 1d) and orthogonal cross sections (Fig. 1e) revealed the layered vessel anatomy (GFP-HUVECs endothelium on top of BFP-AoSMC media) and showed the open lumen

structure (~500µm in diameter) of these tissue-engineered human macrovessels. Phenotypical characterization of these macrovessels by immunostaining of alpha SMA demonstrated that BFP-AoSMC maintained VSMC marker expression (Supplemental Fig. 8).

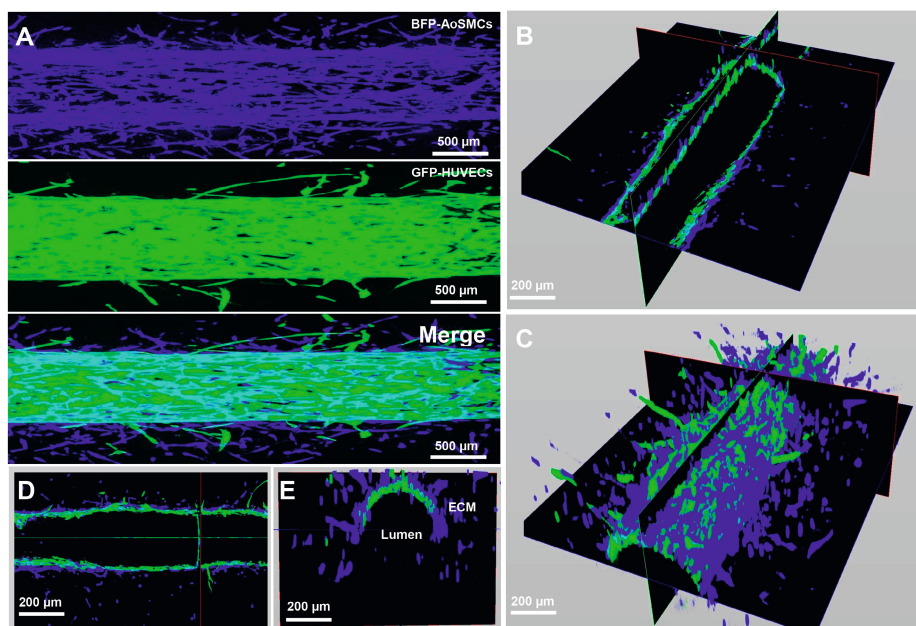


Figure 1. Fluorescent labeled human macrovessels mimicked in an in-house developed microfluidic device for live confocal imaging after 4 days of static co-culture.

(A) Confocal micrographs of vessel wall with an endothelial monolayer formed by GFP- labelled HUVECs (mid panel, in green) surrounded by BFP-labelled human AoSMCs (upper panel, in blue) and merged image (lower panel) of the created human macrovessel. (B) Composite display of the longitudinal and orthogonal cross section micrographs. (C) 3D reconstruction of half of the macrovessel wall. (D) Longitudinal cross section of the vessel. (E) Composite display of the orthogonal cross section micrographs showing the open lumen and layered structure of half of a macrovessel.

Continuous vessel stability after introduction of flow in human macrovessels in the microfluidic system

Flow was introduced in the human macrovessels after 4 days of static co-culture by connecting the microfluidic device to a closed circulating Ibidi pump system (Supplemental Fig. 2c and d). Cocktail medium (SMGM2:EGM2) was perfused unidirectionally through the macrovessel lumens at a flow rate of 20 µl/min for 1 h to allow the vessels to adapt from static condition to flow, before it was increased to 40 µl/min and maintained for 48 h (Supplemental Fig. 2e, timeline b). This flow rate

is within the range previously used in microfluidic platforms to study leukocyte-endothelium interaction under controlled flow²¹⁻²³. Confocal imaging of the perfused channel after 48 h revealed preservation of the human macrovessel with an intact GFP-HUVECs (green) monolayer and sub-endothelial smooth muscle cell layers (BFP-hAoSMCs (blue)) surrounding the endothelium, composing the vessel wall (Fig. 2a). Evaluation by confocal 3D reconstruction (Fig. 2b and c) and analysis of the longitudinal (Fig. 2d) and orthogonal cross sections (Fig. 2e) further confirmed conservation of the endothelium and media and revealed full preservation of open lumen structures without noticeable changes in lumen diameter (Fig. 2 b-e). In line with these observations, quantification of the confocal images revealed that perfusion of the vessel for 48 h after 4 days of static co-culture did not significantly affect the peri-luminal BFP-hAoSMCs+ and GFP-HUVECs+ areas when compared to 4 days static co-culture (Supplemental Fig. 4a and b).

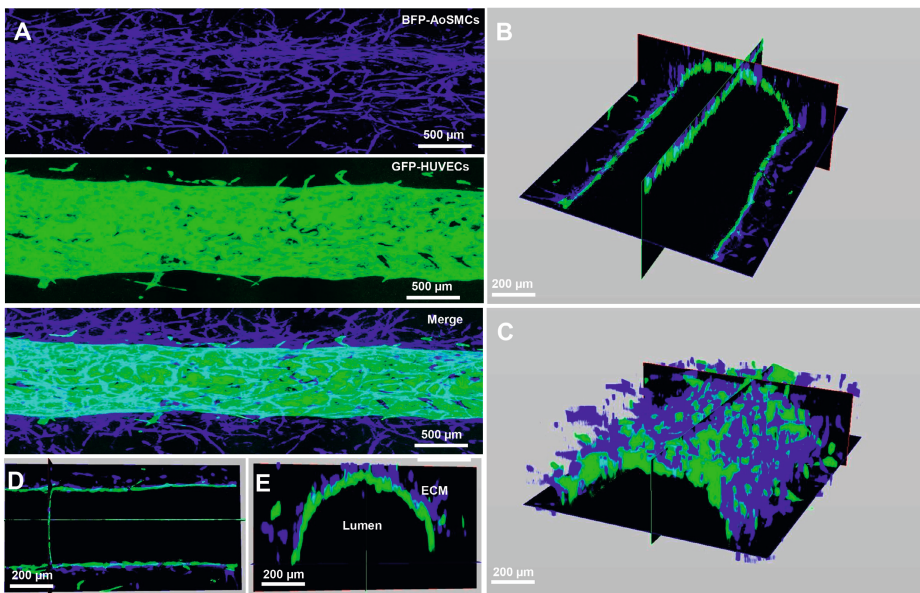
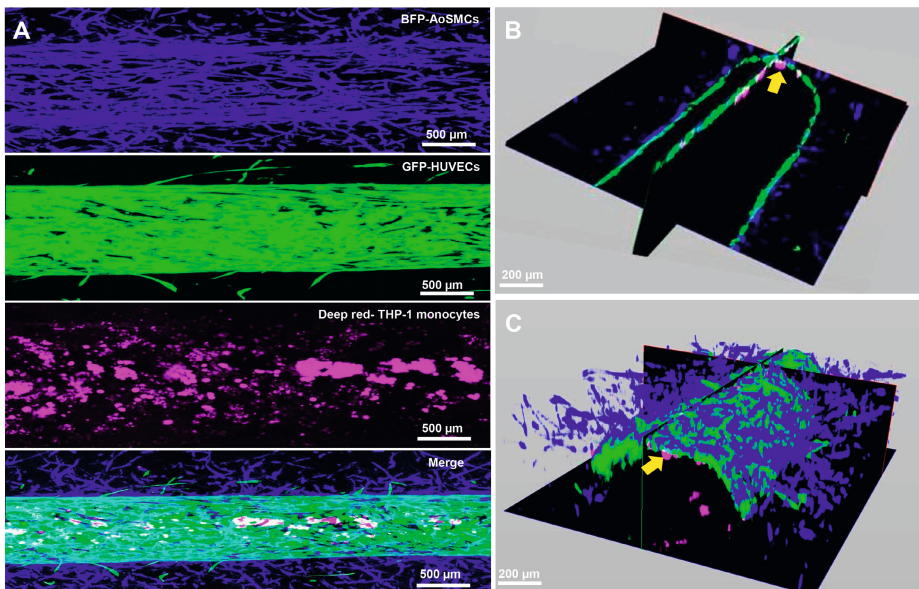


Figure 2. Human macrovessels after 48h of perfusion.

(A) Confocal micrograph shows the preserved endothelial monolayer formed by GFP-HUVECs (mid panel, in green) surrounded by BFP- AoSMCs (upper panel, in blue), and merged image (lower panel) after 6 days of co-culture, from which 4 days static and 2 days perfused at a flow rate of 40μl/min. (B) Composite display of the longitudinal and orthogonal cross section micrographs. (C) 3D reconstruction of half of a wall of the perfused macrovessel. (D) Longitudinal cross section of the vessel. (E) Composite display of the orthogonal cross section micrographs showing half of a macrovessel, demonstrating preservation of the open lumen and layered structure. Experiments were repeated three times (N=3) and representative images are shown in the figures.

Preserved integrity after flowing with circulating monocytes in human macrovessels

In atherogenesis, monocyte recruitment and subsequent differentiation into macrophages and foam cells in the sub-endothelial space represent a hallmark process in disease onset and progression²⁴. We introduced deep red labelled THP-1 monocytes in the cocktail medium and perfused these through the (healthy) control human macrovessels (Supplemental Fig. 2e, time line c) to assess THP-1 cell interaction with the vascular wall. Cell concentrations for circulating THP-1 monocytes were at 5×10^5 cells/ml in SMGM2:EGM2:RPMI, at a flow rate of 40 μ l/min. Confocal live imaging demonstrated limited THP-1 monocyte interaction with the control vessels (Fig. 3b-e). Confocal analysis after 48 h of continuous flow with THP-1 monocytes revealed preservation of the human macrovessels with intact lumen and endothelial and medial layers, similar to the perfused macrovessels without circulating THP-1 cells (Fig. 3a-e). Evaluation by confocal 3D reconstruction and analysis of the longitudinal and orthogonal cross sections further revealed that THP-1 monocytes (magenta) were mostly present in the lumen area (Fig. 3c-e, indicated by white arrows). A limited number of THP-1 localized at the adluminal surface of the GFP-HUVECs endothelial monolayer (Fig. 3b-e, indicated by yellow arrows), but none of these cells transmigrated deeper into the BFP-hAoSMCs medial layer or further into the surrounding ECM. Similar to the flow condition without THP-1 cells, the BFP-hAoSMC⁺ and GFP-HUVEC⁺ areas were not affected by flowing with circulating THP-1 cells (Supplemental Fig. 4a and b).



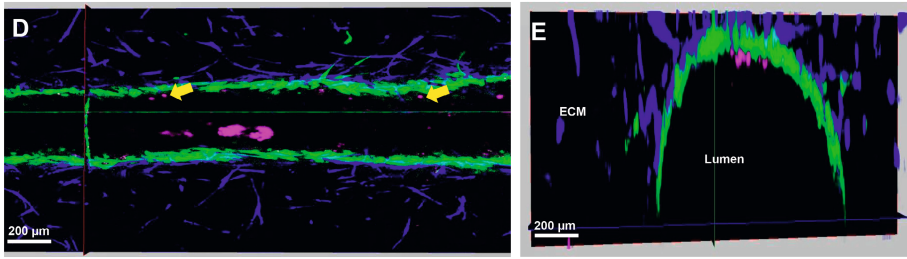


Figure 3. Human macrovessels after 48h of perfusion with circulating THP-1 monocytes.

(A) Confocal micrograph shows the preserved endothelial monolayer formed by GFP-HUVECs (second panel, in green) surrounded by BFP-AoSMCs (first upper panel, in blue), as well as the deep red cell tracker stained THP-1 monocytes (third panel, in magenta) that were perfused in the human macrovessel after 6 days of co-culture, from which 4 days static and 2 days perfused with medium with circulating THP-1 cells at flow rate of 40 $\mu\text{l}/\text{min}$. Lower panel shows merged image. (B) Composite display of the longitudinal and orthogonal cross section micrographs. (C) 3D reconstruction of half of a wall of the perfused macrovessel. (D) Longitudinal cross section of the vessel. (E) Composite display of the orthogonal cross section micrographs showing half of a macrovessel, with preservation of the open lumen and layered structure. THP-1 cells remained mainly free-floating in flow medium and were localized in the lumen, although some of the THP-1 cells were interacting with the endothelium (yellow arrows). Experiments were repeated three times (N=3) and representative images are shown in the figures.

Optimization of Ox-LDL dose and introduction of foam cells in human macrovessels to create atherosclerotic macrovessels

Foam cell formation and accumulation in the sub-endothelial space of arteries is a hallmark of atherosclerotic lesions. We first determined the optimal oxidized-LDL (Ox-LDL) dose that is required for foam cells induction. In 2D culture conditions, THP-1 monocytes were differentiated into macrophages using PMA and treated with Dil-labelled Ox-LDL for live fluorescent monitoring at a concentration of 20 $\mu\text{g}/\text{mL}$ or 40 $\mu\text{g}/\text{mL}$ for 24 h or 48 h. Ideal cell concentration for seeding was established at 5×10^4 cells/mL of RPMI bare medium. Confocal imaging confirmed uptake of Ox-LDL (red) by macrophages at different doses and time points (Supplemental Fig. 3a). Ox-LDL presence within the cell was confirmed by overlapping bright field image with Ox-LDL signal (Supplemental Fig. 3b). Quantification of the images showed a significant reduction in nuclei count at 40 $\mu\text{g}/\text{mL}$ of Ox-LDL after 48 h of stimulation, whereas 20 $\mu\text{g}/\text{mL}$ Ox-LDL did not impact cell numbers (Supplemental Fig. 3c). Similarly, quantification of the Dil-Ox-LDL signal showed that 20 $\mu\text{g}/\text{mL}$ of Ox-LDL induced a higher number of Dil-Ox-LDL⁺ foam cells versus stimulation with 40 $\mu\text{g}/\text{mL}$ (Supplemental Fig. 3d). Cell viability and proliferation of THP-1 macrophages with and without exposure Dil- Ox-LDL was also evaluated by PrestoBlue and PicoGreen analysis. Similar to non-treated THP-1 macrophages, cell viability and proliferation declined over time (24 h versus 48 h) after 20 and 40 $\mu\text{g}/\text{mL}$ Ox-LDL stimulation,

although there was no impact of different Ox-LDL concentration on viability compared with the control macrophages (Supplemental Fig. 3e). The DNA content also declined over time for control macrophages, and macrophages stimulated with 20 and 40 $\mu\text{g}/\text{mL}$ Ox-LDL. Ox-LDL stimulation (both 20 and 40 $\mu\text{g}/\text{mL}$) significantly enhanced the decline compared with control macrophages (Supplemental Fig. 3f). Based on these findings, we proceeded with 20 $\mu\text{g}/\text{mL}$ 24 h Ox-LDL loading for foam cell induction.

Foam cells differentiated under 2D were harvested and stained with cell tracker deep red before seeding into the microfluidic system along with BFP-hAoSMCs on day 1 (at a concentration of 25000 foam cells to 10 million BFP-hAoSMCs - 1:400) followed by GFP-HUVECs (Supplemental Fig. 2e, time line d). Confocal maximum projections at day 4 under static condition showed successful intra-wall foam cell accumulation (Fig. 4a, third panel in magenta) without negative impact on vessel integrity, shown by the general preservation of the endothelial monolayer (green) and VSMC layers (blue) (Fig. 4a, upper two panels). No significant differences were observed in the quantified BFP-hAoSMCs⁺ and GFP-HUVECs⁺ areas between static co-culture with and without foam cell loading (Supplemental Fig. 4e and f). 3D reconstructions and cross sections demonstrate that an open lumen was also maintained (Fig. 4b-d). Higher magnification observation showed that most of the magenta⁺ foam cells were located at the abluminal surface of the GFP-HUVECs endothelial monolayer with pockets of foam cells located deeper in the BFP-hAoSMCs medial layer further away from the endothelium (Fig. 4d and e, indicated by white arrows). Combined, this data indicates that this optimized protocol for foam cell introduction in “healthy” vessels, has successfully created a mimic of an early-stage atherosclerotic human vessel.

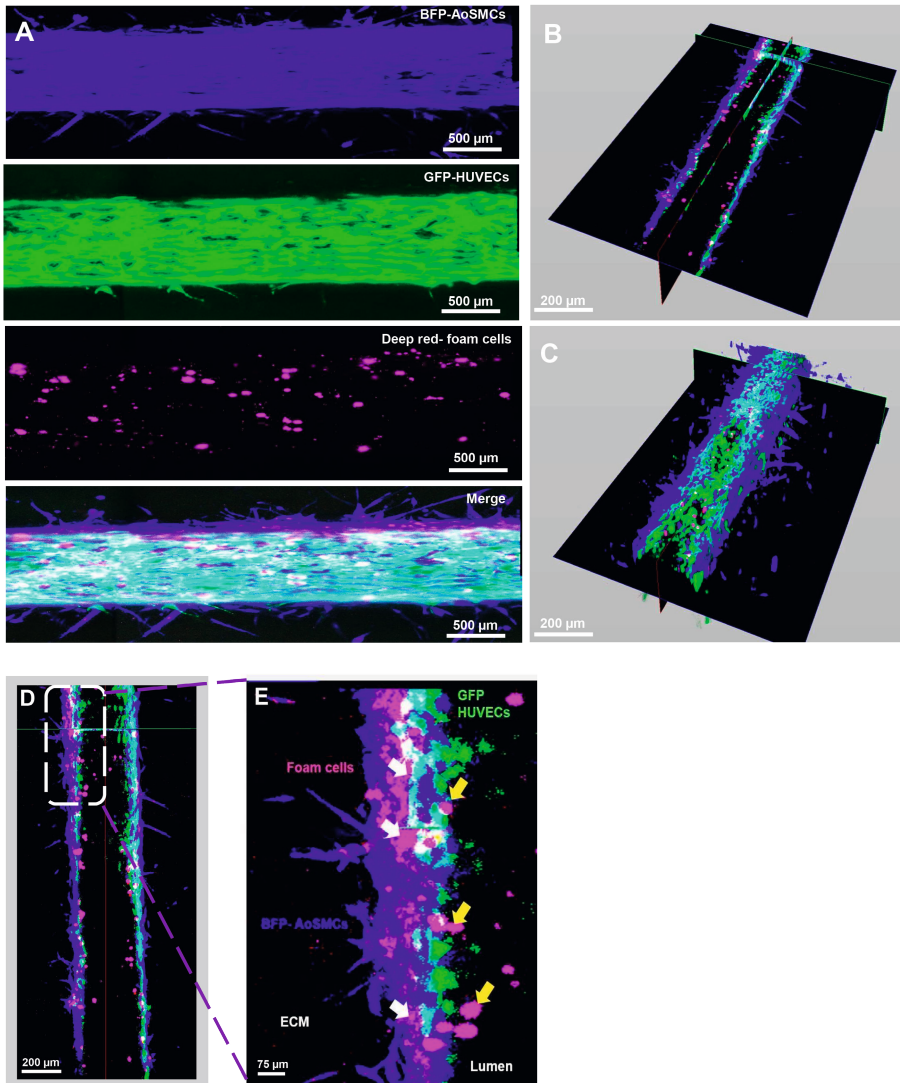
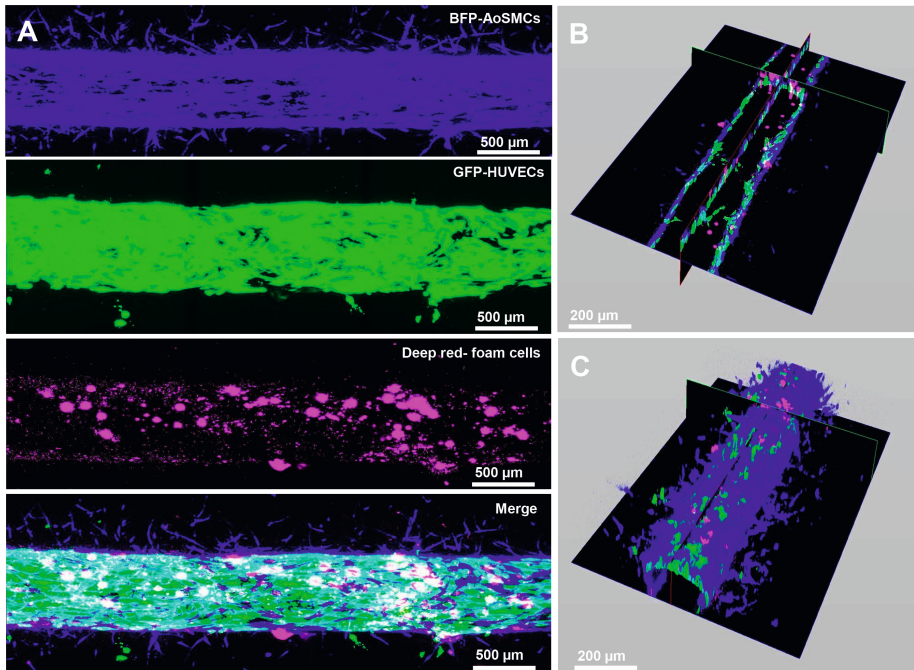


Figure 4. Introduction of foam cells in human macrovessels in the microfluidic system after 4 days of static co-culture.

(A) Confocal micrographs of the preserved endothelial monolayer formed by GFP-labelled HUVECs (second panel, in green) surrounded by preserved BFP-labelled hAoSMCs (upper panel, in blue) co-cultured (static) with foam cells (third panel in magenta) and merged image (lower panel) of the created human atherosclerotic macrovessel. (B) Composite display of the longitudinal and orthogonal cross section micrographs. (C) 3D reconstruction of half of the macrovessel wall. (D) Longitudinal cross section of the vessel. (E) High magnification of a selected area in the longitudinal cross section showing most foam cells (magenta) accumulated in the smooth muscle cell layer (blue) just below the endothelium (green) (the sub-endothelial space (indicated by white arrows)) and some foam cells on the luminal surface (indicated by yellow arrows). Experiments were repeated three times (N=3) and representative images are shown in the figures.

Preserved vessel stability in perfused human atherosclerotic macrovessels in the microfluidic system

To allow studies of tissue adaptation to hemodynamic stimulation, the atherosclerotic vessels were subsequently tested with hemodynamic loading. Confocal live imaging following perfusion with the select cocktail medium for 24 h at a flow rate of 40 $\mu\text{l}/\text{min}$ (Supplemental Fig. 2e, time line e) showed preservation of the vascular wall bilayer structure, and a conservation of the open lumen structure with the presence of foam cell accumulation in the sub-endothelial space, as shown by maximum projection images, 3D composite display, 3D reconstruction and longitudinal cross sections (Fig. 5 a-e). In line with these findings, quantification of the composite images showed no significant differences in BFP-hAoSMCs⁺ and GFP-HUVECs⁺ areas when compared to static atherosclerotic vessels (Supplemental Fig. 4c, d) or when compared to perfused control vessels (Supplemental Fig. 4g and h). Foam cell area in atherosclerotic vessels increased non-significantly in response to circulating cell perfusion, but was significantly amplified by additional, systemic stimulation with pro-inflammatory TNF α (Supplemental Fig. 7).



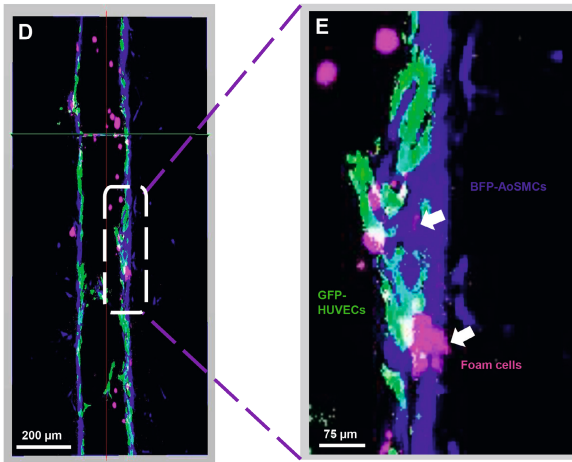


Figure 5. Flow perfusion for 24 hours in a human atherosclerotic vessel in the microfluidic system.

(A) Confocal micrograph shows the preserved endothelial monolayer formed by GFP-HUVECs (second panel, in green) surrounded by preserved BFP-AoSMCs (upper panel, in blue) and accumulated foam cells (third panel in magenta), with the merged image (lower panel) after 5 days of co-culture, from which 4 days static and 1 day perfused at a flow rate of 40 $\mu\text{l}/\text{min}$. (B) Composite display of the longitudinal and orthogonal cross section micrographs. (C) 3D reconstruction of half of a wall of the perfused macrovessel. (D) Longitudinal cross section of the vessel. (E) High magnification of a selected area in the longitudinal cross section showing foam cells (magenta) accumulation in the sub- endothelial space (indicated by white arrows) in the smooth muscle cell layer (blue) under the endothelium (green) as well as foam cells on the luminal side. Experiments were repeated three times (N=3) and representative images are shown in the figures.

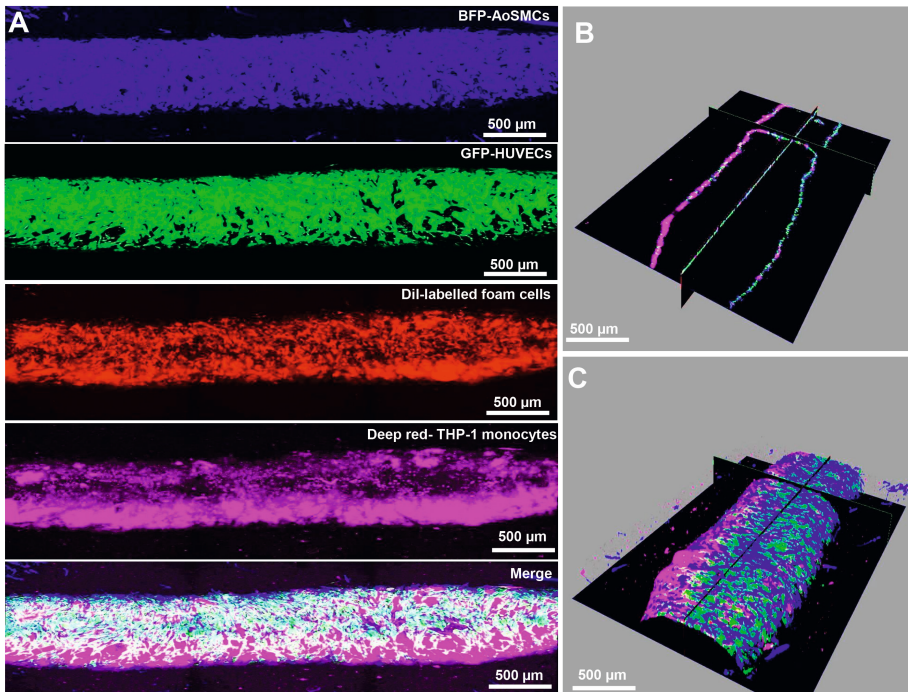
Perfusion of human atherosclerotic vessels with circulating monocytes

Circulating monocytes extravasate into the sub-endothelium of the atherosclerotic plaque in response to local inflammatory signals, followed by macrophage differentiation and contribution to the foam cell core after Ox-LDL uptake during lesion progression. To develop the microfluidic human atherosclerotic chip model into a platform that can facilitate the study of this process, atherosclerotic vessels were perfused with cell tracker deep-red stained THP-1 monocytes, at a concentration of 5×10^5 cells/ mL for 24 h at a flow rate of 40 $\mu\text{l}/\text{min}$ (Supplemental Fig. 2e, timeline f). Confocal live imaging demonstrated a high level of interaction between THP-1 cells and the vascular wall: Confocal maximum projections images showed distributions of GFP-HUVECs (green), BFP-AoSMCs (blue), Dil-OxLDL foam cells (red), and deep-red labelled circulating immune cells (magenta) in the vessel with general preservation of the atherosclerotic vascular wall anatomy (Fig. 6a). In the images of 3D composite display (Fig. 6b) and 3D reconstruction (Fig. 6c)

infiltration of circulating monocytes (magenta) in the media was observed. High magnification display of a longitudinal cross-section with separated colour channels demonstrated significant THP-1 cells interaction with the endothelium, showing a high degree of THP-1 colocalization with HUVECs (Fig. 6d).

Circulating THP-1 cells were also recruited to the sub-endothelial space, showing colocalization with VSMCs (Fig. 6e). The Dil-OxLDL signal indicated that most of the foam cells remained in the sub-endothelial space, co-localizing with the VSMCs (Fig. 6f). Recruited THP-1 cells also colocalized partly with Dil-OxLDL loaded foam cells, implying THP-1/foam cell interaction (Fig. 6g).

In line with these findings, quantification of the composite images showed no significant change in BFP-hAoSMCs⁺ and GFP-HUVECs⁺ areas when compared to static atherosclerotic vessels, or atherosclerotic vessels perfused without circulating cells (Supplemental Fig. 4c, d). No differences in BFP-hAoSMCs⁺ and GFP-HUVECs⁺ area was observed between THP-1 perfused atherosclerotic vessels when compared to THP-1 perfused control vessels (Supplemental Fig. 4i and j).



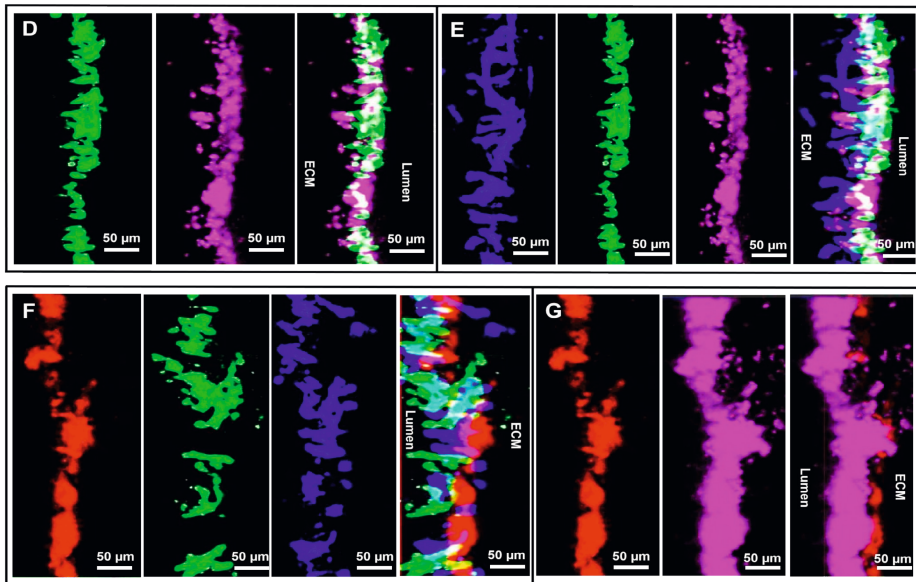


Figure 6. Human atherosclerotic vessel perfused for 24 hours with circulating monocytes in the microfluidic system.

(A) Confocal micrograph shows the preserved endothelial monolayer formed by GFP-HUVECs (second panel, in green) surrounded by preserved BFP- AoSMCs (upper panel, in blue), and accumulated foam cells (third panel in red), with extravasated deep red stained THP-1 monocytes (fourth panel in magenta) and the merged image (lower panel) after 5 days of co- culture, from which 4 days static and 1 day perfused with circulating monocytes at a flow rate of $40\mu\text{l}/\text{min}$ in a human atherosclerotic vessel. (B) Composite display of the longitudinal and orthogonal cross section micrographs. (C) 3D reconstruction of half of a wall of the perfused macrovessel. (D) High magnification of a selected area in the longitudinal cross section with separated colour channels show GFP-HUVECs (green), recruited circulating THP-1 cells (magenta), and composite image. Similar type of panels (E) showing BFP-AoSMCs (blue), GFP-HUVECs (green), recruited circulating THP-1 cells (magenta), and composite image, (F) Dil-OxLDL foam cells (red), GFP-HUVECs (green), BFP-AoSMCs (blue), and composite image, (G) Dil- OxLDL foam cells (red), recruited circulating THP-1 cells (magenta), and composite image. Experiments were repeated three times ($N=3$) and representative images are shown in the figures.

Difference in response of vascular smooth muscle cells in static and perfused healthy and diseased vessels

VSMCs respond to biomechanical and inflammation signals in the atherosclerotic plaque and can switch between a quiescent contractile state to a migratory, proliferative synthetic phenotype²⁵⁻²⁷. To evaluate the impact of flow with and without circulating cells on the migratory response of VSMCs in the (atherosclerotic) vessels, accumulation of VSMCs in the area between the lumen and ECM borders were analysed using confocal maximum projection images. In healthy control vessels, 48 h of flow at $40\mu\text{l}/\text{min}$ increased the overall BFP-hAoSMC signal intensity (V/H- static-

4d + flow, orange line) compared to static controls (V/H- static-4d, grey line) based on the peri-luminal distribution (Fig. 7a). However, segmentation of the periluminal space (into regions of 0-100, 100-200, and 200-300 micron away from the lumen) followed by quantification of the BFP-hAoSMC⁺ area in each segment, showed no significant changes in healthy control vessels in response to flow (Fig.7b). Likewise, no significant change in delta BFP-hAoSMC⁺ area (signal⁺ area in the 200-300 micron region subtracted from the signal⁺ area in the 0-100 micron region (delta segments) was observed, indicating that flow did not alter VSMCs distribution (Fig. 7c). In atherosclerotic vessels, flow decreased the overall BFP-hAoSMC⁺ signal intensity (V/F/H- static-4d + flow, red line) compared to static controls (V/F/H- static-4d, black line) (Fig. 7d). Quantification of the GFP+ VSMC area in each segment, showed no significant changes in atherosclerotic vessels in response to flow (Fig. 7e). However, a significant decrease in delta BFP-hAoSMC⁺ area (delta segments) was observed indicating that flow promoted accumulation of VSMCs away from the lumen (Fig. 7f). To evaluate the impact of foam cells on VSMC distribution, atherosclerotic vessels were compared to control vessels after 4 days of static culture. A non- significant general increase in BFP-hAoSMC⁺ area was observed over all segments in foam cells loaded (atherosclerotic) vessels versus healthy controls without foam cell loading (Supplemental Fig. 5a). A significant increase in the delta BFP-hAoSMC⁺ area was observed in the static atherosclerotic vessels versus control vessels under static conditions (Supplemental Fig. 5b). These data clearly demonstrate that presence of foam cells impacts VSMC distribution in the ECM. Similar results were observed when vessels were perfused with THP-1 cells: VSMC distribution away from the lumen was significantly decreased in atherosclerotic vessels (V/F/H- static- 4d + THP-1 flow) compared to control vessels (delta segments of atherosclerotic vessels < healthy controls, Fig. 8a). Flowing with THP-1 cells significantly reduced the BFP-hAoSMC⁺ area in all segments in atherosclerotic vessels compared to control vessels (Fig.8b).

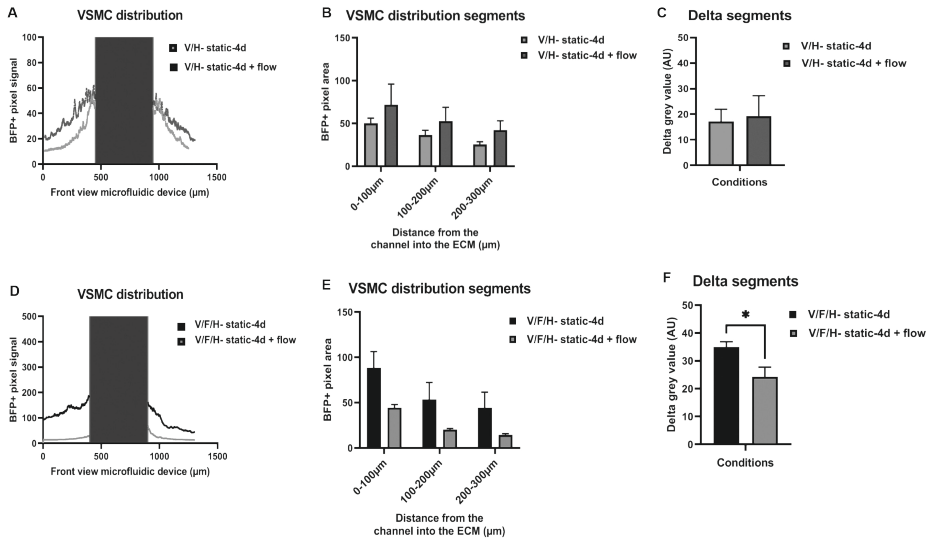


Figure 7. Impact of flow on VSMC distribution in healthy control (V/H) and atherosclerotic (V/F/H) vessels.

(A) Representative view of BFP-VSMC distribution in a static and a perfused healthy control vessel. Distribution of average BFP signal intensity (grey value) over the cross-sectional vessel wall area of static control vessels (grey line) and control vessels perfused for 48 h (orange line). The green box marks the lumen area. (B) BFP-VSMC+ area distribution over predefined cross-sectional wall segments ranging 0-100, 100-200, 200-300 micron from the lumen, of static control vessels (grey bars) and control vessels perfused for 48 h (orange bars), $N=3$. (C) Bar graph showing the delta segments value of static and perfused control vessels, which was calculated by subtracting BFP-VSMC+ area values of segment 200-300 micron from segment 0-100-micron, $N=3$. (D) Representative view of BFP-VSMC distribution in a static and a perfused atherosclerotic vessel. Distribution of average BFP signal intensity over the cross-sectional vessel wall area of static atherosclerotic vessels (black line) and atherosclerotic vessels perfused for 24 h (red line). The green box marks the lumen area. (E) BFP-VSMC+ area distribution over predefined cross-sectional wall segments ranging 0-100, 100-200, 200-300 micron from the lumen, of static (black bars) and perfused atherosclerotic vessels for 24 h (red bars), $N=4$. (F) Bar graph showing the delta segments value of static and perfused atherosclerotic vessels, which was calculated by subtracting BFP-VSMC+ area values of segment 200-300 micron from segment 0-100-micron, $N=4$, $*P<0.05$.

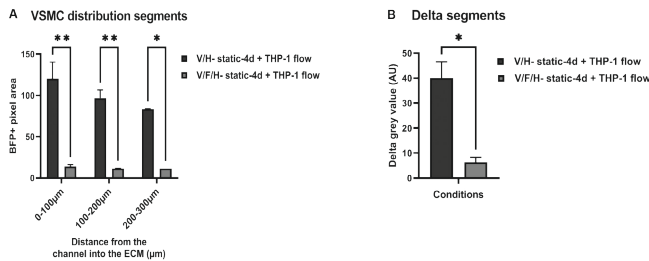


Figure 8. Impact of circulatory monocytes on VSMC distribution in healthy and atherosclerotic vessels.

(A) BFP-VSMC⁺ area distribution over pre-defined cross-sectional wall segments ranging 0-100, 100-200, 200-300 micron from the lumen, of control (blue bars) and atherosclerotic vessels (red bars), perfused for 24 h with THP-1 monocytes, $N=3$, $**P<0.01$, $*P<0.05$. (B) Bar graph showing the delta segments value of control and atherosclerotic vessels, perfused for 24 h with THP-1 monocytes, calculated by subtracting BFP-VSMC⁺ area values of segment 200-300 micron from segment 0-100-micron, $N=3$, $*P<0.05$.

Enhanced recruitment of circulating monocytes in atherosclerotic versus control vessels

In response to *in vivo* inflammatory signals, circulatory monocytes migrate into the vessel wall and merge with the foam cell core during atherosclerosis progression. To evaluate if the model can mimic this process, we next evaluated total THP-1 monocyte area and their distribution in the lumen (free flowing monocytes) and sub-endothelial space (extravasated monocytes) of perfused healthy control (without foam cells) and atherosclerotic (with foam cells) vessels. Quantification of the deep red area showed significant increase in the total area of THP-1 monocytes in the atherosclerotic vessels with foam cells perfused for 24 h (pink bar) compared to control (blue bar, Fig. 9a), indicating that more THP-1 cells were present in the analysed atherosclerotic versus control vessels. Significantly higher significant grey values of the THP-1 deep-red signal were detected in the sub-endothelial space of atherosclerotic versus control vessels indicating that more THP-1 cells were recruited into the vessel wall (Fig. 9b). At the same time, no significant difference in free flowing THP-1 cells was found between atherosclerotic and control vessels (Fig. 9c) These data indicate that our microfluidic system can indeed successfully mimic the events of circulating cell recruitment in human atherosclerotic vessels. Previously our group demonstrated increased THP-1 cell recruitment to the endothelium in response to TNF α treatment using a pericyte-endothelial co-culture in our microfluidic device²⁰. TNF α is a key cytokine in the regulation of the atherogenic inflammatory response²⁸. To evaluate the impact of systemic high levels of TNF α on the transmigration and binding capacity of THP-1 cells in atherosclerotic vessels, THP-1 cells were flowed in healthy and atherosclerotic vessels with prior perfusion

of TNF α for 24 h. THP-1 cell recruitment was significantly higher in atherosclerotic versus control vessels (Supplemental Fig 10). In control vessels, a more than two-fold significant increase of THP-1 signal was observed in the vessel wall after TNF α treatment. THP-1 recruitment in atherosclerotic vessels significantly increased in response to TNF α with similar levels were observed in TNF α treated control vessels (Supplemental Fig 10). Furthermore, TNF α treatment of atherosclerotic vessels in combination with flowing with circulating cells significantly enhanced foam cell areas in atherosclerotic vessels (Supplemental Fig 7).

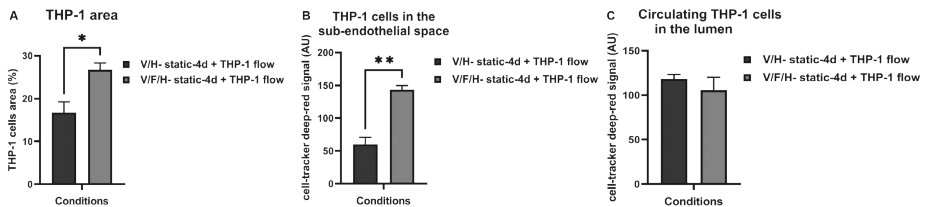


Figure 9. Distribution of circulatory monocytes in healthy and atherosclerotic vessels.

(A) Bar graph presenting the total area of recruited deep-red labelled circulating THP1 monocytes in the atherosclerotic vessels (pink bar) compared to the control vessels (blue bar), after flowing for 24 h with THP-1 cells, $N=3$, $*P<0.05$. (B) Average quantified deep-red signal intensity (grey value) over the sub-endothelial area of the cross-sectional vessel wall, in control and atherosclerotic vessels perfused with THP-1 cells, $N=3$, $**P<0.05$. (C) Average quantified deep-red signal intensity (grey value) over luminal area, in control and atherosclerotic vessels perfused with THP-1 cells, $N=3$.

Adaptation in gene expression of atherosclerotic vessels in response to flow and circulating monocytes

To evaluate the impact of flow, foam cells and circulating monocytes on the mRNA expression level of known atherogenic lipid, inflammation and adhesion markers, microfluidic channels were excised from the ECM gel after the last confocal readout. The qPCR analysis of the macrovessels showed significant upregulation of Low-density lipoprotein-receptor, (LDLR) (a receptor that binds to Ox-LDL particles) under static culture in atherosclerotic versus control vessels (Fig. 10a). LDLR expression significantly decreased under flow compared to static in atherosclerotic vessels, whereas no flow response was observed in control vessels (Fig. 10b). The introduction of circulating monocytes did not impact LDLR expression in both atherosclerotic and control vessels (Fig. 10c). Next, expression levels of inflammatory cytokines Interleukin-6 (IL-6) and Interleukin-8 (IL-8) were analysed. IL-6 but not IL-8 mRNA levels were upregulated under static conditions in atherosclerotic versus control vessels (Fig. 10d, g) Flow downregulated IL-6 but not IL-8 in atherosclerotic vessels and did not affect IL-6 expression in control vessels

(Fig. 10e, h). When circulating monocytes were incorporated in the system, both IL-6 and IL-8 mRNA levels were significantly upregulated in the atherosclerotic vessels. IL-8 mRNA was also increased in control vessels with perfused THP-1 cells (Fig. 10f, i). Adhesion molecules E-selectin and Intercellular adhesion molecule-1 (ICAM-1) were also analysed. Under static conditions, ICAM-1 but not E-selectin was significantly downregulated in the atherosclerotic vessels versus healthy controls (Fig. 10j, m). Flow had no significant impact on expression levels of both E-selectin and ICAM-1 (Fig. 10k, n). Perfusion with circulating THP-1 cells significantly upregulated E selectin expression in atherosclerotic vessels (Fig. 10l) but had no impact on ICAM-1 expression (Fig. 10o). Expression of monocyte chemoattractant protein-1 (MCP-1), a cytokine involved in monocyte recruitment, was significantly upregulated in static atherosclerotic versus control vessels (Fig. 10p). Flow alone did not significantly affect MCP-1 expression in healthy and diseased vessels (Fig. 10q), whereas perfusion with circulating THP-1 cells significantly enhanced MCP-1 expression in both atherosclerotic and control vessels (Fig. 10r). Next, the impact of atherosclerosis, flow and circulation cells on vessel stability was evaluated, by assessing expression of maturation markers: Collagen-4A1 (COL4A1) is a critical major component of the vascular basement membrane that is deposited during neovessel maturation, with COL4A1 defects known to be associated vascular disease in adults²⁹. QPCR analysis showed no significant difference in Collagen-4A1 (COL4A1) expression in response to flow or exposure to circulating cells in healthy vessels. Under static conditions, atherosclerotic vessels showed a significant higher level of COL4A1 expression compared to healthy vessels, which declined in response to flow. However, flowing with circulating cells restored COL4A1 expression (Supplemental Fig 6a). Angiotensin-converting enzyme 1 (ACE1) is expressed in quiescent vasculature and promotes vascular stability, whereas Angiotensin-converting enzyme 2 (ACE2) triggers vessel activation and destabilization. ACE2 expression was increased healthy vessels in response to flow with and without exposure to circulating cells. Atherosclerotic vessels showed a generally higher but non-significant ACE2 expression compared under static conditions, which further increased in response to flow and is significantly higher after flowing with circulating cells compared to healthy vessels (Supplemental Fig 6b), whereas ACE1 levels was not different between conditions (data not shown). The calculated ACE2/ACE1 ratio further confirmed mainly flow induced increase in ACE2/ACE1 ratio in healthy vessels, and significant higher ratios in atherosclerotic vessels in response to flow and flowing with circulating cells compared to similar conditions in healthy vessels (Supplemental Fig 6c). These findings are indicative of a more instable state in atherosclerotic versus healthy vessels, particularly under flow and exposure to circulating cells.

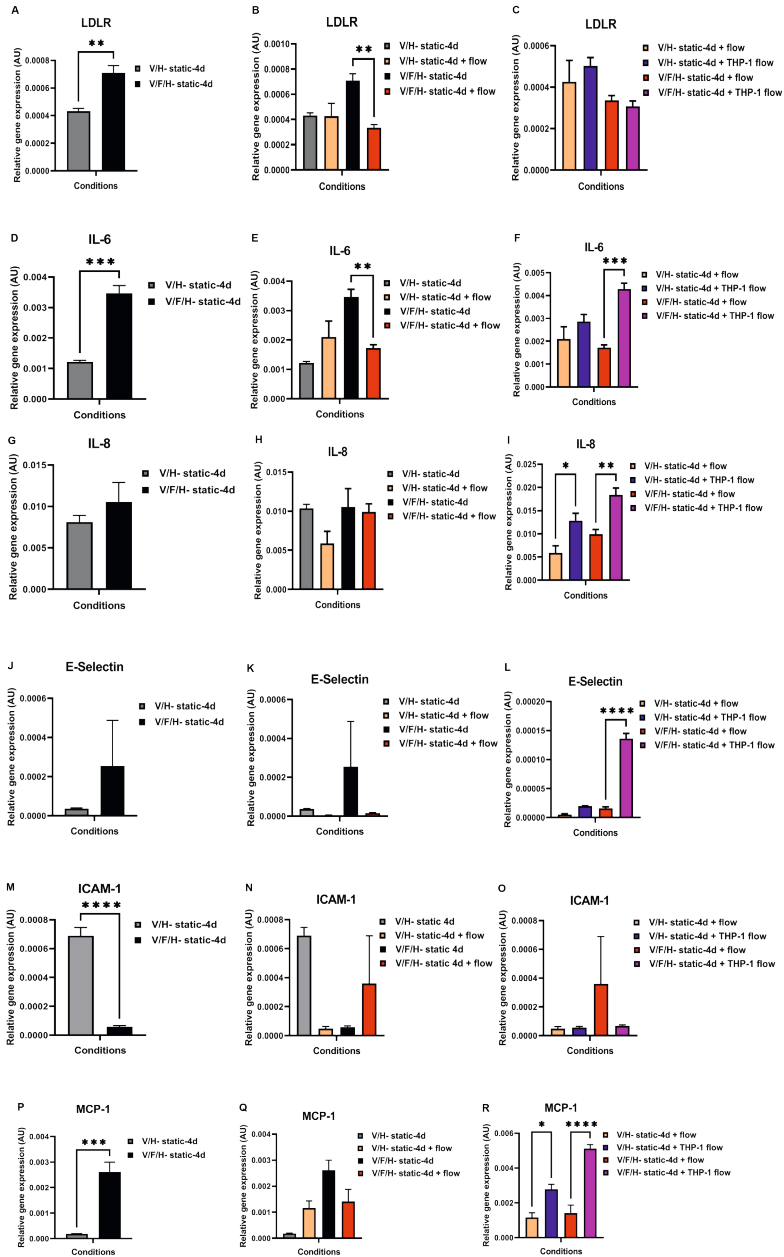


Figure 10. Effect of flow and circulating monocytes on foam cell, inflammatory and adhesion molecule marker expression.

Relative mRNA levels expression of (A-C) LDLR, (D-F) IL6, (G-I) IL8, (J-L) E-selectin, (M-O) ICAM1, and (P-R) MCP-1 in comparison between (A, D, G, J, M, P) control (grey bar) and atherosclerotic vessels (Black bar) under static co-culture, (B, E, H, K, N, Q) in comparison between control and atherosclerotic vessels with and without flow, (C, F, I, L, O, R) in comparison between perfused control and atherosclerotic vessels with and without circulating THP-1 cells, $N=4$, * $P<0.05$, ** $P<0.01$, *** $P<0.001$, **** $P<0.0001$.

Cytokine protein levels in response to flow and circulatory monocytes in atherosclerotic vessels

IL-8 is involved monocyte recruitment and is released by atherosclerotic plaques³⁰. IL8 protein levels were assessed in protein lysate samples of atherosclerotic vessels perfused with or without circulatory THP-1 cells by ELISA analysis, to evaluate the impact of the presence of circulating immune cells on IL-8 production. Although not significant, flowing with circulating cells tended to increase IL-8 protein levels in atherosclerotic vessels versus flowing without cells ($P < 0.118$) indicating that circulatory immune cells can aggravate the inflammatory response of lipid bearing vessels (Supplemental Fig. 9).

Discussion

The aim of the study was to create a complex, perfused human atherosclerosis-OAC model. Here we present, for the first time, a microfluidics-based system with human atherosclerotic vessel-like structures. The most important findings in the present study are that the new system offers: 1) Perfusable macrovessels with preservation of endothelial monolayer, VSMC layers, and open lumen structure after exposure to controlled, unidirectional, continuous flow, with and without circulating monocytes. 2) Introduction of ox-LDL loaded foam cells creates atherosclerotic vessels with a triple-layered lesion-like structure (endothelium, foam cells, VSMC media layer) and an open lumen that is similarly preserved under flow, with and without circulating monocytes. (3) These human (early) atherosclerotic vessels show adaptation to hemodynamic and circulating cell exposure, including distinct changes in expression of lipid-associated, inflammatory and adhesion molecule markers, reduced accumulation of VSMCs near the lumen area in response to flow and circulation cells, and more THP-1 cell recruitment in the sub-endothelial space, compared to healthy control vessels. Combined, these findings demonstrate that our human atherosclerosis-OAC platform can be used to study the complex mechanistic events in early-stage atherosclerosis. Using a PDMS mould casting technique²⁰, the system is suitable for upscaling and high efficiency & low-cost testing of drug targets in atherogenesis.

In the native atherosclerotic lesion, interactions between VSMCs, ECs, and foam cells are vital for disease onset and progression. Early lesions are characterized by the sub-endothelial accumulation of foam cells forming the intima, VSMCs migration into same region followed by VSMCs proliferation, and the activation of the endothelium that facilitates recruitment of circulating immune cells, while the endothelium/media bilayer structure of the vessel wall generally remains mostly intact^{10,31}. Exposure to

(changes in) hemodynamical forces is crucial to provide a continuous trigger for the lesion's adaptive response during growth, and is a critical force that governs lesion interaction with circulating cells, which subsequently lead to local cell recruitment, enhanced inflammation and further plaque expansion³¹⁻³³.

To generate an ideal atherosclerosis-OAC model, all these factors should be considered. Despite the recent advances in microfluidic technology, only a few atherosclerosis-OAC models have thus far been reported, with most of them showing a significant trade-off in their designs for the before mentioned important factors. Qu *et al.* presented a tune-able microfluidic stenosis model for the study of endothelium-leukocyte interactions during atherosclerosis, which lacked incorporation of VSMCs and foam cells¹⁷. Other studies presented systems based on VSMC and EC coculture that lacked foam cells incorporation^{34, 35}. In contrast, our new atherosclerosis-OAC platform not only incorporates 3D co-culture of ECs, VSMCs and foam cells, but also uses a protocol that allows the cells to form a layered structure that mimics the endothelium and media, with Ox-LDL loaded THP-1 cells located in the sub-endothelial space, thereby creating a more plaque-like organization. HUVECs were used in this study based on their proven capacity to easily form distinct monolayer structures on top of mural cells *in vitro*^{16, 17} while exhibiting similar athero-related behaviour with endothelial cells derived from the aorta³⁶⁻³⁸. Combined this 3D layered setup allows the study of cell migration behaviour towards typical plaque anatomical reference points (endothelium, media, foam cell core), and could help reveal interaction patterns between ECs, VSMCs, and (recruited) THP-1 cells in both static and dynamic conditions. In a more advanced platform recently presented by Su *et al.*, co-cultures of VSMCs and ECs were set up in an adapted version of the tension surface-based ECM patterning design to obtain a layered structure. The vessel wall was mimicked by seeding VSMCs and ECM in separate square channels, with ECs on top of the VSMCs layer. Ox-LDL loading of the model was combined with the addition of THP-1 cells and cytokine stimulation, but no experiments were conducted with foam cells, controlled laminar flow or circulating immune cells¹⁸. Similarly, Gu *et al.* presented a 3D stretch design with the co-culture of ECs and VSMCs forming a layered vascular wall structure, and THP-1 monocytes seeded on top, followed by Ox-LDL loading. This platform was capable of testing cell response to stretch, but the structure was grown on a flat surface, lacking the tubular vessel geometry. Flow as well as circulating cell interaction experiments were also not performed in this design¹⁶. Indeed, most of these advanced microfluidics systems use square channels or other geometries that deviate from the native tubular form to recreate the atherosclerotic vessel tissue^{16, 18}. However, to be able to conduct physiologically relevant flow (and

circulating cell) experiments, continuous laminar flow should be introduced in a round tube structure that allows a symmetrical distribution of circulating particles. This cannot be optimally achieved by e.g. using square tubes, which cause particle disturbances³⁹. Recently, Mallone *et al.* developed a new atherosclerosis-on-a-chip model using hiPSCs-derived vascular cells for building plaques. The system utilized a synthetic polyglycolic acid (PGA) tubular scaffold and combined this with bioreactor perfusion and circulating immune cells. While the mesh provides mechanical support to the cells and fibrin was used as a carrier during seeding, it creates an environment in which cells would primarily interact both mechanically and biologically with the synthetic material and its (biodegraded) derivatives instead of natural ECM constituents. Prior investigations have demonstrated that PGA evokes pronounced (localized) inflammation *in vivo*, a phenomenon attributed to the enzymatic and/or hydrolytic (bio)degradation of the material⁴⁰⁻⁴². This suggests the potential for PGA to disrupt the very immune responses that researchers aim to replicate and examine within an *in vitro* atherosclerosis model. The PGA mesh material also interferes with live confocal imaging. For our platform, we used an ECM casting technique incorporating fibrinogen and collagen-1. This approach yielded cylindrical luminal structures, closely resembling native vessels, which were utilized as a foundation for cell seeding. Notably, this ECM construct is devoid of synthetic constituents, enabling real-time confocal imaging of dynamic cell-cell and cell-ECM interactions that closely mimic the conditions in native vessels. Additionally, the here presented model generates atherogenic vessels within a time span of 7 days, in contrast to the PGA mesh-derived system which requires a duration of 4 weeks⁴³.

Our findings demonstrated that controlled, continuous unidirectional flow of healthy control and atherosclerotic arteries in our microfluidic system was feasible up to 48 hours, as no detrimental impact on vessel integrity in response to flow was observed, and arterial layered structure and sub-endothelial location of foam cells were overall conserved. More importantly, unlike previously described atherosclerosis-OAC designs, in which THP-1 cells were added under static conditions²¹, we showed that flowing with circulating THP-1 cells were also feasible in this system. Completely in line with observations in natural human atherogenesis²⁴, enhanced adhesion and recruitment of circulating THP-1 cells into the sub-endothelial space of atherosclerotic vessels was observed compared to control vessels. Perfusion of the atherosclerotic versus healthy vessels with and without circulating cells in our system also led to changes in VSMC behaviour. Previous findings in human atherosclerosis and murine models demonstrated that during atherogenesis, accumulation of ox-LDL in the sub-endothelial space and subsequent foam cell differentiation, is coincided by phenotypic switching of VSMCs from a quiescent,

contractile state to a proliferative synthetic phenotype, with migration of synthetic VSMCs into the intima to advance plaque growth^{27, 44}. VSMCs migration has been explored in the previously described channel system presented by Su *et al.*, where it was demonstrated that VSMCs recruitment towards the sub-endothelial ECM space was enhanced after ox-LDL and/or inflammatory cytokine loading under static conditions¹⁸. In line with these findings, we observed increased accumulation of VSMCs in the vessel segments closest to the sub-endothelium in atherosclerotic vessels compared to the controls after 4 days of static co-culture in our system. Su's model could not test the impact of flow on VSMC behavior¹⁸ but using our model we could demonstrate that flow reduced VSMCs accumulation in the direct sub-endothelial space of the atherosclerotic vessels to baseline values (comparable to control vessels), whereas VSMC distribution in control vessels was not affected by flow. It has been reported that flow-induced shear stress in direct exposure experiments suppresses VSMCs proliferation and migration behaviour compared to static conditions^{45, 46}. In addition, studies using perfused EC and VSMCs co-cultures demonstrated that shear stress sensed by the endothelium promotes synthetic to contractile phenotype switching in the underlying VSMCs via paracrine interaction⁴⁷ and inhibits (contractile phenotype-associated) migration⁴⁸. The findings in our atherosclerosis-OAC model are in line with these previous reports, demonstrating that our system can be used to study complex shear-induced crosstalk mechanisms between vascular cells. In native vessels, atherogenesis typically occurs at vascular sites exposed to deviations in shear stress such as oscillatory shear, and *in vivo* evidence have also demonstrated that they can act as causative factors⁴⁹. As our atherosclerosis-OAC model is pump regulated, the current setup can also be used to study intra-plaque cell behaviour and monocyte recruitment in response to unidirectional versus oscillatory shear stress.

Increased expression of atherogenic factors LDLR, IL-6 and MCP-1⁵⁰⁻⁵² was observed in atherosclerotic vessels compared to control vessels in static conditions. This enhanced expression was suppressed (mainly for LDLR and IL-6) after exposure to flow. It has been reported that phenotypic switching from contractile to synthetic VSMCs promoted expression of atherogenic factors such as IL-6 and MCP-1 (reviewed in⁵³). The decline in expression of atherogenic factors by the atherosclerotic vessels in our platform may be caused by the induction of a more contractile phenotype in perfused versus static conditions. *In vivo* and *in vitro* studies show that recruitment of circulating monocytes into the atherosclerotic vessel wall coincides with increased expression of atherogenic factors⁵⁰⁻⁵³. Similarly, perfusion with circulating monocytes in our microfluidic platform enhanced expression of atherogenic factors IL-6, IL-8, and MCP-1 as well as the expression of adhesion molecule E-selectin, in

atherosclerotic vessels as compared to flowing without circulating cells (Fig. 10l). E-selectin is upregulated in ECs during inflammation responses and is essential for circulating leukocyte-endothelial interaction during extravasation, implying active positive feedback on THP-1 cell recruitment in our atherosclerosis-OAC model⁵⁴. Combined, these data indicates that our new atherosclerosis-OAC platform mimics complex flow and circulating monocytes related processes in human atherogenesis on a tissue anatomical, cell-cell interaction and cell functional level.

Limitations of the study

Without a necrotic core, fibroblasts, and VSMC/fibrous cap, the atherosclerosis-OAC model presented in this study mostly mimics a lesion in the early stage of atherosclerosis. This may limit the suitability of this system to studies that focus on flow and circulating cell (monocytes) interaction with the early lesion environment. The current model could be further adapted for use of vascular cells of different sources, including induced pluripotent stem cells (iPSC) derived vascular cells from CAD patients, opening the door for the use of this system in high throughput personalized drug screening. Secondly, lesion area assessment *in vivo* conventionally involves quantifying cellular accumulation within the intimal region, which is demarcated by the area on top of the internal elastic lamina. Regrettably, our model, akin all other currently available *in vitro* models, lacks this demarcation. Changes in foam cell area (Supplementary Fig. 7) and monocyte area (shown in Fig. 9a) within the vascular wall may be used as proxies, but this would overlook the contribution of VSMCs to lesion size. Third, in our microfluidic system, a flow rate of 40 $\mu\text{l min}^{-1}$ was employed, yielding a shear rate of 38.3 s^{-1} and a wall shear stress of 0.286 dyn cm^{-2} . This is notably lower compared to the 10-70 dyn/cm^2 range observed in straight segments of arteries. However, regions prone to atherosclerosis development, like the inner curvature of vessel branches, exhibit low and/or disturbed shear stress patterns⁵⁵. Research altering shear stress in straight artery segments has shown that reduced shear stress triggers atherosclerosis^{56,57}. Our setup's shear stress aligns with levels used in microfluidic studies focusing on leukocyte-endothelium interaction under controlled flow²¹⁻²³. Yet, the ECM substrate's mechanical weakness restricts raising the flow rate. *In vivo*, tissue cells and the vascular basement membrane counteract intraluminal blood pressure, thereby preserving vessel integrity. Future studies should explore strategies bolstering ECM substrate support for increased flow rates without compromising cell interactions.

Conclusions

The current study demonstrates, to our knowledge for the first time, a fluorescent labelled, quadruple cell co-culture-based atherosclerosis-OAC microfluidic platform that mimics the complexity of the 3D tubular atherosclerotic vessel with layered media and endothelium structure and sub-endothelial foam cell accumulation, which can be exposed to controlled continuous flow with and without circulatory THP-1 monocytes. This new system provides an advanced platform for 3D studies of vascular cell/immune cell interactions in early-stage atherosclerosis. Furthermore, this novel microfluidics model provides live-confocal imaging with side-to-side comparison between healthy with atherosclerotic vessels. Engineered with human cells it offers a humanized platform for in-depth mechanistic studies. Further adaptations of the model may include incorporation of patient-derived cells of iPSC and/or peripheral blood mononuclear cells (PBMCs) origin. Integration of this new atherosclerosis-OAC with genetic and GWAS studies with established biobanks could be especially rewarding, when dedicated disease platforms for patient subpopulations are created for personalized drug screening.

Acknowledgments

We would like to thank Gert-Jan Kremers for providing training on Leica-SP8 DLS confocal microscopy at the Erasmus Optical Imaging Centre (OIC) and Lau Blonden for producing BFP-lentiviral supernatants. This research was financially supported by EC RESCUE grant (no. 801540 to C.C) and the Dutch CardioVascular Alliance (an initiative with support of the Dutch Heart Foundation) Grant 2020B008 RECONNECT (to D.J.D., M.C.V. and C.C.). We gratefully acknowledge the Gravitation Program “Materials Driven Regeneration”, funded by the Netherlands Organization for Scientific Research (024.003.013).

Conflicts of interest

The authors declare no conflict of interest in this study.

Data availability

The datasets generated during and/or analysed during the current study are available from the corresponding author on a reasonable request.

References

1. Schwartz CJ, Valente AJ, Sprague EA, et al. Atherosclerosis. Potential targets for stabilization and regression. *Circulation*. 1992;86(6 Suppl):III117-23.
2. Hansson GK. Inflammation, atherosclerosis, and coronary artery disease. *N Engl J Med*. 2005;352(16):1685-95.
3. Emini Veseli B, Perrotta P, De Meyer GRA, et al. Animal models of atherosclerosis. *Eur J Pharmacol*. 2017;816:3-13.
4. Getz GS, Reardon CA. Animal models of atherosclerosis. *Arterioscler Thromb Vasc Biol*. 2012;32(5):1104-15.
5. Suo J, Ferrara DE, Sorescu D, et al. Hemodynamic shear stresses in mouse aortas: implications for atherogenesis. *Arterioscler Thromb Vasc Biol*. 2007;27(2):346-51.
6. Chen J, Zhang X, Millican R, et al. Recent Progress in in vitro Models for Atherosclerosis Studies. *Front Cardiovasc Med*. 2021;8:790529.
7. Dorweiler B, Torzewski M, Dahm M, et al. A novel in vitro model for the study of plaque development in atherosclerosis. *Thromb Haemost*. 2006;95(1):182-9.
8. Wada Y, Sugiyama A, Kohro T, et al. In vitro model of atherosclerosis using coculture of arterial wall cells and macrophage. *Yonsei Med J*. 2000;41(6):740-55.
9. Robert J, Weber B, Frese L, et al. A three-dimensional engineered artery model for in vitro atherosclerosis research. *PLoS One*. 2013;8(11):e79821.
10. Zhang X, Bishawi M, Zhang G, et al. Modeling early stage atherosclerosis in a primary human vascular microphysiological system. *Nat Commun*. 2020;11(1):5426.
11. Tehranirokh M, Kouzani AZ, Francis PS, et al. Microfluidic devices for cell cultivation and proliferation. *Biomicrofluidics*. 2013;7(5):51502.
12. Wong KH, Chan JM, Kamm RD, et al. Microfluidic models of vascular functions. *Annu Rev Biomed Eng*. 2012;14:205-30.
13. Haase K, Kamm RD. Advances in on-chip vascularization. *Regen Med*. 2017;12(3):285-302.
14. Kim S, Kim W, Lim S, et al. Vasculature-On-A-Chip for In Vitro Disease Models. *Bioengineering (Basel)*. 2017;4(1).
15. Poussin C, Kramer B, Lanz HL, et al. 3D human microvessel-on-a-chip model for studying monocyte-to-endothelium adhesion under flow - application in systems toxicology. *ALTEX*. 2020;37(1):47-63.
16. Gu X, Xie S, Hong D, et al. An in vitro model of foam cell formation induced by a stretchable microfluidic device. *Sci Rep*. 2019;9(1):7461.
17. Venugopal Menon N, Tay HM, Pang KT, et al. A tunable microfluidic 3D stenosis model to study leukocyte-endothelial interactions in atherosclerosis. *APL Bioeng*. 2018;2(1):016103.
18. Su C, Menon NV, Xu X, et al. A novel human arterial wall-on-a-chip to study endothelial inflammation and vascular smooth muscle cell migration in early atherosclerosis. *Lab Chip*. 2021;21(12):2359-71.
19. Chen R, Wang B, Liu Y, et al. Gelatin-based perfusable, endothelial carotid artery model for the study of atherosclerosis. *Biomed Eng Online*. 2019;18(1):87.
20. van Dijk CGM, Brandt MM, Poulis N, et al. A new microfluidic model that allows monitoring of complex vascular structures and cell interactions in a 3D biological matrix. *Lab Chip*. 2020;20(10):1827-44.

21. Lamberti G, Prabhakar Pandian B, Garson C, et al. Bioinspired microfluidic assay for in vitro modeling of leukocyte-endothelium interactions. *Anal Chem*. 2014;86(16):8344-51.
22. Lawrence MB, Kansas GS, Kunkel EJ, et al. Threshold levels of fluid shear promote leukocyte adhesion through selectins (CD62L,P,E). *J Cell Biol*. 1997;136(3):717-27.
23. Simon SI, Hu Y, Vestweber D, et al. Neutrophil tethering on E-selectin activates beta 2 integrin binding to ICAM-1 through a mitogen-activated protein kinase signal transduction pathway. *J Immunol*. 2000;164(8):4348-58.
24. Kim KW, Ivanov S, Williams JW. Monocyte Recruitment, Specification, and Function in Atherosclerosis. *Cells*. 2020;10(1).
25. Zhang MJ, Zhou Y, Chen L, et al. An overview of potential molecular mechanisms involved in VSMC phenotypic modulation. *Histochem Cell Biol*. 2016;145(2):119-30.
26. Biroš E, Reznik JE, Moran CS. Role of inflammatory cytokines in genesis and treatment of atherosclerosis. *Trends Cardiovasc Med*. 2022;32(3):138-42.
27. Chaabane C, Coen M, Bochaton-Piallat ML. Smooth muscle cell phenotypic switch: implications for foam cell formation. *Curr Opin Lipidol*. 2014;25(5):374-9.
28. McKellar GE, McCarey DW, Sattar N, et al. Role for TNF in atherosclerosis? Lessons from autoimmune disease. *Nat Rev Cardiol*. 2009;6(6):410-7.
29. Van Agtmael T, Bailey MA, Schlotzer-Schrehardt U, et al. Col4a1 mutation in mice causes defects in vascular function and low blood pressure associated with reduced red blood cell volume. *Hum Mol Genet*. 2010;19(6):1119-28.
30. Apostolopoulos J, Davenport P, Tipping PG. Interleukin-8 production by macrophages from atheromatous plaques. *Arterioscler Thromb Vasc Biol*. 1996;16(8):1007-12.
31. Chistiakov DA, Melnichenko AA, Myasoedova VA, et al. Mechanisms of foam cell formation in atherosclerosis. *J Mol Med (Berl)*. 2017;95(11):1153-65.
32. Hahn C, Schwartz MA. The role of cellular adaptation to mechanical forces in atherosclerosis. *Arterioscler Thromb Vasc Biol*. 2008;28(12):2101-7.
33. Kwak BR, Back M, Bochaton-Piallat ML, et al. Biomechanical factors in atherosclerosis: mechanisms and clinical implications. *Eur Heart J*. 2014;35(43):3013-20, 20a-20d.
34. Heydarkhan-Hagvall S, Helenius G, Johansson BR, et al. Co-culture of endothelial cells and smooth muscle cells affects gene expression of angiogenic factors. *J Cell Biochem*. 2003;89(6):1250-9.
35. Sarwar M, Samuel CS, Bathgate RA, et al. Enhanced serelaxin signalling in co-cultures of human primary endothelial and smooth muscle cells. *Br J Pharmacol*. 2016;173(3):484-96.
36. Vion AC, Kheloufi M, Hammoutene A, et al. Autophagy is required for endothelial cell alignment and atheroprotection under physiological blood flow. *Proc Natl Acad Sci U S A*. 2017;114(41):E8675-E84.
37. Seebach J, Donnert G, Kronstein R, et al. Regulation of endothelial barrier function during flow-induced conversion to an arterial phenotype. *Cardiovasc Res*. 2007;75(3):596-607.
38. Bharath LP, Cho JM, Park SK, et al. Endothelial Cell Autophagy Maintains Shear Stress-Induced Nitric Oxide Generation via Glycolysis-Dependent Purinergic Signaling to Endothelial Nitric Oxide Synthase. *Arterioscler Thromb Vasc Biol*. 2017;37(9):1646-56.
39. Aminian M, Bernardi F, Camassa R, et al. Squaring the Circle: Geometric Skewness and Symmetry Breaking for Passive Scalar Transport in Ducts and Pipes. *Phys Rev Lett*. 2015;115(15):154503.

40. Ceonzo K, Gaynor A, Shaffer L, et al. Polyglycolic acid-induced inflammation: role of hydrolysis and resulting complement activation. *Tissue Eng.* 2006;12(2):301-8.
41. Wang M, Li Q, Shi C, et al. Oligomer nanoparticle release from polylactic acid plastics catalysed by gut enzymes triggers acute inflammation. *Nat Nanotechnol.* 2023;18(4):403-11.
42. Luo X, Zhou G, Liu W, et al. In vitro precultivation alleviates post-implantation inflammation and enhances development of tissue-engineered tubular cartilage. *Biomed Mater.* 2009;4(2):025006.
43. Human induced pluripotent stem cell-derived arteries as personalized models of atherosclerosis on-a-chip. *bioRxiv.* 2020.
44. Campbell GR, Campbell JH. The phenotypes of smooth muscle expressed in human atheroma. *Ann N Y Acad Sci.* 1990;598:143-58.
45. Kang H, Fan Y, Deng X. Vascular smooth muscle cell glycocalyx modulates shear-induced proliferation, migration, and NO production responses. *Am J Physiol Heart Circ Physiol.* 2011;300(1):H76-83.
46. Palumbo R, Gaetano C, Melillo G, et al. Shear stress downregulation of platelet-derived growth factor receptor-beta and matrix metalloprotease-2 is associated with inhibition of smooth muscle cell invasion and migration. *Circulation.* 2000;102(2):225-30.
47. Tsai MC, Chen L, Zhou J, et al. Shear stress induces synthetic-to-contractile phenotypic modulation in smooth muscle cells via peroxisome proliferator-activated receptor alpha/delta activations by prostacyclin released by sheared endothelial cells. *Circ Res.* 2009;105(5):471-80.
48. Wang HQ, Huang LX, Qu MJ, et al. Shear stress protects against endothelial regulation of vascular smooth muscle cell migration in a coculture system. *Endothelium.* 2006;13(3):171-80.
49. Cheng C, Tempel D, van Haperen R, et al. Atherosclerotic lesion size and vulnerability are determined by patterns of fluid shear stress. *Circulation.* 2006;113(23):2744-53.
50. Herijgers N, Van Eck M, Groot PH, et al. Low density lipoprotein receptor of macrophages facilitates atherosclerotic lesion formation in C57Bl/6 mice. *Arterioscler Thromb Vasc Biol.* 2000;20(8):1961-7.
51. Lin J, Kakkar V, Lu X. Impact of MCP-1 in atherosclerosis. *Curr Pharm Des.* 2014;20(28):4580-8.
52. Hartman J, Frishman WH. Inflammation and atherosclerosis: a review of the role of interleukin-6 in the development of atherosclerosis and the potential for targeted drug therapy. *Cardiol Rev.* 2014;22(3):147-51.
53. Krokoski M, Monslow J, Pure E. The CD44-HA axis and inflammation in atherosclerosis: A temporal perspective. *Matrix Biol.* 2019;78-79:201-18.
54. Wong D, Dorovini-Zis K. Regulation by cytokines and lipopolysaccharide of E-selectin expression by human brain microvessel endothelial cells in primary culture. *J Neuropathol Exp Neurol.* 1996;55(2):225-35.
55. Nigro P, Abe J, Berk BC. Flow shear stress and atherosclerosis: a matter of site specificity. *Antioxid Redox Signal.* 2011;15(5):1405-14.
56. den Dekker WK, Tempel D, Speelman L, et al. Effect of shear stress alteration on atherosclerotic plaque vulnerability in cholesterol-fed rabbits. *Vasc Med.* 2014;19(2):94-102.
57. Cheng C, Tempel D, van Haperen R, et al. Shear stress-induced changes in atherosclerotic plaque composition are modulated by chemokines. *J Clin Invest.* 2007;117(3):616-26.

Supplemental information



PART 3

CHAPTER

8



Matrigel-free alternatives for hiPSC-derived blood vessel organoid culture

Elana M. Meijer, Rachel Giles, Renée G.C. Maas, Christian G.M. van Dijk,
Marianne C. Verhaar, Caroline Cheng

In preparation

Abstract

The use of induced pluripotent stem cell (hiPSC) -derived blood vessel organoids (BVOs) offers significant promise in vascular regeneration research. However, the reliance on Matrigel, a murine sarcoma-derived matrix, in differentiation and culture of BVOs poses challenges regarding reproducibility and translational potentials. Here, we propose and evaluate alternatives to Matrigel to enhance the clinical applicability of hiPSC-derived BVOs. Vitronectin™ emerges as a suitable replacement for Matrigel in hiPSC culture and expansion, maintaining pluripotency and facilitating subsequent differentiation into BVOs. Additionally, we demonstrate that fibrin-based hydrogels effectively support BVO differentiation, promoting vascular network formation and endothelial cell sprouting comparable to Matrigel-based cultures. Through gene expression analysis, surface area quantification, and immunohistochemistry, we validate the efficacy of Vitronectin™ and fibrin in supporting hiPSC-derived BVO differentiation. This Matrigel-free protocol not only enhances reproducibility but is a step forward in xeno-free culture conditions, offering a versatile platform for disease modeling, vascular tissue engineering, and patient-specific therapeutic screening.

Introduction

Organoids, derived from among others induced pluripotent stem cells (iPSCs), are 3D-multicellular structures that mimic organ functions *in vitro* and have become a popular platform for studying organ development, drug discovery and various diseases¹. Compared to conventional 2D cultures and animal models, organoid culture allows patient specificity by including their unique genetic makeup while also recapitulating *in vivo* tissue-like structures and functions *in vitro*. Organoids are typically expanded in extracellular matrix (ECM) protein-based hydrogels, such as Matrigel, or similar alternatives such as Cultrex BME and Geltrex^{2,3}. Matrigel, a reconstituted basement membrane matrix obtained from Engelbreth-Holm-Swarm mouse sarcomas, exhibits high concentrations of laminin, collagen, and extracellular matrix (ECM) proteins⁴⁻⁶. This composition facilitates cellular processes such as adhesion, proliferation, and differentiation, mimicking the inherent characteristics of the natural 3D matrix environment.

Blood vessel organoids (BVOs), derived from (h)iPSCs, are increasingly favoured in vascular regeneration research. These structures, composed of organized endothelial cells (ECs) and mural cells, were first reported in 2019⁷ and have demonstrated functionality when implanted under the renal capsule of mice, connecting to the host vasculature. BVOs find applications in disease modeling, developmental biology studies, genetic engineering, and high-throughput drug screening⁸. The differentiation protocol involves Matrigel embedding, and the expansion of hiPSCs typically requires Matrigel-coated plates⁸. While Matrigel promotes BVO maturation and angiogenic sprouting, its batch variability and murine origin, along with tumor-derived growth factors, hinder reproducibility and human applicability⁴. Identifying a Matrigel-free hydrogel becomes crucial for enhancing reproducibility and translational potential in hiPSC BVO-based *in vitro* assays. For 2D hiPSC culture, several Matrigel-free (and xeno-free) options have been proposed as alternative coating material. Cell-adhesive ECMs such as Vitronectin™ and laminin (laminin-511 recombinant laminin, and laminin fragments) are promising approaches to establish fully defined cell culture conditions for clinical grade hiPSCs⁹⁻¹¹. Nonetheless, it has been reported that the use of different coatings on cell culture plates significantly affects the growth and expansion of hiPSCs, as well as their subsequent effectiveness in differentiation. Furthermore, distinct hiPSC lines from different origins (skin or blood cells) may exhibit varied responses to different substrates. Therefore, it is crucial to assess the selected coating method for its suitability in the intended application with the desired line. Chemical Matrigel-free substrates often lack the necessary stiffness and essential bioactive molecules

crucial for cell interaction and subsequent angiogenic sprouting, rendering them unsuitable for *in vitro* blood vessel models¹². The selected Matrigel alternative for the 3D ECM culture of BVOs should mirror Matrigel characteristics in terms of stiffness and polymerization that enable sprouting behavior.

We propose replacing Matrigel-based steps in the BVO differentiation protocol with Matrigel-free alternatives, aiming to enhance the clinical translatability of vascular regeneration strategies. For hiPSC expansion in 2D culture, Vitronectin™ XF™ serves as a potential Matrigel alternative, providing a xeno-free matrix supporting growth and differentiation under serum- and feeder cell-free conditions. Vitronectin™, a recombinant human protein, enables enzyme-free passaging, supports mesoderm induction, making it suitable for hiPSC-derived vascular organoid culture¹³⁻¹⁵. As a substitute for the 3D ECM in BVO differentiation, fibrin emerges as a viable option. Fibrin, commonly used in sprout formation assays^{12, 16-18}, is a naturally angiogenic provisional matrix in wound healing¹⁸. Fibrin-based hydrogels, known for biocompatibility, non-toxic degradation products, and controllable gelation time through thrombin concentration adjustment, offer versatility in supporting cell proliferation^{19,20}.

In this study we aim to replace Matrigel for hiPSC-derived vascular organoid culture, creating a Matrigel-free BVO differentiation protocol. The suitability of Vitronectin™ for hiPSC expansion in 2D culture and fibrin gels for BVO differentiation in 3D culture, as a substrate replacement of Matrigel, were evaluated. Our findings demonstrate that in both expansion and differentiation steps, Matrigel can be replaced by these alternatives, offering a complete Matrigel-free and near xeno-free method for vascular organoid culture derived from human iPSC origin.

Methods

hiPSC and vascular organoid culture

Derivation and Culture of Human iPSCs on Matrigel and Vitronectin™

The hiPSCs used in this study were donated by the Joseph Wu Lab (Stanford Medicine, Department of Medicine and Radiology, Stanford CVI Biobank) as described previously²¹. hiPSC line was generated from peripheral blood mononuclear cells by Sendai viral reprogramming. Donors gave informed consent under protocols approved by the Stanford University Human Subjects Research Institutional Review Board as previously described. Cells were thawed and cultured on Matrigel (1.2mg/mL in E8 medium, Corning) coated 6-well plates for the Matrigel controls. For the

Vitronectin™ group, cells were thawed and cultured on Vitronectin™ (10µl/mL in PBS) coated 6-well plates. Both groups were supplemented with E8+ medium with 1:1000 ROCK inhibitor (Calbiochem) for the first 24 h. Medium was changed every other day.

hiPSCs in both groups were nonenzymatically passaged using 0.5×10^{-3} M EDTA (Invitrogen) every 4 to 5 days at 90% confluence. They were passaged in a splitting ratio of 1:10. Medium was changed every other day. To improve cell survival, split ratio reliability and to reduce selective pressure, 1:2000 ROCK inhibitor (Calbiochem) was used in the first 24 h. Cells were passaged at least twice before proceeding to vascular organoid differentiation.

Vascular organoid differentiation – suspension culture

Schematic overview of the experimental procedures is represented in figure 2. Both groups of hiPSCs were harvested using EDTA and subsequently resuspended in differentiation medium (Knock-out Dulbecco's modified Eagle's culture medium (KO-DMEM); 20% Knock Out Serum (KOSR), 1% Penicillin Streptomycin (PS), 1% Glutamax and 1% non-essential amino acids (NEAA); all Gibco), including 1:1000 ROCK-inhibitor Y-27632 (Calbiochem). Cells were plated into an ultra-low attachment six-well plate (Corning), in a final concentration of approximately 2×10^5 cells per well. Cells were incubated on a shaker plate at 37°C for 24 h to form aggregates and subsequently transferred to hypoxic conditions (5% O₂). Cell aggregates were treated with 13×10^{-6} M GSK-3 inhibitor CHIR99021 (Tocris) on day 3 to start mesoderm induction. On days 5, 7 and 9, the aggregates were treated with bone morphogenetic protein 4 (BMP4) (30 ng/mL; Stemcell Technologies), vascular endothelial growth factor A (VEGF-A) (30 ng/mL; Peprotech) and Fibroblast Growth Factor 2 (FGF-2) (30 ng/mL; Miltenyi Biotec) to promote the vascular lineage formation. On day 11, differentiation medium was supplemented with VEGF-A (30 ng/mL), FGF-2 (30 ng/mL) and transforming growth factor β (TGFβ)-inhibitor SB43152 (10×10^{-6} M; Stemcell Technologies) to increase the yield of endothelial cells and suppress excessive differentiation into mesenchymal/mural like cells.

Vascular organoid differentiation – 3D culture

In this project 3 different 3D matrix combinations were compared (table 1).

Table 1. hiPSC coating and 3D matrices used in the different research groups.

	Matrigel-Matrigel	Vitronectin™ - Matrigel	Vitronectin™-Fibrin
hiPSC coating	Matrigel	Vitronectin™	Vitronectin™
3D Matrix	Matrigel + Collagen	Matrigel + Collagen	Fibrinogen + Thrombin

The aggregates were collected on day 13, embedded in a 1:1 Matrigel:collagen mixture (Matrigel-Matrigel group and Vitronectin™-Matrigel group) (Corning Matrigel, phenol red free and Atelocollagen Bovine Dermis 3 mg/mL, Bio-connect) or in a 7.5mg/mL fibrinogen (Gibco) + 0.1 U/mL thrombin (Sigma) gel (Vitronectin™-Fibrin group) and supplemented with differentiation medium containing 15% KOSR, VEGF-A (100 ng/mL) and FGF-2 (100 ng/mL). Medium was changed every other day. Vascular organoids were collected on day 18 and either disaggregated for further experiments or cultured in a 96-well round bottom plate without ECM support to stimulate self-assemble into spheroid-shaped vascular organoids.

Cell sorting and analysis

Organoid dissociation

Vascular organoids from both groups were mechanically disrupted after 18 days and disaggregated using 3 U/mL dispase (Gibco), 2 U/mL liberase (Roche) and 100 U DNase (Stemcell Technologies) in warm DMEM + PS for 20 min at 37°C while rotating. Every 5 minutes, the cells were resuspended. To remove excess gel and remaining aggregates from the suspension, the solution was filtered using a 70 µm cell strainer and 5mL DMEM + PS and subsequently spun down for 5 min at 400 g.

Flow cytometry

Single cell organoids were plated into a 96-well flat bottom plate, approximately 25.000 cells per well. Cells were washed with PBS supplemented with 2% FBS and 2mM NaN₃. Cells were stained with anti-CD31 and anti-CD140b antibodies (Supplemental table 1) together with Sytox blue (Invitrogen) to exclude dead cells. CytoFLEX flow cytometer (Beckman Coulter) was used for cell analysis and data analysis was performed using FlowJo software (Version 10.2) and analyzed using Graphpad Prism 9.

Quantitative Polymerase Chain Reaction (qPCR) Analysis

Total RNA was isolated from hiPSCs and vascular organoids on day 0, 5, 11, 15 and 18 of differentiation using Trizol (Invitrogen) according to the manufacturer's instructions. The purity and concentrations of RNA were quantified using spectrophotometry (DS-11; DeNovix) absorbance measurements at 260/280 nm. cDNA synthesis was performed according to the Bioline cDNA synthesis kit. Gene expression patterns were determined using FastStart SYBR-green (Roche) following the quantitative polymerase chain reaction (qPCR) program: 8,5' 95°C, 38 cycles (15" 95°C; 45" 60°C) 1' 95°C, 1' 65°C, 62 cycles (10" 65°C + 0.5°C) in the SYBR-Green-Cycler IQ5 detection protocol (Biorad CFX384), performed in 384-well plates (Merck).

The primer sequences used are listed in Supplemental table 2. All results were normalized for house-keeping genes β -actin and RPLP0 resulting in relative mRNA expression. Results are shown as the fold change of the Δ ct values.

Immunohistochemistry

Immunofluorescent staining of 2D hiPSC cultures

Cultured hiPSCs were fixed using paraformaldehyde (4%) for 15 minutes and incubated with blocking/permeabilization buffer (5% BSA/0.3% Triton-X-100 in PBS) for 30 minutes. After blocking with 1:5 diluted blocking buffer DPBS, the primary antibodies (Table 3) were added and incubated overnight at 4°C. After washing with PBS, Alexa-conjugated secondary antibodies (life technologies) (Table 3) diluted in 1:5 diluted blocking/permeabilization buffer were incubated for one hour in the dark-room at room temperature (RT). Cell nuclei were visualised using μ g/ml Hoechst or DAPI (Life Technologies), before imaging using a Leica DMI8 confocal microscope or Nikon Ti2 Widefield microscope (Trilineage).

Whole mount staining of 3D organoid cultures

Vascular organoids were extracted from wells or a 96-well plate and fixed for 1hr with 4% PFA at RT. Organoids were blocked and permeabilized using 3% FBS, 1% BSA, 0.5% Triton x-100 and 0.5% Tween in PBS for 2 h at RT. 3D cell cultures were stained with anti-CD31 and anti-PDGFr β antibodies (supplemental table 3) for 2 h at RT. The organoids were washed three times with PBS-/Tween (PBST) and secondary antibody incubation (supplemental table 3) was performed for 2 h at RT. Organoids were washed again three times with PBST. DAPI was used as a counterstain and 3D cell cultures were mounted with Mowiol4-88. Samples were stored at 4°C prior to imaging.

Imaging and Analysis

Bright field images for surface area analysis were taken using the Olympus CKX41. 3D Imaging was performed using the Leica Confocal SP8X (10X, 20X magnifications). Images were analyzed using ImageJ software (V1.47). 3D images were composed in LASX (version 3.5.7.23225).

Statistical Analysis

Statistical analyses was performed using GraphPad Prism (version 8.3). Values are shown as individual data points with mean \pm SEM. Prior to statistical testing, outliers were removed when detected using a Grubbs' test ($\alpha = 0.05$). The paired, two-sided t-test and ordinary one-way ANOVA test with Tukey post hoc test were used

when appropriate. Experiments were performed at least in triplicate. The detailed sample size for each result is listed in the legend of the figures. A p-value of $p \leq 0.05$ was accepted as statistically significant.

Results

hiPSCs cultured on Vitronectin™-coated substrate yield similar pluripotent characteristics.

hiPSCs were cultured on either Matrigel or Vitronectin™ for 5 consecutive days before passaging (Fig. 1A). Based on cell number, confluency and morphology, no significant differences were detected between the two groups (fig. 1B-D). Cells were stained for pluripotency markers Nanog and OCT3/4 and counterstained with Hoechst (fig. 1E). Quantification of the images showed no significant differences in the immunofluorescent signal/nucleus for all markers analyzed. These results indicate that Vitronectin™ is a suitable animal-free substitute for Matrigel.

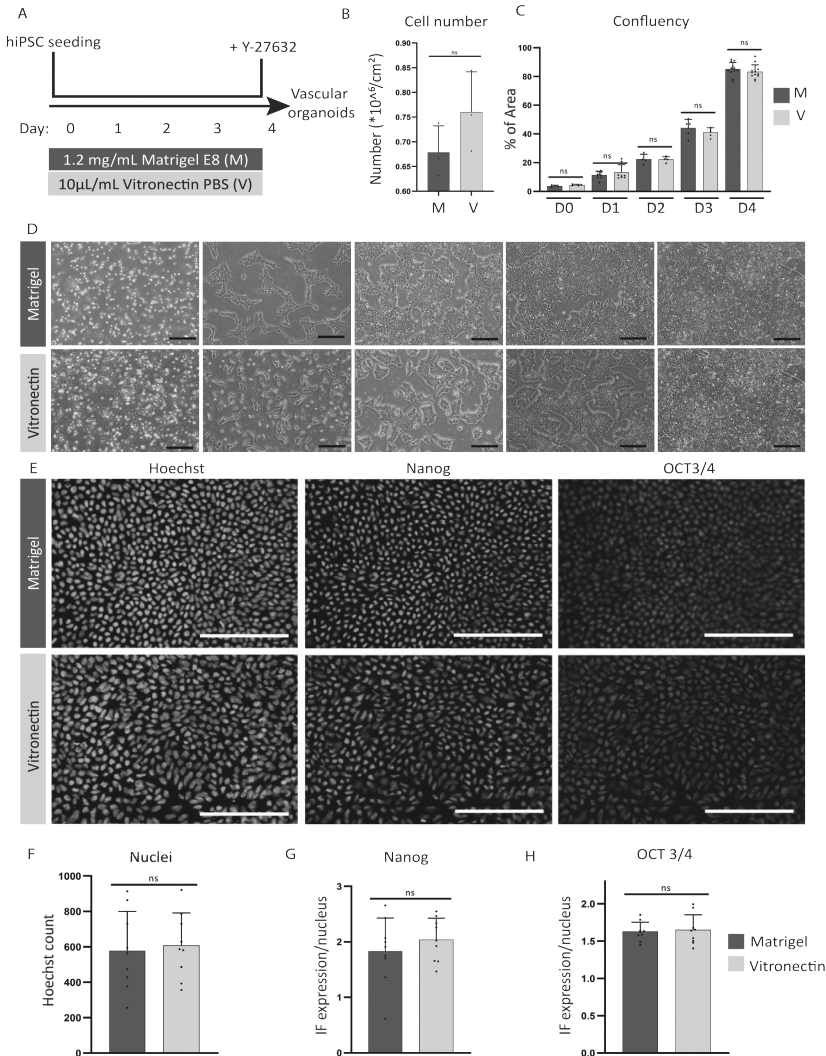
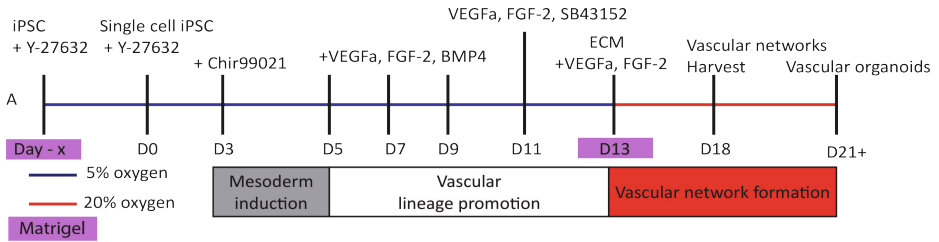


Figure 1. hiPSCs cultured on Vitronectin-coated substrate yield similar pluripotent characteristics.

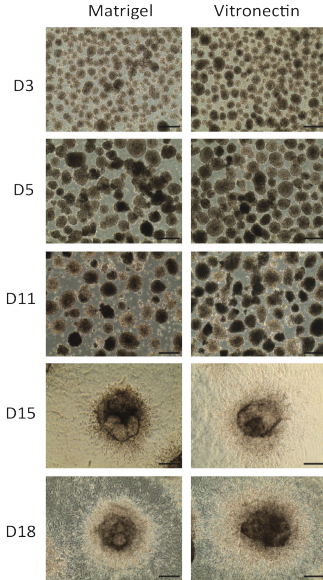
A. Schematic timeline of culturing hiPSCs until the step of induction of embryoid bodies (EB) in different coating conditions. **B.** Total cell number after 4 days of culturing. Error bars represent SD (standard deviation) of three consecutive passages. **C.** Confluency analysis per day of culturing. Error bars represent SD of three consecutive passages. **D.** hiPSCs cultured on Matrigel or Vitronectin during one passage (day 0 - 4). Scale bar depicts 200 μm. **E.** Immunostaining of hiPSC cultured on Matrigel or Vitronectin on day 4. Cells were stained for pluripotency markers NANOG, OCT4 and nuclei counterstained with Hoechst (left panel). Scale bars depict 200 μm. **F.** Total nuclei numbers on day 4 of culturing. Error bars represent SD of three consecutive passages. **G.** Quantification of pluripotency marker Nanog on day 4 of culturing. Error bars represent SD of three consecutive passages. **H.** Quantification of pluripotency marker OCT3/4 on day 4 of culturing. Error bars represent SD of three consecutive passages. Significance is determined by unpaired T-test or One-way ANOVA with tukey post hoc test, ns = not significant.

Vascular organoids derived from Vitronectin™ based hiPSCs show a similar differentiation pattern compared to Matrigel based hiPSCs.

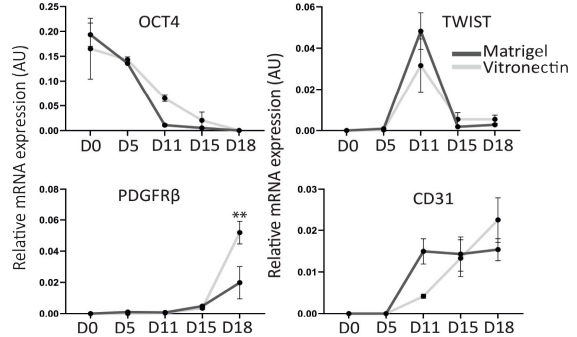
Vascular organoid differentiation takes 18-21 days, incorporating originally 2 Matrigel-based steps (Fig. 2A). To see whether Vitronectin™ coating for hiPSC culture impairs differentiation, the differentiation protocol was first continued in Matrigel, described in previous research ^{7,21}. During the differentiation process, bright field images were taken to detect any differences in size or shape between the vascular differentiation of Vitronectin™ derived hiPSCs and Matrigel derived hiPSCs (Fig. 2B). Gene expression analysis for pluripotency marker OCT4 did not show any significant differences in typical differentiation induced decline. Mesoderm marker TWIST indicated that the mesoderm developed as normal. Expression of mature vascular cell markers such as CD31 and PDGFr β were increased at the later timepoints in both groups, with the differentiation of Vitronectin derived hiPSCs inducing a significant higher expression of PDGFr β at D18 (fig. 2C). Additional markers for the different stages (Nanog, SNAIL, SLUG, CD34, VE-cadherin and ACTA2) were also tested showing similar results except for Matrigel derived hiPSCs producing higher expression levels of CD34 and VE-cadherin at D18 (Supplemental figure 1B).



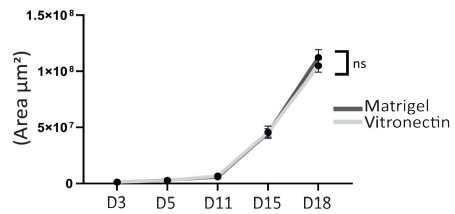
B Organoid growth timeline



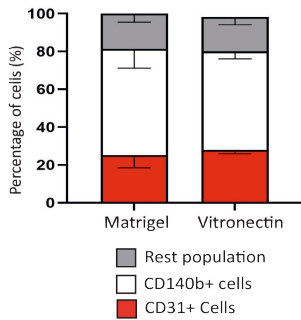
C Gene-expression pattern



D Surface area vascular organoids



E Vascular organoid composition



F Whole-mount staining

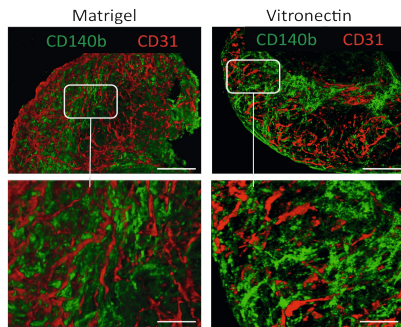


Figure 2. Vascular organoids derived from vitronectin based hiPSCs show a similar differentiation pattern compared to Matrigel based hiPSCs.

A. Schematic timeline of the differentiation process for both organoid groups. **B.** Bright field images of the organoids during the differentiation process (D0 – D18). Scale bar depicts 200 μm . **C.** Gene expression analysis of vascular organoids at different timepoints. Results represented as mean \pm SEM, $n = 4$ for Matrigel-based organoids and $n = 6$ for vitronectin-based organoids. One-way ANOVA with Tukey post hoc test. ** $p > 0.01$. **D.** Surface area over time (D3 – D18). $n = 24$ organoids for both groups. Results represented as mean \pm SEM. Unpaired T-test between timepoints, no significant differences between the organoid groups detected. **E.** Vascular organoid composition based on FACS results. Cell content is represented as the percentage of total cells measured. Results represented as mean \pm SEM, $n = 4$ for Matrigel-based organoids and $n = 6$ for vitronectin-based organoids. Unpaired T-test, no significant differences between organoid groups detected. **F.** Whole-mount staining of vascular organoids. Organoids are stained for endothelial cell marker CD31 (Red) and mural cell marker PDGFR β (Green). Scale bar depicts 200 μm for top panels (whole organoid) and 50 μm for bottom panels (zoomed-in on specific region).

Surface area quantification based on bright field imaging shows no significant differences in size at all timepoints (Fig. 2D). FACS analysis conducted on both groups on day 18 showed no significant differences in the composition of the vascular organoids (Fig. 2E). Whole mount staining confirmed the presence of similar structures in both Matrigel-based and Vitronectin™-based organoids (fig. 2F). These data indicate that Vitronectin™ can be used as an effective Matrigel replacement in standard hiPSCs culture.

Vascular organoids embedded in a fibrin gel show similar differentiation characteristics to vascular organoids embedded in Matrigel.

Based on our previous findings, hiPSC culture was switched from Matrigel to Vitronectin™ for all vascular organoid differentiation procedures for the rest of the experiments as previously described. The standard differentiation protocol requires a transfer from free floating culture (From day 0) to imbedding into a Matrigel 3D culture environment to initiate sprouting behavior at day 13.

To evaluate if this second Matrigel step can also be replaced, the culture was split into 2 groups on day 13; one group was embedded in a Matrigel-collagen gel according to the original protocol⁷ and the other group in a fibrin gel, as shown in the schematic timeline in figure 3A. The fibrin gel was created by mixing 0.1U/mL thrombin with 7.5mg/mL of fibrinogen. Bright field images show a similar growth-pattern in both conditions from day 13 with both conditions facilitating organoid sprouting (fig. 3B). Gene-expression analysis comparing both groups during differentiation shows no significant differences in expression of endothelial and mural cell markers between

fibrin-based and Matrigel-based organoids (fig. 3C). Mesoderm markers were also tested, showing a decrease in mesoderm expression as expected in both groups after embedding (supplemental fig. 2B).

Surface area quantification of bright field images confirms these findings, showing no significant differences in growth pattern up to day 18 (fig. 3D). FACS analysis of 18-day old organoids similarly shows that there are no significant differences in vascular organoid composition, indicating that both conditions facilitate vascular organoid development (fig. 3E). Whole mount staining of sprouting fibrinogen-embedded organoids, showed vascular structures composed of both endothelial and mural cells (fig. 3F), which are comparable to Matrigel-embedded organoids. These results indicate that fibrin-based gels can be used as a Matrigel alternative in hiPSC differentiation into vascular organoids.

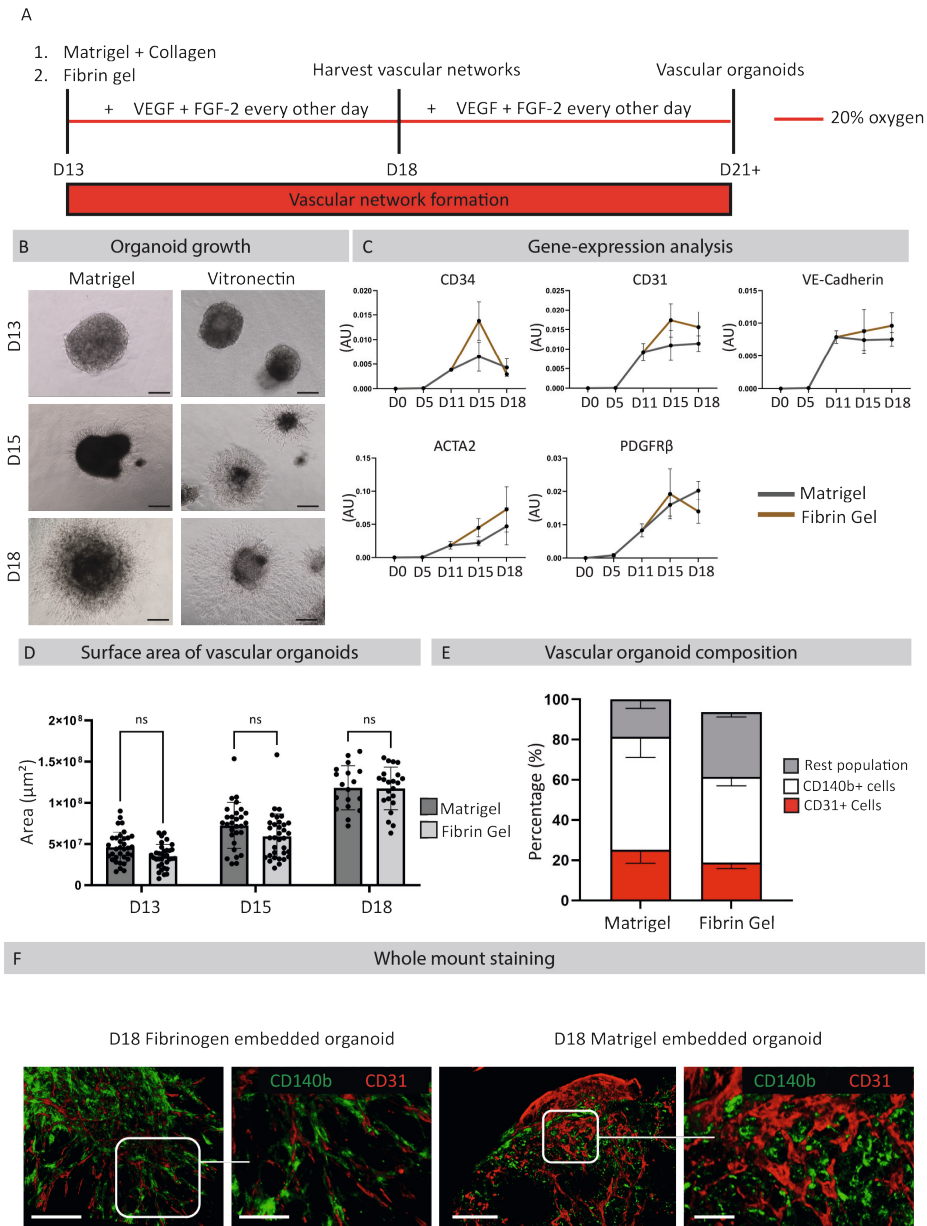


Figure 3. Vascular organoids embedded in fibrin gel show a similar differentiation pattern compared to organoids embedded in matrigel/collagen.

A. Schematic timeline of the differentiation process for both organoid groups. **B.** Bright field images of the organoids during the differentiation process (D13 – D18). Scale bar depicts 200 μm . **C.** Gene expression analysis of vascular organoids at different timepoints. Results represented as mean \pm SEM, $n = 6$ for both groups. One-way ANOVA with Tukey post hoc test. No significant differences between the organoid groups detected. **D.** Surface area over time (D13 – D18). $n = 12$ organoids for both groups. Results represented

as mean \pm SEM. Unpaired T-test between timepoints, no significant differences between the organoid groups detected. **E.** Vascular organoid composition based on FACS results. Cell content is represented as the percentage of total cells measured. Results represented as mean \pm SEM, $n = 6$ for both groups. Unpaired T-test, no significant differences between organoid groups detected. **F.** Whole-mount staining of vascular organoids. Organoids are stained for endothelial cell marker CD31 (Red) and mural cell marker PDGFR β (Green). Scale bar depicts 200 μ m for top panels (whole organoid) and 50 μ m for bottom panels (zoomed-in on selected region).

Discussion

Although Matrigel is cost-effective, versatile, and widely employed in BVO and other organoid cultures, its intricate hydrogel nature poses challenges. With over 1800 distinct proteins, it displays notable batch-to-batch variations in composition and mechanical properties, influencing both cell and organoid growth²²⁻²⁶. Considering these limitations, there is a pressing need to develop Matrigel-independent culture systems. In this context, we explored two potential alternatives to Matrigel within a previously described protocol^{7,21}, to work towards Matrigel-free vascular organoid differentiation.

When cultured on a Vitronectin™-coated substrate, hiPSCs exhibit pluripotent characteristics comparable to Matrigel-based hiPSCs and undergo similar differentiation into vascular organoids.

Multiple animal-free matrices, such as laminin, fibronectin and Vitronectin™ support human iPSC and ESC growth. For large scale usage, Vitronectin™ is the cheapest option with different types of vitronectin available on the market²⁷. It was described that, in combination with the use of a ROCK-inhibitor, Vitronectin™ supports initial attachment and survival of human ES and iPSCs as effectively as Matrigel^{13,28,29}. In line with these previous reports, in our study, hiPSCs expansion on Vitronectin™ coated plates did not affect the hiPSCs in terms of morphology, proliferation capacities, and gene-expression profiles. Previous studies have highlighted the impact of cell culture substrates on differentiation efficacy, suggesting a potential negative impact on the cells' pluripotency³⁰⁻³³. Here, we repeated the original protocol as described to differentiate hiPSCs derived BVOs^{7,21} but with hiPSC expanded on Vitronectin versus Matrigel coated substrate, to assess the impact on subsequent organoid differentiation. Based on gene-expression patterns, proliferation and differentiation capacities of hiPSCs and blood vessel organoids, our results indicate that vitronectin-based expansion of hiPSCs does not negatively influence the differentiation process of hiPSC derived vascular organoids. Consistent with these findings, prior research has shown the successful utilization of vitronectin as a substrate for hiPSC culture in the differentiation protocols for some organoids

and cell types such as cerebral organoids, pancreatic progenitor cells, and renal organoids^{27,34-36}. Here, our findings demonstrate for the first time, that vitronectin based hiPSC culture is also suitable for vascular organoid differentiation.

Vascular organoids embedded in a fibrin gel show similar differentiation characteristics to vascular organoids embedded in Matrigel.

In recent years, extensive research has explored alternatives to Matrigel for organoid culture, including decellularized ECM, gel-forming recombinant proteins, and synthetic hydrogels.

Customizing the organoid ECM substrate to match specific organoids is essential, as there is no universal alternative that fulfills all requirements. Different groups have successfully identified alternatives tailored to their applications; for example, gastrointestinal tissue-derived extracellular matrix hydrogels have proven effective for gastro-intestinal organoids, offering tissue-mimetic microenvironments³⁷. The use of decellularized ECM reduces the risk of immune responses and provides additional cues enhancing tissue regeneration³⁸. Different decellularization methods have been demonstrated for various tissues, such as human and murine kidneys, murine heart, human and porcine lung, and porcine testicular tissues, each presenting distinct challenges¹. However, different tissues requires distinct decellularization methods, hindering standardization and impacting reproducibility. Incomplete cellular remnants removal during decellularization may also trigger immune responses and reduce functionality. The complex native ECM, consisting of over 300 proteins with unique functions and stiffness levels, also complicates isolating variables for detailed studies on its impact on organoid behavior and development. Consequently, decellularized ECM may not be the most favorable option.

Alternatively, collagen based hydrogels have been used for intestine, kidney, colon and stomach organoids³⁹⁻⁴¹, alginate for PSC-derived intestinal organoids^{42,43} and fibrin-laminin for adult stem cell (ASC)-derived small intestinal, pancreatic and liver organoids⁴⁴. As chemical alternatives, PEG and PGLA have been used as an ECM alternative for cardiac, intestinal and lung organoids⁴⁵⁻⁴⁹. Combined, these studies highlight that the hydrogel requirements for organoid development may be different per organoid type, composition, and application, and should consider the biological and mechanical properties of the chosen substrate.

For vascular organoids or organoids containing ECs and vascular structures, there are currently no alternatives for Matrigel use in (human induced pluripotent) stem cell expansion and subsequent organoid differentiation. So far, only co-cultures involving mature primary human endothelial cells and supporting cells (pericytes or vascular smooth muscle cells (VSMCs) along with sprouting assays using Matrigel or animal-free gel types have been documented. Sprout formation can be triggered in both collagen and fibrin gels, with or without the supplementation of growth factors, across these different *in vitro* angiogenesis models⁵⁰⁻⁵⁴.

Fibrin stands out as a suitable choice for BVOs due to its rapid crosslinking, effectively preventing large organoids from settling to the plate's bottom and ensuring their encapsulation within the gel. Moreover, research indicates that fibrin-based hydrogels not only facilitate the growth of epithelial organoids, mesenchymal stem cells (MSCs), and endothelial cells but also support angiogenesis. Hence, they are theoretically ideal for vascular organoid differentiation^{19, 44, 55, 56}. Although fibrin is involved in the blood-clotting cascade and may not be the most suitable for use in graft implantation, the gel characteristics and potential human origin (in case of e.g. fibrinogen extraction from blood of donors, or the use of human recombinant fibrinogen) improves disease modeling and therapeutic screening options compared to Matrigel. Based on previous findings, a fibrin gel (7.5mg/mL fibrinogen, 0.1U/mL thrombin) was evaluated as a Matrigel substitute in the current study⁵⁷. In terms of differentiation efficacy, replacement of the Matrigel of the original protocol with fibrin showed no significant impact on gene-expression patterns, organoid size and end composition. Organoids cultured with vitronectin and fibrin exhibited sprouting vascular networks similar to Matrigel-derived controls. Further comprehensive examination of these organoids might involve employing sequencing techniques or proteomics to explore how the hydrogel composition impacts essential matrix elements, as observed in the context of gastrointestinal organoids³⁷.

In conclusion here we present, for the first time, a Matrigel-free protocol for hiPSC-derived vascular organoid culture. Culturing hiPSCs on Vitronectin™ yielded comparable morphology and growth efficacy to Matrigel-cultured hiPSCs. The change in cell culture substrate didn't hinder vascular organoid differentiation, confirming Vitronectin as a viable Matrigel alternative. Moreover, adopting a fibrin-based gel facilitated organoid differentiation, promoting vascular network formation and endothelial cell sprouting, with no significant differences observed in the final obtained organoids when compared to differentiation in Matrigel.

The new Matrigel-free protocol presented in this study, may find its use in a variety of applications where either Matrigel replacement or adherence to xeno-free culture conditions is preferred or required. Such applications include disease modeling, vascular tissue engineering, and patient-specific therapeutic screening.

Acknowledgements

This work was funded by the NWO vidi grant (no. 91714302 to CC). The authors gratefully acknowledge the Gravitation Program “Materials Driven Regeneration”, funded by the Netherlands Organization for Scientific Research (024.003.013).

Conflicts of interest

The authors declare no conflicts of interest

References

1. Kozlowski MT, Crook CJ, Ku HT. Towards organoid culture without Matrigel. *Commun Biol*. 2021;4(1):1387.
2. Hughes CS, Postovit LM, Lajoie GA. Matrigel: a complex protein mixture required for optimal growth of cell culture. *Proteomics*. 2010;10(9):1886-90.
3. Passaniti A, Kleinman HK, Martin GR. Matrigel: history/background, uses, and future applications. *J Cell Commun Signal*. 2022;16(4):621-6.
4. Heo JH, Kang D, Seo SJ, et al. Engineering the Extracellular Matrix for Organoid Culture. *Int J Stem Cells*. 2022;15(1):60-9.
5. Kleinman HK, Martin GR. Matrigel: basement membrane matrix with biological activity. *Semin Cancer Biol*. 2005;15(5):378-86.
6. Kleinman HK, Philp D, Hoffman MP. Role of the extracellular matrix in morphogenesis. *Curr Opin Biotechnol*. 2003;14(5):526-32.
7. Wimmer RA, Leopoldi A, Aichinger M, et al. Human blood vessel organoids as a model of diabetic vasculopathy. *Nature*. 2019;565(7740):505-10.
8. Lam MT, Longaker MT. Comparison of several attachment methods for human iPS, embryonic and adipose-derived stem cells for tissue engineering. *J Tissue Eng Regen Med*. 2012;6 Suppl 3(0 3):s80-6.
9. Rodin S, Domogatskaya A, Strom S, et al. Long-term self-renewal of human pluripotent stem cells on human recombinant laminin-511. *Nat Biotechnol*. 2010;28(6):611-5.
10. Pouliot N, Kusuma N. Laminin-511: a multi-functional adhesion protein regulating cell migration, tumor invasion and metastasis. *Cell Adh Migr*. 2013;7(1):142-9.
11. Miyazaki T, Futaki S, Hasegawa K, et al. Recombinant human laminin isoforms can support the undifferentiated growth of human embryonic stem cells. *Biochem Biophys Res Commun*. 2008;375(1):27-32.
12. Morin KT, Tranquillo RT. Guided sprouting from endothelial spheroids in fibrin gels aligned by magnetic fields and cell-induced gel compaction. *Biomaterials*. 2011;32(26):6111-8.
13. Chen G, Gulbranson DR, Hou Z, et al. Chemically defined conditions for human iPSC derivation and culture. *Nat Methods*. 2011;8(5):424-9.
14. Shen J, Zhu Y, Zhang S, et al. Vitronectin-activated alphavbeta3 and alphavbeta5 integrin signalling specifies haematopoietic fate in human pluripotent stem cells. *Cell Prolif*. 2021;54(4):e13012.
15. Fontes A, Macarthur CC, Lieu PT, et al. Generation of human-induced pluripotent stem cells (hiPSCs) using episomal vectors on defined Essential 8 Medium conditions. *Methods Mol Biol*. 2013;997:57-72.
16. Morin KT, Tranquillo RT. In vitro models of angiogenesis and vasculogenesis in fibrin gel. *Exp Cell Res*. 2013;319(16):2409-17.
17. Nakatsu MN, Davis J, Hughes CC. Optimized fibrin gel bead assay for the study of angiogenesis. *J Vis Exp*. 2007(3):186.
18. Nakatsu MN, Sainson RC, Aoto JN, et al. Angiogenic sprouting and capillary lumen formation modeled by human umbilical vein endothelial cells (HUVEC) in fibrin gels: the role of fibroblasts and Angiopoietin-1. *Microvasc Res*. 2003;66(2):102-12.

19. Brinkmann J, Malyaran H, Enezy-Ulbrich MAA, et al. Assessment of Fibrin-Based Hydrogels Containing a Fibrin-Binding Peptide to Tune Mechanical Properties and Cell Responses. *Macromolecular Materials and Engineering*. 2023;2200678.
20. Janmey PA, Winer JP, Weisel JW. Fibrin gels and their clinical and bioengineering applications. *J R Soc Interface*. 2009;6(30):1-10.
21. Meijer EM, Koch SE, van Dijk CGM, et al. 3D Human iPSC Blood Vessel Organoids as a Source of Flow-Adaptive Vascular Cells for Creating a Human-Relevant 3D-Scaffold Based Macrovascular Model. *Adv Biol (Weinh)*. 2023;7(1):e2200137.
22. Vukicevic S, Kleinman HK, Luyten FP, et al. Identification of multiple active growth factors in basement membrane Matrigel suggests caution in interpretation of cellular activity related to extracellular matrix components. *Exp Cell Res*. 1992;202(1):1-8.
23. Huch M, Knoblich JA, Lutolf MP, et al. The hope and the hype of organoid research. *Development*. 2017;144(6):938-41.
24. Nemir S, West JL. Synthetic materials in the study of cell response to substrate rigidity. *Ann Biomed Eng*. 2010;38(1):2-20.
25. Chaudhuri O. Viscoelastic hydrogels for 3D cell culture. *Biomater Sci*. 2017;5(8):1480-90.
26. Dahl-Jensen S, Grapin-Botton A. The physics of organoids: a biophysical approach to understanding organogenesis. *Development*. 2017;144(6):946-51.
27. Braam SR, Zeinstra L, Litjens S, et al. Recombinant vitronectin is a functionally defined substrate that supports human embryonic stem cell self-renewal via alphavbeta5 integrin. *Stem Cells*. 2008;26(9):2257-65.
28. Rowland TJ, Miller LM, Blaschke AJ, et al. Roles of integrins in human induced pluripotent stem cell growth on Matrigel and vitronectin. *Stem Cells Dev*. 2010;19(8):1231-40.
29. Rivera T, Zhao Y, Ni Y, et al. Human-Induced Pluripotent Stem Cell Culture Methods Under cGMP Conditions. *Curr Protoc Stem Cell Biol*. 2020;54(1):e117.
30. LaFosse PK, Zamponi M, Mollica PA, et al. Effect of substrate coating material on spontaneous activity of human-induced pluripotent stem cell-derived neuronal stem cells.
31. Lee CH, Hunt D, Roth JG, et al. Tuning pro-survival effects of human induced pluripotent stem cell-derived exosomes using elastin-like polypeptides. *Biomaterials*. 2022;291:121864.
32. Sagrac D, Senkal S, Hayal TB, et al. Surface coating materials regulates the attachment and differentiation of mouse embryonic stem cell derived embryoid bodies into mesoderm at culture conditions. *Cytotechnology*. 2022;74(2):293-307.
33. Prajapati C, Ojala M, Lappi H, et al. Electrophysiological evaluation of human induced pluripotent stem cell-derived cardiomyocytes obtained by different methods. *Stem Cell Res*. 2021;51:102176.
34. Pedraza-Arevalo S, Cujba AM, Alvarez-Fallas ME, et al. Differentiation of beta-like cells from human induced pluripotent stem cell-derived pancreatic progenitor organoids. *STAR Protoc*. 2022;3(3):101656.
35. Wiersma LE, Avramut MC, Lievers E, et al. Large-scale engineering of hiPSC-derived nephron sheets and cryopreservation of their progenitors. *Stem Cell Res Ther*. 2022;13(1):208.
36. Hong YJ, Lee SB, Choi J, et al. A Simple Method for Generating Cerebral Organoids from Human Pluripotent Stem Cells. *Int J Stem Cells*. 2022;15(1):95-103.

37. Kim S, Min S, Choi YS, et al. Tissue extracellular matrix hydrogels as alternatives to Matrigel for culturing gastrointestinal organoids. *Nat Commun.* 2022;13(1):1692.
38. Giobbe GG, Crowley C, Luni C, et al. Extracellular matrix hydrogel derived from decellularized tissues enables endodermal organoid culture. *Nat Commun.* 2019;10(1):5658.
39. Jabaji Z, Sears CM, Brinkley GJ, et al. Use of collagen gel as an alternative extracellular matrix for the in vitro and in vivo growth of murine small intestinal epithelium. *Tissue Eng Part C Methods.* 2013;19(12):961-9.
40. Sachs N, Tsukamoto Y, Kujala P, et al. Intestinal epithelial organoids fuse to form self-organizing tubes in floating collagen gels. *Development.* 2017;144(6):1107-12.
41. Jee JH, Lee DH, Ko J, et al. Development of Collagen-Based 3D Matrix for Gastrointestinal Tract-Derived Organoid Culture. *Stem Cells Int.* 2019;2019:8472712.
42. Capeling MM, Czerwinski M, Huang S, et al. Nonadhesive Alginate Hydrogels Support Growth of Pluripotent Stem Cell-Derived Intestinal Organoids. *Stem Cell Reports.* 2019;12(2):381-94.
43. Patel SN, Ishahak M, Chaimov D, et al. Organoid microphysiological system preserves pancreatic islet function within 3D matrix. *Sci Adv.* 2021;7(7).
44. Broguiere N, Isenmann L, Hirt C, et al. Growth of Epithelial Organoids in a Defined Hydrogel. *Adv Mater.* 2018;30(43):e1801621.
45. Cruz-Acuna R, Quiros M, Huang S, et al. PEG-4MAL hydrogels for human organoid generation, culture, and in vivo delivery. *Nat Protoc.* 2018;13(9):2102-19.
46. Hoang P, Kowalczewski A, Sun S, et al. Engineering spatial-organized cardiac organoids for developmental toxicity testing. *Stem Cell Reports.* 2021;16(5):1228-44.
47. Cruz-Acuna R, Quiros M, Farkas AE, et al. Synthetic hydrogels for human intestinal organoid generation and colonic wound repair. *Nat Cell Biol.* 2017;19(11):1326-35.
48. Dye BR, Youngblood RL, Oakes RS, et al. Human lung organoids develop into adult airway-like structures directed by physico-chemical biomaterial properties. *Biomaterials.* 2020;234:119757.
49. Davoudi Z, Peroutka-Bigus N, Bellaire B, et al. Intestinal organoids containing poly(lactic-co-glycolic acid) nanoparticles for the treatment of inflammatory bowel diseases. *J Biomed Mater Res A.* 2018;106(4):876-86.
50. Dietrich F, Lelkes PI. Fine-tuning of a three-dimensional microcarrier-based angiogenesis assay for the analysis of endothelial-mesenchymal cell co-cultures in fibrin and collagen gels. *Angiogenesis.* 2006;9(3):111-25.
51. Rioja AY, Tiruvannamalai Annamalai R, Paris S, et al. Endothelial sprouting and network formation in collagen- and fibrin-based modular microbeads. *Acta Biomater.* 2016;29:33-41.
52. Feng X, Tonnesen MG, Mousa SA, et al. Fibrin and collagen differentially but synergistically regulate sprout angiogenesis of human dermal microvascular endothelial cells in 3-dimensional matrix. *Int J Cell Biol.* 2013;2013:231279.
53. Lawley TJ, Kubota Y. Induction of morphologic differentiation of endothelial cells in culture. *J Invest Dermatol.* 1989;93(2 Suppl):59S-61S.
54. Kanzawa S, Endo H, Shioya N. Improved in vitro angiogenesis model by collagen density reduction and the use of type III collagen. *Ann Plast Surg.* 1993;30(3):244-51.

55. Murphy KC, Whitehead J, Zhou D, et al. Engineering fibrin hydrogels to promote the wound healing potential of mesenchymal stem cell spheroids. *Acta Biomater.* 2017;64:176-86.
56. Chung E, Rytlewski JA, Merchant AG, et al. Fibrin-based 3D matrices induce angiogenic behavior of adipose-derived stem cells. *Acta Biomater.* 2015;17:78-88.
57. van Dijk CGM, Brandt MM, Poulis N, et al. A new microfluidic model that allows monitoring of complex vascular structures and cell interactions in a 3D biological matrix. *Lab Chip.* 2020;20(10):1827-44.

Supplemental information



CHAPTER

9



General Discussion

Summary and general discussion

The heterogeneity and complexity of the vasculature requires in-depth fundamental research to gain a deeper comprehension of the interactions among various vascular cell types in development and disease. This understanding is crucial for improving strategies in vascularized tissue engineering, the development of pre-vascularization constructs, and the creation of personalized disease models. In this thesis, we aimed to create and test a human induced pluripotent stem cell (hiPSC)-derived cell source for various vascular (re-)generation strategies and enhance our understanding of their use in the development of advanced disease models. We hypothesized that vascular cells derived from hiPSCs vascular organoids are suitable for micro-and macrovascular regeneration strategies and disease modeling.

The use of tissue specific cells is crucial in the development of vascular models

In the first part of this thesis, we focused on the use of suitable vascular cells for tissue engineering purposes and disease modeling. The critical factor we considered is the significant variation in the morphology, density, and functionality of vascular cell populations found throughout the human body. In these first chapters, we focused on the development and characterization of a suitable cell source; hiPSC-derived blood vessel organoids (BVOs).

In **Chapter 2** we described the distinctions among microvascular pericytes distributed throughout the vascular network. These cells exhibit varying morphological features and functions that are influenced by their specific locations within the vascular tree. In microvascular research, brain pericytes are often used, mostly in a pool derived from isolated human brain tissue from different donors. As outlined in **Chapter 2**, pericytes located in the brain exhibit distinctly different morphological characteristics and functions when compared to those found in other organs such as the lungs, heart, or kidneys. The process of extracting pericytes from various tissue locations is both invasive and complex, underscoring the growing necessity and demand for the differentiation of patient-derived pluripotent cells into these specific mural cell types for regenerative and disease modeling use.

HiPSCs, more so than embryonic stem cells (ESCs), hold promise in the field of regenerative medicine as therapeutic products. ESCs, despite their ability to differentiate into any desired cell type, come with two significant drawbacks¹. Firstly, there's an ethical concern because the acquisition of these cells requires human embryos². Secondly, since ESCs cannot be obtained from individual patients,

the transplantation of constructs based on ESCs is associated with a high risk of immunological rejection³. Conversely, hiPSCs can be obtained non-invasively from adult individuals, including the patients requiring therapy, and exhibit comparable differentiation capabilities to ESCs.

In **chapter 2** we described the heterogeneity of pericytes throughout the human body, and reviewed their interaction mechanism and that of vascular smooth muscle cells (VSMCs) with endothelial cells (ECs)⁴⁻⁷. In the case of ECs, one of the primary challenges is maintaining organ specific cell functions *in vitro*. Fortunately, for modeling purposes, a wide array of commercially available ECs makes it feasible to adequately mimic particular segments of the vascular tree *in vitro*. Nonetheless, the clinical application of these primary human endothelial cells for *in vivo* regeneration is severely limited due to the potential for immune responses since they do not mirror the genetic and immunogenic background of individual patients. Recently, multiple differentiation protocols for hiPSCs into various cell types have been published, leading to the development of mature cells that closely resemble the morphology, gene expression patterns, and functions of the desired cell types. For example, in the context of cardiac regeneration, hiPSC-derived cardiomyocytes recapitulate phenotypic differences caused by (disease associated) genetic variations in patients⁸. In **Chapter 4 and 5** of this thesis, both vascular organoid based hiPSC-derived ECs and VSMCs are directed via our newly developed differentiation protocols into a specific functional subtype of their cell type.

Evaluating human iPSC-derived blood vessel organoids as a viable source for vascular cells

In **chapter 3**, we differentiated hiPSCs into blood vessel organoids (BVOs) following a previously described protocol⁹. These BVOs form vascular networks that contain ECs and mural cells with both pericyte and VSMC characteristics. In the past, the creation of vascular structures using hiPSCs primarily relied on a combination of 2D differentiation methods to establish a vascular network *in vitro*^{10,11}. However, since the introduction of BVOs in 2019, these 3D models have found diverse applications, ranging from developmental studies and disease modeling to the development of (pre-)vascularization constructs. In the original study, BVOs were transplanted beneath the renal capsule in mice, where they successfully integrated with the host vasculature, indicating the functionality of the vascular cells after implantation⁹. In 2023, it was confirmed that BVOs are capable of rapidly responding to metabolic changes. Using BVOs, this research also identified connective tissue growth factor as a new component in maintaining microvascular stability¹². Co-differentiation of both ECs and mural cells in 3D, as described in another protocol, enables EC-

mural cell interactions which promote self-organization into vascular networks. Different growth factor treatments during differentiation enable the specification of arterial and venous structures, facilitating the study of early aspects of vascular development¹³. In **chapter 3**, vascular ECs and mural cells were extracted from the BVOs (respectively Organoid-derived Endothelial Cells (ODECs) and Organoid-derived Mural cells (ODMCs)) and expanded for in-depth validation. It has frequently been described that cells exhibit distinct different behavior in a two-dimensional (2D) setting compared to a more natural 3D environment^{14, 15}. The differentiation protocol for blood vessel organoids involves the use of growth factors and internal cellular responses to direct differentiation into mature vascular cells within a 3D environment. This allows for the monitoring of various differentiation steps, as described in the chapter. Upon extraction from the BVOs, gene and protein expression levels in ODECs and ODMCs are comparable to their expression in the 3D organization. Furthermore, validation of the ODECs demonstrated barrier functionality and shear stress responsiveness that were equivalent to those observed in HUVECs, serving as the control group. In **chapter 3**, ODECs and ODMCs were used to seed a PCL-BU scaffold, enabling the examination of shear stress response and remodeling in a 3D macrovascular setting. This experimental set-up confirmed the functionality of these vascular cells. While the cells successfully integrated and colonized the scaffold and responded to shear stress, these constructs do not closely resemble physiological blood vessels due to limited tissue formation during short period of *ex vivo* culture. However, it has been previously described that pre-cellularization of constructs further improves anastomosis and tissue formation upon implantation^{16, 17}. Thus, using patient-(hiPSCs) derived cells for pre-cellularization of scaffolds has the potential to enhance the likelihood of a successful anastomosis following implantation. Extended cultivation of these constructs could result in improved colonization of the scaffold for regenerative applications, which may also facilitate the development of patient-specific disease models and drug screening platforms that we aim to develop in the field.

Due to the variability of ECs found across the vascular network, it is necessary to select appropriate cells tailored to the specific needs of either a disease model or a tissue-engineered structure. In **chapter 4**, we explored the feasibility of generating a fenestrated EC culture from the naturally non-fenestrated ODECs. We demonstrated that iPSC-derived cells can be guided toward a desired subtype of their cell population even after initial differentiation to a “mature” state. The significance of fenestrations is discussed in **chapter 4**, yet the use of fenestrated cells in tissue-engineered constructs is only very limitedly explored. Recently, electrospinning was used to create artificial fenestrated capillary vessels¹⁸. These

nano porous microtubes have tunable morphological features and could serve as capillary vessels for microvascular tissue engineering. However, fenestrae are not solid structures, but dynamic diaphragms developing and disappearing according to the vascular network's needs and surrounding stimuli. Therefore, an improved understanding of the requirements in the environment that need to be met to introduce and stabilize functional fenestrated ECs in semi and fully biological microvascular constructs is essential. Current understanding of fenestrae biology is limited, with most of the research dating back several decades and lacking updates. Research for exerting control over fenestrae in iPSC-derived ECs is currently completely lacking. In structure, each fenestra has a cart-wheel shaped membrane acting as a diaphragm. The best-known component of these fenestral diaphragms in fenestrated primary ECs is Plasmalemma Vesicle Associated Protein (PLVAP)¹⁹⁻²³, which is involved in regulating endothelial permeability. It has been established that PLVAP *in vivo* is present in vascular beds containing diaphragmed fenestrae and is only absent from fenestrated endothelia of the adult liver sinusoids and kidney glomerulus, which are devoid of diaphragms^{22, 24, 25}. *In vitro* assays suggest that fenestrae formation is unlikely to depend only on the presence of PLVAP²⁶. However, the dysmorphic appearance of fenestrae and disorganized sieve plates after PLVAP knockdown suggest that PLVAP presence is required for the fenestrae development and stabilization²³. The reduction of diaphragms in fenestrae, observed after PLVAP knockdown, is consistent with previous reports showing that PLVAP is the major constituent of caveolar and fenestral diaphragms. Our main findings in **chapter 4** suggest that the use of both VEGF and PMA induces fenestral diaphragm formation in our ODECs. However, these diaphragms are not located within the structures termed "sieve plates," which consist of a small cluster of fenestrae on the cell membrane. The formation of fenestral diaphragms that we observed in ODECs after treatment was accompanied by increased PLVAP levels, were similar in size as previously described *in vivo* counterparts²⁷ and demonstrated permeability function. This suggests that fenestrae formation indeed occurs, but it is possible that the development of sieve plates may necessitate supplementary factors that have not yet been identified. Future studies may include omics analysis to gain further insights in these additional factors required for fenestrae and fenestral diaphragm formation and alteration, as well sieve plate clustering. The discovery of these new components could potentially pave the way for novel targets in the regulation of fenestrae within cells, both in advanced *in vitro* disease model systems and advanced (pre-)vascularization constructs.

Ranging from microvascular arterioles to macrovascular structures, it is crucial to consider the plasticity of VSMCs when designing vascular constructs. In **chapter 5**, our primary goal was focused on whether our ODMCs could successfully transition their more pericyte like cell-type in the vascular organoids to mimic arterial VSMCs and, if so, what biological and mechanical stimuli are responsible for this cell type and phenotypic switch. One of the key attributes of mature vessel VSMCs is their state of (contractile) quiescence, enabling them to manage vessel dynamics and prevent infiltration in the intima and (hyper)proliferation of mural cells. In the context of neovascularization, VSMCs are in their synthetic state with elevated rates of proliferation, migratory behavior, and ECM deposition. When cultivated in 2D, VSMCs are maintained in their synthetic (proliferative) state to facilitate the expansion of the cells. To successfully mimic a functional tunica media for a disease model or tissue engineered construct, the VSMCs must switch to a quiescent, more contractile state. Introducing this contractile phenotype in VSMC in e.g. (pre) vascularized graft strategies or *in vitro* disease model poses a challenge as this limits effective expansion. A viable solution may lie in developing a culture protocol capable of inducing the contractile state in a mature VSMC population, after tissue generation for the application is complete. Induction of the contractile phenotype can be achieved using suitable scaffold designs, cell culture media formulations, cell-cell interactions, and the application of mechanical stimulation to VSMCs in dynamic cell culture systems. These factors can be particularly effective when applied in combination²⁸. In **chapter 5**, the influence of growth factors, environmental stiffness and mechanical stretch are studied and evaluated for their potential of creating VSMCs from ODMCs and subsequently guiding these into the desired contractile or synthetic phenotype. The combination of these findings with the model described in **chapter 3** could lead to increased functionality of the construct upon implantation. Based on our findings in **chapter 5**, we can conclude that the hiPSC-derived VSMCs are able to sense and respond to mechanical cues and adapt their phenotype accordingly.

The use of vascular shear stress and wall stretch in vascularized tissue engineering: a step closer to physiological differentiation and development.

In the second part of this thesis, we included mechanical cues in a complex atherosclerosis-on-a-chip model to see the effect on immune response and plaque development. In an extensive review in **chapter 6**, the effect of mechanical forces on vascular homeostasis and regenerative processes are described. As outlined in the introduction, ECs and mural cells have the capability to detect mechanical stress and respond to alterations in vascular motion. This chapter highlights that vascular shear

stress levels are maintained through diameter adaptations via vaso-regulation, adjusting vascular tone. Likewise, wall stretch elicits a physiological response that induces and maintains a contractile VSMC phenotype. However, excessive mechanical forces result in pathological deviations in vascular wall adaptation and remodeling. Hence, considering mechanical forces and providing such stimuli within a physiological range should therefore be considered crucial for the development of new *in vitro* vascular models, as well as new vascular regenerative strategies. **chapters 3 and 5** subjected both ODECs and ODMCs to mechanical stretch and shear stress. It has been documented that incorporating shear stress along with growth factors in differentiation protocols enhances EC differentiation and maturation by activating the notch signaling pathways²⁹⁻³¹. The methods presented in **chapter 3**, where the ODECs were used to line the inner wall of the PCL-BU scaffold supported by the ODMCs in the media, represent a complex *in vitro* model in which the impact of mechanical forces such as shear stress can be evaluated. Given our findings in **chapter 5**, where we observed that hiPSC-derived VSMCs transition to a contractile phenotype when exposed to stretching, adaptations in the scaffold design that would allow future incorporation of physiological relevant strain dynamics would further advance this model to one that allows the study of phenotype switching of VSMCs. The response of blood vessels to physiological and pathological stimuli partly depends on the crosstalk between EC lining the luminal side and VSMCs in the inner part of the vascular wall. To sustain the functional contractile phenotype of the VSMCs, a continuous release of paracrine compounds from ECs is also required³². However, in instances of mechanical or chemical injury or endothelial loss, the crosstalk between the VSMCs and ECs is disturbed. This perturbation serves as a catalyst for phenotypic and functional alterations in VSMCs, transitioning them from a contractile to a proliferative state, accompanied by inflammatory responses and extracellular matrix (ECM) deposition^{33, 34}. Collectively, these events characterize the manifestation of pathological vascular wall remodeling. The combination of using suitable cell populations and the application of shear stress and wall stretch during a cell-seeded scaffold formation and maturation could contribute to the creation of a more physiologically relevant disease model or a construct suitable for transplantation.

The benefits of using hiPSC-derived cells in advanced 3D disease models

Monitoring of early disease progression using animal models is very time-consuming and expensive. Moreover, animal models often do not precisely replicate human systems. In **chapter 7**, we established an atherosclerosis-on-a-chip model to closely examine cell-cell interactions during the initial phases of this disease and assess the

impact of mechanical factors on disease progress without the use of animals. This approach also offers the potential to employ patient-derived cells in the system. The chip model enables the co-culture of different cell types and here we included ECs, VSMCs, foam cells, and THP-1 monocytes, as demonstrated in **chapter 7**. Organ-on-a-chip models have recently gained significant attention for investigating early disease development *in vitro*. All models have different forms and functions, but most of them have hollow channels where cells can be seeded and the material in the construct is able to give or receive mechanical cues to better mimic the organ or disease state³⁵. In 2011, Huh et al. developed the “lung-on-a-chip”, where human lung alveolar epithelial cells were co-cultured with vascular endothelium to recreate the alveolar-capillary interface³¹. This model introduced living bacteria to the construct to mimic pulmonary inflammation and infection which resulted in recruitment of circulating immune cells, mimicking the innate cellular response to these pathologies. Perfusion with anti-cancer drug interleukin-2 (IL-2) in this system resulted in vascular leakage and infiltration of fluids in the air channel. This approach was able to replicate pulmonary oedema *in vitro*³⁶. In the case of the heart, a 3D printed construct was utilized to culture hiPSC-derived cardiomyocytes alongside ECs to assess the impacts of the anti-cancer drug doxorubicin³⁹. They observed that doxorubicin has a notable impact on reducing the beating rate of cardiomyocytes. However, endothelialized cardiac organoids continued to exhibit a high beating rate, indicating that endothelial cells may play a role in enhancing cardiac performance. Incorporating hiPSCs into these organ-on-a-chip systems offers the potential to create disease models and drug screening platforms tailored to the (epi)genetic makeup of specific diseases. Thus, utilizing patient-derived cells could offer valuable insights into issues related to vascular development, immune responses, and drug reactions.

The validation of the atherosclerosis-on-a-chip model, as elucidated in **chapter 7**, was conducted using standardized cell lines, namely HUVECs and aortic VSMCs. To enhance the clinical applicability, the integration of hiPSC-derived vascular and PBMCs (derived immune cells) from the same donor source, employing both ODECs and ODMCs as previously detailed, could be considered for this system. While this thesis thoroughly covers the differentiation of hiPSCs into vascular cells, it's worth noting that previous research has also successfully differentiated both macrophages and monocytes from hiPSCs. Consequently, either the PBMCs from matched donors, or hiPSC immune cells could also be incorporated into early-stage disease models, allowing disease modeling with all required cell types to recreate a unique patient-specific construct.⁴⁰⁻⁴².

Replacing animal-derived ECM is an important step towards clinical translation

Finally, we highlight a concern in molecular research concerning the utilization of 3D (organoid) cultures. Many 3D organoid cultures involve embedding in a 3D extracellular matrix (ECM), with Matrigel or similar products being commonly used in most protocols. Furthermore, a majority of hiPSCs are cultivated in 2D on Matrigel. It is important to note that Matrigel, or the alternatives Cultrex BME, and Geltrex are all derived from Engelbreth-Holm-Swarm sarcomas in mice. The benefits of using these products are that they are packed with ECM proteins, including laminin, collagen IV, entactin and heparin sulphate proteoglycan perlecan, allowing extensive cell growth and proliferation. Nevertheless, these ECM-like gels have significant batch-to-batch variations due to their origin, and the precise composition remains inadequately characterized, thus prohibiting their clinical use. To develop uniform, xeno-free stem cell populations for disease modeling and regenerative strategies, it is necessary to explore alternatives to these matrices. Over the past years, multiple synthetic alternatives to animal-based cell culture substrates for hiPSCs have been proposed. Human- and other animal-derived alternatives such as gelatin, collagen and fibrinogen have been used as natural alternatives for hiPSC culture and expansion. Additionally, vitronectin, a xeno-free, defined recombinant human protein alternative, has been used⁴³ and shows promising results towards clinical translation^{44, 45}. Vitronectin is a multifunctional glycoprotein present in blood and ECM, coded by the VTN gene. Standardized recombinant gene products offer advantages such as optimized protocol control and limited batch to batch differences, as well as reduced chance of immunogenic rejection, thanks to its human origin. As described in **chapter 8**, we found that vitronectin as a recombinant human ECM-based substrate is a suitable cell culture alternative for hiPSC derived BVO differentiation. In the original BVO differentiation protocol, Matrigel is employed as a 3D extracellular matrix to facilitate sprouting and the maturation of cells. Synthetic alternatives to Matrigel have been explored, including polyacrylamide (PAM) and polyethylene glycol (PEG) derived gels⁴⁶. These materials offer advantages such as tunable physical and biological properties, control over composition, and defined biofunctional characteristics. Nevertheless, the development of suitable synthetic alternatives presents challenges such as the constrained ability to replicate the complexity of the natural ECM, the inherently bioinert characteristics, issues related to polymerization, and a shortfall in addressing cell-specific requirements. Despite these hurdles, the widespread interest in this field has inspired numerous research groups to actively pursue the development of synthetic alternatives that closely emulate Matrigel-like ECMs. The next best option would be a human-derived alternative, such as a fibrin gel. Fibrin is a gel formed by the rapid crosslinking of

fibrinogen and thrombin when combined. In previous research, fibrin has effectively played a role in guiding, enhancing, and sustaining sprout development⁴⁷⁻⁵⁰. As described in **chapter 8**, fibrin is a suitable human-derived alternative to Matrigel matrices for 3D BVO development. Further validation, which includes the extraction of ODECs and ODMCs from the BVOs as previously described in **chapter 3**, would represent a significant stride towards facilitating the clinical translation of these organoids. Furthermore, the adoption of human alternatives can reduce the number of animals needed for both fundamental and translational research.

Concluding remarks and future directions

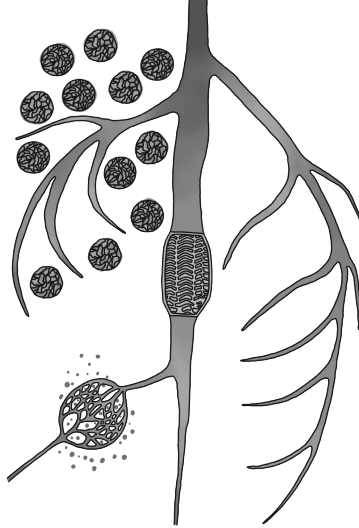
The studies described in this thesis conclude that hiPSC-derived vascular cells hold promise for both macrovascular and microvascular tissue engineering strategies. The findings presented lay a foundation for future studies exploring the application of tissue-specific cells derived from patients for vascularized tissue engineering applications. The advantages associated with the use of human-derived and, in the future, patient-specific cells represent a significant stride towards personalized disease modeling, offering prospects for new therapeutic targets, treatment alternatives, and, ideally, enhanced patient care. In-depth investigation if both ODECs and ODMCs show that these cells, derived from BVOs are able to adapt to their environment, differentiate into the desired cell type and show functional behavior comparable to primary human vascular cells. This opens up possibilities of using a single hiPSC population for multiple (vascular) regeneration strategies. The benefits of hiPSCs encompass the ability to generate not only vascular cells but also other cell types, such as immune cells, from the same cell population. This would enable the development of entirely patient-specific disease models, facilitating drug screening and the identification of therapeutic targets. The combination of vascularized tissue engineering strategies and advanced disease modeling will improve the translation of *in vitro* generated data to clinical applications. Based on this, we conclude that the vascularized tissue engineering research field would greatly benefit from future research into the use, expansion, and application of patient-derived hiPSCs into advanced disease models and personalized medicine.

References

1. Takahashi K, Tanabe K, Ohnuki M, et al. Induction of pluripotent stem cells from adult human fibroblasts by defined factors. *Cell*. 2007;131(5):861-72.
2. Takahashi K, Yamanaka S. Induction of pluripotent stem cells from mouse embryonic and adult fibroblast cultures by defined factors. *Cell*. 2006;126(4):663-76.
3. Taylor CJ, Bolton EM, Bradley JA. Immunological considerations for embryonic and induced pluripotent stem cell banking. *Philos Trans R Soc Lond B Biol Sci*. 2011;366(1575):2312-22.
4. Gifre-Renom L, Daems M, Luttun A, et al. Organ-Specific Endothelial Cell Differentiation and Impact of Microenvironmental Cues on Endothelial Heterogeneity. *Int J Mol Sci*. 2022;23(3).
5. van Kuijk K, Kuppe C, Betsholtz C, et al. Heterogeneity and plasticity in healthy and atherosclerotic vasculature explored by single-cell sequencing. *Cardiovasc Res*. 2019;115(12):1705-15.
6. Rensen SS, Doevendans PA, van Eys GJ. Regulation and characteristics of vascular smooth muscle cell phenotypic diversity. *Neth Heart J*. 2007;15(3):100-8.
7. Denzer L, Muranyi W, Schrotten H, et al. The role of PLVAP in endothelial cells. *Cell Tissue Res*. 2023;392(2):393-412.
8. Di Baldassarre A, Cimetta E, Bollini S, et al. Human-Induced Pluripotent Stem Cell Technology and Cardiomyocyte Generation: Progress and Clinical Applications. *Cells*. 2018;7(6).
9. Wimmer RA, Leopoldi A, Aichinger M, et al. Human blood vessel organoids as a model of diabetic vasculopathy. *Nature*. 2019;565(7740):505-10.
10. Kurokawa YK, Yin RT, Shang MR, et al. Human Induced Pluripotent Stem Cell-Derived Endothelial Cells for Three-Dimensional Microphysiological Systems. *Tissue Eng Part C Methods*. 2017;23(8):474-84.
11. Vila Cuenca M, Cochrane A, van den Hil FE, et al. Engineered 3D vessel-on-chip using hiPSC-derived endothelial- and vascular smooth muscle cells. *Stem Cell Reports*. 2021;16(9):2159-68.
12. Romeo SG, Secco I, Schneider E, et al. Human blood vessel organoids reveal a critical role for CTGF in maintaining microvascular integrity. *Nat Commun*. 2023;14(1):5552.
13. Bertucci T, Kakarla S, Winkelmann MA, et al. Direct differentiation of human pluripotent stem cells into vascular network along with supporting mural cells. *APL Bioeng*. 2023;7(3):036107.
14. Kapalczyńska M, Kolenda T, Przybyła W, et al. 2D and 3D cell cultures - a comparison of different types of cancer cell cultures. *Arch Med Sci*. 2018;14(4):910-9.
15. Duval K, Grover H, Han LH, et al. Modeling Physiological Events in 2D vs. 3D Cell Culture. *Physiology (Bethesda)*. 2017;32(4):266-77.
16. Scarritt ME, Pashos NC, Bunnell BA. A review of cellularization strategies for tissue engineering of whole organs. *Front Bioeng Biotechnol*. 2015;3:43.
17. Fayon A, Menu P, El Omar R. Cellularized small-caliber tissue-engineered vascular grafts: looking for the ultimate gold standard. *NPJ Regen Med*. 2021;6(1):46.
18. Qavi I, Tan G. Process control of electrospinning artificial fenestrated capillary vessels. *Materials & Design*. 2023;227:111708.

19. Aird WC. Phenotypic heterogeneity of the endothelium: I. Structure, function, and mechanisms. *Circ Res*. 2007;100(2):158-73.
20. Auvinen K, Lokka E, Mokkalala E, et al. Fenestral diaphragms and PLVAP associations in liver sinusoidal endothelial cells are developmentally regulated. *Sci Rep*. 2019;9(1):15698.
21. Bosma EK, van Noorden CJF, Schlingemann RO, et al. The role of plasmalemma vesicle-associated protein in pathological breakdown of blood-brain and blood-retinal barriers: potential novel therapeutic target for cerebral edema and diabetic macular edema. *Fluids Barriers CNS*. 2018;15(1):24.
22. Stan RV, Kubitzka M, Palade GE. PV-1 is a component of the fenestral and stomatal diaphragms in fenestrated endothelia. *Proc Natl Acad Sci U S A*. 1999;96(23):13203-7.
23. Herrnberger L, Seitz R, Kuespert S, et al. Lack of endothelial diaphragms in fenestrae and caveolae of mutant Plvap-deficient mice. *Histochem Cell Biol*. 2012;138(5):709-24.
24. Braet F, Wisse E. Structural and functional aspects of liver sinusoidal endothelial cell fenestrae: a review. *Comp Hepatol*. 2002;1(1):1.
25. Reeves WH, Kanwar YS, Farquhar MG. Assembly of the glomerular filtration surface. Differentiation of anionic sites in glomerular capillaries of newborn rat kidney. *J Cell Biol*. 1980;85(3):735-53.
26. Ioannidou S, Deinhardt K, Miotla J, et al. An in vitro assay reveals a role for the diaphragm protein PV-1 in endothelial fenestra morphogenesis. *Proc Natl Acad Sci U S A*. 2006;103(45):16770-5.
27. Ichimura K, Stan RV, Kurihara H, et al. Glomerular endothelial cells form diaphragms during development and pathologic conditions. *J Am Soc Nephrol*. 2008;19(8):1463-71.
28. Bacakova L, Travnickova M, Filova E, et al. Vascular smooth muscle cells (VSMCs) in blood vessel tissue engineering: the use of differentiated cells or stem cells as VSMC precursors. *Muscle Cell and Tissue-Current Status of Research Field London, UK: IntechOpen*. 2018:289-307.
29. Huang Y, Chen X, Che J, et al. Shear Stress Promotes Arterial Endothelium-Oriented Differentiation of Mouse-Induced Pluripotent Stem Cells. *Stem Cells Int*. 2019;2019:1847098.
30. Huang Y, Qian JY, Cheng H, et al. Effects of shear stress on differentiation of stem cells into endothelial cells. *World J Stem Cells*. 2021;13(7):894-913.
31. Wang H, Riha GM, Yan S, et al. Shear stress induces endothelial differentiation from a murine embryonic mesenchymal progenitor cell line. *Arterioscler Thromb Vasc Biol*. 2005;25(9):1817-23.
32. Sandoo A, van Zanten JJ, Metsios GS, et al. The endothelium and its role in regulating vascular tone. *Open Cardiovasc Med J*. 2010;4:302-12.
33. Gimbrone MA, Jr., Garcia-Cardena G. Endothelial Cell Dysfunction and the Pathobiology of Atherosclerosis. *Circ Res*. 2016;118(4):620-36.
34. Li M, Qian M, Kyler K, et al. Endothelial-Vascular Smooth Muscle Cells Interactions in Atherosclerosis. *Front Cardiovasc Med*. 2018;5:151.
35. Ingber DE. Human organs-on-chips for disease modelling, drug development and personalized medicine. *Nat Rev Genet*. 2022;23(8):467-91.
36. Huh D, Matthews BD, Mammoto A, et al. Reconstituting organ-level lung functions on a chip. *Science*. 2010;328(5986):1662-8.
37. Lee PJ, Hung PJ, Lee LP. An artificial liver sinusoid with a microfluidic endothelial-like barrier for primary hepatocyte culture. *Biotechnol Bioeng*. 2007;97(5):1340-6.

38. Ortega-Prieto AM, Skelton JK, Wai SN, et al. 3D microfluidic liver cultures as a physiological preclinical tool for hepatitis B virus infection. *Nat Commun.* 2018;9(1):682.
39. Huh D, Leslie DC, Matthews BD, et al. A human disease model of drug toxicity-induced pulmonary edema in a lung-on-a-chip microdevice. *Sci Transl Med.* 2012;4(159):159ra47.
40. Nenasheva T, Gerasimova T, Serdyuk Y, et al. Macrophages Derived From Human Induced Pluripotent Stem Cells Are Low-Activated “Naive-Like” Cells Capable of Restricting Mycobacteria Growth. *Front Immunol.* 2020;11:1016.
41. Cui D, Franz A, Fillon SA, et al. High-Yield Human Induced Pluripotent Stem Cell-Derived Monocytes and Macrophages Are Functionally Comparable With Primary Cells. *Front Cell Dev Biol.* 2021;9:656867.
42. Tanaka T, Shiba T, Honda Y, et al. Induced Pluripotent Stem Cell-Derived Monocytes/Macrophages in Autoinflammatory Diseases. *Front Immunol.* 2022;13:870535.
43. Nguyen EH, Daly WT, Le NNT, et al. Versatile synthetic alternatives to Matrigel for vascular toxicity screening and stem cell expansion. *Nat Biomed Eng.* 2017;1.
44. Upton Z, Wallace HJ, Shooter GK, et al. Human pilot studies reveal the potential of a vitronectin: growth factor complex as a treatment for chronic wounds. *Int Wound J.* 2011;8(5):522-32.
45. Wang Y, Cheng L, Gerecht S. Efficient and scalable expansion of human pluripotent stem cells under clinically compliant settings: a view in 2013. *Ann Biomed Eng.* 2014;42(7):1357-72.
46. Aisenbrey EA, Murphy WL. Synthetic alternatives to Matrigel. *Nat Rev Mater.* 2020;5(7):539-51.
47. Morin KT, Tranquillo RT. In vitro models of angiogenesis and vasculogenesis in fibrin gel. *Exp Cell Res.* 2013;319(16):2409-17.
48. Morin KT, Tranquillo RT. Guided sprouting from endothelial spheroids in fibrin gels aligned by magnetic fields and cell-induced gel compaction. *Biomaterials.* 2011;32(26):6111-8.
49. van Dijk CGM, Brandt MM, Poulis N, et al. A new microfluidic model that allows monitoring of complex vascular structures and cell interactions in a 3D biological matrix. *Lab Chip.* 2020;20(10):1827-44.
50. Murphy KC, Whitehead J, Zhou D, et al. Engineering fibrin hydrogels to promote the wound healing potential of mesenchymal stem cell spheroids. *Acta Biomater.* 2017;64:176-86.



Appendices

Nederlandse Samenvatting

Dankwoord

List of publications

Curriculum vitae

Nederlandse Samenvatting

Achtergrond

De bloedsomloop bestaat uit verschillende typen vaten die samen zorgen voor de bloedcirculatie in het menselijk lichaam. De circulatie voor de grote bloedsomloop begint in het hart; waar de arteriën zuurstofrijk bloed meenemen naar de verschillende orgaansystemen. Deze slagaders vertakken in kleinere arteriolen en uiteindelijk in nog kleinere capillairen, waar uitwisseling van zuurstof, voedingsstoffen en afvalstoffen plaatsvindt. Zuurstofarm bloed wordt vervolgens via die capillairen, daarna via de venulen en uiteindelijk via de venen teruggevoerd naar het hart. De kleine bloedsomloop loopt via de longen, waar de longslagaders het zuurstofarme bloed van het hart naar de longen vervoeren om het bloed weer van zuurstof te voorzien. Via de longaders loopt dit bloed terug naar het hart; waar het weer gebruikt wordt in de grote bloedsomloop.

Bloedvaten bestaan in de basis uit drie verschillende lagen. De binnenste laag, de tunica intima, is een enkele laag endotheelcellen (ECs), die zorgt voor een barrièrefunctie en in direct contact staan met de bloedstroom. Deze laag wordt beschermd door het basaalmembraan, een dun laagje bindweefsel. De middelste laag, de tunica media, bestaat uit een laag gladde spiercellen (SMCs) die zorgen voor het samentrekken en ontspannen van de bloedvaten. De tunica adventita, de buitenste laag, bestaat uit bindweefsel dat ervoor zorgt dat het vat goed hecht aan het omliggende weefsel. Een uitzondering hierop zijn capillairen, die bestaan enkel uit twee lagen om de uitwisseling van zuurstof, voedings- en afvalstoffen mogelijk te maken. Net als grote vaten hebben deze een binnenste laag van endotheelcellen, gesterkt door een dun laagje bindweefsel. Deze laag wordt ondersteund door een laag murale cellen, de pericyten. Die zorgen voor stabiliteit en functionele interactie met andere cellen, omliggende weefsels en organen.

Afhankelijk van de locatie in het menselijk lichaam hebben de vaten orgaan specifieke functies. Hierdoor hebben de cellen in deze vaten allemaal een unieke vorm en functie en ook de hoeveelheid spiercellen verschilt per type bloedvat. Bij het onderzoek doen naar bloedvaten is het dus belangrijk rekening te houden met de locatie waarin het bloedvat zich in de normale situatie bevindt. De ontwikkeling van bloedvaten begint tijdens de ontwikkeling van het lichaam in de embryonale fase. Daar zorgt vasculogenese voor het ontstaan van nieuwe vaten, beginnend met capillairen die doorgroeien naar grotere (slag)aders en venen. Eenmaal volgroeid zorgt een ander ontwikkelingsproces, angiogenese, voor het ontstaan van nieuwe capillairen uit bestaande capillairen. Dit proces noemen we sprouting. Zo ontstaat

er uiteindelijk een complex vaatnetwerk door het hele lichaam. Angiogenese is naast cruciaal voor het ontwikkelen van dit stelsel, ook betrokken bij (wond)heling en herstel na vaatschade.

Ziekte en dysfunctie van bloedvaten kan leiden tot ernstige complicaties. Verkalking van de grote vaten, atherosclerose, leidt tot verslechterde bloedsomloop van- en naar het hart. In het proces van atherosclerose ontstaat er een steeds groter wordende plaque, door ophoping van witte bloedcellen en vette stoffen. Ook kan atherosclerose onbehandeld resulteren in ruptuur van de plaque, waarbij de inhoud van de plaque naar buiten komt en gaat circuleren. Hierdoor kunnen verderop in de bloedsomloop blokkades of nieuwe laesies ontstaan. Als de bloedsomloop geblokkeerd is krijgen achterliggende organen niet genoeg zuurstof meer, waardoor deze achteruit gaan in functie en uiteindelijk voor verdere problemen zorgen.

Regeneratieve geneeskunde focust zich op het herstellen of vervangen van de fysiologische functie van weefsels en organen. Dit kan door regeneratie in het lichaam zelf, of door het maken van vervangende structuren om op de aangedane plek te kunnen implanteren. Bloedvaten spelen daarin een grote rol. Niet alleen op zichzelf staand, maar zoals hierboven beschreven hebben organen zuurstof en voedingsstoffen nodig om te kunnen functioneren. Bij het (re-)genereren van orgaanstructuren is het dus belangrijk om ook de bijbehorende bloedvaten in acht te nemen. Het ontbreken van een functioneel vasculair netwerk in ontwikkelde orgaanstructuren zorgt voor verminderde functionaliteit buiten het lichaam en na implantatie omdat er niet voldoende zuurstof en voedingsstoffen beschikbaar zijn om het volledige construct te voorzien. Daarom is het belangrijk om onderzoek te doen naar het creëren van verschillende vaatstructuren om zo zowel bloedvaten, als geïntegreerde vaatstructuren voor orgaanconstructen te kunnen ontwikkelen.

Het namaken van functionele organen voor transplantatie zou natuurlijk de meest ideale uitkomst zijn in een wereld waar er een schrijnend tekort is aan donororganen. Echter is er over veel onderliggende mechanismen van bepaalde aandoeningen nog weinig bekend. Onderzoek doen naar ziektes en afwijkingen in het menselijk lichaam is vaak invasief voor de patiënt en lastig voor de onderzoeker omdat elke patiënt een unieke genetische code heeft, waardoor niet elke behandeling voor iedereen werkt, ook al is de aandoening in de basis hetzelfde. Het buiten het lichaam namaken van het zieke orgaan of weefsel zou daarvoor uitkomst bieden. Als je daarbij gebruik maakt van stamcellen, en daarbij specifiek geïnduceerde pluripotente stamcellen (iPSCs) is het mogelijk om voor elke patiënt een eigen construct te maken met het juiste genetische materiaal. iPSCs kunnen worden gemaakt van bijvoorbeeld

fibroblasten uit de huid, waardoor ze voor elk individu te maken zijn. Deze cellen hebben het vermogen om te differentiëren tot bijna elk celtype in het menselijk lichaam en zijn daardoor bij uitstek geschikt voor het ontwikkelen van complexe orgaanstructuren. Met het gebruik van patiënt-eigen cellen maak je niet alleen een construct waar je bepaalde therapieën op kunt testen, maar is het ook mogelijk om de ontwikkeling en progressie van een bepaalde aandoening te kunnen onderzoeken zonder dat de patiënt daar zelf last van heeft.

Voor het maken van dergelijke constructen zijn verschillende wegen te bewandelen. Één daarvan is het gebruik van biomaterialen die, zowel in het lichaam als erbuiten een bepaalde (structurele) functie kunnen overnemen. Om dat volledig te kunnen doen is daar ook organisch materiaal voor nodig, om te zorgen dat de cellen zich op de juiste manier oriënteren, bijvoorbeeld in een tubulair construct. Een combinatie van een biomateriaal en (patiënt-specifieke) cellen zou kunnen leiden tot een functioneel construct, voor zowel implantatie, als therapeutisch screenings platform en als ziektemodel.

Ook het gebruik van organoïden, kleine 3D structuren die de vorm en functie van een specifiek orgaan of weefsel kunnen nabootsen zijn populair. In dit proefschrift maken we gebruik van bloedvat organoïden, gemaakt van iPSCs. Hiermee hebben we direct een populatie van diverse vaatcellen beschikbaar, die we kunnen gebruiken voor de ontwikkeling van verschillende modellen. De cellen gewonnen uit deze organoïden zijn geschikt voor het maken van zowel macro- als microvaatmodellen voor regeneratie en het ontwikkelen van ziektemodellen.

De belangrijkste bevindingen binnen dit proefschrift

Verder onderzoek naar de verschillende functies van vaatcellen in het lichaam is nodig om uiteindelijk orgaan- of vaatspecifieke constructen te kunnen maken. In **hoofdstuk 2** hebben we de belangrijkste bevindingen over de diversiteit in functie, vorm en dichtheid van pericyten op verschillende locaties in de bloedsomloop uiteengezet. We concludeerden dat daar veel verschil in zit en dat het dus belangrijk is om de juiste populatie te kiezen (of te differentiëren vanuit stamcellen) wanneer er onderzoek gedaan wordt naar een bepaalde vaataandoening. In **hoofdstuk 3** hebben we ECs en SMCs gewonnen uit bloedvat organoïden (ODECs en ODMCs), gemaakt van stamcellen. Deze cellen zijn toen gezaaid op een biologisch afbreekbare scaffold, een tubulair construct gemaakt van polycaprolactone-bisurea (PCL-BU). Deze is vervolgens getest in een bioreactor, waar de cellen op de scaffold blootgesteld werden aan mechanische stress, net zoals in het menselijk lichaam. Analyse van het construct wees uit dat er een dubbellaagse celstructuur is ontstaan,

met een laag ODECs aan de lumenale zijde, ondersteund door de ODMCs. Deze structuur bleef onaangetaast na het blootstellen aan mechanische stress, waardoor we kunnen concluderen dat deze cellen geschikt zijn voor het creëren van een vaatmodel zoals beschreven in **hoofdstuk 3**.

De multi inzetbaarheid van de ODECs is verder getest in **hoofdstuk 4**. In het lichaam zijn verschillende soorten capillairen te vinden, waar gefenestreeerde capillairen één soort van is. Fenestrae zijn openingen van ongeveer 70nm in diameter in het celmembraan van een EC waardoor uitwisseling van grotere moleculen mogelijk is. Deze capillairen zijn te vinden in het endocriene (hormonale) systeem, de nieren en in het maag-darmstelsel. Fenestrae zijn dynamisch, ze verschijnen en verdwijnen afhankelijk van de vereiste permeabiliteit van het vat. Over het ontstaan, maar voornamelijk over het verdwijnen van deze structuren is helaas weinig bekend. Er is één gen en bijbehorend eiwit geassocieerd met deze fenestrae, Plasmalemma Vesicle Associated Protein (PLVAP). In **hoofdstuk 4** hebben we met behulp van groeifactoren opregulatie van PLVAP verkregen, waardoor fenestrae in het membraan van iPSC gedifferentieerde stamcellen ontstonden. Er werd aangetoond dat het gebruik van deze groeifactoren geen invloed heeft op de expressie van EC specifieke markers of op de barrière functie. Wel is er, na inductie van de fenestrae, verhoogde permeabiliteit van de ODECs waardoor grotere moleculen het membraan kunnen passeren. Deze resultaten worden vergeleken met cellen die van nature gefenestreeerd zijn en daaruit konden we concluderen dat de ODECs vergelijkbare functionaliteit vertoonden. Door meer onderzoek te doen naar het ontstaan en het controleren van fenestrae, ook buiten het lichaam, is het mogelijk om functionele capillaire te creëren, die uiteindelijk gebruikt kunnen worden voor regeneratieve toepassingen.

Ook de ODMCs werden uitgebreid getest voor verschillende toepassingen. Nadat ze functioneel bleken in een macro-vaat model in **hoofdstuk 3**, werden ze in **hoofdstuk 5** vergeleken met SMCs uit de aorta. SMCs hebben als unieke eigenschap dat ze verschillende fenotypen kunnen aannemen afhankelijk van de behoeften van een bloedvat. In functionele volgroeide vaten zijn ze contractiel en voornamelijk verantwoordelijk voor vasoconstrictie en vasodilatatie. Tijdens de ontwikkeling, zowel in embryogenese als in herstel na schade veranderen ze naar een synthetisch fenotype. Deze cellen vermenigvuldigen zich snel en zorgen voor snel vaatherstel door het uitscheiden van extracellulaire matrix (ECM) en het aantrekken van ECs. De switch tussen deze twee fenotypen wordt gemedieerd door signalen vanuit de omgeving. Het begrijpen en kunnen controleren van deze switch is essentieel voor het gebruik van SMCs in regeneratieve toepassingen om te voorkomen dat SMCs

blijven groeien op het moment dat een construct volledig volgroeid is. In **hoofdstuk 5** hebben we de switch van synthetisch, zoals ze zijn in een 2D celkweek, naar contractiel geïnitieerd met behulp van groeifactoren, verandering in stijfheid van de omgeving en het gebruik van mechanische stretch. Hier hebben we gezien dat de ODMCs in staat zijn beide fenotypes aan te nemen in een 2D celkweek, gelijkend op de SMCs uit de aorta. Daarnaast resulteert het verhogen van de stijfheid van de omgeving, door middel van verschillende concentraties GelMa ervoor dat deze cellen meer richting een contractiel fenotype gaan en stoppen met prolifereren. Ook het toevoegen van mechanische stretch, net als in de fysiologische omgeving zorgt ervoor dat deze cellen contractiele eigenschappen krijgen. Verder onderzoek zal moeten uitwijzen of deze cellen gebruikt kunnen worden in combinatie met ECs in een model als beschreven in **hoofdstuk 3** of **hoofdstuk 7**. Het kunnen creëren en behouden van een contractiele populatie SMCs is een stap dichterbij het maken van een functioneel macrovaatmodel.

Het (re)modelleren van bloedvaten is een dynamisch proces en in de fysiologische situatie zijn daar verschillende mechanische factoren bij betrokken. Door de bloedstroom vanuit het hart is er altijd druk op de wanden van het bloedvat. De bloedstroom veroorzaakt zowel shear stress (de oppervlaktespanning die ontstaat doordat er druk op de lumenale endotheellaag wordt uitgeoefend) als wall stretch (het uitrekken van het vat door de bloeddruk). Deze krachten hebben invloed op de gedragingen van vasculaire cellen, zoals uiteengezet in **hoofdstuk 6**. We concludeerden dat deze biomechanische factoren verschillende mechanosensors activeren. De activatie van deze sensoren stimuleert vaatgroei, wat essentieel is in de regeneratieve geneeskunde. Echter; een verhoogde bloeddruk kan leiden tot ongewilde vaatgroei of andere vasculaire pathologieën. Verschillende mechanosensors in vaatcellen zijn betrokken bij de ontwikkeling en progressie van vaatziekten, maar verder onderzoek is noodzakelijk om nieuwe therapeutische targets voor vaatregeneratie te identificeren. Het gebruik van mechanische factoren in ziektemodellen is hierdoor essentieel om de ontwikkeling en progressie van ziektes in kaart te brengen. In **hoofdstuk 7** hebben we een ziektemodel voor atherosclerose ontwikkeld, waarbij we gebruik hebben gemaakt van verschillende celtypes betrokken bij deze ziekte. Het gebruik van patiënt-eigen cellen in een ziektemodel zoals beschreven in hoofdstuk 7 zou de vertaling naar de kliniek voor regeneratieve toepassingen makkelijker maken. Naast vaatcellen zoals beschreven in dit proefschrift, is het mogelijk om ook de benodigde immuuncellen van iPSCs te differentiëren waardoor er voor elke patient een uniek model met het bijbehorende genetische materiaal kan worden ontwikkeld.

Een belangrijke limitatie in de vertaling van het lab naar de kliniek voor regeneratie in de patient zelf (*in vivo*) of het terugplaatsen van buiten het lichaam gekweekt materiaal (*ex vivo/ in vitro*) is het gebruik van dierlijke (bij)producten. Een veelgebruikt product in celkweek, zowel in iPSCs als in organoids is Matrigel. Matrigel is een basaalmembraanmatrix die wordt uitgescheiden door Engelbreth-Holm-Swarm-muissarcoomcellen. De samenstelling van deze matrix, bestaande uit verschillende groeifactoren waardoor celgroei gepromoot wordt, is doordat het een dierlijk product is per batch enigszins verschillend, waardoor replicatie van proeven bemoeilijkt wordt. Het gebruik van tumor(bij)producten is in de kliniek natuurlijk niet wenselijk, dus er is veel behoefte aan een alternatief. Omdat elk type cel andere behoeftes heeft, dienen alternatieven per protocol getest te worden. **In hoofdstuk 8** hebben we voor zowel de iPSCs als voor onze bloedvat organoïden een alternatief getest. Voor de iPSC kweek is dit een synthetisch alternatief, waardoor de celkweek een continue kwaliteit behoudt en proeven makkelijk gerepliceerd kunnen worden. Voor de vasculaire organoïden is dit alternatief gebaseerd op een uit de mens afkomstige fibrine gel, omdat de beschikbare synthetische alternatieven niet voldoen aan de eigenschappen die dit protocol vereist. Fibrine gellen zijn combinaties van fibrinogeen en thrombine, onderdeel van de bloedstollingscascade en werden eerder in verband gebracht met het promoten van vaatgroei. Het gebruik van deze alternatieven leverden vergelijkbare eindproducten op; waardoor deze cellen in de toekomst mogelijk gebruikt kunnen worden voor regeneratieve toepassingen in de kliniek, maar ook een beter beeld geven bij gebruik in ziektemodellen.

Conclusie

De hypothese van dit proefschrift luidde; hiPSC afgeleide bloedvatorganoïden zijn een goede bron van vaatcellen voor het namaken van zowel macro- als microvaat modellen. Door gebruik te maken van verschillende *in vitro* technieken hebben we aangetoond dat dat klopt. Onze iPSC afgeleide ECs (ODECs) expresseren de karakteristieke EC markers en reageren op mechanische stress zoals ze in de fysiologische situatie ook zouden doen. Daarnaast is het mogelijk een subpopulatie ECs te creëren die fenestrae bevatten om zo stofuitwisseling mogelijk te maken in een capillair bed. De iPSC afgeleide SMCs (ODMCs) hebben pericyte-(micro-vaat) karakteristieken in hun 3D formatie binnen de bloedvat organoïden. Daarbuiten zijn ze in staat om een macrovaatmodel te bevolken, maar ook om de verschillende SMC fenotypes aan te nemen onder invloed van groeifactoren en mechanische stress. Dit betekent dat deze cellen voor verschillende vaatmodellen kunnen worden gebruikt, waarmee, wanneer de iPSCs van de patiënt afkomstig zouden zijn, patiënt specifieke ziektemodellen kunnen worden gemaakt waar verschillende therapieën op kunnen

worden getest. Door het vervangen van Matrigel in het differentiatieprotocol komen we een stap dichterbij de kliniek. In de projecten binnen dit proefschrift hebben we gebruik gemaakt van stamcellen van gezonde donoren. Echter zal het gebruik van stamcellen van patiënten met vaatziekten wellicht meer inzicht geven in de interactie tussen de verschillende vaatcellen en het verschil in ontwikkeling van nieuwe vaten. Verder onderzoek naar het specificeren van subpopulaties van vaatcellen die corresponderen met de locatie waar er sprake is van ziekte of abnormaliteiten zal uiteindelijk bijdragen aan het creëren van constructen die zowel orgaan- als patiënt-specifiek zijn.

Dankwoord/acknowledgements

Hora est! Het afronden van dit proefschrift was niet mogelijk geweest zonder de ondersteuning van mijn promotieteam, collega's, familie en lieve vrienden. Hieronder wil ik een aantal mensen in het bijzonder bedanken.

Promotiecommissie

Prof. Dr. Marianne verhaar

Lieve **Marianne**, bedankt voor het mogelijk maken van mijn promotietraject, de input in mijn projecten en de interesse in mijn werk maar ook in mij persoonlijk. Ik heb onze samenwerking als heel waardevol en leerzaam ervaren en kijk met een heel goed gevoel terug op mijn tijd als PhD student in het UMCU!

Dr. Caroline Cheng

Lieve **Caroline**, allereerst ontzettend bedankt voor de fijne begeleiding tijdens mijn promotietraject. Jouw kennis, input en vertrouwen in mij hebben mij uiteindelijk gebracht waar ik nu ben; bij het einde van mijn PhD en het begin van een nieuwe carrière. Ik wist de afgelopen jaren altijd waar ik aan toe was en heb ontzettend veel geleerd van onze samenwerking. Ik heb de ruimte gekregen mijzelf te ontwikkelen, zelf een project op te starten (en af te ronden) en mijn werk te presenteren binnen en buiten het UMCU. Ik ga dit traject en de dingen die ik erin geleerd heb nooit vergeten.

Daarnaast wil ik de leden van mijn promotiecommissie, **Prof. dr. J.P.G. Sluijter, Dr. Y.M. Ruigrok, Dr. J. Essers, Prof. dr. C.V.C. Bouten** en **Prof. dr. ir. J. Malda** hartelijk bedanken voor het zitting nemen in mijn leescommissie en het kritisch lezen van dit proefschrift.

Collega's

Petra de Bree en **Rachel**, my dear paranymphs. I'm honored that you wanted to stand by my side for this very special occasion. **Petra**, mijn koffiedrinkmaatje, mede fietsliefhebber en heerlijke collega, ik heb onwijs genoten van onze tijd samen op het lab. Samen het foute uur luisteren (en klagen over Paradise in the dashboard lights), uren praten over fietsen (en fietsen) en onze koffiedates. Met als hoogtepunt natuurlijk fietsen op Lanzarote samen. Ik ga het werken met jou enorm missen, maar we zetten onze koffiedates op de fiets voort!

Rachel, thanks for making my last year in the lab great fun and one to remember. We got along from the first week you were here and although you sometimes had a hard time with me being stressed to finish this dissertation, we had a lot of fun and good talks in our office corner. Let's keep the advent calendar tradition alive! We do need to work a bit on the relationship with your tiny raptor at home though, but we will get there. Happy to have you as my friend!

De (rest van de) Cheng groep. Allereerst **Chris**, bedankt voor onze samenwerking de afgelopen jaren! Ik heb veel van je geleerd en onze tripjes naar München en Manchester waren onwijs leuk. Ik hoop dat we af en toe de tijd kunnen vinden om een biertje te drinken en bij te praten in de toekomst! **Ihsan(e)** 😊, bedankt voor jouw werk aan onze projecten, maar vooral ook de gezelligheid in het lab en op kantoor. Onze discussies, vaak met een knipoog, ga ik niet snel vergeten! **Ijsbrand**, bedankt voor de gezelligheid in de groep en succes met het afronden van je promotietraject! Also, although not working in the lab in Utrecht, **Ranga** and **Maarten** thanks for you input and collaboration on some projects! I wish you both all the best in the future!

Dan de rest van de Nefrologiegroep, bedankt voor al jullie input, gezelligheid en samenwerkingen binnen het RMCU. **Paul**, bedankt voor alles! Jouw energie, kennis over van alles en nog wat en input in mijn projecten hebben mij door mijn PhD heen gesleept. Ik heb enorm genoten van onze gesprekken, al dan niet met een biertje erbij, en ga jou als collega erg missen! **Merle**, ondanks dat we niet hebben samengewerkt aan projecten heb ik jouw input altijd heel erg gewaardeerd. Daarnaast was er altijd tijd voor "even gezellig kletsen", ook al hadden we het allebei superdruk. We blijven contact houden! **Tobias**, bedankt voor alle gezelligheid, alle uren hardlopen (al dan niet in de regen) en goede gesprekken. Veel succes met de rest van je opleiding! **Bas**, ik heb jou als collega de afgelopen jaren enorm gewaardeerd. Ik bewonder jouw passie voor wetenschap en ik was erg onder de indruk van je vindingrijkheid in projecten. Daarnaast had ook jij altijd tijd voor een praatje (of snoepjacht op kantoor) en heb je veel waardevolle, kritische en eerlijke adviezen gegeven omtrent mijn werk. Daar ben ik je super dankbaar voor! **Petra de Graaf**, ik vond het heerlijk dat je onze groep kwam versterken al hoor je natuurlijk stiekem bij de Urologie. Bedankt voor je altijd waardevolle input, gezellige kletspraatjes, mooie keramieke aandenkens en ons tripje naar Polen! **Melanie**, bedankt voor alle gezelligheid in het lab en tijdens onze koffiedates! Ook **Krista**, bedankt voor jouw gezelligheid, met name tijdens de uurtjes in het histolab.

Ook **Tom, Kate, Gisela, Julia, Robin, Isabel, Joost de Vries, Joost Fledderus** en **Babette**, bedankt voor de gezelligheid! Ik wens jullie het allerbeste! **Vivian, Murillo, Vasiliki, Silvia** and **Jaap**, I enjoyed the research meetings and your input on my projects. I wish you all the best for the future!

Inge, bedankt voor alle gezellige uren in de kweek, goeie gesprekken en het verzorgen van mijn cellen in het weekend. Ik kon alles altijd met een gerust hart aan je over laten, waarvoor eeuwig dank! Gelukkig blijven we elkaar spreken buiten werk! Lieve **Marijn**, ik heb genoten van alle uren samen op kantoor, smoothie bowls bij Loua en al het andere dat we hebben meegemaakt. Heel leuk dat je er de laatste maanden van mijn PhD weer bij was en ik wens je heel veel succes in je ongetwijfeld prachtige carrière! Ook **Iris**, met wie we uren op kantoor hebben zitten kletsen, dankjewel voor alles! **Renée**, bedankt voor onze leuke samenwerking op mijn grootste project! Honderduit kletsen in de kweek over van alles en nog wat en soms even “samen klagen” tijdens een kopje koffie. En dan nu allebei klaar, trots op ons! Ik wens je heel veel succes in de toekomst! **Roos-Anne**, jou wil ik ook heel erg bedanken voor alle gezelligheid op het lab. Bedankt voor het scheppen van orde in de chaos die celweek heet en alle leuke gesprekken die we hebben gehad! **Nino**, thanks for all the good talks and laughs in the lab, we had a good time! **Ook de rest van de collega's van Diergeneeskunde en het UMCU, die er echt te veel zijn om op te noemen, dankjulliewel!**

Onze projecten zouden niet zijn afgerond zonder de samenwerking met de Tu/E. Met name **Suzanne, Anthal** en **Tamar** heel erg bedankt voor jullie harde werk, maar ook de gezellige meetings en goede feedback. Ik wens jullie het allerbeste voor de toekomst! Also, a special thanks to **Wojchech and Carlijn** for the help on my projects.

Als laatste van het lab; “mijn” studenten. Jullie hebben allemaal een bijdrage geleverd aan dit proefschrift en daar ben ik jullie onwijs dankbaar voor. **Esmee, Karlijn, Ymke, Stijn, Jurjen, Elena, Lisa** en **Vera**, ik wens jullie veel succes in jullie verdere carrière!

Vrienden en familie

Mijn vrienden en vriendinnen uit Leiden, van Aug en daarbuiten die er altijd waren voor afleiding, een luisterend oor of een goed gesprek. **Daan** en **Danique**, bedankt voor alle uren die ik bij jullie op de bank mocht doorbrengen, de cocktailavondjes en de spelletjesstrijd, op nog heel veel momenten samen! Ook **Steeff, Sebas, Dion, Claire** en **Suus**, dank voor jullie liefde en support. **Vivian**, heerlijk dat we

tegenwoordig een gedeelde passie hebben. Altijd kletsen over sport (of samen trainen), daar geniet ik heel erg van. Ook onze spelletjesavonden, samen met **René** en **Dennis**, zijn favoriet! **Tamara** en **Maarten**, bedankt voor de fancy dinertjes, goede wijntjes en af en toe een random theatervoorstelling tussendoor, een welkome afleiding tussen het sporten en werken door. **Sophie Geelen**, van triatlons naar gemeenschappelijk irritainment, ik ben blij met onze vriendschap! **Anne** en **Pauline**, mijn lievelingsbestuurders, jullie zijn er vanaf het begin van mijn PhD ook altijd bij geweest. Dank voor jullie luisterend oor en avondjes gezelligheid!

Lieve **Roni**, mijn studiemaatje en later PhD sparringpartner, bedankt voor alle wijze raad, gezelligheid en luisterend oor de afgelopen jaren. Van twee net afgestudeerde broekies naar zelfstandige onderzoekers, ik ben trots op ons!

Mijn treintje op de baan, met name **Lisa, Anne en Silke**, bedankt voor alle uren training, gezelligheid en wijze raad ten tijde van mijn promotietraject en mijn weg naar de IRONMAN afgelopen jaar. Het Kalmar clubje, met **Paul, Christiaan** en **Dennis** (en **Veerle** natuurlijk) was een heerlijk geheel! **Bas van Boven**, bedankt voor het altijd zijn van een luisterend oor, mijn eerste hulp bij fietsproblemen oplosser en trainingsmaatje. Alle uren zwemmen, fietsen en hardlopen hebben me veel plezier en afleiding gebracht de afgelopen jaren. **Mijn andere trainingsmaatjes van ZVL, het hele Luxemburg clubje** en alle andere (tri)atleten die met mij mee hebben getraind en geleefd de afgelopen jaren, ik ben jullie heel dankbaar! Ook de lieve mensen van **dansschool Dance Fit**, met name **Robin, Sandra, Esther** en **Reinier**, bedankt voor het zijn van het allerleukste avondje uit van de week!

Hanne, mijn allergrootste (maar allerkleinste) vriendinnetje. Bedankt voor het er altijd zijn, voor leuke en minder leuke dingen, voor grote en kleine geluksmomentjes. Niet veel woorden nodig; love you!

Papa en **Mama**, jullie hebben altijd met 100% support en enthousiasme achter mij gestaan tijdens mijn PhD. Ondanks dat ik soms een woordenwaterval ben en met termen gooi die ik daarna even moet uitleggen is jullie enthousiasme over mijn werk nooit minder geworden. Ik ben blij dat ik altijd bij jullie terecht kan en dat jullie mij alle ruimte hebben gegeven om mij te ontwikkelen tot mijn grote (maar toch ook nog steeds kleine 😊) zelf! Ook **Peter** en **Josine**, mijn bonusouders, bedankt voor jullie steun, support en interesse! Ik houd van jullie! **Juul**, liefste nuunt, waar we elkaar vroeger liever kwijt dan rijk waren zijn we nu 2 handen op 1 buik. Ook jij hebt altijd met veel liefde, interesse en bemoedigende woorden klaargestaan voor mij de afgelopen jaren en daar ben ik je super dankbaar voor. En **Enverney**;

bedankt voor bemoedigende woorden, kritische vragen en ruimdenkende blik; fijn om jou erbij te hebben! **Rob**, mijn (niet meer zo) kleine broertje, in de afgelopen jaren ben jij gegroeid tot een slimme, kritische en ambitieuze jongvolwassene, ik ben heel trots op jou! Bedankt dat je er altijd bent. **Ron, Joke** en **Janine**, mijn lieve schoonouders en schoonzusje, waar altijd de koffie klaar staat en we terecht kunnen met al onze verhalen. Bedankt voor jullie interesse, steun en luisterend oor tijdens de afgelopen jaren!

Oma Witte, bedankt voor uw interesse, vragen en verhalen over wetenschap, onze gemeenschappelijke deler. Naast paarden natuurlijk, onze ritjes ga ik nooit vergeten. Ik vind het heel bijzonder dat u er bent nu ik mijn proefschrift afrond. **Oma Meijer**, ook u bent altijd geïnteresseerd geweest in mijn werk en ik kan met al mijn verhalen altijd terecht. Samen met **André** een kaas en wijn avondje houden blijft favoriet! Ook **Co** en **Wilma**, misschien niet altijd dichtbij, maar wel altijd enthousiast en geïnteresseerd. Bedankt voor alles! Ook de rest van de **familie Meijer**, de **familie Witte** en mijn **schoonfamilie van Rooden** en **van der Reijden**, bedankt voor jullie vertrouwen in mij! In het bijzonder **Annemieke**, die eventjes tegelijk met mij PhD student was.

Als laatste mijn liefste man, lieve **Dennis**, samen kunnen wij de wereld aan. Bedankt voor je onvoorwaardelijke steun, wijze raad en kritische blik. Voor altijd aan een half woord genoeg. De afgelopen jaren hebben we veel avonturen beleefd waaronder prachtige reizen, ons huwelijk en het kopen van ons (nu nog) toekomstige droomhuis. Ik kijk met liefde terug op deze tijd, en met nog meer liefde vooruit naar de toekomst. Ik houd van je!

List of publications

Published

Meijer, E. M., van Dijk, C. G., Kramann, R., Verhaar, M. C., & Cheng, C. (2022). Implementation of pericytes in vascular regeneration strategies. *Tissue Engineering Part B: Reviews*, 28(1), 1-21.

Meijer, E. M., Koch, S. E., van Dijk, C. G., Maas, R. G., Chrifi, I., Szymczyk, W., ... & Cheng, C. (2023). 3D Human iPSC Blood Vessel Organoids as a Source of Flow-Adaptive Vascular Cells for Creating a Human-Relevant 3D-Scaffold Based Macrovascular Model. *Advanced Biology*, 7(1), 2200137.

Meijer, E. M., van Dijk, C. G. M., Giles, R., Gijsen, K., Chrifi, I., Verhaar, M. C., & Cheng, C. (2023). Induction of Fenestrae in hiPSC-Derived Endothelial Cells for Disease Modeling. *Tissue engineering. Part A*.

Meijer, E. M., Giles, R., van Dijk, C. G., Maringanti, R., Wissing, T. B., Appels, Y., ... & Cheng, C. (2023). Effect of Mechanical Stimuli on the Phenotypic Plasticity of Induced Pluripotent Stem-Cell-Derived Vascular Smooth Muscle Cells in a 3D Hydrogel. *ACS Applied Bio Materials*, 6(12), 5716-5729.

Maringanti, R., **Meijer, E.**, Brandt, M. M., Duncker, D. J., & Cheng, C. (2021). Contributions of wall stretch and shear stress to vascular regulation: Molecular mechanisms of homeostasis and expansion. *Vascular Mechanobiology in Physiology and Disease*, 21-46.

In submission

Maringanti, R., van Dijk, C. G., **Meijer, E. M.**, Brandt, M. M., Krebber, M. M., Chrifi, I., ... & Cheng, C. (2023). A complex three-dimensional microfluidic model that mimics the early stage events in the human atherosclerotic artery. *bioRxiv*, 2023-02.

Curriculum Vitae

Elana Marianne Meijer was born in Amsterdam on the 25th of May, 1995. In 2013, she graduated from the Gymnasium Education at 'Het Amsterdams Lyceum' and started the bachelor BioPharmaceutical Sciences in Leiden. Her final internship was on the development of lipid plaques in ApoE-deficient mice. During her studies she worked as a research assistant at the Center for Human Drug research in phase II and III clinical trials. After receiving her diploma in 2016, Elana continued her education at the University of Amsterdam. During her master Experimental Internal Medicine, she performed two internships. Under supervision of dr. Phil Barnett in the Amsterdam Medical Center, her first internship was on the capacity of EMERGE predicting cardiac enhancers. Her second internship was under supervision of dr. Ruud Jansen and dr. Wil van der Reijden at Streeklab Haarlem, where they developed an Next-Generation Screening pipeline for HLA-DQ genotyping. Her final thesis was on the role of platelets in diabetic nephropathy. After finishing her masters, Elana started her PhD at the department of Nephrology and hypertension under supervision of dr. Caroline Cheng and Prof. dr. Marianne Verhaar. The results obtained during her PhD are presented in this thesis. After her PhD, she started working as a Pharmaceutical Specialist at MSD in Haarlem.



